Validation of Australian Bureau of Meteorology High Resolution Wave Model (HI-WAM)

Author:
Coghlan, I R

Publication details:
Report No. UNSW Water Research Laboratory Technical Report No. 237

Publication Date:
2010

DOI:
https://doi.org/10.26190/unsworks/634

THE UNIVERSITY OF NEW SOUTH WALES
water research laboratory
Manly Vale N.S.W. Australia

VALIDATION OF AUSTRALIAN BUREAU OF METEOROLOGY HIGH RESOLUTION WAVE MODEL (HI-WAM)

by

I R Coghlan

Research Report 237
May 2010

BIBLIOGRAPHIC DATA SHEET

Report No. 237	Report Date: May 2010	ISBN: 0/85824/084/X

Title: Validation of Australian Bureau of Meteorology High Resolution Wave Model (HI-WAM)

Author(s) I R Coghlan

Sponsoring Organisation:

Australian Bureau of Meteorology

Supplementary Notes

Abstract

The Water Research Laboratory (WRL) of the University of New South Wales has undertaken the first national assessment of the performance of the HI-WAM wave model developed by the Australian Bureau of Meteorology (BoM). The model was validated against wave buoy measurements from 18 locations around Australia over an 11 year period 1 (1997 to 2008).

This high resolution, modified version of WAM was found to generally reproduce the overall natural variability of the sea state in terms of Significant Wave Height, Mean Wave Period and Wave Direction.

However, while the HI-WAM model reproduces the overall natural patterns of the Australian climate and is considered to perform very well in moderate wave conditions, predictions for extreme measured wave heights are not considered to be suitable for engineering design purposes.

Distribution Statement

For general distribution.

Descriptors

Ocean wave, Numerical simulation, Wave models, Hindcast, WAM, Wave buoys, Statistical analysis, Error estimation.

Identifiers

Number of Pages: 185	Price: On Application.

THE UNIVERSITY OF NEW SOUTH WALES
SCHOOL OF CIVIL AND ENVIRONMENTAL ENGINEERING
WATER RESEARCH LABORATORY

VALIDATION OF AUSTRALIAN BUREAU OF METEOROLOGY HIGH RESOLUTION WAVE MODEL (HI-WAM)

by

I R Coghlan

Internal Supervisor: W L Peirson (UNSW)
External Supervisor: D J M Greenslade (BoM)

Research Report No. 237
(Thesis Fulfilling 12 Credit Point Masters Project - CVEN9930)

May 2010

CONTENTS

LIST OF TABLES

LIST OF FIGURES

ABSTRACT

The Water Research Laboratory (WRL) of the University of New South Wales has undertaken the first national assessment of the performance of the HI-WAM wave model developed by the Australian Bureau of Meteorology (BoM). The model was validated against wave buoy measurements from 18 locations around Australia over an 11 year period 1 (1997 to 2008). Several major storms were experienced at most wave buoy locations during this time.

This high resolution, modified version of WAM was found to generally reproduce the overall natural variability of the sea state. The contemporary skill of the model was assessed in terms of Significant Wave Height, Mean Wave Period and Wave Direction using only the most recent six months of data (September 2007 to February 2008). For any given location in Australia within the range of water depths tested, HI-WAM wave parameter predictions were found to have a general accuracy (when compared to measured values) as follows:

- Significant Wave Height predictions within ± 0.4 m
- Mean Wave Period predictions within ± 0.9 s
- Wave Direction predictions within ± 10 ° (for H_S greater than or equal to 1 m).

Summary time series plots and box plots comparing measured and predicted values for each site and wave parameter are presented as "thumbnails" overlaid on the model domain in Figures 7.51 to 7.56 so that regional trends in model skill can be viewed at a glance.

When extreme wave events occurred in the real world (H_S greater than 3.0 m), considerable systematic differences in wave energy were noted between HI-WAM predictions and the measured data. Wave energy (height and period) was vastly over predicted at only one site, Sydney (NSW), for extreme wave heights but, conversely, energy was under predicted for those sites exposed to full swell in Victoria, Tasmania, South Australia and Western Australia.

While the HI-WAM model reproduces the overall natural patterns of the Australian climate and is considered to perform very well in moderate wave conditions, predictions for extreme measured wave heights are not considered to be suitable for engineering design purposes.

A preliminary comparison of HI-WAM with the performance of another wave model, NOAA Wave Watch III (NWWIII) at one representative location indicated that NWWIII appeared to have slightly superior performance for all statistical measures of model skill.

Further analysis of the HI-WAM model identified several interesting trends in model performance as follows:

- Model skill generally reduced with depth for H_S and T_1 (poorer performance in shallower depths);
- Model skill increased as a function of time (wind field descriptions input into HI-WAM are constantly being improved);
- Model skill was not correlated with latitude (considerable differences in model skill were not noted between Australian latitudinal extremes);
- Model skill increased with increase in measured H_S for Wave Direction (better Wave Direction predictions in more energetic conditions).

Recommendations were made to install more wave buoys in strategic regions of the coast, to further extended validation of HI-WAM and to consider the future use of HI-WAM if NWWIII is shown (by more extensive comparisons) to provide superior wave predictions.

1. INTRODUCTION

The Australian Bureau of Meteorology (BoM) executes a high resolution, modified version of the third generation ocean wave prediction model, WAM (WAve Model). This form of the model, known as "HI-WAM", was developed for a research project undertaken by Geoscience Australia for the purposes of scientific examination of sediment mobility on the Australian continental shelf. HI-WAM is the most detailed (and computationally intensive) wave model of the Australian coastline developed by BoM but its output is not publically available at present. The model also remains unvalidated against real wave measurements. The Water Research Laboratory (WRL) of the University of New South Wales approached BoM to develop a collaborative research project to validate the skill of HI-WAM.

A brief literature review of the current state of wave models was undertaken. Background knowledge of the Action Balance Equation and its source terms was developed. An overview of WAM physics and its numerical implementation are provided in addition to modifications made to the original code by BoM to best suit Australian conditions.

HI-WAM model output data for wave height, period and direction was available for a duration of 11 years (1997 to 2008). This model data was compared with wave buoy measurements from 18 carefully selected locations around Australia during the same time period. Several adjustments were required to transform the wave buoy data into a common format for comparison with the HI-WAM model. It was also necessary to interpolate model output values between grid points to approximate the location of each wave buoy. To undertake a robust analysis of the model skill of HI-WAM for engineering design purposes, several statistical measures were determined in two distinct validation stages.

Phase 1 involved a review of all available data without any filtering to ensure that the maximum possible variability in ocean conditions was replicated. The likelihood of predictions falling within ± of one RMSE for each parameter was determined. The performance of HI-WAM as a function of measured significant wave height was also evaluated. Since the input wind fields to HI-WAM are constantly being improved by BoM, the variation in model skill over time was assessed for one representative location.

Phase 2 of the model validation was then conducted using only the most recent six months of data. This eliminated the variability of the input winds influencing the assessment of contemporary model skill. Wave directions were also filtered during this phase in accordance with methodologies presented in existing literature. Finally, comparisons were made between HI-WAM model skill and wave buoy depth and latitude.

2. LITERATURE REVIEW

2.1 Historical Background

Even the most casual of observers are able to note that a relationship exists between surface winds and the generation of water waves. Ocean waves are initially generated by random pressure fluctuations in turbulent winds, and are then reinforced in a feedback process that involves the airflow over the wavy surface. The stronger the wind and the greater the distance over which it blows, the longer and larger are the dominant waves.

Basic wind wave research was undertaken as early as the 19th century by Airy (1845) and Stokes (1847), but intensive empirical observations were not carried out until the Second World War by Sverdrup and Munk (1944a, 1944b) and Bretschneider (1952). Studies of wind-wave generation by Miles (1957) and Phillips (1957) led to the development of a theoretical framework. Insight into non-linear interactions by Hasselmann (1962) provided a more extensive appreciation of the full wind wave evolution process. By the mid 1960's, the basic processes involved in the growth of the wind wave spectrum had been recognised.

2.2 Contemporary Wave Models

The goals of wind wave research are simple: to be able to predict the wind wave field and its effect on the environment. Two basic types of mathematical models for the description of the evolution of the wind wave spectrum exist: phase averaging models and phase resolving models (not discussed in this report). At the time of writing, the two most popular phase averaging models (defined as "third generation models") available in the public domain are WAM (formerly maintained by KNMI - Royal Netherlands Meteorological Institute; now overseen by ECMWF - European Centre for Medium-Range Weather Forecasts) and Wave Watch III (maintained by NOAA – United States National Oceanic and Atmospheric Administration). It should also be noted that a third phase averaging model, SWAN (Simulating WAves Nearshore) maintained by Delft University of Technology, is commonly used to hindcast waves in deep, intermediate and finite depths for geographically small study areas.

2.3 Pertinent Examples of Contemporary Wave Model Performance

The skill of coarse gridded, deepwater applications of these two models was assessed by Hemer *et al.* (2007) around the Australian coast by comparing the predictions to measurements from 27 wave buoys. The WAM model dataset (denoted "CERA-40" -

ECMWF Re-Analysis of the global atmosphere and surface conditions for 45-years) had a Root-Mean-Square-Error (*RMSE*) for significant wave height (H_S) of 0.59 m. The Wave Watch III dataset had an *RMSE* of 0.63 m for H_S.

It is noteworthy that New Zealand's NIWA (National Institute of Water & Atmospheric Research) operate a version of WAM. Gorman and Stephens (2003) compared the NIWA WAM model outputs to the measurements from 8 wave buoy sites around New Zealand and found *RMSE* ranging from 0.27 m to 0.84 m, with a Bias towards under estimating H_S.

Typical errors for predicting H_S in the Australasian region are of the order of 0.5 m for these contemporary phase averaging wave models. The skill of these models for predicting wave period and direction was not assessed in these studies.

Wave model performance outside of Australia, but under extreme forcing wind conditions, is also of interest and was documented by Moon *et al.* (2003). A high resolution version of Wave Watch III (WWIII) was run for four days to simulate wave growth as Hurricane Bonnie (1998) approached the East Coast of the USA. The model results were compared with NASA Scanning Radar Altimeter (SRA) data in the open ocean. The *RMSE* for Significant Wave Height between the WWIII and SRA data was 0.5 m for this study.

2.4 Action Balance Equation

Global third generation wave models (such as WAM and Wave Watch III) solve the Action Balance Equation in Equation 2.1 in spherical co-ordinates for the two-dimensional action density ocean wave spectrum $F(\omega,\theta,\phi,\lambda,t)$ with respect to wave frequency (ω) and direction (θ), as a function of latitude (ϕ), longitude (λ) and time (t).

$$\frac{\partial F}{\partial t} + (\cos\phi)^{-1}\frac{\partial}{\partial\phi}(\dot{\phi}\cos\phi F) + \frac{\partial}{\partial\lambda}(\dot{\lambda}F) + \frac{\partial}{\partial\omega}(\dot{\omega}F) + \frac{\partial}{\partial\theta}(\dot{\theta}F) = S \quad \text{(Eq. 2.1)}$$

where:

$\dot{\phi}$:	component of group velocity with respect to latitude
$\dot{\lambda}$:	component of group velocity with respect to longitude
$\dot{\omega}$:	rate of change of the dispersion relation
$\dot{\theta}$:	rate of change of direction (due to great circle propagation)
S:	net source function describing the change of energy of a propagating wave group as shown in Equation 2.2

$$S = S_{in} + S_{nl} + S_{ds} + S_{bot} \qquad \text{(Eq. 2.2)}$$

where:

S_{in}:	atmospheric input from the wind
S_{nl}:	non-linear interactions between spectral components
S_{ds}:	dissipation due to "white capping"
S_{bot}:	dissipation due to interaction with the bottom

Mathematical models to solve Equation 2.1 need to have a numerical scheme to approximate the left hand side of the equation and to parameterise each of the physical processes on the right hand side which transfer energy to, from and within the spectrum.

These numerical scheme and source term parameterisation used in the WAM model will be discussed further in Section 3.

2.5 Sources of Error in Wave Model Predictions

Komen *et al.* (1994) suggested three possible sources of error in the WAM model:

1) Inadequate input wind
2) Inadequate wave model physics
3) Inadequate numerics and resolution.

Young (1999) believes that the first error source is the most important, stating that:

"the most significant source of error in deep water wave models is the driving wind. Further advances in our understanding of the physics of wave evolution will result in only marginal improvements in the prediction capability."

A 10 per cent error in the estimate of surface wind speed can lead to 10-20 per cent errors in Significant Wave Height and 20-50 per cent errors in wave energy (Komen *et al.* 1994). However, Janssen (2004) notes that rapid improvements in the quality of the input wind fields "seen in the past 5 to 10 years and ongoing" make it easier to identify and resolve wave-model errors. Despite these differences, no author would argue that a complete knowledge of the physics of wind wave generation has been grasped by modern science, particularly in finite depth regions.

2.6 Future Improvements to Model Performance

Many authors have noted that although steady increases in the accuracy of phase averaging wave models has been achieved, that continued development exhibits diminished returns; the added computational expense of more sophisticated (higher order) wave models yields only marginal improvements in performance.

Liu *et al.* (2002) argue that traditional approaches to the Action Balance Equation need to be overhauled. They state that the next generation of wave models should include wave groups and reject the premise of the stationarity of wind waves. It is speculated that:

"the traditional approach to wave modelling based on the wave energy spectrum may have reached its limit in terms of reproducing observed wave characteristics and that a whole new approach to wind wave modelling focused specifically on the wave group processes and non-stationary energy transfer might be an appropriate route for further development."

3. PHYSICS OF WAM AND NUMERICAL IMPLEMENTATION

The following discourse on the basics of WAM operation is founded on more extensive discussions by the WAMDI Group (1988), Komen *et al.* (1994), Young (1999) and Janssen and Bidlot (2003). Note that a concise historic account of the Wave Modelling Group responsible for the development of WAM is given by Komen (2004).

Solving the Action Balance Equation (Equation 2.1) requires the specification of appropriate initial and boundary conditions, the implementation of an appropriate advection scheme to represent the transport of energy within the computational domain and the specification of the forcing term, S. The manner in which the WAM model determines this solution is briefly outlined in Sections 3.1 and 3.2. Note that the following discussion relates to unmodified Cycle 2 WAM physics.

3.1 Physical Mechanisms of Wave Evolution

3.1.1 Atmospheric Input, S_{in}

The wind input source term represents the work done by the wind on the ocean surface to produce waves. The wind generation of waves takes place in the high frequency part of the spectrum; producing relatively short waves. The wind input source function for WAM, S_{in}, was adopted from physics developed by Snyder *et al.* (1981) as shown in Equation 3.1, where γ_{in} is the growth rate parameter (defined in Equation 3.2) (Bender and Leslie, 1994).

$$S_{in} = \gamma_{in} F \qquad \text{(Eq. 3.1)}$$

$$\gamma_{in} = \max\left\{0, 0.25\frac{\rho_a}{\rho_w}\left[28\frac{u_*}{c}\cos(\theta - \theta_w) - 1\right]\right\}\omega \qquad \text{(Eq. 3.2)}$$

$$u_* = \left(\frac{\tau_a}{\rho_a}\right)^{\frac{1}{2}} \qquad \text{(Eq. 3.3)}$$

where:

ρ_a:	density of air
ρ_w:	density of water
c:	phase velocity of the wave
u_*:	friction velocity (defined in Equation 3.3)
θ_w:	wind direction
τ_a:	surface wind stress

The surface wind stress is related to the wind velocity by means of a wind speed dependent drag coefficient, C_D, in Equation 3.4. C_D is defined by Wu (1982) in Equation 3.5. However, defining the drag co-efficient over the sea remains an unsolved problem. Later versions of WAM relate aerodynamic drag directly to the sea state (Janssen, 2004).

$$\frac{\tau_a}{\rho_a} = C_D(U_{10})U_{10}^{\ 2} \qquad \text{(Eq. 3.4)}$$

$$C_D = (0.8 + 0.065U_{10}) \times 10^{-3} \qquad \text{(Eq. 3.5)}$$

3.1.2 Non-Linear Quadruplet Interactions Atmospheric Input, S_{nl}

Since the wind input only produces short surface waves in the energy spectrum, another process is at work to indirectly produce long swell waves. These longer waves are the result of energy "cascades" that take energy from the short wind waves and feed the longer waves with energy. When the short wave amplitudes become large, three waves with different wavelengths may interact through mechanical resonance and create a fourth wavelength. These processes are known as Non-Linear Quadruplet Interactions and they are responsible for forming and maintaining the shape of the spectrum.

The exact form of the Non-Linear transfer expression is shown in Equation 3.6 (WAMDI Group, 1988). Note that this expression is also known as the Boltzmann equation.

$$S_{nl}(k_4) = \int \omega_4 \sigma \delta(k_1 + k_2 - k_3 - k_4) \times \delta(\omega_1 + \omega_2 - \omega_3 - \omega_4)[n_1 n_2 (n_3 + n_4) - n_3 n_4 (n_1 + n_2)]\, dk_1 k_2 k_3 \qquad \text{(Eq. 3.6)}$$

However, the evaluation of the exact form of S_{nl} requires an enormous amount of computation because a three dimensional integral needs to be evaluated. A more economical evaluation of the Non-Linear transfer was employed by Hasselmann *et al.* (1985) and included in WAM; as shown in Equation 3.7.

$$S_{nl}(k_4) = \sum_{j=1,2} A_j \omega_4 \left[n_1^j n_2^j (n_3^j + n_4^j) - n_3^j n_4^j (n_1^j + n_2^j) \right] \qquad \text{(Eq. 3.7)}$$

$$n_1^j = F_1^j \omega_1^j \qquad \text{(Eq. 3.8)}$$

where:

ω:	angular frequency
A_j:	denotes a tuned coupling coefficient
n_1^j:	denotes the action densities at the four wave components $i = 1,\ldots,4$ of each of the two (mirror-image) discrete resonant interaction quadruplets $j = 1,2$ (defined in Equation 3.8).

The parameterisation is both fast and it respects the basic properties of the Non-Linear transfer, such as conservation of momentum, energy and action, while it also produces the proper high-frequency spectrum. The Discrete Interaction Approximation (DIA) was constructed by considering only a small number of interaction configurations consisting of neighbouring and finite distance interactions. Hasselmann and Hasselmann (1981) showed that only 5-10 % of the interacting wave number quadruplets contribute 95 % of the Non-Linear transfer. However, the neglect of so many possible interactions has consequences. The DIA typically produces spectra with broader directional spreading than do models based on a full solution to S_{nl} (Young *et al.* 1987; Van Vledder, 1990).

3.1.3 White-Cap Dissipation, S_{ds}

The energy transfer from the wind to the waves results in an increase in wave amplitude. This process continues until the wave eventually becomes unstable and breaks. This form of breaking is generally termed "white-capping" in contrast to depth limited breaking, which might occur on a beach. The loss of energy from this process is called White-Cap Dissipation, S_{ds}, and is represented in WAM as Equation 3.9 (Bender and Leslie, 1994), where the dissipation rate, γ_{ds}, is a function of the spectral density (Equation 3.10).

$$S_{ds} = \gamma_{ds} F \qquad \text{(Eq. 3.9)}$$

$$\gamma_{ds} = -c\hat{\omega}\left[\frac{\hat{\alpha}}{\hat{\alpha}_{PM}}\right]^2\left[\left(\frac{\omega}{\hat{\omega}}\right)^2 + \left(\frac{\omega}{\hat{\omega}}\right)^n\right] \qquad \text{(Eq. 3.10)}$$

$$\hat{\omega} = \left[E^{-1}\iint F(f,\theta)\omega^{-1} df d\theta\right]^{-1} \qquad \text{(Eq. 3.11)}$$

$$E = \iint F(f,\theta) df d\theta \qquad \text{(Eq. 3.12)}$$

$$\hat{\alpha} = E\hat{\omega}^4 g^{-2} \qquad \text{(Eq. 3.13)}$$

$$\hat{\alpha}_{PM} = 0.66\alpha_{PM} \qquad \text{(Eq. 3.14)}$$

where:

- c: a constant equal to 2.33×10^{-5}
- $\hat{\omega}$: mean frequency defined by the inverse of the mean period (as described in Equation 3.11)
- E: total energy (surface elevation variance) (Equation 3.12)
- $\hat{\alpha}$: integral wave steepness parameter (Equation 3.13)
- $\hat{\alpha}_{PM}$: theoretical value of $\hat{\alpha}$ for a Pierson-Moskowitz spectrum, where $\alpha_{PM} = 4.57\times10^{-3}$ (Equation 3.14)

Young (1999) states that "white-cap dissipation is a process which is poorly understood. No rigorous theory exists for either the onset of white-capping or the resulting energy loss."

3.1.4 Finite Depth Processes, S_{bot}

Processes occurring due to finite depth are collectively represented by S_{bot} in Equation 3.15.

$$S_{bot} = S_{bf} + S_{brk} + S_{tri} \qquad \text{(Eq. 3.15)}$$

where:

S_{bf} : bottom friction

S_{brk} : depth limited wave breaking

S_{tri} : triad non-linear interactions

However, the WAM model only includes the first term, bottom friction, in its determination of finite depth processes and may be approximated by Equation 3.16 (Young, 1999). Consequently, depth limited wave breaking and triad non-linear interactions are not considered in this wave model. For this reason, it is of extreme interest to examine the performance of the HI-WAM model in relatively shallow water depths (say, 20 to 30 m).

$$S_{bot} \approx S_{bf} \qquad \text{(Eq. 3.16)}$$

In shallow water the orbital motions of the water particles, induced by surface waves, extend down to the sea floor. This gives rise to an interaction between the surface waves and the bottom. These interactions may include scattering on bottom irregularities, motion of a soft bottom, percolation into a porous bottom and friction in the turbulent bottom boundary layer. The last two processes, percolation and bottom friction, both dissipate energy and are parameterised in WAM with Equation 3.17 after Hasselmann *et al.* (1973). Note that percolation is usually much less important than bottom friction.

$$S_{bf} = -\frac{\Gamma}{g^2}\frac{\omega^2}{\sinh^2 kD}F \qquad \text{(Eq. 3.17)}$$

where:

$\Gamma = 0.038\ \mathrm{m^2\ s^{-3}}$ (constant)

$\omega = (gk \tanh kD)^{1/2}$ (finite depth dispersion relation for depth, D)

3.1.5 The Spectral Balance, S

In the preceding discussion, each of the source terms has been considered in isolation, however, it is the sum of the individual terms, S, which is responsible for the evolution of the wave spectrum. As the spectrum matures, the spectral peak gradually shifts to lower frequencies and the spectrum broadens. The source terms are completely balanced when $S = 0$; this state is commonly referred to as full development (Young, 1999).

3.2 Numerical Implementation

3.2.1 Implicit Integration of the Source Functions

An implicit scheme was introduced for the source function integration to enable the use of an integration time step that was greater than the dynamic adjustment time of the highest frequencies still treated prognostically in the model. The energy balance of the spectrum is evaluated in detail up to a high cut-off frequency. An implicit second order, centred difference integration scheme (whose time step is matched to the evolution of the lower frequency waves) is used in WAM and given in Equation 3.18 (without advection terms). Notice the following treatise is based on the outline given by the WAMDI Group (1988).

$$F_{n+1} = F_n + \frac{\Delta t}{2}(S_{n+1} + S_n) \qquad \text{(Eq. 3.18)}$$

where: Δt: time step
n: time level index

If S_{n+1} depends linearly on F_{n+1}, Equation 3.18 could be solved directly for the spectrum F_{n+1} at the new time step. Unfortunately, only the input source function (S_{in}) is linear, this term is described in Equation 3.19.

$$S^{in}_{n+1} = \beta_{n+1} F_{n+1} = \beta_{n+1} \Delta F + \beta_{n+1} F_n \qquad \text{(Eq. 3.19)}$$

where: $\beta_{n+1} = \beta(u_*^{n+1})$
$\Delta F = F_{n+1} - F_n$

For the remaining source functions, described in Equation 3.20, a Taylor expansion is introduced in Equation 3.21.

$$S^{rest}_{n+1} = S^{nl}_{n+1} + S^{ds}_{n+1} + S^{bot}_{n+1} \qquad \text{(Eq. 3.20)}$$

$$S^{rest}_{n+1} = S^{rest}_{n} + \frac{\partial S^{rest}_n}{\partial F} \Delta F + \cdots \qquad \text{(Eq. 3.21)}$$

The functional derivative in Equation 3.21 (numerically a discrete matrix M_n) can be divided into a diagonal matrix Λ_n and a non-diagonal residual N_n in Equation 3.22.

$$\frac{\partial S_n}{\partial F} = M_n = \Lambda_n + N_n \qquad \text{(Eq. 3.22)}$$

Substituting Equations 3.19, 3.21 and 3.22 into 3.18, yields the expression in Equation 3.23.

$$\left[1-\frac{\Delta t}{2}\{\Lambda_n + N_n + \beta_{n+1}\}\right]\Delta F = \Delta t\left[\left(\frac{\beta_n+\beta_{n+1}}{2}\right)F_n + S_n^{rest}\right] \qquad \text{(Eq. 3.23)}$$

If the non-diagonal terms are not too large, the matrix on the left-hand side can be inverted by expanding with respect to the non-diagonal contributions, yielding Equation 3.24. Note that the diagonal term is given by 3.25 and the first non-diagonal matrix in the expansion takes the form of Equation 3.26.

$$\Delta F(f,\theta) = A(f,\theta) + \sum_{f',\theta'} B(f,\theta;f',\theta')A(f',\theta') + \cdots \qquad \text{(Eq. 3.24)}$$

$$A(f,\theta) = \left\{\left[\Delta t\frac{(\beta_n+\beta_{n+1})}{2}F_n + S_n^{rest}\right]\times\left[1-\frac{\Delta t}{2}(\Lambda_n+\beta_{n+1})\right]^{-1}\right\}_{(f,\theta)} \qquad \text{(Eq. 3.25)}$$

$$B(f,\theta;f',\theta') = \frac{N_n(f,\theta;f',\theta')\frac{\Delta t}{2}}{\left\{1-\frac{\Delta t}{2}(\Lambda_n+\beta_{n+1})\right\}_{(f,\theta)}} \qquad \text{(Eq. 3.26)}$$

3.2.2 Propagation

The unmodified WAM code uses a first order upwind scheme as shown in Equation 3.27 (WAMDI Group, 1988).

$$F_j^{n+1} = F_j^n - \sum_k \frac{\Delta t}{\Delta x_k \cos\theta_j}\left[(u\cos\phi F^n)_j - (u\cos\phi F^n)_{k\_}\right] \qquad \text{(Eq. 3.27)}$$

where:

n:	time level index
$k\_$:	neighbouring grid point in the upstream propagation direction, relative to the reference grid point j
k:	index running over the three propagation directions λ, ϕ and θ
u_k:	velocity component in the relevant direction (λ, ϕ, θ)
Δx_k:	grid spacing in the relevant direction (λ, ϕ, θ)

3.2.3 Refraction

In addition to the change of wave direction due to great circle propagation ($\dot{\theta}_{gc}$), refraction due to variation in water depth ($\dot{\theta}_D$) is included in WAM in Equation 3.28.

$$\dot{\theta}_D = \frac{1}{kR}\frac{\partial \omega}{\partial D}\left(\sin\theta\frac{\partial D}{\partial \phi} - \frac{\cos\theta}{\cos\phi}\frac{\partial D}{\partial \lambda}\right) \qquad \text{(Eq. 3.28)}$$

This process (more generally described as shoaling) causes waves in deepwater which are propagating initially parallel to the coast to slow, steepen and bend towards more shallow water resulting in focusing phenomena and caustics. It affects the spectral and spatial energy distribution of the wave field without changing the overall energy budget.

Overall refraction in the model is the addition of these two processes in Equation 3.29.

$$\dot{\theta} = \dot{\theta}_{gc} + \dot{\theta}_D \qquad \text{(Eq. 3.29)}$$

It should be emphasised though, that in the final stages of shoaling in coastal areas (approaching the break point), this kinematic description of waves breaks down because of strong non-linearity (Komen *et al.* 1994).

3.2.4 Boundary Conditions and Grid Nesting

The wave model grid can be surrounded by both land and ocean points. For locations where there is a land boundary, there is no energy flux into the grid and free advection of energy out of the grid at the coastline (Young, 1999).

The generation and propagation of ocean waves covers a wide range of space and time scales. A wave model which covers all scales uniformly is not practicable because of computer limitations. The use of variable wave model grids; (i.e. high resolution near the coast and course in the open ocean) has not been followed with WAM. Instead, WAM is set up to run on nested grids.

This nesting approach gives the opportunity to use results of a coarse mesh model from a large region in a fine mesh regional model. Several successive levels of nesting may be necessary. The two-dimensional spectra computed by the coarse mesh model are saved at grid points which are on the boundary of the limited area, high-resolution grid. These spectra are then interpolated in space and time to match the high resolution at the grid boundaries (Komen *et al.* 1994).

4. SPECIFICATIONS OF THE HI-WAM MODEL

The following section outlines specific details of the HI-WAM model complementing the preceding discussion of generalised WAM application. In addition to model particulars, modifications to the original WAM code for implementation as HI-WAM are also outlined. Note that the HI-WAM model is not "operational" in the same sense as other versions of WAM at the BoM; it is executed in hindcast mode on an ad hoc basis rather than running it routinely to make forecasts.

4.1 Nesting

Two different techniques for nesting the HI-WAM domain were applied during two consecutive periods of the validation study; the first from March 1997 to February 1998 and the second approach from March 1998 to February 2008.

During the first nesting period (1997 to 1998), the HI-WAM domain was nested inside two coarser WAM models; "global" and "regional". The details of the domain and resolution of each of these three are summarised in Table 4.1.

Table 4.1
BoM WAM Model Nesting Details

Model Name	Latitude Range	Longitude Range	Spatial Resolution
Global	78° N to 78° S	180° W to 180° E	3.0°
Regional	12° N to 60° S	69° E to 180° E	1.0°
HI-WAM	7° S to 46° S	110° E to 156° E	0.1°

A "global" model with a spatial resolution of 3.0° and a domain spanning longitudes from 180°W to 180°E and latitudes ranging from 78°N to 78°S is the coarsest WAM application.

Within the global model domain, a "regional" WAM application with a moderate spatial resolution of 1.0° and a domain spanning longitudes from 69°E to 180°E (West to East) and latitudes ranging from 12°N to 60°S exists. This model spans the oceans around Australia and provides the boundary conditions for input to the high-resolution model.

Finally, within the "regional" domain, the HI-WAM model spans longitudes ranging from 110°E to 156°E (West to East) and latitudes ranging from 7°S to 46°S (North to South) as shown in Figure 4.01. HI-WAM has the highest spatial resolution of the three; 0.1°. Note that the spectral resolution is the same for both the "regional" model and HI-WAM.

During the second nesting period (1998 to 2008), a different technique was used whereby the spatial resolution of the "global" model was increased to 1.0° and the HI-WAM model was nested directly inside of it (i.e. the "regional" model was not used during this period). The latitude and longitude domains remained unchanged from the first approach for the "global" and HI-WAM models when this second technique was employed.

4.2 Scope of Model Parameters

The source terms and propagation terms are integrated every 5 minutes. In terms of the wave spectrum, the directional resolution is 15° and there are 25 frequency bins ranging from 0.0418 to 0.4114 Hz. This represents wave periods from approximately 24 to 2.5 s. Three parameters: Significant Wave Height, Mean Wave Period and Mean Wave Direction are predicted at six-hourly intervals. An example of model output is shown in Figure 4.02.

4.3 Input Wind Fields

The quality of the surface wind speed estimates generated by the BoM's Numerical Weather Prediction (NWP) systems is of critical importance to the WAM models which are dependent on the accuracy of the atmospheric forcing (S_{in}).

There are several varieties of NWP systems operated by BoM, but the Meso-LAPS (Limited Area Prediction System) model forces the HI-WAM model. Meso-LAPS has a resolution of 0.125° and a domain spanning longitudes from 95°E to 169.875°E and latitudes ranging from 4.875°N to 55°S. The system employs a data assimilation scheme using observational sources including conventional (surface synoptic, ship, synthetic and radiosonde), automatic (buoy and land based), satellite (radiances, retrieved profiles and cloud drift winds) and aircraft.

Schulz *et al.* (2007) compared the predictions from Meso-LAPS to scatterometer wind data from the QuikSCAT satellite (which were not used in the data assimilation scheme at that time) over a two year period from 2003 to 2004. Meso-LAPS tended to underestimate marine near-surface winds, with a bias of -0.4 ms^{-1}. Note that the Meso-LAPS model cannot resolve the effects of local processes such as sea breezes.

An operational verification suite exists at the BoM which provides estimates of the performance of the NWP marine surface wind analysis and forecasts. This suite has shown

that *Bias* and *RMSE* in wind speed are constantly reducing over time. These improvements should result in more accurate wave predictions by HI-WAM over the same time period.

Note too that the input wind fields for the coarser nesting WAM models are different; the global WAM model is forced by the BoM's Global Assimilation and Prediction System (GASP) and the regional WAM model is forced by a system called LAPS-375.

4.4 Bathymetry

The bathymetric data for defining the water depths in HI-WAM originated from two sources (Porter-Smith *et al.* 2004).

The great majority of the bathymetry data was taken from a high-resolution ($1/120^{th}$ °) survey of the Australian continental shelf undertaken by Geoscience Australia (formerly the Australian Geological Survey Organisation - AGSO) (Buchanan, Unpublished Manuscript). The AGSO dataset spans most of the HI-WAM domain, with longitudes ranging from 110°E to 156°E (West to East) and latitudes ranging from 9°S to 45°S (North to South).

The small remainder of area in the model not covered by the AGSO survey was supplemented with data from the ETOPO5 bathymetric dataset (United States National Geophysical Data Center, 1998). The ETOPO5 bathymetry has a resolution of $1/12^{th}$ °.

The bathymetric model to be coupled with HI-WAM was constructed from both datasets (AGSO and ETOPO5) by interpolating to a grid spacing of $1/12^{th}$ ° (approximately 0.01°).

4.5 Modifications to WAM Code for HI-WAM Development

The version of WAM code used as the "foundation" for HI-WAM is physics Cycle 2. Note that the most recent official version of WAM physics is Cycle 4.5 (released September 2006).

However, some changes were made to the WAM software code for HI-WAM application (Bender and Leslie, 1994 and Bender, 1996). Numerous validations of the wind input physics for WAM Cycle 2 by the wave modelling community had shown a consistent under prediction of wave heights in the Southern Hemisphere.

Bender and Leslie showed that WAM Cycle 2 could be improved by simply upgrading the propagation numerics. The first order upwinding scheme (outlined in Section 3.2.2) is

highly diffusive and leads to excessive numerical dissipation of swell that travels long distances (experienced along much of the Australian coast). A change to the third-order upwinding scheme remedied this deficiency and improved wave parameter predictions.

In order to maintain numerical stability for the third order upwinding scheme, the iterative time integration scheme of Miller and Pearce (1974) which alternates between forward and backward time differencing was used. When the model with upgraded numerics was re-tuned, the optimal White-Cap Dissipation constant (c) in Equation 3.10 was found to be 2.95×10^{-5} in contrast to the specified value of 2.33×10^{-5}.

Note that the modified WAM Cycle 2 physics are executed at BoM from within the software layout of WAM Cycle 4 to take advantage of nesting capabilities.

Note too that the rotated wave spectrum discretisation outlined by Greenslade (2000) was implemented in the HI-WAM model from March 1998 to February 2008. This spectral rotation eliminates the possibility of wave energy propagating directly along east-west and north-south coordinate axes, which can result in elongated north-south patterns of Significant Wave Height due to excessive shadowing of wave energy by islands.

5. WAVE MEASUREMENT RECORDS FOR MODEL VALIDATION

5.1 Overview

In order to validate the performance of the HI-WAM model (i.e. to quantify how well it models wave height, period and direction), ocean measurements are required to make comparisons with the modelled values. Wave buoys are the most common instrument for making these recordings of the "real" ocean surface and are deployed around Australia. These units are typically administered by state governments, port authorities or the BoM.

In total, 18 different wave buoy records were sourced from around the Australian coastline (Figure 5.01). Each of these sites was carefully chosen with the following criteria in mind:

- Measured records within the HI-WAM model domain (spatial and temporal)
- Selecting "directional" wave buoys, where possible
- Ensuring the wave buoys were deployed in a variety of water depths (15 to 100 m)
- Maximising the range of latitudes where wave buoys were located (19° S to 42° S)
- Having a spatial coverage to represent the Australian wave climate, where possible.

A summary of the observation details for each wave buoy site is provided in Table 5.1. This table includes the location (latitude and longitude), water depth, time step (elapsed time between measurements), time zone, record duration (start and end dates) and wave parameters measured (height, period and direction) by each buoy. A detailed discussion of further particulars for each of the wave buoys is provided in Sections 5.2 through 5.9.

It should be noted that there are important differences in wave parameter definition between the wave buoy administrators. All sites except for those in Western Australia measure mean wave period in terms of T_Z. Cottesloe, Rottnest Island and Exmouth record mean wave period in terms of T_1. These differences in definition for wave period are later addressed in Section 6.5. In addition to these differences, for directional wave buoy sites not operated by Melbourne Ports (Datawell buoys), wave direction is measured as the direction corresponding to the peak spectral wave period (Peak Direction). However, for Point Nepean and Point Lonsdale (Triaxys buoys), wave direction is measured as the weighted average of all directions in the spectrum (Mean Direction). These differences in definition for wave direction are later addressed in Section 6.6.

All wave buoy records have been provided for this study subject to data consent conditions. Where available, copies of these conditions have been reproduced in Appendix A.

Table 5.1
Wave Buoy Observations Details: Deployment Location, Duration and Available Parameters

Buoy #	Location	Latitude	Longitude	Depth (m)	Time Step (mins)	Time Zone (hrs GMT)	Start Date	End Date	Parameters
1	Townsville &	19° 09.487' S	147° 03.793'E	15	30*	+10	01/03/1997	27/09/2004	H_S, T_Z, *Drn* (Peak)~
2	Mackay &	21° 02.389' S	149° 32.795' E	29	30*	+10	01/03/1997	01/03/2008	H_S, T_Z, *Drn* (Peak)
3	Mooloolaba	26° 33.945' S	153° 10.888' E	33	30	+10	01/09/2007	29/02/2008	H_S, T_Z, *Drn* (Peak)
4	Brisbane	27° 29.767' S	153° 37.762' E	79	30	+10	01/09/2007	29/02/2008	H_S, T_Z, *Drn* (Peak)
5	Gold Coast	27° 57.930' S	153° 26.530' E	18	30	+10	03/09/2007	29/02/2008	H_S, T_Z, *Drn* (Peak)
6	Tweed River	28° 10.766' S	153° 34.592' E	23	30	+10	01/09/2007	29/02/2008	H_S, T_Z, *Drn* (Peak)
7	Byron Bay &	28° 49.600' S	153° 39.800' E	68	60	+10	26/10/1999	01/03/2008	H_S, T_Z, *Drn* (Peak)
8	Sydney &	33° 46.517' S	151° 25.067' E	85	60	+10	17/04/1997	01/03/2008	H_S, T_Z, *Drn* (Peak)
9	Batemans Bay &	35° 42.433' S	150° 20.917' E	73	60	+10	23/02/2001	29/02/2008	H_S, T_Z, *Drn* (Peak)
10	Lakes Entrance	37° 54.600' S	147° 58.800' E	23	30	+10	23/08/2007	11/02/2008	H_S, T_Z, *Drn* (Peak)
11	Kingfish B	38° 35.982' S	148° 11.334' E	78	60	+10	10/12/1998	07/10/1999	H_S
12	Point Nepean	38° 21.643' S	144° 41.639' E	26	30	+10	13/01/2003	28/02/2008	H_S, T_Z, *Drn* (Mean)
13	Point Lonsdale	38° 18.242' S	144° 34.235' E	27	30*	+10	31/12/2000	30/08/2003	H_S, T_Z, *Drn* (Mean)
14	Cape Sorell	42° 07.200' S	145° 01.800' E	100	30#	+10	07/01/1998	01/03/2008	H_S, T_Z
15	Cape du Couedic	36° 04.200' S	136° 37.200' E	80	30^	+9.5	29/11/2000	11/12/2007	H_S, T_Z
16	Cottesloe	31° 59.667' S	115° 41.200' E	15	60	+8	03/09/1999	01/03/2008	H_S, T_1, *Drn* (Peak)~
17	Rottnest Island	32° 05.650' S	115° 24.467' E	48	30*	+8	15/09/2004	29/02/2008	H_S, T_1, *Drn* (Peak)
18	Exmouth	21° 41.967' S	114° 05.917' E	54	30	+8	03/10/2006	29/02/2008	H_S, T_1, *Drn* (Peak)

& the position and depth of this buoy was variable, refer to detailed text for full location history.
* an earlier (minor) part of this record had a time step of 60 minutes, rather than 30 minutes.
# an earlier (minor) part of this record had a time step of 20 minutes, rather than 30 minutes.
^ an earlier (minor) part of this record had a time step of 15 minutes, rather than 30 minutes.
~ this wave buoy was "directional" for only part of the study duration (i.e. it simply recorded H_S, T_Z for an earlier part of this record).

5.2 Department of Environment and Resource Management (Queensland)

Six wave buoys operated by the Queensland Department of Environment and Resource Management (DERM) have been referred to in this study; Townsville, Mackay, Mooloolaba, Brisbane, Gold Coast and Tweed River. Each of these wave boys measures H_S, T_Z and Peak Wave Direction via Datawell Directional Waverider Buoys.

The location of the Townsville wave buoy is illustrated in Figure 5.02 (with the 0.1 ° HI-WAM model grid overlain on the image); the buoy is exposed to swell attack in an approximate window clockwise from the North around to the East. However, as shown in Figure 5.02, the buoy is located leeward of the Great Barrier Reef. Incident swell is broken, attenuated and refracted by this morphology, effectively protecting the site from the full energy at sea. Observed data is available for the period 1 March, 1997 through to 27 September, 2004. Note that directional data is only available from 12 December, 2000 onwards. The location of the Townsville wave buoy was variable; its spatial history is shown in Table 5.2. When comparing HI-WAM model skill against water depth in Section 7.6.1, a weighted average depth of 15 m was assumed for the Townsville wave buoy.

Table 5.2
Townsville Waverider Buoy: Location History

Deployment Location	Latitude	Longitude	Depth (m)	Start Date	End Date
1	19° 09.470'S	147° 03.770'E	22.0	01/03/1999	03/06/1997
2	19° 09.420'S	147° 03.110'E	16.2	03/06/1997	09/07/1998
3	19° 09.440'S	147° 03.240'E	15.1	09/07/1998	02/09/1999
4	19° 09.470'S	147° 03.750'E	14.4	02/09/1999	07/08/2001
5	19° 09.470'S	147° 03.770'E	15.1	07/08/2001	15/10/2002
6	19° 09.370'S	147° 03.803'E	16.3	15/10/2002	20/05/2003
7	19° 09.487'S	147° 03.793'E	15.5	20/05/2003	27/09/2004

The location of the Mackay wave buoy is illustrated in Figure 5.03; the buoy is exposed to swell attack in an approximate window clockwise from the North around to the South. However, as shown in Figure 5.03, the buoy is again located leeward of the Great Barrier Reef. Observed data is available for the period 1 March, 1997 through to 1 March, 2008. It should be noted that a significant data gap exists for this site between 31 July 1997 and 13 February 2002. The location of the Mackay wave buoy was variable; its spatial history is shown in Table 5.3. When comparing HI-WAM model skill against water depth in Section 7.6.1, a weighted average depth of 29 m was assumed for the Mackay wave buoy.

Table 5.3
Mackay Waverider Buoy: Location History

Deployment Location	Latitude	Longitude	Depth (m)	Start Date	End Date
1	21° 02.620' S	149° 32.220' E	27.0	01/03/1997	31/07/1997
2	21° 02.495' S	149° 32.806' E	26.0	13/02/2002	16/07/2002
3	21° 02.593' S	149° 32.875' E	31.0	16/07/2002	10/02/2004
4	21° 02.492' S	149° 32.891' E	29.0	10/02/2004	29/08/2005
5	21° 02.507' S	149° 32.840' E	29.0	29/08/2005	24/05/2006
6	21° 02.424' S	149° 32.782' E	29.0	24/05/2006	29/03/2007
7	21° 02.389' S	149° 32.795' E	29.0	29/03/2007	01/03/2008

The locations of the Mooloolaba (33 m depth) and Brisbane (79 m depth) wave buoys are illustrated in Figure 5.04. The buoys are exposed to swell attack in an approximate window clockwise from the North around to the South. However, the Mooloolaba buoy is offered some protection to the South by Fraser Island. Observed data is available for the period 1 September, 2007 through to 29 February, 2008.

The locations of the Gold Coast (18 m depth) and Tweed River (23 m depth) wave buoys are illustrated in Figure 5.05. Again, the buoys are exposed to swell attack in an approximate window clockwise from the North around to the South. However, the Gold Coast buoy is offered some protection to the South by Point Danger. Observed data is available for the period 1 September, 2007 (Tweed River) and 3 September, 2007 (Gold Coast) through to 29 February, 2008.

5.3 Department of Environment, Climate Change and Water and the Department of Services, Technology and Administration: Manly Hydraulics Laboratory (New South Wales)

Manly Hydraulics Laboratory (NSW DSTA) operates three directional wave buoys on the New South Wales coast which have each been referred to in this study; Byron Bay, Sydney and Batemans Bay. Each of these wave boys measures H_S, T_Z and Peak Wave Direction via Datawell Directional Waverider Buoys.

The location of the Byron Bay wave buoy is illustrated in Figure 5.05; the buoy is exposed to swell attack in an approximate window clockwise from the North around to the South. Observed data is available for the period 26 October, 1999 through to 1 March, 2008. The location of the Byron Bay wave buoy was variable; its spatial history is shown in Table 5.4.

When comparing HI-WAM model skill against water depth in Section 7.6.1, a weighted average depth of 68 m was assumed for the Byron Bay Waverider Buoy.

Table 5.4
Byron Bay Waverider Buoy: Location History

Deployment Location	Latitude	Longitude	Depth (m)	Start Date	End Date
1	28° 43.533' S	153° 44.592' E	72	26/10/1999	28/11/2000
2	28° 50.150' S	153° 43.717' E	71	29/11/2000	23/01/2001
3	28° 49.233' S	153° 43.633' E	71	10/02/2001	29/08/2003
4	28° 49.733' S	153° 43.133' E	71	29/08/2003	12/08/2004
5	28° 50.033' S	153° 43.400' E	71	12/08/2004	01/01/2005
6	28° 49.600' S	153° 39.800' E	62	04/02/2005	01/03/2008

The location of the Sydney wave buoy is illustrated in Figure 5.06; the buoy is exposed to swell attack in an approximate window clockwise from the North-North-East around to the South-South-West. Observed data is available for the period 17 April, 1999 through to 1 March, 2008. It is the longest measured data set for a site exposed to full ocean swell. The location of the Sydney wave buoy was also variable; its spatial history is shown in Table 5.5. When comparing HI-WAM model skill against water depth in Section 7.6.1, a weighted average depth of 85 m was assumed for the Sydney Waverider Buoy.

Table 5.5
Sydney Waverider Buoy: Location History

Deployment Location	Latitude	Longitude	Depth (m)	Start Date	End Date
1	33° 46.183' S	151° 25.300' E	87	17/04/1997	11/02/1998
2	33° 46.517' S	151° 25.650' E	87	11/02/1998	01/10/1998
3	33° 46.483' S	151° 25.117' E	85	01/10/1998	07/02/1999
4	33° 46.883' S	151° 25.150' E	85	26/03/1999	23/11/1999
5	33° 46.950' S	151° 25.283' E	85	23/11/1999	20/07/2001
6	33° 46.900' S	151° 25.483' E	85	11/09/2001	18/05/2004
7	33° 46.750' S	151° 25.250' E	85	18/05/2004	15/01/2005
8	33° 46.517' S	151° 25.067' E	85	15/02/2005	01/03/2008

The location of the Batemans Bay wave buoy (73 m depth) is illustrated in Figure 5.07; the buoy is exposed to swell attack in an approximate window clockwise from the North-North-East around to the South-South-West. Observed data is available for the

period 23 February, 2001 through to 29 February, 2008. The location of the Batemans Bay wave buoy was again variable; its spatial history is shown in Table 5.6.

Table 5.6
Batemans Bay Waverider Buoy: Location History

Deployment Location	Latitude	Longitude	Depth (m)	Start Date	End Date
1	35° 42.400' S	150° 20.683' E	73	23/02/2001	30/07/2004
2	35° 42.433' S	150° 20.917' E	73	30/07/2004	29/02/2008

5.4 Department of Sustainability and Environment: Gippsland Ports (Victoria)

Gippsland Ports (within the Victorian State Government Department of Sustainability and Environment) administers a Datawell Directional Waverider Buoy offshore from Lakes Entrance on the South-Eastern Victorian coast. Its location is illustrated in Figure 5.08; the buoy is exposed to swell wave attack in an approximate window clockwise from the East around to the South-West. As detailed in Table 5.1, the buoy is located in 23 metres of water depth. Observed data is available for H_S, T_Z and Peak Wave Direction for the period 23 August, 2007 through to 11 February, 2009.

5.5 Esso Australia (Victoria)

Esso Australia operates an oil rig called "Kingfish B" in the Eastern Bass Strait (offshore of the South-Eastern Victorian coast). The platform gathers wave information, not with a wave buoy, but with an instrument submerged approximately 10 m below Mean Sea Level. This instrument is called a SeaData 624XP Directional Wave, Tide and Current Meter. Its location is illustrated in Figure 5.08; due to its offshore position, the platform is exposed to swell wave attack from all directions. As detailed in Table 5.1, the platform is located in 78 metres of water depth. Observed data is available for H_S for the period 10 December 1998 through to 7 October, 1999. Data for wave direction was available, however, upon review of the data (and detailed correspondence with the instrument administrator), the directional data was determined to be of a poor quality and was not used. Data was also available for T_P, but not for T_Z; no attempt was made to convert the T_P values to T_Z to maintain consistency with the other data sets.

5.6 Port of Melbourne Corporation (Victoria)

Two wave buoys operated by the Port of Melbourne Corporation (Victoria) have been referred to in this study; Point Nepean and Lonsdale. Note that the Point Nepean buoy is identified internally by the port as "Portsea Buoy C". Each of these wave boys measures H_S, T_Z and Mean Wave Direction via Triaxys Directional Waverider Buoys.

The locations of the Point Nepean (26 m depth) and Point Lonsdale (27 m depth) wave buoys are illustrated in Figure 5.09. The buoys are exposed to swell attack in an approximate window clockwise from the South-East around to the South-West. Observed data for Point Nepean is available for the period 13 January, 2003 through to 28 February, 2008. Data for Point Lonsdale is available for the period 31 December, 2000 through to 30 August, 2003.

5.7 Australian Government: Bureau of Meteorology (Tasmania & South Australia)

The Australian Bureau of Meteorology operates two non-directional wave buoys which have both been referred to in this study; Cape Sorell (Tasmania) and Cape du Couedic (South Australia). Each of these wave boys measures H_S and T_Z via Datawell non-directional Waverider Buoys. Note that although neither of these wave buoys measure wave direction, they have been included to increase the spatial coverage of Australia.

The location of the Cape Sorell wave buoy (100 m depth) is illustrated in Figure 5.10; the buoy is exposed to swell attack in an approximate window clockwise from the South-South-East around to the North-North-West. This location has the highest wave energy of all validation sites. Observed data is available for the period 7 January, 1998 through to 1 March, 2008.

The location of the Cape du Couedic wave buoy (80 m depth) is illustrated in Figure 5.11; the buoy is exposed to swell attack in an approximate window clockwise from the South-East around to the West. Observed data is available for the period 29 November, 2000 through to 11 December, 2007.

5.8 Fremantle Ports (Western Australia)

One of the wave buoys operated by Fremantle Ports (WA), Cottesloe, has been referred to in this study. Note that the Cottesloe buoy is identified internally by the port as "Outer Harbour, Deep Channel". This wave buoy measures H_S, T_1 and Peak Wave Direction via a Datawell Directional Waverider Buoy. The location of the Cottesloe wave buoy

(15 m depth) is illustrated in Figure 5.12; the buoy is exposed to swell attack in an approximate window clockwise from the South around to the North-North-West. However, the Cottesloe buoy is offered significant protection to the West by Rottnest Island. Observed data is available for the period 3 September, 1999 through to 1 March, 2008. Note that directional data is only available from 11 February, 2008 onwards.

5.9 Department of Transport (Western Australia)

Two of the wave buoys operated by the Department of Transport (WA), Rottnest Island and Exmouth, have been referred to in this study. These wave boys measures H_S, T_1 and Peak Wave Direction via Datawell Directional Waverider Buoys.

The location of the Rottnest Island wave buoy (48 m depth) is illustrated in Figure 5.12; the buoy is exposed to swell attack in an approximate window clockwise from the South-South-East around to the North. Observed data is available for the period 15 September, 2004 through to 29 February, 2008.

The location of the Exmouth wave buoy (54 m depth) is illustrated in Figure 5.13; the buoy is exposed to swell attack in an approximate window clockwise from the South-East around to the North-East. Observed data is available for the period 3 October, 2006 through to 29 February, 2008.

5.10 Comment on Wave Buoy Accuracy

Verification of the HI-WAM model is to be performed by comparison with observations obtained from each of the in situ wave buoys detailed in the preceding discussion. In effect, the wave buoy observations are used to "ground truth" the HI-WAM model output, which implies that the errors and uncertainties associated with the observations are significantly smaller than those associated with the modelled waves.

However, it has been documented that wave buoys do not necessarily have insignificant errors when measuring wave climate. Bettington and Wilkinson (1997) noted that when wave heights exceed three metres, the significant wave height may be consistently under estimated. The authors suggested that this may be due to the accelerometer buoys becoming submerged at the crests of the higher waves due to drag on the mooring line. These systematic errors in the prediction of the wave crest elevation by accelerometer buoys may under estimate the heights of storm waves by 8 per cent. **No attempt has been made to correct wave buoy records used in validation to alleviate this phenomenon.**

6. DATA PREPARATION: MODELLED AND OBSERVED RECORDS

To undertake a robust analysis of the model skill of HI-WAM for engineering design purposes, a series of preparatory operations were carried out on the records from the model and each wave buoy. Since the wave buoy records are administered by many different organisations, the data was not in a common format and definitions for wave statistics were not consistent. Consequently, several adjustments were required to transform the wave buoy data into a common format for comparison with the HI-WAM model. It was also necessary to make several assumptions about each parameter which are detailed in the following sections.

6.1 Time

The HI-WAM model fields are at six-hourly intervals, such that there are four records at each grid point for wave height, period and direction per day. The model source terms and propagation terms are integrated every 5 minutes. The model outputs are in Greenwich Mean Time (GMT). For example, the daily time-steps for 01 January, 2008, are as follows:

1) 00:00 GMT on 01 January, 2008
   (midnight between 31 December, 2007 and 01 January, 2008)
2) 06:00 GMT on 01 January, 2008
3) 12:00 GMT on 01 January, 2008
4) 18:00 GMT on 01 January, 2008.

Note that GMT was replaced by Coordinated Universal Time (UTC) in all Australian states from 01 September 2005; although the fractional second difference between UTC and GMT is inconsequentially small for engineering purposes.

The available model records are from 06:00 GMT 01 March, 1997 to 00:00 GMT 01 March, 2008 (11 years duration). Note that when a leap year occurred, an additional day (29 February) was included in the model.

Wave buoy records in different time zones around Australia were each adjusted to GMT to synchronise the modelled and observed data. Note too that none of the wave buoys referred to daylight saving time in states where this is observed during the year (NSW, Victoria, Tasmania and South Australia); all buoy records were logged with the standard time for the relevant local time zone. As such, it was not necessary to change the time offset between modelled and observed data throughout each year.

6.2 Spatial Location

The high resolution HI-WAM model grid has a spatial resolution of 0.1° in the Geocentric Datum of Australia 1994 (GDA94) coordinate system. As noted previously, HI-WAM spans longitudes ranging from 110°E to 156°E (West to East) and latitudes ranging from 7°S to 46°S (North to South). This is a matrix with 461 × 391 points. Grid cells have a width of between 7.33 and 11.05 km (the distance between 0.1° of longitude) and a height of 11.13 km (the distance between 0.1° of latitude). Where grid points lie over land (including islands), rather than the ocean, no model output is returned.

Wave buoys were not co-located exactly with model grid points. Consequently, to ensure that the most accurate model output values were compared with the wave buoy data, the four model grid points surrounding each wave buoy were extracted to interpolate values for wave height, period and direction at the location of the wave buoy. Three different techniques for interpolation were used depending on the occurrence of land in the grid cell containing the wave buoy as shown in Figure 6.01. Note that there were always three or four "ocean" grid points available at each wave buoy site; it never occurred that only one or two points were on hand.

6.2.1 Interpolation with Four "Ocean" Grid Points

For the majority of wave buoy locations, four "ocean" grid points were available for interpolation. At these locations, the technique proposed by Cook *et al.* (1989) was used to weight the value of each grid point based on the inverse of the area between it and the wave buoy location.

6.2.2 Interpolation with Three "Ocean" Grid Points (Wave Buoy inside Triangle)

Where one of the grid points surrounding a wave buoy location was co-incident with land, only three grid points were available for interpolation. A triangle could then be drawn between the three available grid points. If the wave buoy location fell within this triangle, another interpolation technique set out by Cook *et al.* (1989) for triangles was used.

This interpolation technique was used for two buoy locations: Cape du Couedic (SA) and Rottnest Island (WA).

6.2.3 Simplification with Three "Ocean" Grid Points (Wave Buoy outside Triangle)

Further to Section 6.2.2, if the wave buoy location fell outside of the triangle, interpolation was not possible and extrapolation was considered precarious due to shoaling and friction processes. A simplification was made for these occurrences and the model values from the closest grid point were assumed for comparison with the wave buoy record.

This simplification was necessary for six buoy locations: Mooloolaba (Qld), Gold Coast (Qld), Tweed River (Qld), Byron Bay (NSW), Batemans Bay (NSW) and Lakes Entrance (Victoria).

6.3 Temporal Data Smoothing

Wave buoy records from around Australia typically had a time step of 30 or 60 minutes; this is a much higher frequency than the HI-WAM model. If only the wave buoy values co-incident with the HI-WAM model time steps are compared, some information may be lost (such as peak values, etc). Temporal data smoothing was used to average the wave buoy data so the temporal scales of variability were the same in the HI-WAM model as with the buoy observations.

Since the HI-WAM model output values are representative of some time period either side of each model time step, the wave buoy records were averaged for a two-hour "window" centred about each model time step. That is, an average was taken of all wave buoy values (height, period and direction) from one hour prior to the model step to one hour after. An example of this process, for wave height only, is shown below for Point Nepean (Victoria) in Table 6.1. Clearly, the buoy records for H_S for five time steps are more "noisy" than the single HI-WAM model value over the same two-hour period.

Table 6.1
Example of Temporal Data Smoothing for Point Nepean Wave Buoy (H_S Only)

Time/Date (GMT)	Wave Buoy H_S (m)	Model H_S (m)
17:00 02 February, 2005	5.73	4.79
17:30 02 February, 2005	5.48	
18:00 02 February, 2005	5.65	
18:30 02 February, 2005	6.27	
19:00 02 February, 2005	5.52	
Average (18:00 02 February, 2005)	5.73 ± 0.54	4.79

This approach attempts to manage the sampling problem that exists when comparing model output values with wave buoy records.

6.4 Significant Wave Height

The HI-WAM model output for height is called "Significant Wave Height", H_S, and is defined in the frequency domain in Equation 6.1 (USACE-CEM, 2006):

$$H_s = 4\sqrt{m_0} \qquad \text{(Eq. 6.1)}$$

where m_n is the nth order spectral moment, given by:

$$m_n = \int_0^\infty f^n S(f) df \qquad n = 0, 1, 2, \ldots$$

and $S(f)$ is the spectral density at frequency f. Note that m_0 is the total variance (energy) of the wave system.

The wave buoys each measured "Significant Wave Height" which is defined in the time domain as the average of the highest one-third of the wave heights calculated with an (up or down) zero-crossing analysis as Equation 6.2 (USACE-CEM, 2006):

$$H_S = H_{1/3} = \frac{1}{\frac{N}{3}} \sum_{i=1}^{N/3} H_i \qquad \text{(Eq. 6.2)}$$

where N is the number of individual wave heights H_i in a record ranked highest to lowest.

For a wave system whose spectrum contains only a narrow band of frequencies, $H_{1/3} = 4\sqrt{m_0}$, however, Tucker (1991) has noted that for more typical sea states, $0.9 \times (4\sqrt{m_0}) < H_{1/3} < 4\sqrt{m_0}$.

For this study, no adjustment has been made for the two definitions for Significant Wave Height (modelled in the frequency domain, observed in the time domain) and the values from each have been directly compared.

6.5 Mean Wave Period

The HI-WAM model output for period is called "Mean Wave Period", T_1, and is defined as the inverse of mean frequency of the spectrum (f_{mean}, Hz), shown in Equation 6.3:

$$f_{mean} = \frac{\int\int E df d\theta}{\int\int \frac{E}{f} df d\theta} \qquad \text{(Eq. 6.3)}$$

T_1 may also be expressed in terms of spectral moments in Equation 6.4:

$$T_1 = \frac{m_0}{m_1} \qquad \text{(Eq. 6.4)}$$

Three wave buoys; Exmouth, Cottesloe and Rottnest Island record T_1 and were easily comparable to the model output without any adjustments.

However, the majority of the wave buoys did not measure T_1 (in the frequency domain) but instead measured a different definition for Mean Wave Period, T_Z; the Zero Crossing Period (in the time domain). T_z is defined as the average of all wave periods calculated with an (up or down) zero-crossing analysis in Equation 6.5 (USACE-CEM, 2006):

$$T_z = \frac{T_r}{N_z} \qquad \text{(Eq. 6.5)}$$

where T_r is the total wave record length and N_z is the number of zero-crossings in the wave record.

For Gaussian stochastic processes, T_z is approximated in the frequency domain as Equation 6.6 (Longuet-Higgins, 1962 and USACE-CEM, 2006):

$$T_z = \sqrt{\frac{m_0}{m_2}} \qquad \text{(Eq. 6.6)}$$

As such, there is a difference between the modelled and observed definitions for period which requires adjustment.

Carter (1982) demonstrated that if the input parameters for a JONSWAP spectrum (JOint North Sea WAve Project – a field campaign undertaken to develop an understanding of the evolution of the wave spectrum) are assumed as the mean values of the experiment (that is, γ = 3.3, α_a = 0.07 and α_b = 0.09), the relationship between T_1 and T_z may be best estimated via Equation 6.7:

$$T_1 = 1.073 \times T_z \qquad \text{(Eq. 6.7)}$$

Accordingly, for all wave buoys which did not record T_1, each value for T_z was multiplied by a factor of 1.073 before being compared with the modelled results from HI-WAM.

Note that for engineering purposes, the peak spectral period, T_p, is generally used. However, the high resolution version of the HI-WAM model was originally constructed for the purposes of scientific examination of sediment mobility on the Australian continental shelf (Porter-Smith *et al.* 2004), and hence T_1 was the preferred wave period statistic. Carter (1982) also determined a best-fit relationship between T_p and T_1 may be expressed in Equation 6.8:

$$T_p = 1.199 \times T_1 \qquad \text{(Eq. 6.8)}$$

No effort was made to convert model or buoy wave period values to T_p. This relationship has been provided for the interest of the reader; all processed wave period values corresponded to T_1.

6.6 Wave Direction

The HI-WAM model output for direction is called "Mean Wave Direction" and is defined as the energy-weighted average direction of all spectral components. It is given in oceanographic co-ordinates (i.e. it is the direction waves are propagating towards) and is measured in degrees clockwise from True North. As this is a coastal engineering study, to compare the model with the wave buoy data, the model wave directions were adjusted by 180° (i.e. the direction waves are propagating from).

As noted in Section 5.1, all directional wave buoys (except for Point Nepean and Point Lonsdale) measure the "Peak Wave Direction" which is defined as the average direction from which waves corresponding to the peak spectral energy, T_P, are coming from. As such, there is a difference between the modelled and observed definitions for direction which requires careful review.

Both definitions for wave direction, Mean and Peak, involve the use of first order Fourier coefficients. However, Peak Wave Direction only retains the directional information for that frequency corresponding to T_P. Mean Wave Direction considers all frequency components; the average direction for each frequency band is determined and then an overall mean direction is calculated by an energy-weighted mean for each frequency band in the spectrum. The equations for determining these values from a wave buoy record are shown in Appendix B.

While the two wave direction definitions are generally of a similar magnitude, analysis of data from the Point Nepean wave buoy (where both wave direction parameters were extracted) indicates that considerable non-linear variations do occur between the two. The typical difference (RMSE) between the definitions was 12°. The full extent of this analysis of recorded Mean and Peak Wave Directions is also discussed in Appendix B.

Due to these observed differences in wave direction definitions at one representative site, the assessment of model skill for Mean Wave Direction at sites measuring Peak Wave Direction should only be considered as illustrative and preliminary.

However, since HI-WAM and the directional wave buoys at Point Nepean and Point Lonsdale both use the same definition for wave direction, the model performance at these locations may be evaluated with confidence.

Note that most wave buoys measured direction in degrees clockwise from True North. However, eight wave buoy locations measured wave direction in degrees clockwise from Magnetic North. These were converted to degrees from True North by the addition of the appropriate local magnetic declination as defined in Table 6.2.

Table 6.2
Local Declinations for Wave Buoys Measuring Direction from Magnetic North

Buoy #	Location	Magnetic Declination
1	Townsville	+ 7.810°
2	Mackay	+ 8.810°
4	Brisbane	+ 11.200°
12	Point Nepean	+ 11.700°
13	Point Lonsdale	+ 11.700°
16	Cottesloe	- 1.587°
17	Rottnest Island	- 1.759°
18	Exmouth	+ 0.865°

Note too that most wave buoys measured direction across all frequencies in the spectra. However, two wave buoys; Exmouth and Rottnest Island recorded two Peak Wave

Directions: one for frequencies up to 0.125 Hz (longer than 8 s – "swell") and another for frequencies greater than 0.125 Hz (less than 8 s – "sea"). For these wave buoys, T_P was known for "swell", "sea" and the full spectrum at each time step. The T_P for the full spectrum was compared with the T_P for "swell" and "sea" to select which component represented the energy peak of the full spectrum. The Peak Wave Direction for this component ("sea" or "swell") was then assumed as that for the full spectrum. An example of this process for wave direction is shown for Exmouth (WA) in Table 6.3. Notice that T_P was only used for the purposes of determining the true Peak Wave Direction and was not included in any direct analysis of model skill for predicting wave period.

Table 6.3
Example of the Selection of Peak Wave Direction for Exmouth Wave Buoy

Time/Date (GMT)	"Swell" (> 8s)		"Sea" (< 8s)		Total	Dominant Component	Selected Full Spectrum *Drn°*
	T_P (s)	*Drn°*	T_P (s)	*Drn°*	T_P (s)		
07:00 08 October, 2006	13.33	260	5.88	228	5.88	Sea	228
07:30 08 October, 2006	12.50	256	5.56	231	12.50	Swell	256
08:00 08 October, 2006	13.33	260	5.56	229	13.33	Swell	260
08:30 08 October, 2006	11.76	248	5.26	228	5.26	Sea	228
09:00 08 October, 2006	13.33	264	5.56	225	13.33	Swell	264
09:30 08 October, 2006	13.33	253	5.56	226	5.56	Sea	226

Finally, when interpolating between grid points for Mean Wave Direction from the HI-WAM model outputs, a simple averaging technique was not used, as this could generate misleading results. Instead, each direction value was converted to radians and broken into two components: east-west and north-south. These components were multiplied by the inverse weighting components for interpolation discussed in Sections 6.2.1 and 6.2.2, summed together, then re-combined as a vector and converted back to degrees. The values generated from this process represented realistic Mean Wave Directions at the approximate location of each wave buoy that were not influenced by the "wrap-around" effect when going from 359° to 1° TN.

6.7 Variability of Measured Wave Conditions

After all data preparations techniques were applied to each of the wave buoy records, the variability of each parameter was tabulated in Table 6.4. The minimum, average and maximum measured values during the study duration are provided for H_S, T_1 and Wave Direction. Note that Townsville (Queensland) had the lowest average H_S of 0.68 m and T_1 of 3.8 s, and Cape Sorrell (Tasmania) had the highest average H_S of 2.95 m and T_1 of 8.5 s. Variability in wave direction is affected by both available wind processes and bathymetry.

Table 6.4
Minimum, Average and Maximum Wave Conditions Measured at each Wave Buoy Location

Buoy #	Location	Depth (m)	Significant Wave Height, H_S (m)			Mean Wave Period, T_1 (s)			Wave Direction (°)		
			Minimum	Average	Maximum	Minimum	Average	Maximum	Minimum	Average	Maximum
1	Townsville	15	0.10	0.68	3.01	2.3	3.8	6.3	0	76	360
2	Mackay	29	0.05	0.91	4.55	2.3	4.5	9.0	0	113	360
3	Mooloolaba	33	0.48	1.38	4.27	3.7	6.0	9.6	24	96	153
4	Brisbane	79	0.57	1.76	5.71	4.0	6.7	9.9	13	116	345
5	Gold Coast	18	0.42	1.26	4.39	4.0	6.3	9.7	30	94	136
6	Tweed River	23	0.48	1.37	3.70	4.2	6.5	10.4	28	93	138
7	Byron Bay	68	0.35	1.64	5.34	3.3	6.6	11.9	4	132	359
8	Sydney	85	0.42	1.66	7.69	3.7	6.7	11.9	9	136	352
9	Batemans Bay	73	0.32	1.40	5.32	3.3	6.5	11.7	27	130	346
10	Lakes Entrance	23	0.37	0.98	4.15	3.5	5.6	9.4	83	142	270
11	Kingfish B	78	0.57	1.67	5.76	N/A			N/A		
12	Point Nepean	26	0.29	1.67	5.73	2.6	7.2	14.6	143	212	347
13	Point Lonsdale	27	0.25	1.48	4.21	2.7	7.0	12.4	82	204	353
14	Cape Sorell	100	0.65	2.95	9.28	4.3	8.5	13.4	N/A		
15	Cape du Couedic	80	0.60	2.63	7.93	3.9	8.3	15.4	N/A		
16	Cottesloe	15	0.24	0.99	3.47	2.7	5.7	11.7	0	250	352
17	Rottnest Island	48	0.57	2.20	6.96	3.6	7.8	15.1	1	249	359
18	Exmouth	54	0.54	1.40	4.83	3.8	6.6	13.2	0	256	357

7. MODEL SKILL: INTERPRETATION AND ANALYSIS

7.1 Overview of HI-WAM Validation

To assess the skill of the HI-WAM model (i.e. how well the modelled values matched the real world observed data), several standard statistical measures were determined for each of the three wave parameters. The detail for each of these measures is discussed in Section 7.2. The data were also plotted as time series at each site for visual examination of the skill of HI-WAM. The model validation procedure was undertaken in two distinct validation stages.

Phase 1 involved a review of all available data without any filtering to ensure that the maximum possible variability in ocean conditions was replicated. This provided a gross assessment of the performance of the model around the entire Australian coastline over an 11 year period. However, as noted in Section 4.3, the input wind fields to HI-WAM are constantly being improved by BoM and as such, constitute an additional model variable which is not accounted for in this phase of validation. One site with an extended directional wave buoy record, Point Nepean, was selected to examine two topics of interest:

- The variation of model skill over time
  (i.e. is HI-WAM improving with improved wind field descriptions?)
- The variation of model skill for predicting wave direction with measured H_S
  (i.e. does HI-WAM have difficulty predicting direction for low wave heights?).

Phase 2 of the model validation was then conducted using only the most recent six months of data. This eliminated the variability of the input winds influencing the assessment of contemporary model skill. Wave directions were also filtered during this phase in accordance with methodologies presented in existing literature (discussed in Section 7.2.3). The results generated from this second and final phase of model validation allowed two further points to be addressed:

- The variation of model skill with water depth
  (i.e. up to which depths can HI-WAM be executed successfully?)
- The variation of model skill with latitude
  (i.e. do trends exist for HI-WAM model skill at Australian latitudinal extremes?).

7.2 Statistical Measures of Model Skill for each Wave Parameter

7.2.1 Significant Wave Height

To examine the HI-WAM model skill for hindcast Significant Wave Height, four statistics were calculated for each wave buoy site: *Bias* (modelled – observed values), *R* (linear correlation coefficient), *RMSE* (Root-Mean-Square Error) and *SI* (Scatter Index). Each of these is defined in Equations 7.1 to 7.4 and yield different information regarding how well the model compares with observed data. Note that the subscript *M* stands for model and *O* stands for observation.

$$Bias = \frac{1}{N_{obs}} \sum_{j=1}^{N_{obs}} H_{SM}^{j} - H_{SO}^{j} \qquad [m] \qquad \text{(Eq. 7.1)}$$

$$R = \frac{\sigma_{OM}}{\sigma_O \sigma_M} \qquad [-] \qquad \text{(Eq. 7.2)}$$

$$RMSE = \left[\frac{1}{N_{obs}} \sum_{j=1}^{N_{obs}} (H_{SM}^{j} - H_{SO}^{j})^2 \right]^{1/2} \qquad [m] \qquad \text{(Eq. 7.3)}$$

$$SI = \frac{\sigma_{ERRORS}}{\overline{H}_{SO}} \qquad [-] \qquad \text{(Eq. 7.4)}$$

where:

N_{obs}:	Number of observed data values
H_{SM}:	Modelled Significant Wave Height
H_{SO}:	Observed Significant Wave Height
σ_{OM}:	Covariance between observed and modelled values
σ_O:	Standard deviation of observed values
σ_M:	Standard deviation of modelled values
σ_{ERRORS}:	Standard deviation of (modelled – observed) values
$\overline{H}_{SO}$:	Mean Observed Significant Wave Height

The *Bias* for H_S indicates whether the HI-WAM model is generally under (negative) or over predicting (positive) the Significant Wave Height. The linear correlation coefficient illustrates how well the model fits the observed data; an *R* value of +1 indicates perfect correlation but an *R* value of 0 indicates no correlation. *RMSE* is a measure of the magnitude of varying error about the line of perfect model skill and is a good relative measure of model accuracy. Scatter Index normalises the standard deviation of individual

errors (through division by the mean observed value) to allow comparison between wave buoy sites regardless of the typical, local wave energy.

R and *SI* are statistics which are independent of the variability of wave climate across different wave buoy sites (i.e. high energy vs low energy regions). Accordingly, these two parameters are primarily used to directly compare model performance between wave buoy sites.

7.2.2 Mean Wave Period

For Mean Wave Period, the same four statistics for T_1 were calculated for each wave buoy site for analysis of HI-WAM model skill, as with H_S. For brevity, these equations have not been repeated in this section. Note that for wave buoys which only measured T_Z, values were adjusted to T_1 (as discussed in Section 6.5) prior to comparison with model T_1 values.

7.2.3 Wave Direction

For Wave Direction, since values are denoted in the form of angles, different statistical techniques (compared to H_S and T_1) were required to examine the HI-WAM model skill. Circular, rather than linear approaches were necessary. Four directional statistics were calculated for each wave buoy site: *Bias* (modelled – observed values), Circular Correlation ($\hat{p}_T$), *RMSE* (Root-Mean-Square Error) and the Concentration Statistic ($\hat{k}$).

Bias is calculated using the technique outlined by Bowers *et al.* (2000). Note that directional differences were defined as the acute angle between the observed and modelled wave directions. The difference was defined such that a positive difference occurs when the modelled wave direction is more clockwise that the observed wave direction. For example, if the modelled wave direction is from 25° TN and the observed wave direction is from 350° TN, the difference is defined as +35°. Equations 7.5 to 7.9 show the calculation steps to determine the model directional *Bias*. Note that *R* (in this context) is called the Resultant and $\overline{R}$ is termed the Mean Resultant Length since it is divided by the number of observed data values.

$$S = \sum_{j=1}^{N_{obs}} \sin(\theta_M^j - \phi_O^j) \qquad [-] \qquad \text{(Eq. 7.5)}$$

$$C = \sum_{j=1}^{N_{obs}} \cos(\theta_M^j - \phi_O^j) \qquad [-] \qquad \text{(Eq. 7.6)}$$

$$R = \sqrt{(C^2 + S^2)} \qquad [-] \qquad \text{(Eq. 7.7)}$$

$$\overline{R} = \frac{R}{N_{obs}} \qquad [-] \qquad \text{(Eq. 7.8)}$$

$$Bias = \tan^{-1}\left(\frac{S}{C}\right) \qquad [°] \qquad \text{(Eq. 7.9)}$$

A measure analogous to the linear correlation coefficient is required for comparing the two wave direction definitions. Toroidal linear association, as defined by Fisher (1983) and adopted by Bowers *et al.* (2000), can be used to determine the degree of association between two circular distributions using the statistic, Circular Correlation ($\hat{p}_T$). Circular Correlation is defined in Equation 7.10 and an alternative form, for computational purposes, is shown in Equation 7.11.

$$\hat{p}_T = \frac{\sum_{1 \le i < j \le N_{obs}} \sin(\theta_M^i - \theta_M^j)\sin(\phi_O^i - \phi_O^j)}{\left[\sum_{1 \le i < j \le N_{obs}} \sin^2(\theta_M^i - \theta_M^j) \sum_{1 \le i < j \le N_{obs}} \sin^2(\phi_O^i - \phi_O^j)\right]^{\frac{1}{2}}} \qquad [-] \qquad \text{(Eq. 7.10)}$$

$$\hat{p}_T = 4(AB - CD)/\left[(N_{obs}^2 - E^2 - F^2)(N_{obs}^2 - G^2 - H^2)\right]^{\frac{1}{2}} \qquad [-] \qquad \text{(Eq. 7.11)}$$

where:

$$A = \sum_{i=1}^{N_{obs}} \cos\theta_M^i \cos\phi_O^i \qquad B = \sum_{i=1}^{N_{obs}} \sin\theta_M^i \sin\phi_O^i$$

$$C = \sum_{i=1}^{N_{obs}} \cos\theta_M^i \sin\phi_O^i \qquad D = \sum_{i=1}^{N_{obs}} \sin\theta_M^i \cos\phi_O^i$$

$$E = \sum_{i=1}^{N_{obs}} \cos(2\theta_M^i) \qquad F = \sum_{i=1}^{N_{obs}} \sin(2\theta_M^i)$$

$$G = \sum_{i=1}^{N_{obs}} \cos(2\phi_O^i) \qquad H = \sum_{i=1}^{N_{obs}} \sin(2\phi_O^i)$$

The closer that $\hat{p}_T$ is to 1, the greater the extent to which the two wave direction distributions (observed and modelled) are correlated.

RMSE was calculated in the same manner as that for H_S and T_1.

The Concentration Statistic ($\hat{k}$), also defined by Fisher (1993) and adopted by Bowers *et al.* (2000) is a relative measure of how the two wave direction distributions compare. If the concentration is greater than or equal to 5.0, the two directional distributions being compared are similar (tight); lower concentration values indicate more spread between the two distributions. The Concentration Statistic is defined in Equation 7.12.

$$\hat{k} = \begin{cases} 2\overline{R} + \overline{R}^3 + 5\overline{R}^5/6 & \text{if } \overline{R} < 0.53 \\ -0.4 + 1.39\overline{R} + 0.43/(1-\overline{R}) & \text{if } 0.53 \le \overline{R} < 0.85 \\ 1/(\overline{R}^3 - 4\overline{R}^2 + 3\overline{R}) & \text{if } \overline{R} \ge 0.85 \end{cases} \quad [-] \qquad \text{(Eq. 7.12)}$$

Two of the parameters, Circular Correlation and the Concentration Statistic, are primarily used to directly compare model performance between wave buoy sites for wave direction.

Note too that when plotting wave direction in the corresponding figures, the direction axis was not set to the conventional range of 0° to 360° TN. Instead, the axis was centred on the approximate mean direction. For example, if the mean wave direction was from 90° TN, the axis' minimum would be -90° TN and the maximum 270° TN. This approach was undertaken to aid in visual analysis of the data when plotted; data plotted on a conventional directional axis of 0° to 360° TN appears very erratic when switching from, say, 359° to 1° TN.

Note that in Phase 2 of HI-WAM model validation; these four directional statistics were determined only when the observed Significant Wave Height was equal to or greater than 1.0 m. Use of this limit follows the approach undertaken by Tracy (2002) for comparing modelled and observed wave directions, because "*directions of low wave heights can diverge and contaminate the directional difference distribution*". This directional divergence is later demonstrated for one example wave buoy site Point Nepean, in Section 7.4.4.

7.3 Phase 1 Model Validation

7.3.1 Summary

The results of Phase 1 of the HI-WAM model validation are presented in two forms:

- The statistical measures of model skill are tabulated overleaf in Table 7.1
- Graphical plots are presented in Figures 7.01 to 7.50 for each site and wave parameter. These figures are each composed of a time series plot (measured and predicted values versus time) for one selected month with high wave energy, and a box plot for all available data (measured versus predicted values); the diagonal line through this plot represents perfect model skill. Note that the measured time series have been plotted discontinuously to show where wave buoy data gaps occurred. All of these same graphical plots for each site and wave parameter are also presented as "thumbnails" overlaid on the model domain in Figures 7.51 to 7.56 so that apparent regional trends in model skill can be compared at a glance.

Observation of the correlation coefficients, R and $\hat{k}$, indicates that HI-WAM has the most skill in predicting wave height (0.84), followed by similar degrees of skill for wave period (0.68) and wave direction (0.69). Note this assessment of skill for model wave direction is only based on the performance of the two wave buoys measuring Mean Wave Direction (Point Nepean and Point Lonsdale).

Table 7.1
Validation Phase 1: Measures of Model Skill for each Wave Buoy Location (All Data)

Buoy #	Location	Depth (m)	Significant Wave Height, H_S					Mean Wave Period, T_1					Wave Direction, *Drn*				
			N_{obs}	*Bias* (m)	*R*	*RMSE* (m)	*SI*	N_{obs}	*Bias* (s)	*R*	*RMSE* (s)	*SI*	N_{obs}	*Bias* (°)	$\hat{p}_T$	*RMSE* (°)	$\hat{k}$
1	Townsville	15	9,924	+0.29	0.77	0.39	0.39	9,924	+1.93	0.10	2.15	0.25	5,152	-1.22	0.63	28.55	4.85
2	Mackay	29	9,058	+0.17	0.91	0.36	0.34	9,058	+0.42	0.58	0.83	0.16	9,058	-11.53	0.57	32.17	4.75
3	Mooloolaba	33	726	+0.06	0.93	0.25	0.18	726	+0.31	0.77	0.70	0.11	726	-5.80	0.65	19.75	9.93
4	Brisbane	79	727	-0.11	0.90	0.37	0.20	727	-0.36	0.72	0.86	0.12	727	-18.08	0.45	40.87	3.45
5	Gold Coast	18	651	+0.08	0.90	0.28	0.21	651	-0.04	0.75	0.72	0.11	651	-6.59	0.46	24.56	6.52
6	Tweed River	23	715	-0.06	0.85	0.29	0.21	715	-0.20	0.70	0.75	0.11	715	-10.46	0.43	27.89	5.63
7	Byron Bay	68	7,619	-0.08	0.73	0.51	0.30	7,619	+0.32	0.57	1.14	0.16	7,619	-18.99	0.58	39.66	3.65
8	Sydney	85	13,46	-0.13	0.83	0.45	0.26	13,464	+0.35	0.64	1.07	0.15	13,464	-7.50	0.64	32.09	4.21
9	Batemans Bay	73	8,558	-0.03	0.80	0.39	0.27	8,558	+0.27	0.64	1.00	0.15	8,558	-8.88	0.64	29.62	4.95
10	Lakes Entrance	23	554	-0.30	0.68	0.45	0.33	554	+0.16	0.68	0.90	0.16	554	-14.08	0.60	31.61	4.96
11	Kingfish B	78	988	+0.03	0.78	0.47	0.28	N/A					N/A				
12	Point Nepean	26	6,535	-0.42	0.87	0.55	0.21	6,535	+0.31	0.73	1.28	0.17	6,535	+3.06	0.69	18.62	12.50
13	Point Lonsdale	27	2,737	-0.53	0.80	0.64	0.25	2,737	+0.16	0.65	1.39	0.20	2,737	+3.22	0.69	17.81	13.61
14	Cape Sorell	100	13,46	-0.63	0.88	0.85	0.19	13,464	-0.26	0.69	1.12	0.13	N/A				
15	Cape du Couedic	80	9,700	-0.52	0.87	0.72	0.19	9,700	-0.46	0.73	1.17	0.13	N/A				
16	Cottesloe	15	12,24	+0.01	0.87	0.26	0.26	12,246	+1.63	0.62	2.19	0.26	69	-30.23	0.46	54.36	2.60
17	Rottnest Island	48	4,558	-0.40	0.85	0.61	0.21	4,558	-0.62	0.74	1.31	0.15	4,558	-19.72	0.51	32.20	6.31
18	Exmouth	54	1,624	-0.36	0.75	0.45	0.19	1,624	-0.22	0.71	1.15	0.17	1,624	+2.08	0.33	42.47	2.78

7.3.2 Significant Wave Height

The *Bias* for H_S (the average of the errors) was variable across the wave buoy sites, but under predictions were more common, with a typical value of -0.18 m. It is noteworthy that that *Bias* was very positive at Townsville and Mackay (Locations 1 and 2), indicating an over prediction of wave height most likely due to wave breaking processes over the Great Barrier Reef not being accounted for in the model (refer to Figures 7.01 and 7.04). Those sites exposed to long period Southern and Indian Ocean Swells: Point Nepean, Point Lonsdale, Cape Sorrell, Cape du Couedic, Rottnest Island and Exmouth (Locations 12, 13, 14, 15, 17 and 18) had quite a negative *Bias*; of the order of -0.50 m. Those sites on the Australian East Coast exposed to full swell (Locations 3 to 11) were generally consistent with a *Bias* of around -0.08 m.

The Linear Correlation Coefficient, *R* (the measure of how well the model fits the observed data), was typically of the order of 0.84. This indicates strong, but certainly not perfect correlation. Lakes Entrance (Location 10) had the poorest correlation at 0.68 which was considerably less than all other sites.

The Root-Mean-Square Error, *RMSE* (which indicates a typical absolute value of the errors in model prediction) had an indicative value of 0.50 m across all sites. This means any given HI-WAM prediction for H_S around Australia is likely to be within ± 0.50 m of the (real) measured value. This measure is, however, not suited to making comparisons across multiple sites as it is considerably affected by depth limiting of available wave climate. Those sites in shallower water: Townsville, Gold Coast, Tweed River, Cottesloe (Locations 1, 5, 6 and 16) have a much smaller *RMSE* of 0.30 m than those in deeper water; Cape Sorrell (Location 14) had an *RMSE* of 0.85 m.

The Scatter Index, *SI* (which normalises the individual standard deviations for error through division by the mean value), had a general value for H_S of 0.26 and is best for comparing error between different locations. It highlighted that there was extensive scatter in three of the shallow water sites: Townsville, Mackay and Lakes Entrance (Locations 1, 2 and 11) with an approximate *SI* value of 0.35, despite them having low local wave energy.

In addition to the problems noted for the two sites leeward of the Great Barrier Reef, HI-WAM shows some difficulty in matching the measured wave heights at Lakes Entrance.

7.3.3 Mean Wave Period

The *Bias* for T_1 was (as with H_S) variable across the wave buoy sites, but over predictions were more common, with a typical value of +0.22 s. Clearly, those sites affected by more complex local breaking and refraction processes, such as Townsville, Mackay and Cottesloe (Locations 1, 2 and 16) showed a gross over prediction of mean wave period, up to +1.93 s (refer to Figures 7.02, 7.05 and 7.43). Again, sites exposed to long period Southern and Indian Ocean Swells: Cape Sorrell, Cape du Couedic, Rottnest Island and Exmouth (Locations 14, 15, 17 and 18) had quite a negative *Bias*; of the order of -0.40 s.

The Linear Correlation Coefficient was typically of the order of 0.68. This indicates robust correlation for mean wave period around Australia. Townsville (Location 1) had the poorest correlation at 0.10 which was less than all other sites by some margin. Mackay and Byron Bay (Locations 2 and 7) also demonstrated poor correlations around 0.57.

The typical *RMSE* value for T_1 around the Australian coastline was 1.20 s. This means any given HI-WAM prediction for T_1 is likely to be within ± 1.20 s of the (real) measured period. Again, Townsville and Cottesloe (Locations 1 and 16) defied this trend, and had very large *RMSE* values of approximately 2.15 s.

The Scatter Index had a common value for T_1 of 0.16. Townsville and Cottesloe (Locations 1 and 16) had the highest *SI* with 0.25, but the smallest measure of scatter for mean wave period was found in south-east Queensland. Mooloolaba, Brisbane, Gold Coast and Tweed River (Locations 3, 4, 5 and 6) had an SI value of around 0.11.

Townsville and Mackay have already been noted as being difficult sites for HI-WAM to predict values for, but an examination of mean wave period has shown that another protected shallow water site, Cottesloe (Location 16), is also a problem.

7.3.4 Wave Direction

The model skill for wave direction is discussed in two parts: those sites measuring Peak Wave Direction and then those measuring Mean Wave Direction.

7.3.4.1 Sites Measuring Peak Wave Direction

For those sites measuring Peak Wave Direction, the Bias for wave direction was approximately -10 ° for most locations. This indicated that the HI-WAM model predictions are biased 10 ° anticlockwise of the real (measured) wave direction values.

The Circular Correlation Coefficient, $\hat{p}_T$ (this is analogous to R for H_S and T_1), was typically of the order of 0.56. This indicates reasonable correlation between modelled and observed values for wave direction. Exmouth (Location 18) had the poorest circular correlation at 0.33 which was considerably less than all other sites (refer to Figure 7.50).

The typical *RMSE* value for wave direction around the Australian coastline was 32 °. This indicates that wave direction predictions are likely to be within ± 32 ° of the (real) measured direction. Mooloolaba (Location 3) had the lowest wave direction *RMSE* of around 20 °. HI-WAM had the worst performances for direction at Brisbane, Byron Bay, Cottesloe and Exmouth (Locations 4, 7, 16 and 18) with an *RMSE* of approximately 45 °.

The Circular Concentration Statistic, $\hat{k}$, had a typical value equal to 5.50 (the modelled and observed directional distributions are considered to be similar if this is ≥ 5.00). As such, the model is considered to predict a reasonably similar directional distribution to that which is observed in the real world. HI-WAM had a very tight match at Mooloolaba (Location 3) with a $\hat{k}$ value 9.93. The most loose concentrations were noted in Western Australia with Cottesloe and Exmouth (Locations 16 and 18) showing $\hat{k}$ around 2.70.

Exmouth has been shown to be the most problematic validated site at which HI-WAM predicts wave direction. It should be noted that the wave buoy at Cottesloe only has a relatively small number of valid directional observations, 69 in total (versus several hundred or more at other sites) and that caution should be applied in criticising the directional performance of HI-WAM at this location. The directional data from Cottesloe will not be included in Phase 2 of the model validation.

The skill of the HI-WAM model for predicting wave direction at the two sites (Rottnest Island and Exmouth) where it was necessary to select the wave direction from "sea" and "swell" components (as described in Section 6.6) is within the acceptable ranges of other sites indicating that this technique was appropriate.

7.3.4.2 Sites Measuring Mean Wave Direction

At the two locations measuring Mean Wave Direction (Point Nepean – Location 12 and Point Lonsdale – Location 13), HI-WAM model skill was superior than all other sites (refer to Figures 7.34 and 7.37). The typical statistical measures were as follows:

- *Bias* $+3°$
- $\hat{p}_T$ 0.69
- *RMSE* $18°$
- $\hat{k}$ 13

It should be noted that these two locations both lie outside of Port Phillip Bay in Melbourne and have very similar wave climates. Accordingly, although these are the only two sites for which observed and predicted wave direction definitions are the same, they do not represent the spatial variability of Australian wave climate.

7.3.4.3 Peak vs. Mean Wave Direction

While the local geography/bathymetry at Point Nepean and Point Lonsdale may constrain the incident wave energy to being from one directional window (between the SWW and the SSW), the exceptional results for wave direction at these locations support the analysis from Appendix B that Peak and Mean Wave Direction definitions cannot be considered to be analogous. This vindicates the separation of data output from these two types of directional wave buoys. Further assessment of HI-WAM model skill for predicting wave direction in validation Phase 2 will be limited to only those sites measuring Mean Wave Direction. As such, spatial variability of the directional performance of HI-WAM will be sacrificed to ensure that the same definitions for wave direction are used to assess its final directional skill in Phase 2.

7.4 Extensions to Analysis from Validation Phase 1

7.4.1 Likelihood of Predictions being within ± One Root-Mean-Square Error of Measurements

Since the *RMSE* is used to provide a measure of typical model accuracy, it is useful to determine the likelihood of individual model predictions falling within its bounds. The *RMSE* may be related to model *Bias* and the standard deviation of all error values (modelled – observed), σ_{ERRORS}, by Equation 7.13.

$$RMSE = \sqrt{Bias^2 + \sigma_{ERRORS}^2} \qquad \text{(Eq. 7.13)}$$

RMSE is distinct from σ_{ERRORS} because it measures the spread about the line of perfect model skill, but σ_{ERRORS} measures the spread about the *Bias* (the line-of-best-fit through the data). *RMSE* and σ_{ERRORS} are only equivalent for a case with zero model *Bias*. As such, *RMSE* is always greater than or equal to σ_{ERRORS} and increases with increasing absolute value of *Bias*. If the errors follow a Gaussian distribution, the likelihood that individual model predictions fall within ± one standard deviation of the *Bias* is 68.2 per cent. This value should serve as a lower threshold for the likelihood that predictions fall within ± one *RMSE*. Since *RMSE* is a function of *Bias*, it is variable for each wave parameter and buoy location. The proportion of model predictions which were within ± one *RMSE* of the measured values for each parameter (wave height, wave period and wave direction) was determined in percentage terms at each location for Phase 1 and presented in Table 7.2.

Table 7.2
Proportion of HI-WAM Predictions within ± one RMSE of Measured Values (by %)

Buoy #	Location	H_S %	T_1 %	*Drn* %
1	Townsville	69.8	65.8	79.4
2	Mackay	77.0	77.1	79.1
3	Mooloolaba	76.2	74.0	76.2
4	Brisbane	71.4	70.8	81.3
5	Gold Coast	73.0	72.5	73.9
6	Tweed River	74.1	73.6	76.6
7	Byron Bay	79.4	71.2	76.6
8	Sydney	76.4	72.1	77.4
9	Batemans Bay	76.7	73.3	77.2
10	Lakes Entrance	72.7	65.0	74.7
11	Kingfish B	72.4	N/A	73.3
12	Point Nepean	66.5	73.1	91.7
13	Point Lonsdale	63.3	73.0	89.7
14	Cape Sorell	65.8	71.5	N/A
15	Cape du Couedic	68.5	73.8	N/A
16	Cottesloe	74.1	69.4	75.4
17	Rottnest Island	71.1	73.0	74.9
18	Exmouth	64.4	74.8	82.8

The likelihood of H_S predictions by HI-WAM being within ± one *RMSE* of the measured values varied between 63 and 80 per cent, with a mean value of 72 per cent. For T_1 predictions, it varied between 65 and 77 per cent for all locations; but with the same mean. Wave direction likelihoods were tabulated for all sites; the mean value was 91 per cent for the two sites measuring Mean Wave Direction (Point Nepean and Point Lonsdale). It should be noted that six of the probability values are slightly lower than the theoretical threshold of 68.2 per cent; indicating a likely divergence from a Gaussian distribution.

These results demonstrate that 28 per cent of predictions for H_S and T_1 will be more than ± one *RMSE* from the measured values. For Mean Wave Direction, 9 per cent of predictions will fall outside these same bounds.

7.4.2 Variation of Model Skill with Significant Wave Height: Examination of Regional Trends

7.4.2.1 Relevance of Model Skill Aspects for Different Stakeholders

The skill of HI-WAM is of interest from (at least) the following perspectives:

- Climate — sciences requiring a model fitting overall natural trends – such as climate or wave energy assessments
- Operational — ports facilities or defence activities relying on day-to-day model predictions for operational decision making
- Design — engineers using model output to design a coastal structure – extreme storms are most important.

The analysis conducted thus far in Validation Phase 1 has concentrated on the overall fit of the HI-WAM predictions to those observed in nature. This focus is of most interest to climate science modellers and to operational stakeholders. To address model skill under extreme wave conditions (infrequent events) more analysis is required. This is important if the HI-WAM model outputs are to be used (in the absence of wave buoy data) at particular locations by coastal engineers to extrapolate predicted wave heights for storm events with long recurrence intervals (i.e. a 1 in 100 year ARI event) using statistical techniques. This same information is also of interest to operational stakeholders to prevent and/or mitigate the loss of life and property in an extreme wave event.

Examination of model skill for predicting the intensity of wave action as a function of measured significant wave height is helpful in verifying if HI-WAM output is suitable for design purposes. To this end, *Bias* and *RMSE* for predicted wave height and period were calculated in 1.0 m bins of measured wave heights for all available data at all buoy locations. The influence of wave direction on the intensity of wave action experienced at each buoy location was not considered in this analysis. For brevity, these values have not been tabulated but are presented graphically in Figures 7.57 to 7.60. Each of these figures has been subdivided into six regions around the Australian coast with similar wave climate to see if regional trends in HI-WAM skill for wave height and period may be observed. The regional groups adopted are defined in Table 7.3.

HI-WAM model prediction performance is evaluated in detail for each sub-region in Section 7.4.2.2 (predicted H_S as a function of measured H_S) and Section 7.4.2.3 (predicted T_1 as a function of measured H_S).

Table 7.3
Six Regional Groups for Analysing Variation of Model Skill with Measured H_S

Regional Group		Buoy #	Location
#	Description		
1	Great Barrier Reef	1	Townsville
		2	Mackay
2	South-East Queensland to New South Wales Border	3	Mooloolaba
		4	Brisbane
		5	Gold Coast
		6	Tweed River
		7	Byron Bay
3	New South Wales	8	Sydney
		9	Batemans Bay
4	South-East Victoria	10	Lakes Entrance
		11	Kingfish B
5	South-West Victoria, West Tasmania, South Australia	12	Point Nepean
		13	Point Lonsdale
		14	Cape Sorell
		15	Cape du Couedic
6	Western Australia	16	Cottesloe
		17	Rottnest Island
		18	Exmouth

7.4.2.2 Significant Wave Height

The following treatise is based on the skill shown in Figures 7.57 (*Bias*) and 7.58 (*RMSE*).

Region 1 is located in lee of the Great Barrier Reef and, as previously mentioned, HI-WAM over predicted wave height under all conditions (positive *Bias*). This prediction error (*RMSE*) increased with increasing measured H_S.

Region 2 (SE Queensland to New South Wales border) over predicted small wave heights (0 to 2 m) by 0.8 m at all locations, but no discernible trends exists for the largest measured H_S (some sites over predict, some under predict). Disparities were also noted for *RMSE*.

Region 3 (New South Wales) showed a negligible *Bias* for wave heights up to 1.0 m. Wave heights were under predicted in the range between 1.0 and 7.0 m. However, for the largest significant wave heights (up to 8.0 m – only recorded at Sydney), HI-WAM over predicted the wave heights by more than 2.5 m. The model error (*RMSE*) was noted to generally increase for Sydney and Batemans Bay with increasing measured wave height.

Region 4 (Lakes Entrance and Kingfish B) showed model *Bias* decreasing with measured H_S from negligible at small heights to under prediction by 1.7 m at large wave heights. Again, *RMSE* generally increased with increasing measured H_S.

Region 5 (West Victoria, West Tasmania and South Australia) demonstrated similar behaviour to Eastern Victoria (Region 4). Wave height was always under predicted (negative *Bias*) and for measured heights up to 10 m it was under predicted by more than 3.0 m. Again, *RMSE* generally increased with increasing measured H_S.

Region 6 (Western Australia) showed a negligible *Bias* for wave heights up to 1.0 m. However, model performance at Cottesloe (in lee of Rottnest Island) was very different to the two exposed sites. Wave heights were over predicted with increasing measured H_S at Cottesloe (similar behaviour was noted for the sites in lee of the Great Barrier Reef in Region 1). For Rottnest Island and Exmouth, *Bias* became more negative with increasing measured Significant Wave Height (the greatest under prediction was -1.25 m for 6 to 7 m wave heights). For all sites, model error increased with increasing measured H_S.

7.4.2.3 Mean Wave Period

The following treatise is based on the skill shown in Figures 7.59 (*Bias*) and 7.60 (*RMSE*).

Region 1 over predicted the mean wave period under all wave conditions (positive *Bias*). Divergent behaviour was noted for *RMSE* (Townsville showed increasing error for decreasing H_S; Mackay behaved in the converse).

Region 2 showed a slight over prediction of T_1 for small wave conditions (H_S up to 1.0 m). This error was reduced for mid-wave heights; with divergence occurring for the larger wave heights. Disparities were again noted for *RMSE* between the five sites.

Region 3 over predicted T_1 for small wave conditions (H_S less than 1.0 m) though *Bias* was negligible for moderate wave conditions. However, for H_S exceeding 7.0 m, T_1 was over predicted by more than 2.8 s. The *RMSE* was moderate for low wave heights, low for medium wave heights, but then increased considerably for large measured H_S.

Region 4 was only composed of one wave buoy site; Lakes Entrance (as Kingfish B did not record mean wave period). For small to moderate wave heights, T_1 was over predicted by 0.25 s and under predicted by the same value for moderate to large wave heights. *RMSE* for mean wave period had a maximum for measured H_S of up to 5 m.

Region 5 over predicted T_1 at Point Nepean and Point Lonsdale but under predicted at Cape Sorrell and Cape du Couedic for small wave heights. For moderate to large H_S, mean wave period was under predicted at all locations, with the most negative *Bias* being -1.3 s. *RMSE* was observed to be high (approximately 1.5 s) for low and high wave conditions but less than 1.0 s for moderate wave conditions.

Region 6 again demonstrated divergent behaviour between the protected site at Cottesloe and the exposed sites at Rottnest Island and Exmouth. Cottesloe over predicted the mean wave period under all wave conditions. The two open-coast locations showed model *Bias* decreasing with measured H_S from negligible at small heights to under prediction by almost 1.0 s at large wave heights. *RMSE* generally decreased with increasing measured H_S.

7.4.2.4 Synopsis of Regional Trends in Model Skill

For small measured significant wave heights (less than 1.0 m), wave energy (both H_S and T_1) was generally over predicted on the eastern coast (Regions 1 to 4), but was under predicted for the western coasts of Australia (Regions 5 and 6).

HI-WAM predictions for wave intensity were generally best (lowest absolute values of *Bias* for wave height and period); for the moderate range of measured H_S values (1.0 to 3.0 m). The following points summarise the regional trends observed for model performance with extreme measured significant wave heights (greater than 3.0 m):

- For tropical regions on the eastern seaboard (Regions 1 and 2 - Great Barrier Reef to NSW border), no overall trend was noted for HI-WAM predictions.
- Wave buoy sites in Region 3 (southern half of the NSW coast) showed an under prediction of wave height for moderate to large conditions but no overall trend for wave period.
- With the exception of the protected Cottesloe station, wave buoys located in Regions 4, 5 and 6 (Victoria, Tasmania, SA and WA) considerably under predicted wave energy (height and period) for extreme H_S.

The most concerning outcome of this analysis was that wave energy (both H_S and T_1) was vastly over predicted at only one site, Sydney (NSW), for extreme wave heights but, conversely, energy was under predicted for those sites exposed to full swell in Victoria, Tasmania, South Australia and Western Australia.

On this basis, great caution should be applied if HI-WAM model outputs are to be for used for engineering design purposes when planning coastal structures exposed to infrequent and extreme storm events.

7.4.3 Variation of Model Skill with Time: Point Nepean Case Study

Since the quality of the Meso-LAPS input wind fields to HI-WAM are constantly being improved by BoM, it was important to determine if these changes resulted in improved performance of the model over time. To verify this, a case study was developed for one example location, Point Nepean (Location 12); selected because it had the longest directional history of those sites recording Mean Wave Direction. The measures of model skill were determined in 11 six month increments (March to August and September to February). The results of this detailed case study are tabulated in Table 7.4.

Table 7.4
Variation of HI-WAM Model Skill with Time (Point Nepean – 6 Month Increments)

Time Period	Start Date	End Date	Significant Wave Height, H_S					Mean Wave Period, T_1					Wave Direction, Drn				
			N_{obs}	*Bias* (m)	*R*	*RMSE* (m)	*SI*	N_{obs}	*Bias* (s)	*R*	*RMSE* (s)	*SI*	N_{obs}	*Bias* (°)	$\hat{p}_T$	*RMSE* (°)	$\hat{k}$
1	13/01/2003	28/02/2003	175	-0.59	0.71	0.69	0.24	175	-0.37	0.76	0.98	0.15	175	-0.13	0.81	11.73	25.91
2	01/03/2003	31/08/2003	649	-0.44	0.89	0.56	0.22	649	-0.06	0.63	1.40	0.19	649	3.96	0.68	22.09	8.67
3	01/09/2003	29/02/2004	254	-0.42	0.87	0.54	0.20	254	0.17	0.78	1.01	0.14	254	2.47	0.53	11.45	29.13
4	01/03/2004	31/08/2004	675	-0.41	0.89	0.56	0.21	675	0.29	0.71	1.32	0.17	675	6.14	0.67	22.01	9.73
5	01/09/2004	28/02/2005	721	-0.43	0.85	0.57	0.23	721	0.29	0.70	1.22	0.17	721	1.57	0.62	13.88	21.21
6	01/03/2005	31/08/2005	705	-0.42	0.85	0.56	0.23	705	0.10	0.74	1.32	0.18	705	8.49	0.60	32.99	4.84
7	01/09/2005	28/02/2006	724	-0.41	0.86	0.53	0.21	724	0.52	0.74	1.31	0.17	724	0.50	0.69	16.79	14.84
8	01/03/2006	31/08/2006	704	-0.38	0.88	0.53	0.21	704	0.54	0.75	1.42	0.17	704	2.52	0.65	13.64	20.51
9	01/09/2006	28/02/2007	724	-0.43	0.87	0.55	0.20	724	0.48	0.71	1.24	0.16	724	2.51	0.79	11.40	29.06
10	01/03/2007	31/08/2007	606	-0.35	0.87	0.47	0.20	606	0.38	0.69	1.26	0.17	606	2.46	0.80	14.17	19.17
11	01/09/2007	28/02/2008	598	-0.43	0.87	0.55	0.19	598	0.40	0.80	1.13	0.15	598	0.90	0.71	13.34	22.05

The key model skill parameters R, SI, $\hat{p}_T$ and $\hat{k}$ are plotted as a function of time in Figures 7.61 (wave height), 7.62 (wave period) and 7.63 (wave direction). As there is some variability in the results, regression lines have also been plotted through each of these data sets to indicate trends over time.

While there is some seasonal variability between the six month increments (switching between Autumn/Winter and Spring/Summer weather patterns), improvements can be qualitatively measured for each wave parameter in HI-WAM from 2003 to 2008. These improvements are summarised in Table 7.5.

Table 7.5
Variation in HI-WAM Model Skill at Point Nepean, Victoria (2003-2008)

Model Skill Parameter	H_S	T_1	*Drn*
R (H_S and T_1), $\hat{p}_T$ (*Drn*)	+0.07	+0.03	+0.07
SI (H_S and T_1), $\hat{k}$ (*Drn*)*	-0.03	0.00	+3.49
RMSE	-0.11	+0.11	-3.49

* Note that an increase in $\hat{k}$ is an improvement of the fit between modelled and observed values (this is analogous to a reduction in *SI*).

Noteworthy improvements were observed for Significant Wave Height predictions: the linear correlation coefficient increased by 0.07 and the Scatter Index was reduced by 0.03. This resulted in a reduction in the *RMSE* for H_S of 0.11 m.

Small improvements were noted in the R value for Mean Wave Period; it increased by 0.03. However, *SI* for T_1 was steady throughout the 11 year study period. Although R improved and *SI* was steady for T_1, there was a small increase in the overall *RMSE* for T_1 of 0.11 s. This trend appears to be particularly affected by a very low *RMSE* value in Time Period 1.

The correlation for Wave Direction was strengthened, with an increase in $\hat{p}_T$ of 0.07. The observed and predicted wave direction distributions were noted to become more similar; $\hat{k}$ increased by 3.49. The improvement in the quality of the Meso-LAPS input wind fields resulted in reduction in the *RMSE* for wave direction at Point Nepean of 3.49 °.

Finally, it should be noted that while trends for improvement of model skill have been observed for each wave parameter; the seasonal and inter-annual variability is of a similar (or slightly larger) magnitude. As such, care should be taken when interpreting results from Validation Phase 2 because even though the variability of input wind fields has been removed, the seasonality signal will persist and may affect the final, contemporary model skill assessment.

7.4.4 Variation of Directional Model Skill with Significant Wave Height: Point Nepean Case Study

As noted in existing literature in Section 7.2.3, extensive divergence between measured and predicted wave directions is observed to occur for low wave heights. This will contaminate the qualitative assessment of the directional skill of HI-WAM. For engineering purposes, prediction of incident direction at low wave heights is not considered to be a high priority.

The Point Nepean case study was extended to include an examination of HI-WAM skill in predicting wave direction as a function of measured significant wave height. The RMSE for wave direction prediction was calculated in 1.0 m bins for all available wave heights and is shown in Table 7.6.

Table 7.6
HI-WAM Skill for Predicting Wave Direction with Variation in H_S (Point Nepean)

Measured H_S (m)	HI-WAM Model Wave Direction *RMSE* (°)
0 to 1	34.30
1 to 2	15.47
2 to 3	8.06
3 to 4	7.77
4 to 5	7.21
5 to 6	5.35

These results indicate that there is a decrease in error for wave direction with measured H_S (i.e. HI-WAM makes better wave direction predictions in more energetic conditions). *RMSE* for wave direction is 34 ° for H_S up to 1.0 m, but is reduced to 8 ° for wave heights between 2.0 and 6.0 m at Point Nepean.

For all available data, the directional errors are plotted as a function of measured significant wave height in Figure 7.64 (top). The same data is replotted as the square of the directional errors in Figure 7.64 (bottom). The trend for reduction in directional wave error with increase in incident wave height is again obvious in these plots.

On this basis, the arbitrary threshold of 1.0 m minimum measured significant wave height is adopted in Validation Phase 2 to produce more consistent directional skill results. Note that no minimum thresholds were applied for assessing model skill for H_S and T_1 in Phase 2.

7.5 Phase 2 Model Validation

7.5.1 Summary

Phase 2 of the model validation was conducted using only the most recent six months of data (September 2007 to February 2008). Consequently, several wave buoy locations (Townsville, Kingfish B and Point Lonsdale) were not included in this analysis as no wave buoy data was available during this timeframe. However, the available wave buoy data from four sites in South-East Queensland (Mooloolaba, Brisbane, Gold Coast and Tweed River) was wholly within this timeframe. As such, at these sites no difference exists for H_S and T_1 skill between validation Phases 1 and 2.

The results of Phase 2 of the HI-WAM model validation are presented overleaf in Table 7.7. Note that the percentage of observations with H_S equal to or greater than 1.0 m is shown for one wave buoy location only (Point Nepean). This indicates how much directional data was used (after filtering) in determining the measures of directional model skill. For brevity, revised figures with time series and box plots of observed and predicted values have not been produced.

In summary, for any given location in Australia within the range of water depths tested, HI-WAM wave parameter predictions are likely to have a general accuracy as follows:

- Significant Wave Height predictions within ± 0.4 m of the measured H_S (negative *Bias*)
- Mean Wave Period predictions within ± 0.9 s of the measured T_1 (no *Bias*)
- Wave Direction predictions within ± 10 ° of the measured *Drn* (no *Bias*)
  (for H_S greater than or equal to 1 m).

These values are based on representative *RMSE* values for all sites in Validation Phase 2.

Table 7.7
Validation Phase 2: Measures of Model Skill for each Wave Buoy Location (September 2007 to February 2008)

Buoy #	Location	Depth (m)	Significant Wave Height, H_S					Mean Wave Period, T_1					Wave Direction, *Drn* ($H_S \geq 1.0$ m)					
			N_{obs}	*Bias* (m)	*R*	*RMSE* (m)	*SI*	N_{obs}	*Bias* (s)	*R*	*RMSE* (s)	*SI*	N_{obs}	% Obs $H_S \geq$ 1 m	*Bias* (°)	$\hat{p}_T$	*RMSE* (°)	$\hat{k}$
2	Mackay	29	726	+0.04	0.94	0.25	0.28	726	+0.35	0.71	0.76	0.15	(Peak Wave Direction Definition Used)					
3	Mooloolaba	33	726	+0.06	0.93	0.25	0.18	726	+0.31	0.77	0.70	0.11	(Peak Wave Direction Definition Used)					
4	Brisbane	79	727	-0.11	0.90	0.37	0.20	727	-0.36	0.72	0.86	0.12	(Peak Wave Direction Definition Used)					
5	Gold Coast	18	651	+0.08	0.90	0.28	0.21	651	-0.04	0.75	0.72	0.11	(Peak Wave Direction Definition Used)					
6	Tweed River	23	715	-0.06	0.85	0.29	0.21	715	-0.20	0.70	0.75	0.11	(Peak Wave Direction Definition Used)					
7	Byron Bay	68	687	-0.21	0.65	0.59	0.31	687	-0.08	0.41	1.06	0.16	(Peak Wave Direction Definition Used)					
8	Sydney	85	701	-0.16	0.80	0.41	0.23	701	+0.15	0.63	0.86	0.13	(Peak Wave Direction Definition Used)					
9	Batemans Bay	73	522	-0.04	0.83	0.33	0.24	522	+0.24	0.63	0.85	0.13	(Peak Wave Direction Definition Used)					
10	Lakes Entrance	23	522	-0.31	0.67	0.46	0.33	522	+0.17	0.48	0.90	0.16	(Peak Wave Direction Definition Used)					
12	Point Nepean	26	598	-0.43	0.87	0.55	0.19	598	+0.40	0.80	1.13	0.15	519	87	+0.87	0.75	9.17	39.93
14	Cape Sorell	100	704	-0.53	0.93	0.67	0.14	704	-0.27	0.83	0.82	0.09	N/A					
15	Cape du Couedic	80	407	-0.44	0.92	0.60	0.15	407	-0.14	0.86	0.81	0.10	N/A					
16	Cottesloe	15	722	+0.07	0.89	0.25	0.26	722	+1.59	0.71	1.98	0.23	(Peak Wave Direction Definition Used)					
17	Rottnest Island	48	711	-0.26	0.89	0.47	0.19	711	-0.37	0.79	1.07	0.14	(Peak Wave Direction Definition Used)					
18	Exmouth	54	475	-0.37	0.86	0.44	0.16	475	-0.16	0.78	0.87	0.13	(Peak Wave Direction Definition Used)					

7.5.2 Significant Wave Height

When comparing the contemporary *Bias* for H_S at each site with the Phase 1 results, there was not a general improvement for all sites. Six sites; Sydney, Batemans Bay, Lakes Entrance, Point Nepean and Exmouth, each had negative Biases in Phase 1 which become slightly more negative (by approximately 0.01 m) in Phase 2. Five sites; Mackay, Cape Sorrell, Cape du Couedic, Cottesloe and Rottnest Island each had commendable improvements in *Bias* of the order of 0.10 m. Byron Bay (Location 7) had the poorest change from Phase 1 to Phase 2; *Bias* changed from -0.08 m to -0.21 m. A typical under predictive *Bias* value of -0.16 m was found when considering all sites around Australia.

The linear correlation coefficient, R, was slightly improved for most sites and was approximately 0.86. Small reductions in correlation (-0.02) were noted at Sydney and Lakes Entrance (Locations 8 and 10). Byron Bay (Location 7) again had the poorest contemporary skill, with R reduced (by 0.08) to 0.65.

The typical RMSE value across all sites was 0.40 m. All sites except Byron Bay and Lakes Entrance (Locations 7 and 10) showed a reduction in RMSE from Validation Phases 1 to 2.

All locations except Byron Bay (which increased by 0.01) showed a reduction in the Scatter Index for H_S. An *SI* of 0.22 was representative of all Australian sites for significant wave height.

7.5.3 Mean Wave Period

The *Bias* for T_1 was reduced between Validation Phases 1 and 2 for all sites except for those in the South Eastern corner of Australia: Lakes Entrance, Point Nepean and Cape Sorrell (Locations 10, 12 and 14) which had minor reductions in performance. It is worth noting that two sites showed considerable improvement with positive changes in *Bias* of 0.30 s; Cape du Couedic changed from -0.46 to -0.14 s and Rottnest Island from -0.62 to -0.37 s *Bias*. In general, there was no overall *Bias* when considering all sites around Australia (over and under predictions are evenly mixed).

The Linear Correlation Coefficient, R, was slightly improved for most sites and was approximately 0.71. Small reductions in correlation (-0.01) were noted at Sydney and Batemans Bay (Locations 8 and 9). Byron Bay and Lakes Entrance (Locations 7 and 10) again had the poorest contemporary correlation, with R reduced to as low as 0.41.

The typical *RMSE* value across all sites was 0.90 s. All sites showed a reduction in *RMSE* from Validation Phases 1 to 2 of the order of 0.14 s.

Similarly, all locations showed a reduction in the Scatter Index for T_1. An *SI* of 0.13 was representative of all Australian sites for mean wave period.

7.5.4 Wave Direction

At the only site measuring Mean Wave Direction during the most recent six months (Point Nepean – Location 12), the contemporary directional skill of HI-WAM was assessed. Filtering out low wave heights (and allowing for higher quality wind fields) improved all statistical measures as shown in Table 7.8.

Table 7.8
Model Skill for Predicting Direction at Point Nepean: (Phase 1 versus Phase 2)

Parameter	Phase 1	Phase 2	Change
Bias (°)	+3.06	+0.87	2.19
$\hat{p}_T$	0.69	0.75	+0.10
RMSE (°)	18.62	9.17	-9.45
$\hat{k}$	12.50	39.93	27.43

These results indicate that HI-WAM model error for Mean Wave Direction may be as low as 10 ° (when H_S is equal to or greater than 1.0 m). However, this assessment of the contemporary directional model skill of HI-WAM is based on only one location on the Australian coast.

Further to this disclaimer, Womersley (2008) noted that:

"the geographic location of the Point Lonsdale wave buoy [which is relatively close to the Point Nepean wave buoy], combined with the relatively shallow depth at the deployment means that wave refraction processes around northwest Tasmania, King Island and Cape Otway, result almost without exception, in the lower frequency swell waves generated in the southern ocean arriving from a very tight direction band centred around 211°."

Accordingly, it is possible that modelling the Mean Wave Direction at this site may not be the most demanding test of HI-WAM skill.

7.6 Extensions to Analysis from Validation Phase 2

7.6.1 Variation of Model Skill with Water Depth

Water depths of approximately 20 to 30 m are considered to be the shallowest depths to which the WAM model can be run successfully (Booij *et al.* 1999 and Porter-Smith *et al.* 2004). This threshold was tested by plotting both of the key model skill parameters R and SI (which are independent of mean wave climate) as a function of water depth at each wave buoy used in Validation Phase 2 in Figures 7.65 (wave height) and 7.66 (wave period). Note that no assessment of the variation of model skill for wave direction with water depth was possible as there was only one appropriate site.

While these plots do not account for regional morphology impacts (reefs, islands, etc), some trends are able to be noted despite the scatter in the data.

With reference to Figure 7.65, there is a general trend for reduction in model skill for H_S (R decreasing and SI increasing) with decreasing water depth. However, the two shallowest sites; Cottesloe (15 m) and the Gold Coast (18 m) maintained reasonable model performance with linear correlation of 0.89 to 0.90 and Scatter Index of 0.21 to 0.26. The obvious outliers in these plots were Lakes Entrance (23 m) and Byron Bay (68 m) which both have very poor model performance ($R \approx 0.66$ and $SI \approx 0.32$).

Model skill for mean wave period is shown in Figure 7.66. Again, a similar trend for reduction in model skill for T_1 (R decreasing and SI increasing) with decreasing water depth is visible. Lakes Entrance and Byron Bay again were outliers for the linear correlation coefficient, with low correlation for T_1 (0.41 to 0.48). The most shallow site, Cottesloe (15 m) also had very high scatter (SI of 0.23) for T_1 which was not observed at the Gold Coast (18 m) and Tweed River (23 m). This strange result at Cottesloe may not be fully attributable to its shallow water depth; complexities in the shadow of Rottnest Island may also exist.

While it has been observed that model skill for significant wave height and mean wave period reduces with depth, it should be acknowledged that there is considerable scatter in the data indicating that other variables are not being accounted for.

Although the Cottesloe record has problems with wave period, HI-WAM has been shown to produce effective results in water depths of 15 to 30 m. The performance of the model at the Gold Coast in 18 m of water for all wave parameters is a particularly good example of this.

7.6.2 Variation of Model Skill with Latitude

It is also of interest to examine if the predictive capability of HI-WAM varies with latitude; that is, to see if trends exists for HI-WAM model skill at Australian latitudinal extremes. It is suggested that distinctions in model performance may exist between the temperate zones with frequently occurring, large storms and the intertropical zones with more infrequent, tighter weather systems.

This supposition was tested by plotting both of the key model skill parameters *R* and *SI* (which are independent of mean wave climate) as a function of latitude for each wave buoy used in Validation Phase 2 in Figures 7.67 (wave height) and 7.68 (wave period). Again, no assessment of the variation of model skill for wave direction with latitude was possible as there was only one appropriate site.

With reference to Figure 7.67, there was no overall trend for model skill for H_S with variation in latitude. In fact, the trends for the individual model skill parameters were contrary to one another (both *R* and *SI* were decreasing with decreasing latitude).

Model skill for mean wave period is shown in Figure 7.68. There was a weak trend for improvement in model skill for T_1 (*R* increasing and *SI* decreasing) with decreasing latitude (i.e. HI-WAM performed better for period at higher (more southern) latitudes in Australia). Lakes Entrance, Byron Bay and Cottesloe were again obvious outliers with low correlation for T_1. However, it is acknowledged that considerable scatter remains in the data and that the noted correlation for model skill for Mean Wave Period is relatively weak with latitude.

An examination of HI-WAM skill versus latitude has demonstrated that, for Significant Wave Height and Mean Wave Period, model skill has no considerable correlation with latitude.

7.7 Comparison of Model Skill: HI-WAM versus NOAA Wave Watch III (Sydney)

During the course of this study it became apparent that it would be helpful to determine how other global wave models performed around the Australian coastline for comparison with HI-WAM. The Wave Watch III global model operated in the United States by NOAA (NWWIII) provides freely available modelled wave data around the world on a 1.0° (latitude) by 1.25° (longitude) model grid at 3 hour time steps (8 values per day). The operational subtleties of the NWWIII (i.e. source term techniques) have not been addressed in this study. However, during another research project (Harley, 2009); WRL undertook validation of NWWIII against the same Sydney wave buoy data used in this study, for H_S only. The NWWIII validation was conducted with data from 2004 to 2008 (13, 081 observations); but no spatial interpolation or temporal smoothing was used. The measures of model skill for significant wave height for NWWIII were compared with those from HI-WAM Validation Phases 1 and 2 in Table 7.9. This comparison should be considered preliminary as no effort was made to ensure that fair conditions existed for both models.

Table 7.9
Comparison of Model Skill for Predicting H_S at Sydney: HI-WAM versus NWWIII

Parameter	HI-WAM (Phase 1)	HI-WAM (Phase 2)	NOAA Wave Watch III
Study Duration	March 1997 to February 2008	September 2007 to February 2008	2004 to 2008
N_{obs}	13,464	701	13,081
Bias (m)	- 0.13	- 0.16	- 0.11
R	0.83	0.80	0.88
RMSE (m)	0.45	0.41	0.38
SI	0.26	0.23	0.22

It can be observed that at Sydney, NWWIII appeared to have slightly superior performance over HI-WAM with respect to *Bias*, linear correlation coefficient, Scatter Index and *RMSE*. Most importantly, the *RMSE* of 0.38 m for NWWIII was at least 30 mm less than that of HI-WAM (both in the long term, 0.45 m or the short term, 0.41 m).

Many more extensive tests are required to determine whether HI-WAM or NWWIII provides more skilful model predictions around the Australian coast. These should include checks of Mean Wave Period and Mean Wave Direction, as well as validation in other regions of the Australian coast, particularly those regions in southern Australia exposed to significant wave energy from distant storm systems. Assessment of skill in areas with more complex offshore topography and bathymetry would also be necessary. The Sydney wave buoy is also located in relatively deep water at 85 m; NOAA Wave Watch III would also need to be tested in shallower water depths (15 to 30 m). The coarse model resolution (of

the public domain output data) may mean NWWIII does not perform as skilfully at these depths.

8. CONCLUSIONS AND RECOMMENDATIONS

This study is the first national assessment of the performance of the HI-WAM wave model developed by the Australian Bureau of Meteorology (BoM). The model was validated against wave buoy measurements from 18 locations around Australia over an 11 year period (1997 to 2008). Several major storms were experienced at most wave buoy locations during this time.

This high resolution, modified version of WAM was found to generally reproduce the overall natural variability of the sea state. The contemporary skill of the model was assessed in terms of Significant Wave Height, Mean Wave Period and Wave Direction using only the most recent six months of data (September 2007 to February 2008). For any given location in Australia within the range of water depths tested, HI-WAM wave parameter predictions were found to have a general accuracy (when compared to measured values) as follows:

- Significant Wave Height predictions within ± 0.4 m
- Mean Wave Period predictions within ± 0.9 s
- Wave Direction predictions within ± 10 ° (for H_S greater than or equal to 1 m).

Note that 28 per cent of predictions by HI-WAM for Significant Wave Height and Mean Wave Period and 9 per cent of predictions for Wave Direction were found to lie outside of these general accuracy bands.

During extreme wave events (H_S greater than 3.0 m), considerable systematic differences in wave energy were noted between HI-WAM predictions and the measured data. Wave energy (height and period) was vastly over predicted at only one site, Sydney (NSW), for extreme wave heights but, conversely, energy was under predicted for those sites exposed to full swell in Victoria, Tasmania, South Australia and Western Australia.

While HI-WAM reproduces the overall natural patterns of the Australian climate and is considered to perform very well in moderate wave conditions, predictions for extreme measured wave heights are not considered to be suitable for engineering design purposes.

Further analysis of the HI-WAM model identified several interesting trends in model performance. It was demonstrated that model skill at one representative location (Point Nepean) increased as a function of time (since the wind field descriptions being input into HI-WAM are constantly being improved). It was also shown there is a decrease

in error for Wave Direction with increase in measured H_S (i.e. HI-WAM makes better Wave Direction predictions in more energetic conditions).

Comparisons were also made between HI-WAM model skill and wave buoy depth and latitude (for wave height and period only). It was observed that model skill for Significant Wave Height and Mean Wave Period generally reduces with depth (poorer performance in shallower depths), however, effective results were shown in water depths of 15 to 30 m. An examination of HI-WAM skill versus latitude demonstrated that, for Significant Wave Height and Mean Wave Period, model skill has no considerable correlation with latitude.

Validation of the HI-WAM model could be improved if even more appropriate measured wave period and direction data from wave buoys was acquired. For example, if T_1 could be directly recorded at more buoy sites (rather than converting T_Z records) and if Weighted Mean Wave Direction could be directly measured (rather than Peak Wave Direction). Such an undertaking would remove some uncertainty from the assessment of HI-WAM model performance.

Further to this, although HI-WAM was originally constructed for the purposes of examining sediment mobility on the Australia coast (with parameters Mean Wave Period and Mean Wave Direction), in the future it would be advantageous to also output Peak Wave Period and Peak Wave Direction parameters. These parameters reflect the behaviour of energy at the peak of the spectrum and are more readily comparable with buoy data.

Additional research should also focus explicitly on examining the performance of the HI-WAM model as a function of storm duration. Such an examination would be of interest to see how quickly the model responds to rapidly changing (increasing and decreasing) storms as opposed to more "steady" storms of a longer duration.

More wave buoys need to be deployed around the Australian coast to record wave data. Enormous stretches of coastline remain without measurement instrumentation and satellite altimetry (a large-scale remote sensing alternative) scans at too low a frequency to capture appropriate wave data from short duration storms. HI-WAM and other wave models still do not predict wave heights to a sufficient degree that existing buoys could be taken offline. On the contrary, it is suggested that buoys should be added to the national network to fill measurement gaps in the following regions: East Coast Tasmania, Cape du Couedic (SA) to Esperance (WA) and from Exmouth (WA) to Weipa (Qld) including the Northern Territory. Wave measurements seaward of the Great Barrier Reef are also desired but not a priority.

Finally, it is recommended that further work be undertaken to make a more robust comparison of model performance between HI-WAM and NOAA Wave Watch III around the Australian coast (the most current version of NWWIII at the time of writing was version 3.14; released in May 2009). If HI-WAM is shown to be a superior wave model for Australian conditions, public access to the output data would be a great asset to the coastal engineering community. If this is not the case, and NOAA Wave Watch III generates better wave predictions than HI-WAM for all wave parameters; BoM ought to consider further modifications to the HI-WAM physics or ceasing WAM application and developing a high resolution, open source licence of Wave Watch III with Meso-LAPS wind fields for all its wave modelling.

9. ACKNOWLEDGEMENTS

The author wishes to express gratitude to a number of people for their assistance with this project.

To Dr William Peirson for his invaluable advice and insightful guidance through this research. His time spent in careful review of all aspects of the work is very much appreciated.

To Dr Diana Greenslade without whom this project would not be possible. Her proposal for this research and ongoing enthusiasm for the results generated were most beneficial. Thanks should also be extended to the Australian Bureau of Meteorology for allowing me access to the HI-WAM model outputs and wave data from two of their buoys.

Several colleagues at WRL also deserve credit for their input to the study: James Carley, Matt Blacka, Duncan Rayner, Conrad Wasko, Dr Bruce Cathers, Dr Mitchell Harley Wendy Thomason-Harper and Caroline Hedges.

Special thanks are extended to each individual and organisation that provided me with wave buoy data for this project and patiently dealt with ongoing technical queries: to Jim Waldron and Catherine Acworth at Queensland Government Hydraulics Laboratory (DERM), Mark Kulmar and Benjamin Modra at Manly Hydraulics Laboratory (NSW DSTA), Mark Spykers at Gippsland Ports, Ray Rice at Cardno Lawson Treloar, Esso Australia, Paul Downie at the Port of Melbourne, Alec Millett at Fremantle Ports, Grant Ryan at Tremarfon and Reena Lowry at the Western Australian Department of Transport.

Satellite imagery reproduced in Figures 4.01, 5.01 through 5.13 and 7.51 through 7.56 was provided courtesy of Google Earth ™ version 5.01.

Finally, the author would like to thank his family for their ongoing support and encouragement: Ross, Therese, Janine, John and Robyn. Thanks also to Neil and Mary for generously allowing much of this work to be carried out in their house in Mount Victoria. Most gratefulness is reserved for Cat; for bearing this charge together.

10. REFERENCES

Airy, G B (1845), "Tides and Waves", Mixed Sciences 3, Encyclopaedia Metropolitana, London.

Bender, L C and Leslie, L M (1994), *Evaluation of a Third Generation Wave Model for the Australian Region*, BMRC Research Report 43, Australian Bureau of Meteorology, Melbourne, Victoria, Australia, pp 1-77.

Bender, L C (1996), "Modification of the Physics and Numerics in a Third-Generation Ocean Wave Model", *Journal of Atmosphere and Oceanic Technology*, Volume 13, pp 726-750.

Bettington, S H and Wilkinson, D L (1997), "Extreme Water Surface Excursions During Storm Events", *Australasian Coasts and Ports Conference*, Christchurch.

Booij, N, Ris, C and Holthukisen, L H (1999), "A Third-Generation Wave Model for Coastal Regions", Part 1 – Model Description and Validation, *Journal of Geophysical Research*, Volume 104, pp 7649 – 7666.

Bowers, J A, Morton, I D and Mould, G I (2000), "Directional Statistics of the Wind and Waves", *Applied Ocean Research*, Volume 22, Issue No. 1, pp. 13-30.

Borgman, L E (1969), "Directional Spectra Models for Design Use", *Proceedings of the Offshore Technology Conference*, Paper No. OTC 1069, pp. 721-746.

Bretschneider, C L (1952), "Revised Wave Forecasting Relationships", *Proceedings of the 2nd Conference on Coastal Engineering*, ASCE, Council on Wave Research.

Buchanan, C, "A Gridded Bathymetric Data Set", *Unpublished Manuscript*, Australian Geological Survey Organisation.

Carter, D J T (1982), "Prediction of Wave Height and Period for a Constant Wind Velocity using the JONSWAP Results", *Journal of Coastal Engineering*, Volume 9, pp 17-33.

Cook, R D, Malkus, D S and Plesha, M E (1989), *Concepts and Applications of Finite Element Analysis,* John Wiley & Sons, Canada, 3rd Edition, p 99.

Fisher, N I and Lee, A J (1983), "A Correlation Coefficient for Circular Data", *Biometrika*, Volume 70, Issue 2, pp. 327-332.

Fisher, N I (1993), *Statistical Analysis of Circular Data*, Cambridge University Press, Cambridge, UK, pp. 88-93 and 151-153.

Gorman, R M and Stephens, S A (2003), "The New Zealand Wave Climate Derived from Buoy, Satellite and Hindcast Data", *Australasian Coasts and Ports Conference,* Auckland.

Harley, M (2009), Personal Correspondence, Wave Watch III Model Skill for Sydney Waverider Buoy.

Greenslade, D J M (2000), "Upgrades to the Bureau of Meteorology's Ocean Wave Forecasting System", *BMRC Research Report No. 79*, Bureau of Meteorology: Australia.

Hasselmann, K (1962), "On the Non-Linear Energy Transfer in a Gravity-Wave Spectrum, Part 1: General Theory", *Journal of Fluid Mechanics*, Volume 12, pp 481-500.

Hasselman, K, Barnett, T P, Bouws, E, Carlson, D E and Hasselmann, P (1973), "Measurements of wind-wave growth and swell decay during the Joint North Sea Wave Project (JONSWAP)", *Deutsche Hydrographische Zeitschrift*, Volume 8, Number 12.

Hasselmann, S and Hasselmann, S (1981), "A Symmetrical Method of Computing the Non-Linear Transfer in a Gravity-Wave Spectrum", *Hamburger Geophysical Einzelschriften*, Serie A 52, p 138.

Hasselmann, S, Hasselmann, K, Allender, J H. and Barnett, T.P. (1985), "Computations and Parameterizations of the Nonlinear Energy Transfer in a Gravity Wave Spectrum, Part 2: Parameterizations of the Nonlinear Energy Transfer for Application in Wave Models", *Journal of Physical Oceanography*, Volume 15, pp 1378-1391.

Hemer, M A, Church, J A and Hunter, J R (2007), "Waves and Climate Change on the Australian Coast", *Journal of Coastal Research Special Issue 50 (Proceedings of the 9th International Coastal Symposium)*, pp 432-437, Gold Coast, Australia.

Janssen, P A E M and Bidlot, J R (2003), *Part VII: ECMWF Wave-Model Documentation*, IFS Documentation Cycle CY23R4, September.

Janssen, P A E M (2004), *The Interaction of Ocean Waves and Wind*, Cambridge University Press, Cambridge, UK.

Kuik, A J, Vledder, G and Holthuijsen, L H (1988), "A Method for the Routine Analysis of Pitch and Roll Wave Buoy Data", *Journal of Physical Oceanography*, Volume 18, pp. 1020-1034.

Komen, G J, Cavaleri, L, Donelan, M, Hasselmann, K, Hasselmann, S and Janssen, P A E M (1994), *Dynamics and Modelling of Ocean Waves*, Cambridge University Press, Cambridge, UK.

Komen, G J (2004), "The Wave Modelling (WAM) Group: A Historical Perspective", *16th BMRC Modelling Workshop*, Melbourne.

Kumar, V S and Anand, N M (2004), "Variations in Wave Direction estimated using First and Second Order Fourier Coefficients", *Journal of Coastal Engineering*, Volume 31, pp 2105-2119.

Liu, P C, Schwab, D J and Jensen, R E (2002), "Has Wind-Wave Modeling Reached its Limit?", *Ocean Engineering*, Volume 29, pp 81-98.

Longuet-Higgins, M S (1957), "The Statistical Analysis of a Random, Moving Surface", *Philosophical Transactions of the Royal Society*, Series A, Volume 249, pp 321-387.

Longuet-Higgins, M S (1962), "The Distribution of Intervals between Zeros of Random Function", *Philosophical Transactions of the Royal Society*, Series A, Volume 254, pp 557-599.

Longuet-Higgins, M S, Cartwright, D E and Smith, N D (1963), "Observations of the Directional Spectrum of Sea Waves using Motions of a Floating Buoy", *Ocean Wave Spectra*, Prentice Hall, pp. 111-136.

Miles, J W (1957), "On the Generation of Surface Waves by Shear Flows", *Journal of Fluid Mechanics*, Volume 3, pp 185-204.

Miller, M J, and Pearce, R P (1974), "A Three Dimensional Primitive Equation Model of Cumulonimbus Convection", *Quarterly Journal of the Royal Meteorological Society*, Volume 100, pp 133-154.

Moon, I-J, Ginis, I, Hara, T, Tolman, H, Wright, C W and Walsh, E J (2003), "Numerical Simulation of Sea-Surface Directional Wave Spectra under Hurricane Wind Forcing", *Journal of Physical Oceanography*, Volume 33, pp 1680-1706.

Phillips, O M (1957), "On the Generation of Waves by Turbulent Wind", *Journal of Fluid Mechanics*, Volume 2, pp 417-445.

Porter-Smith, R, Harris, P T, Anderson, O, Coleman, R, Greenslade, D J M and Jenkins, C J (2004), "Classification of the Australian Continental Shelf based on Predicted Sediment Threshold Exceedance from Tidal Currents and Swell Waves", *Marine Geology*, Volume 211, pp 1-20

Schulz, E W, Kepert, J D and Greenslade, D J M (2007), "An Assessment of Marine Surface Winds from the Australian Bureau of Meteorology Numerical Weather Prediction Systems," *Weather and Forecasting*, Volume 22, No. 3, pp 609 – 632.

Snyder, R L, Dobson, F W, Elliot, J A and Long, R B (1981), "Array Measurements of Atmospheric Pressure Fluctuations above Surface Gravity Waves", *Journal of Fluid Mechanics*, Volume 102, pp 1-59.

Stokes, G G (1847), "On the Theory of Oscillatory Waves", *Transactions of the Cambridge Philosophical Society,* No. 8, pp 441–455.

Sverdrup, H V and Munk, W H (1944a), "Wind Waves and Swell: Principles in Forecasting", Hydrographic Office, US Navy, Miscellaneous 11, 275.

Sverdrup, H V and Munk, W H (1944b), "Breakers and Surf: Principles in Forecasting", Hydrographic Office, US Navy, Publication No. 235.

Tracy, B A (2002), "Directional Characteristics of the 1990-1999 Wave Information Studies Gulf of Mexico Hindcast", *7th International Workshop on Wave Hindcasting and Forecasting*, October 21-25, Banff, Alberta, Canada.

Tucker, M J (1991), *Waves in Ocean Engineering: Measurement, Analysis, Interpretation*, Ellis Horwood Limited, England, 1st Edition, pp 51 and 112.

United States National Geophysical Data Center (1998), "Digital relief of the Surface of the Earth", Data Announcement 88-MGG-02, NOAA, Boulder, Colorado, USA.

U.S. Army Corps of Engineers (2006), *Coastal Engineering Manual*, EM 1110-2-1100, Part II: Chapter 1, p 87.

WAMDI Group (Hasselmann, S, Hasselmann, K, Bauer, E, Janssen, P A E M., Komen, G, Bertotti, L, Lionello, P, Guillaume, A, Cardone, V C, Greenwood, J A, Reistad, M, Zambresky, L and Ewing, J A) (1988), "The WAM model – A Third Generation Wave Prediction Model", *Journal of Physical Oceanography*, Volume 18, pp 1775-1810.

Van Vledder, G Ph. (1990), "Directional Response of Wind Waves to Turning Wind", Faculty of Civil Engineering, Delft University of Technology, Report No. 90-2, The Netherlands.

Womersley, T (2008), "Analysis of 40 Years of Simulated Victorian Wave Climate and Coastal Processes", Department of Civil and Environmental Engineering, UNSW, Masters Degree: Minor Thesis Project.

Wu, J (1982), "Wind-Stress Coefficients over Sea Surface from Breeze to Hurricane", *Journal of Geophysical Research*, Volume 87, pp 9704-9706.

Young, I R (1999), *Wind Generated Ocean Waves*, Elsevier Ocean Engineering Book Series: Volume 2, Elsevier Science Ltd, Oxford, UK.

Young, I R, Hasselmann, S and Hasselmann, K (1987), "Computations of the Response of a Wave Spectrum to a Sudden Change in Wind Direction", *Journal of Physical Oceanography*, Volume 17, pp 1317–1338.

HI-WAM MODEL DOMAIN

Figure 4.01

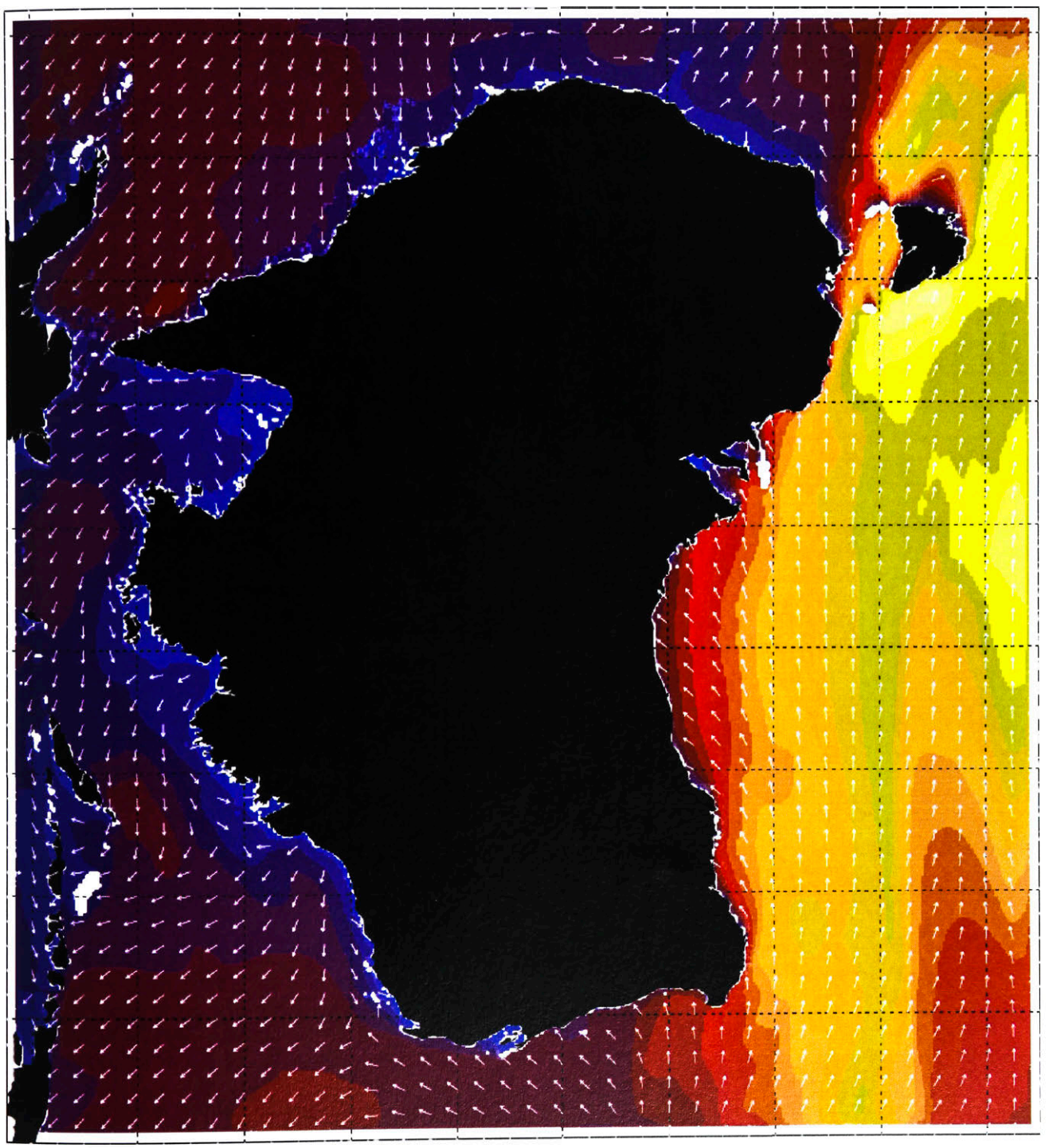

WRL Report No. 237	EXAMPLE HI-WAM MODEL OUTPUT FOR H_S AND DIRECTION 18:00 GMT, 8TH AUGUST, 2007 (WAVE PERIOD NOT SHOWN)	Figure 4.02

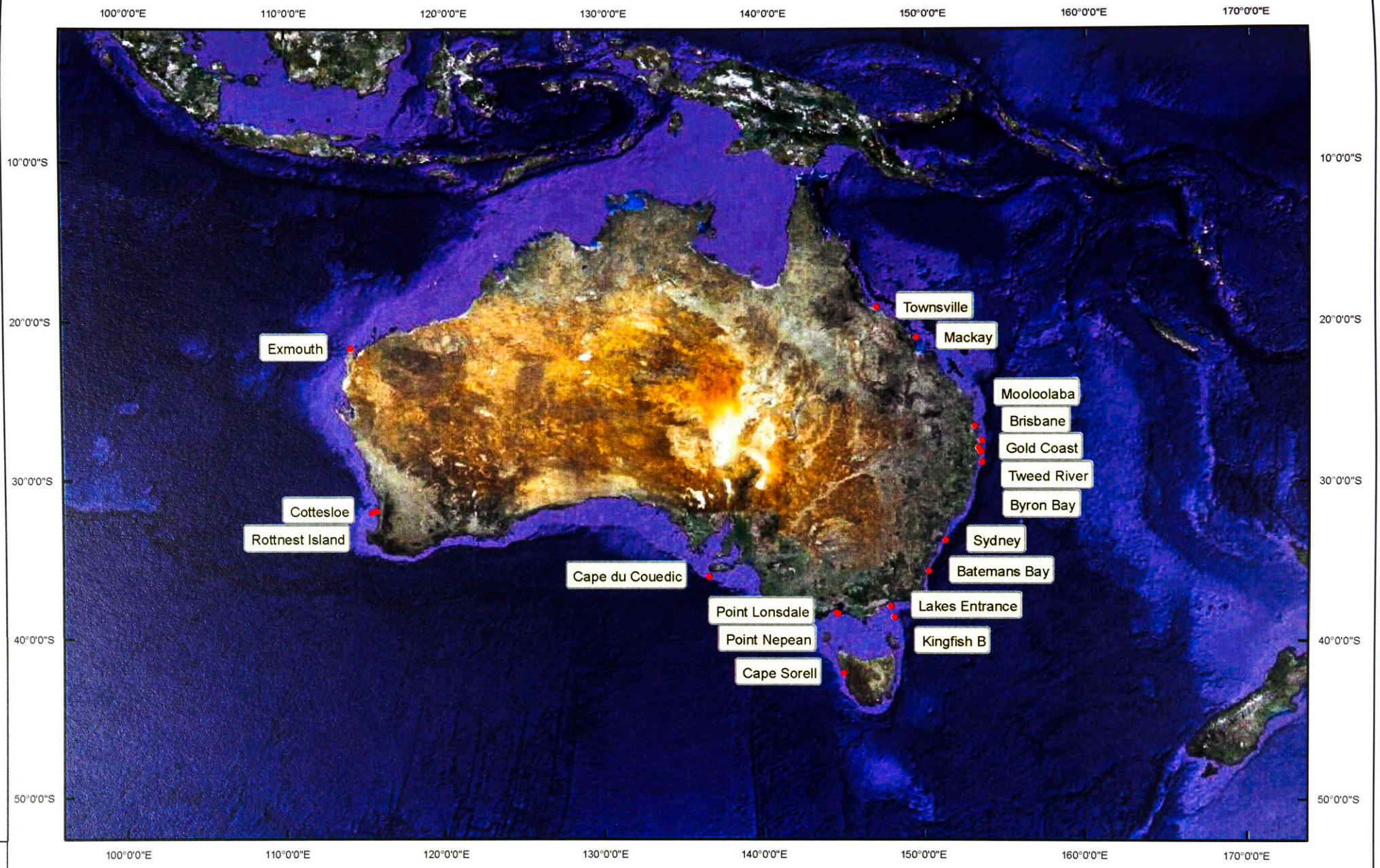

WAVE MEASUREMENT SITES AROUND AUSTRALIAN COAST

Figure 5.01

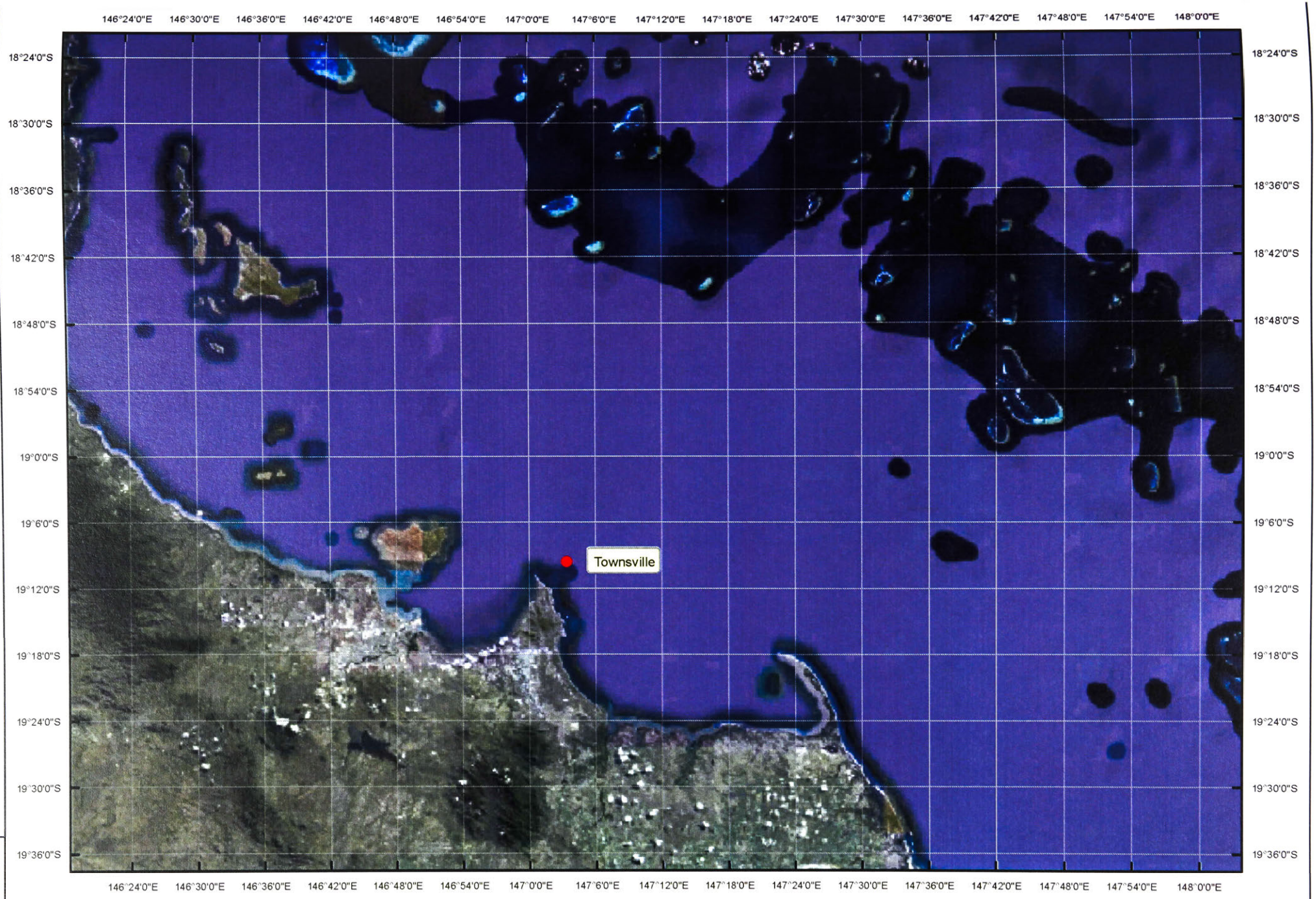

WRL

Report No. 237

TOWNSVILLE WAVE BUOY LOCATION

Figure 5.02

WRL

eport No. 237

MACKAY WAVE BUOY LOCATION

Figure 5.03

WRL

Report No. 237

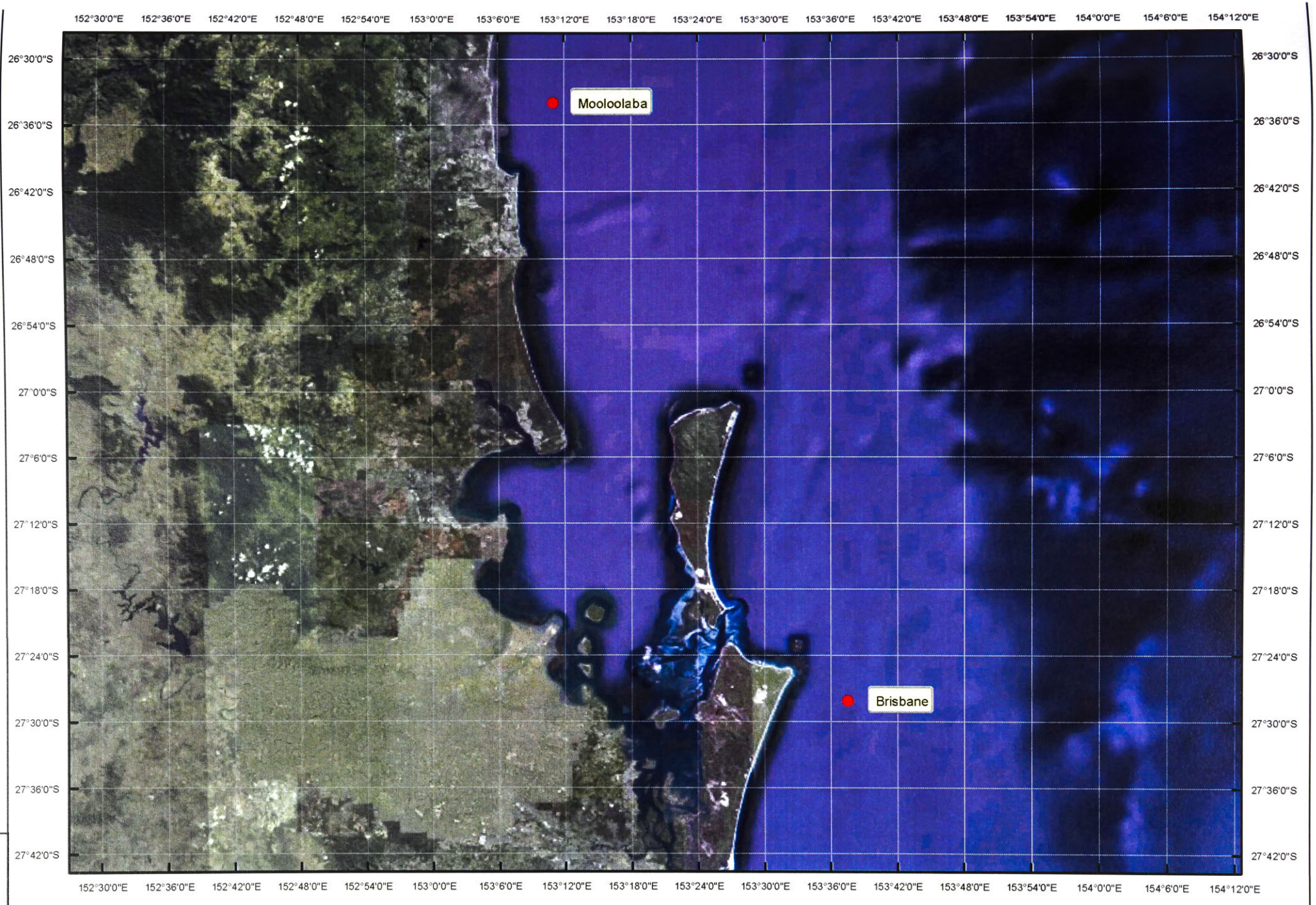

MOOLOOLABA AND BRISBANE WAVE BUOY LOCATIONS

Figure 5.04

WRL

eport No. 237

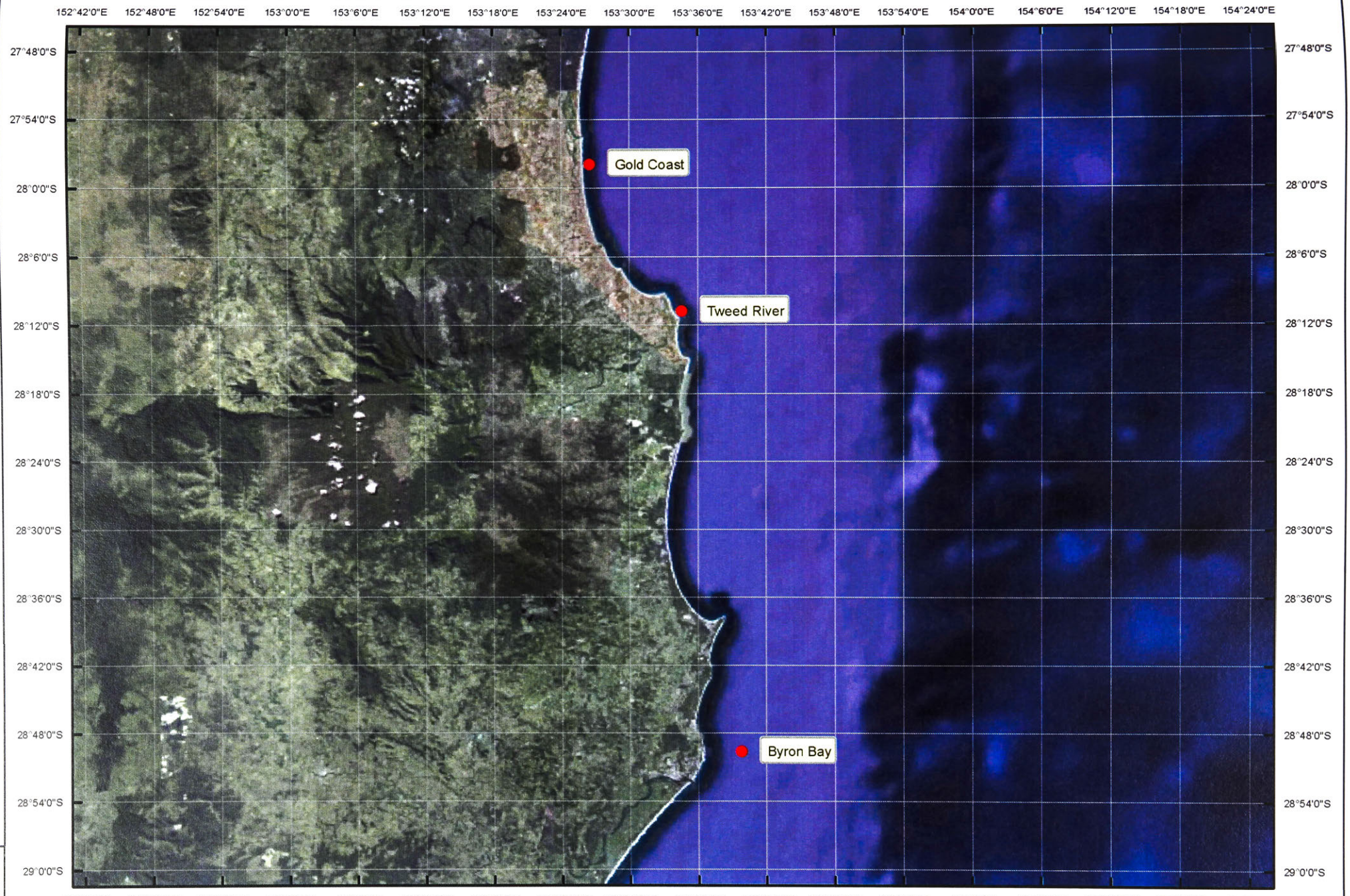

GOLD COAST, TWEED RIVER AND BYRON BAY
WAVE BUOY LOCATIONS

Figure 5.05

WRL

Report No. 237

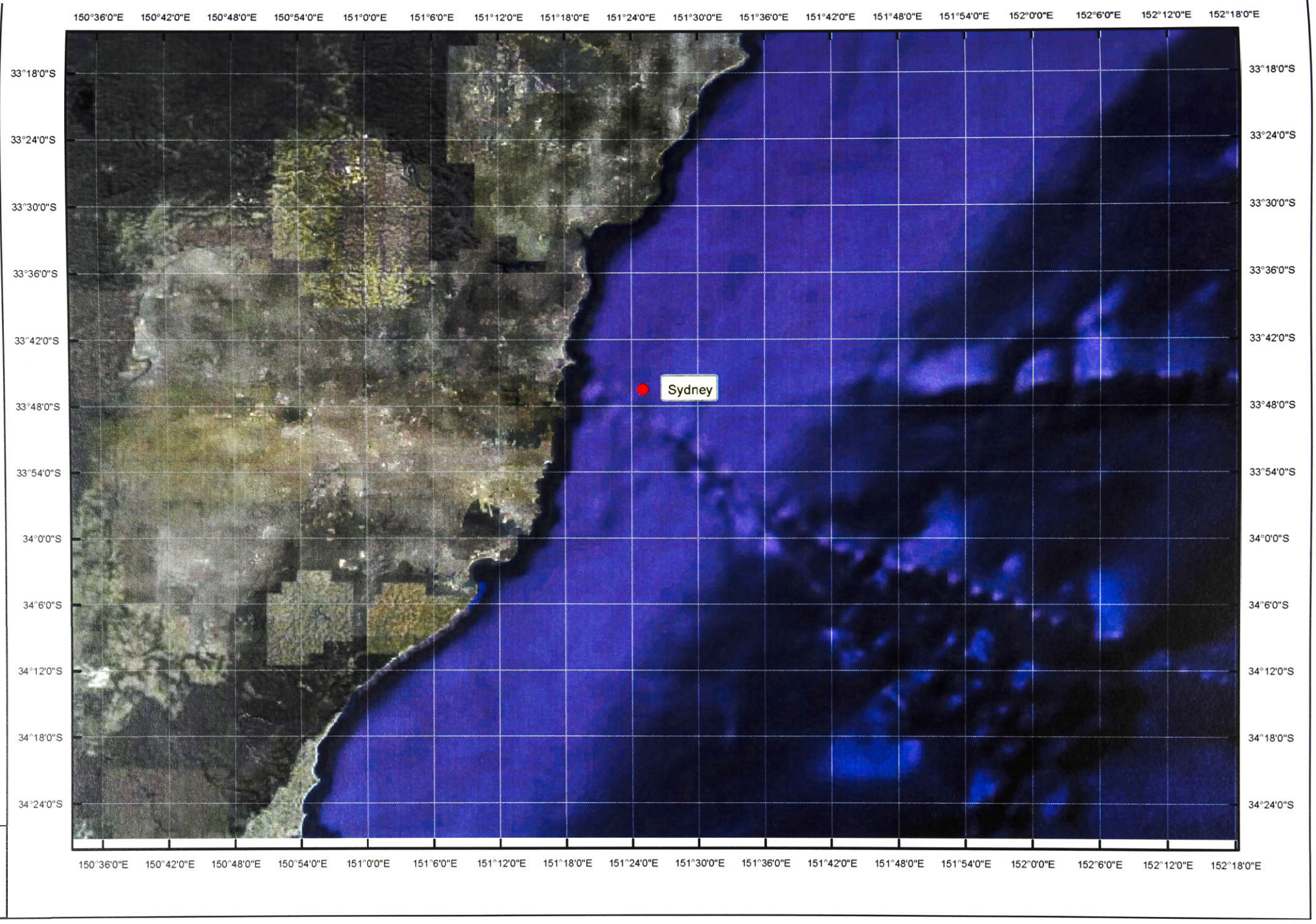

SYDNEY WAVE BUOY LOCATION

Figure 5.06

WRL

eport No. 237

BATEMANS BAY WAVE BUOY LOCATION

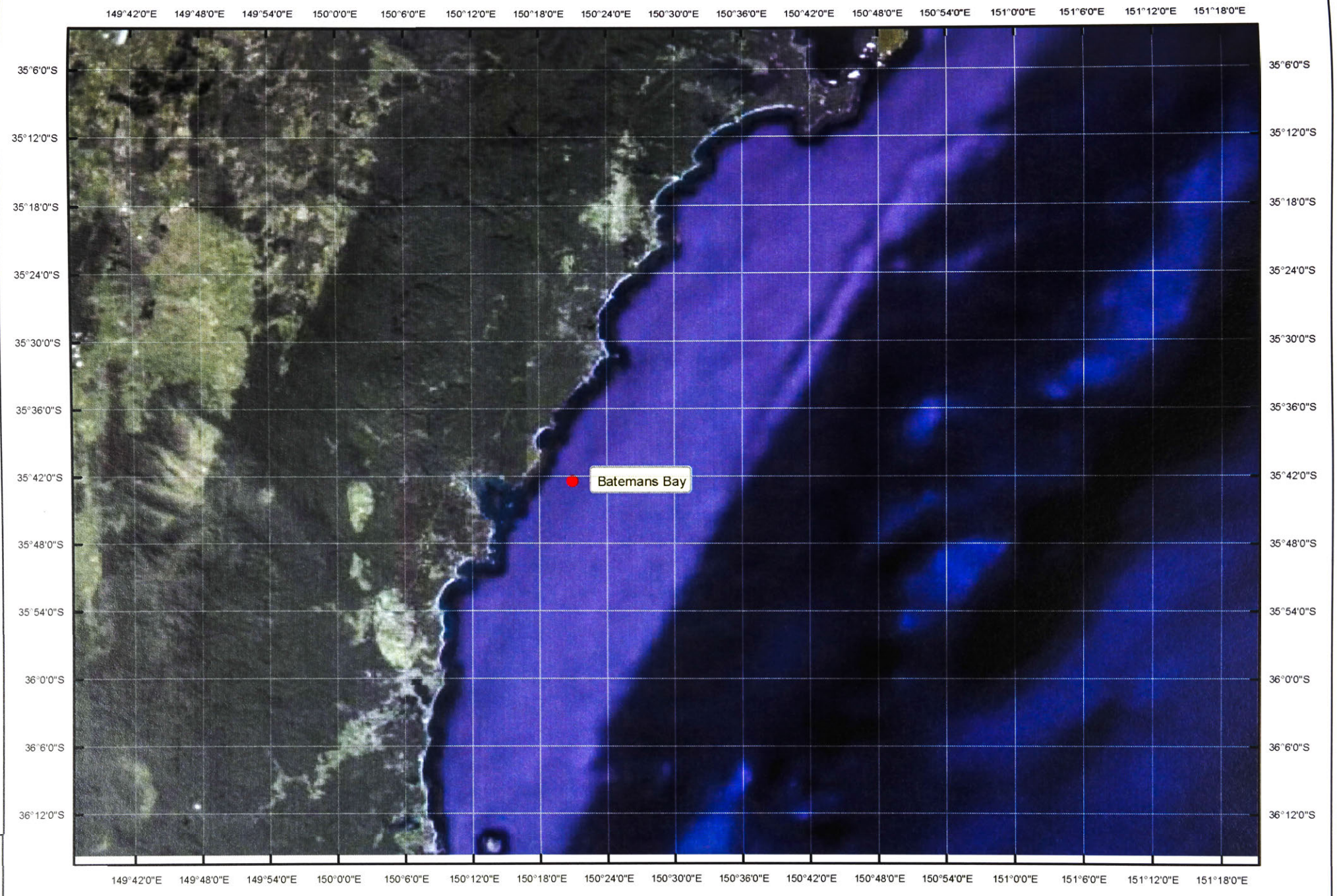

Figure 5.07

WRL

Report No. 237

LAKES ENTRANCE AND KINGFISH B WAVE BUOY LOCATIONS

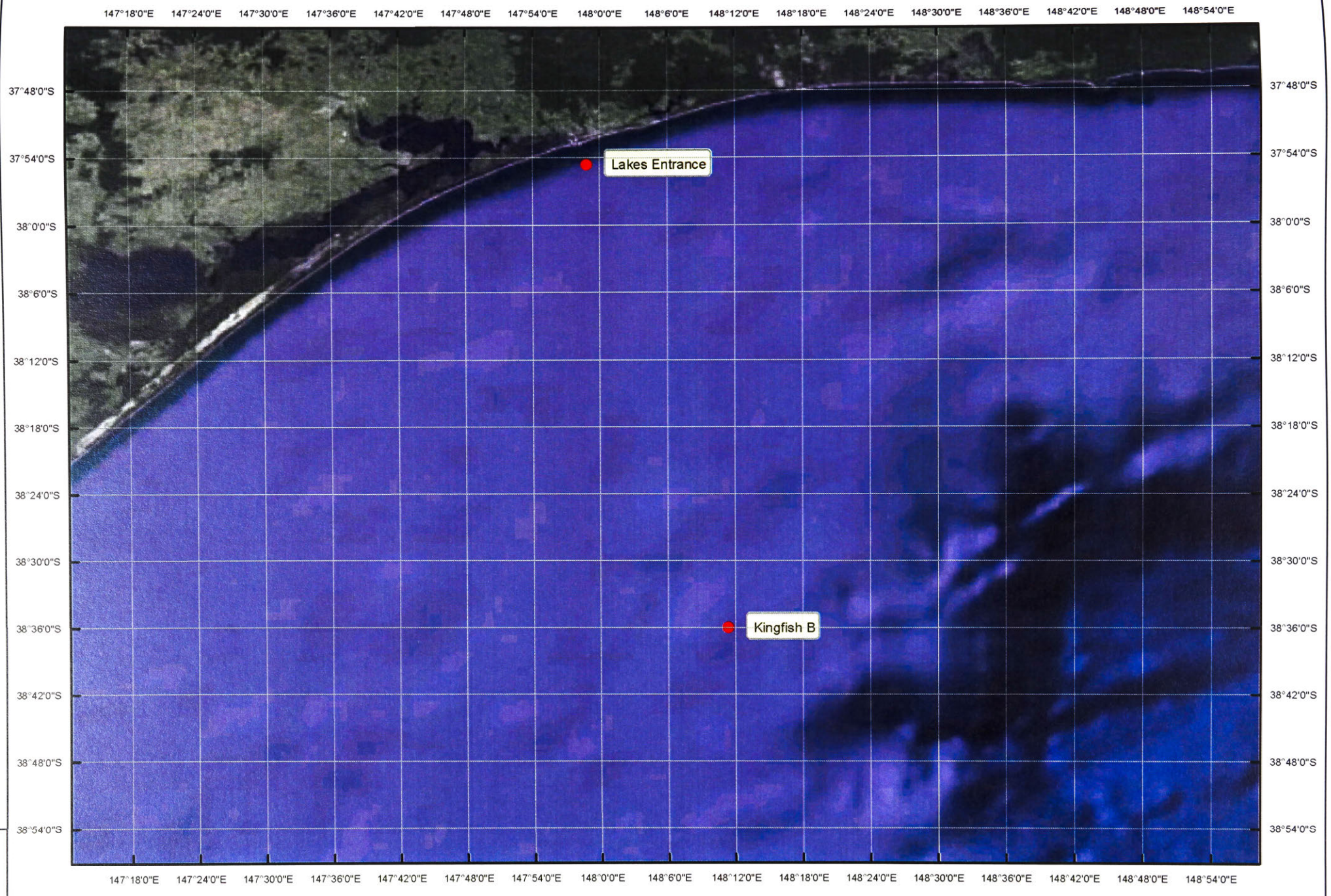

Figure 5.08

WRL

Report No. 237

POINT NEPEAN AND POINT LONSDALE WAVE BUOY LOCATIONS

Figure 5.09

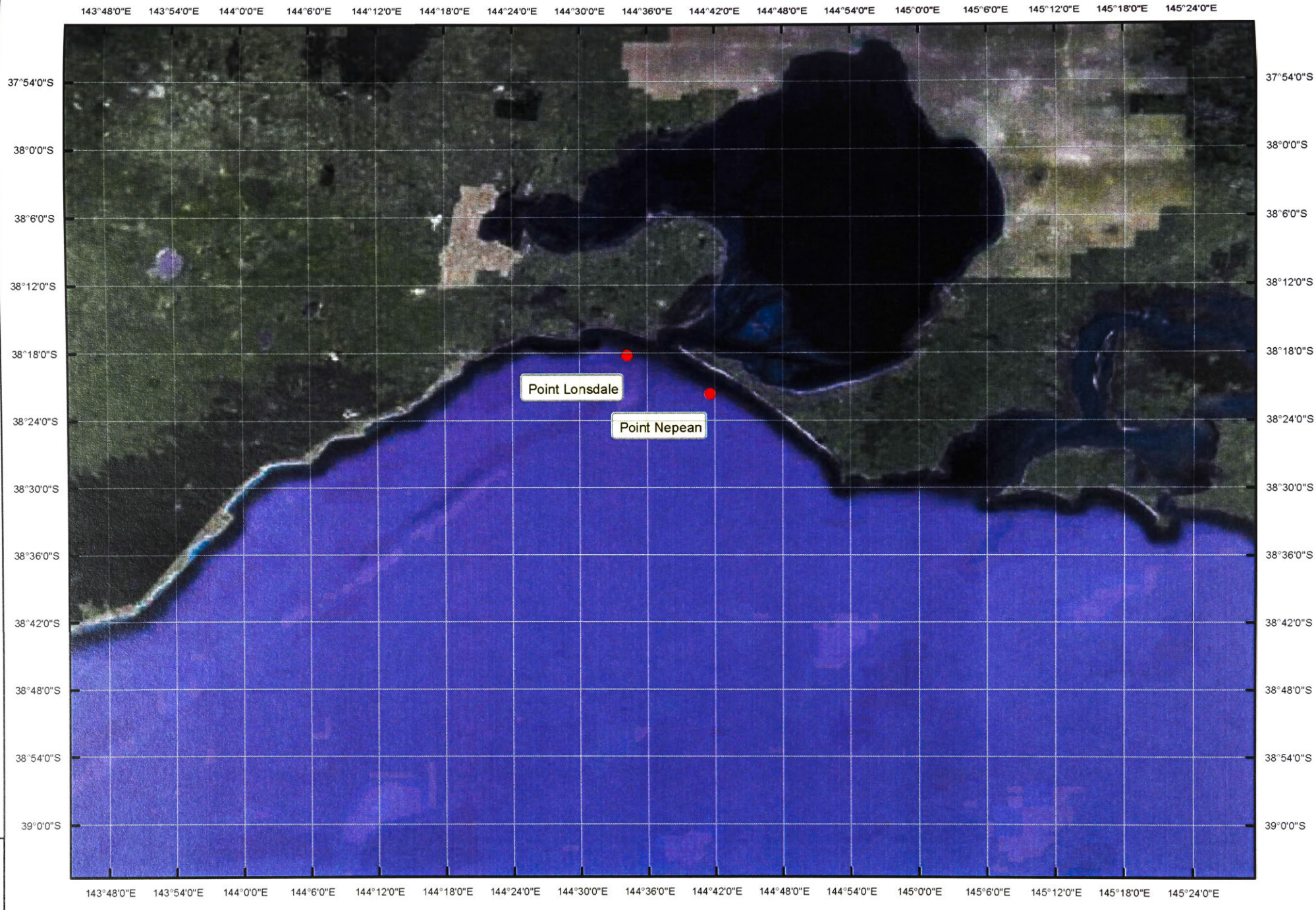

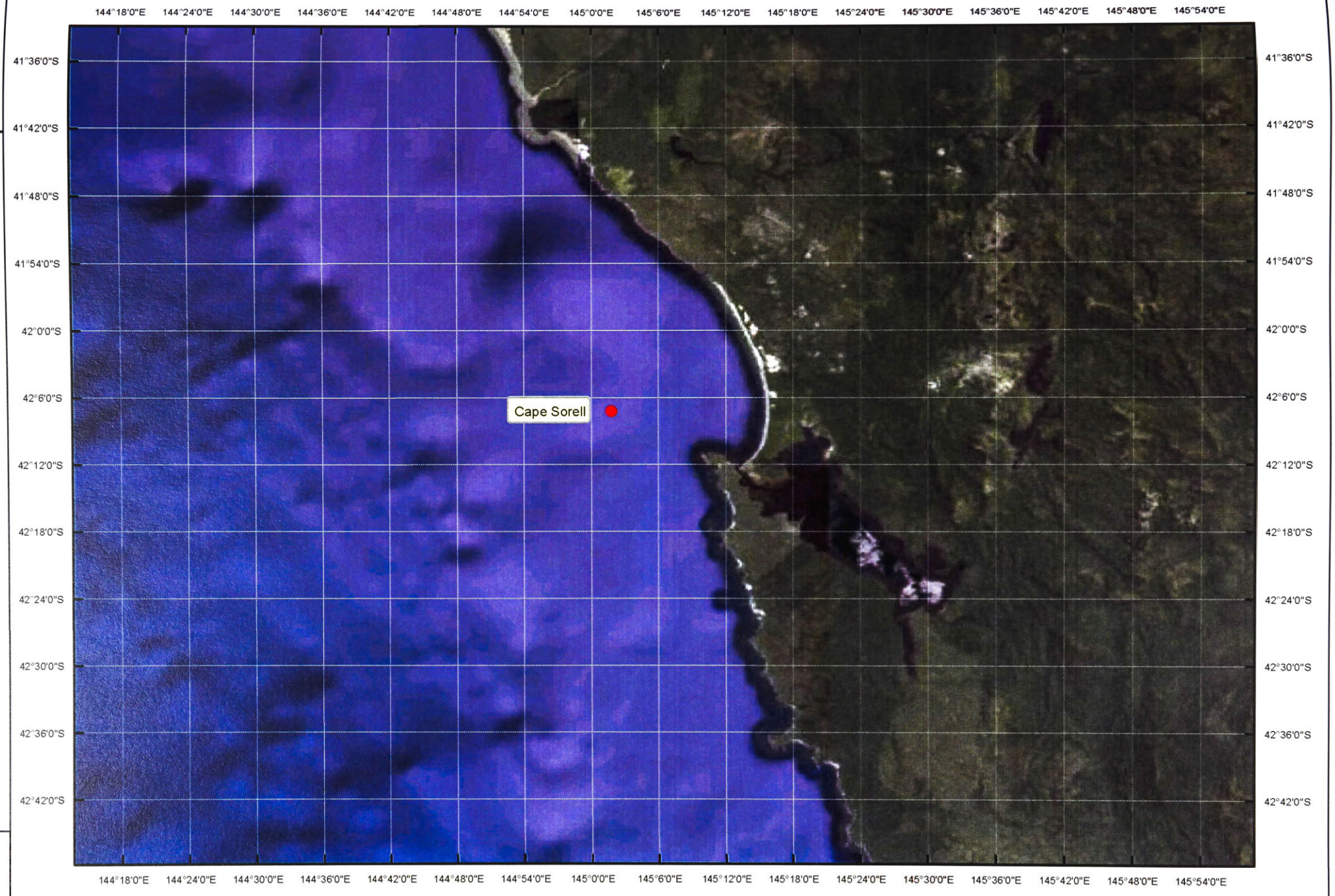

CAPE SORELL WAVE BUOY LOCATION

Figure 5.10

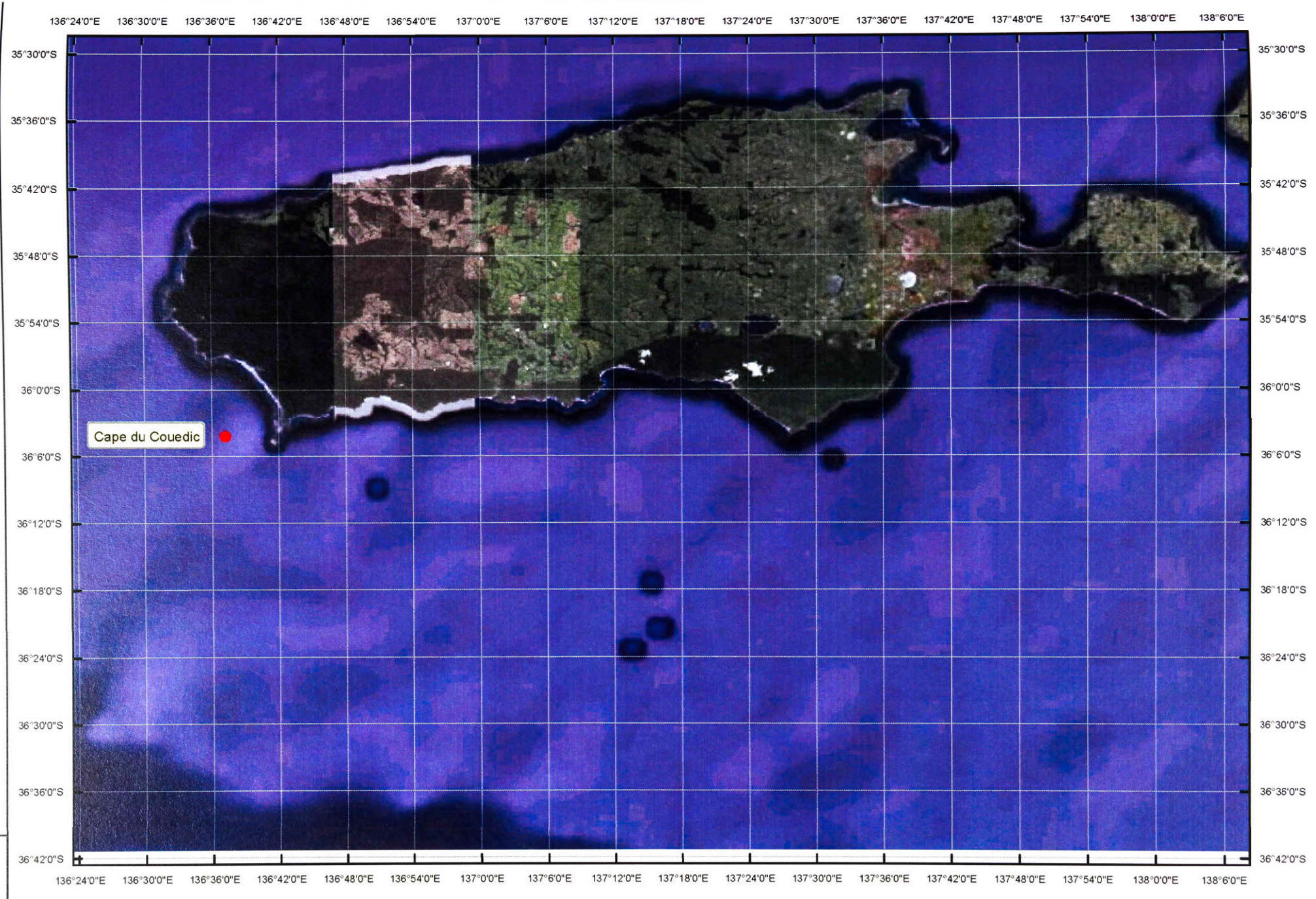

CAPE DU COUEDIC WAVE BUOY LOCATION

Figure 5.11

WRL

Report No. 237

COTTESLOE AND ROTTNEST ISLAND WAVE BUOY LOCATIONS

Figure 5.12

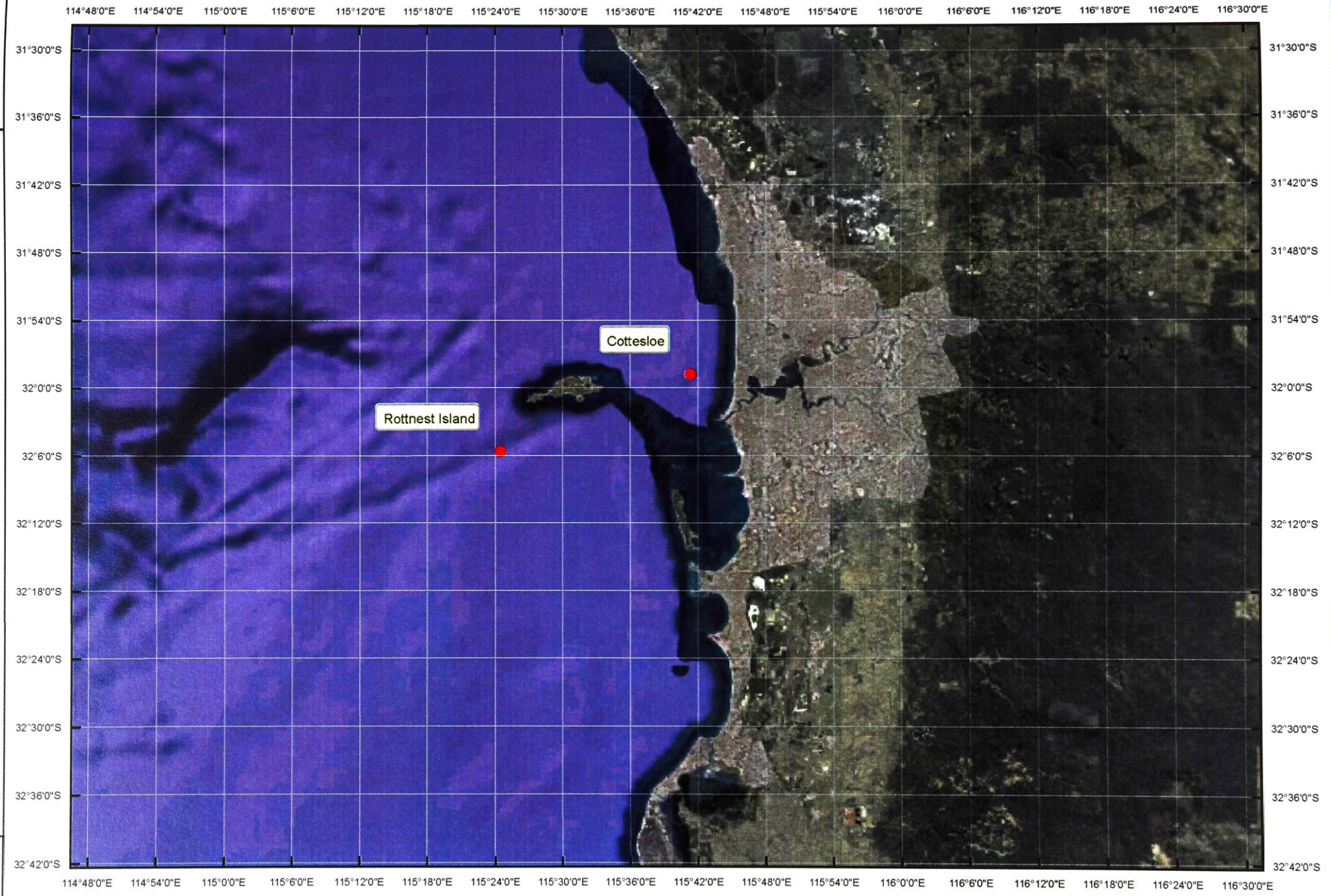

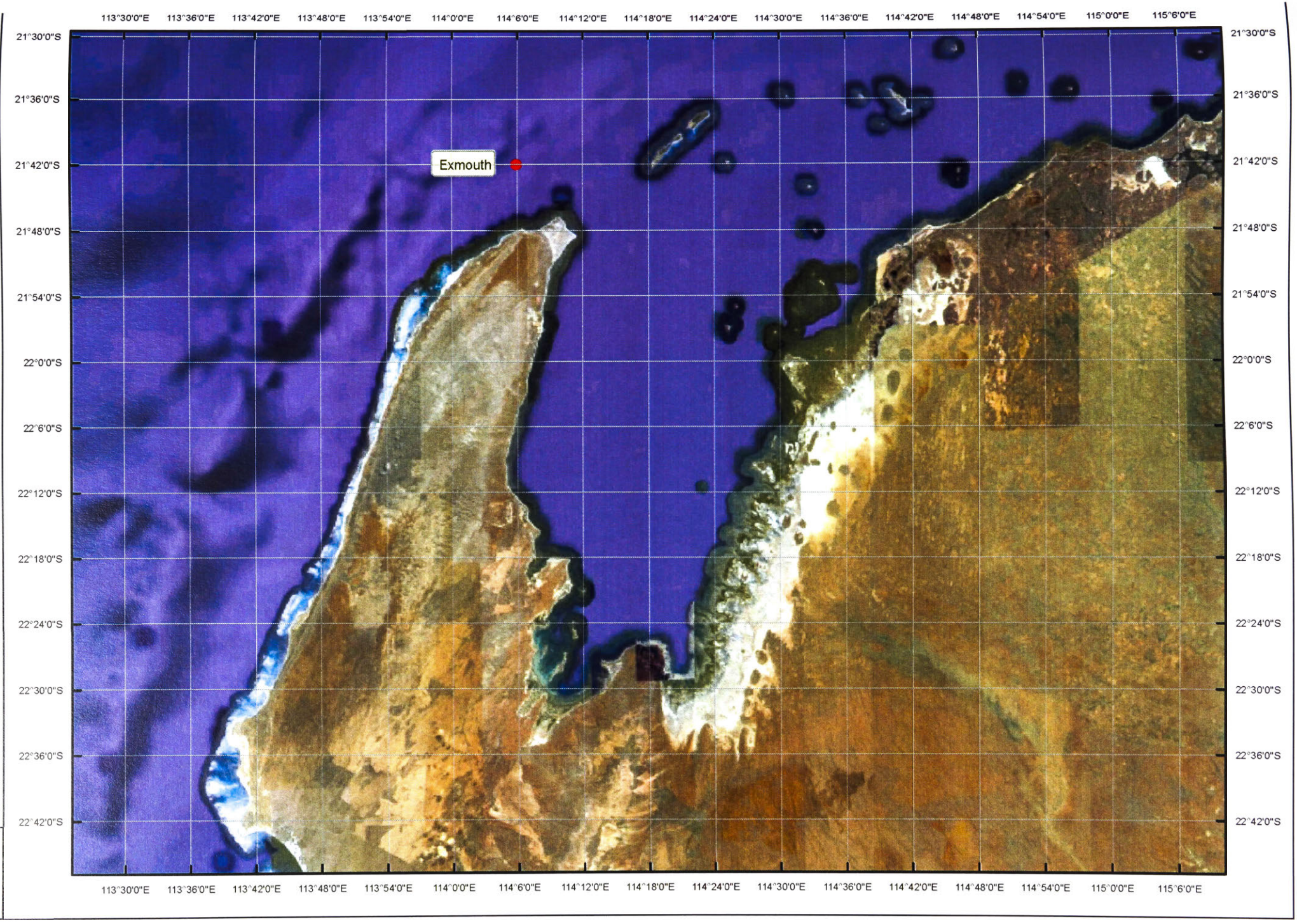

EXMOUTH WAVE BUOY LOCATION

Figure 5.13

KEY

- HI-WAM "Ocean" Grid Point
- HI-WAM "Land" Grid Point (Model Boundary)
- Wave Buoy Location

1. Interpolation with Four "Ocean" Grid Points

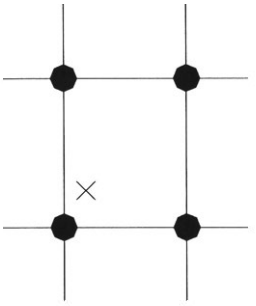

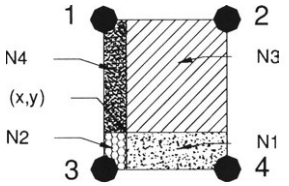

$$\phi(x, y) = N_1\phi_1 + N_2\phi_2 + N_3\phi_3 + N_4\phi_4$$

N_x are fractions of the area of the grid cell.

2. Interpolation with Three "Ocean" Grid Points (Wave Buoy Inside Triangle)

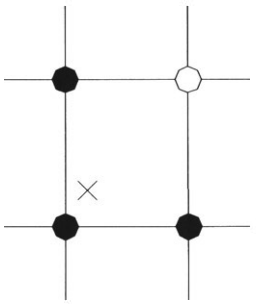

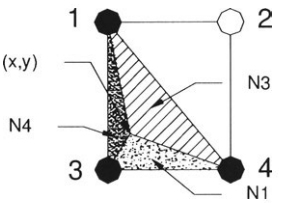

$$\phi(x, y) = N_1\phi_1 + N_3\phi_3 + N_4\phi_4$$

N_x are fractions of the area of the triangle.

3. Simplification with Three "Ocean" Grid Points (Wave Buoy Outside Triangle)

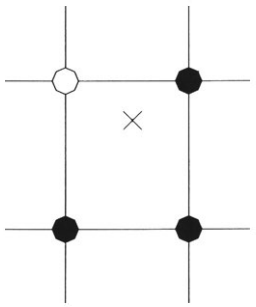

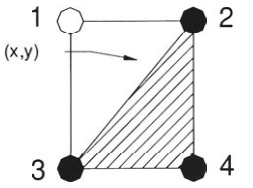

$$\phi(x, y) = \phi_2$$

The closest "ocean" grid point value is assumed (Point 2 in this example).

WRL Report No. 237	THREE INTERPOLATION TECHNIQUES FOR MODEL GRID	Figure 6.01

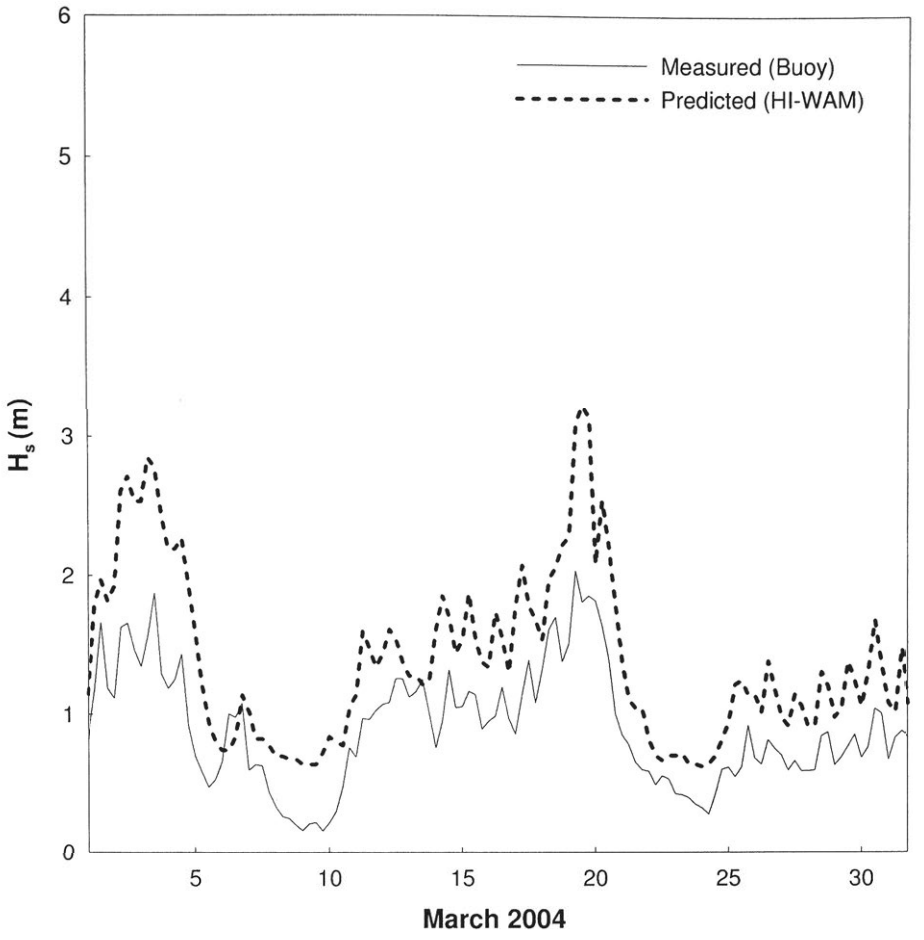

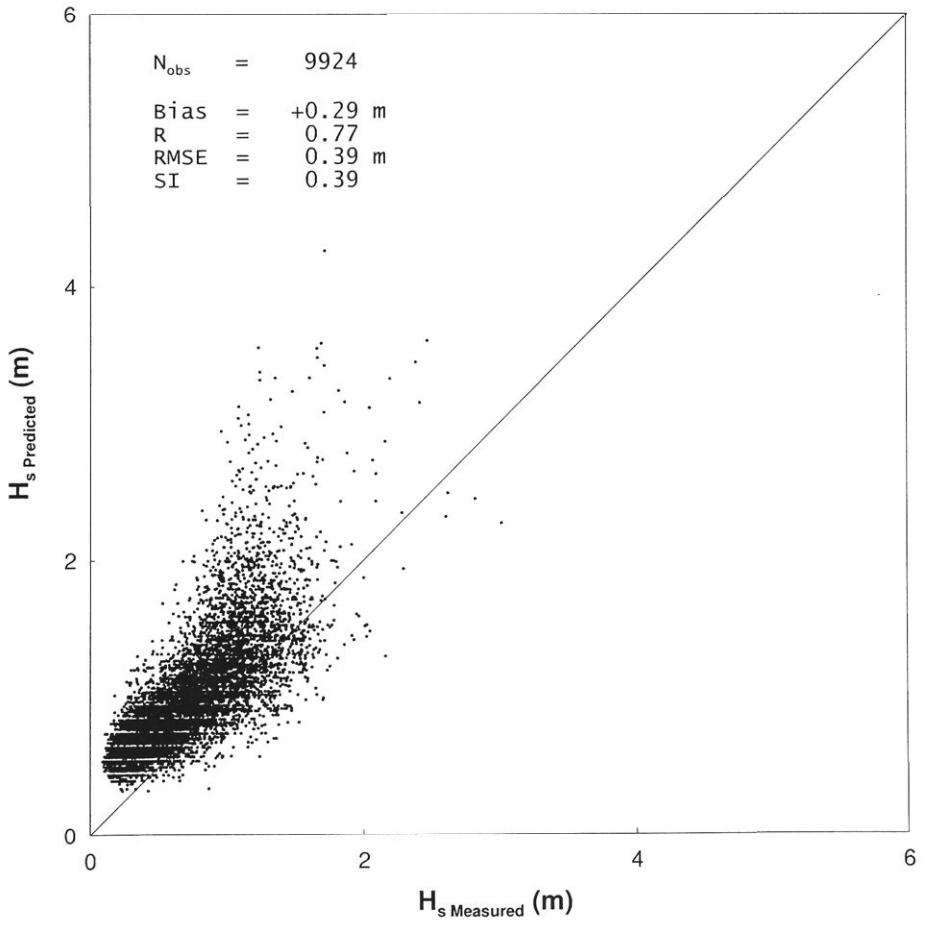

WRL Report No. 237	COMPARISON OF MEASURED & PREDICTED H_s VALUES TOWNSVILLE, QUEENSLAND	Figure 7.01

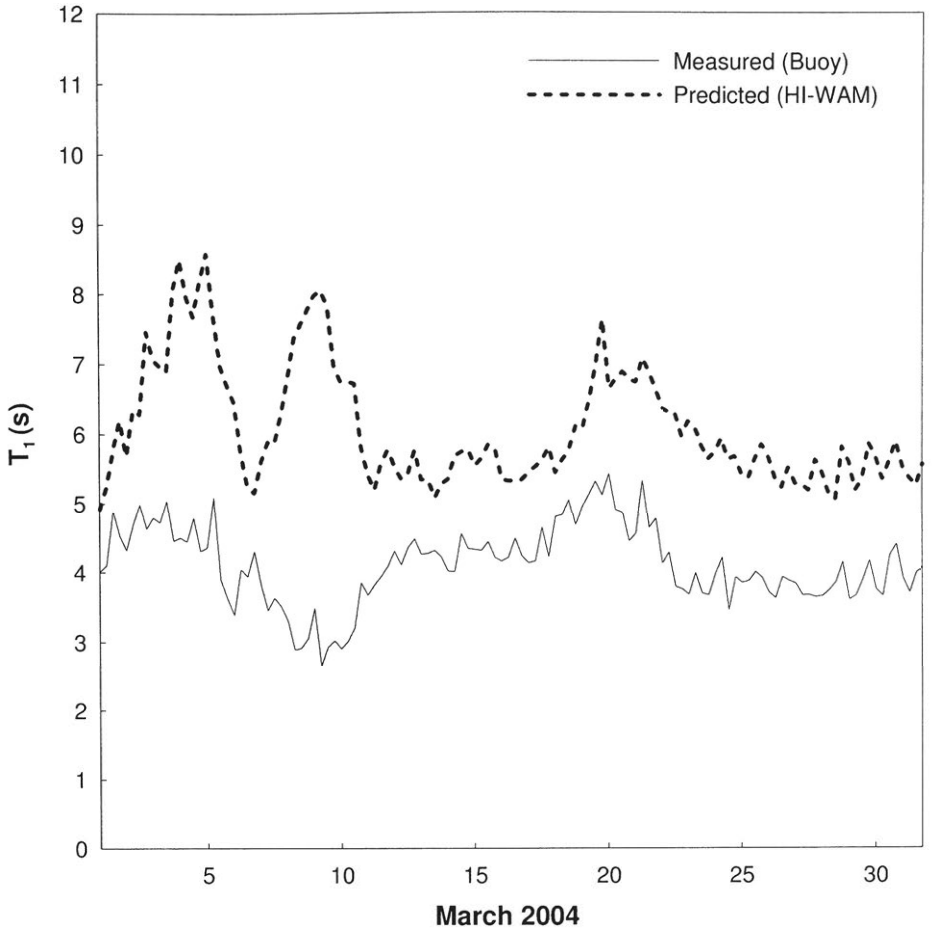

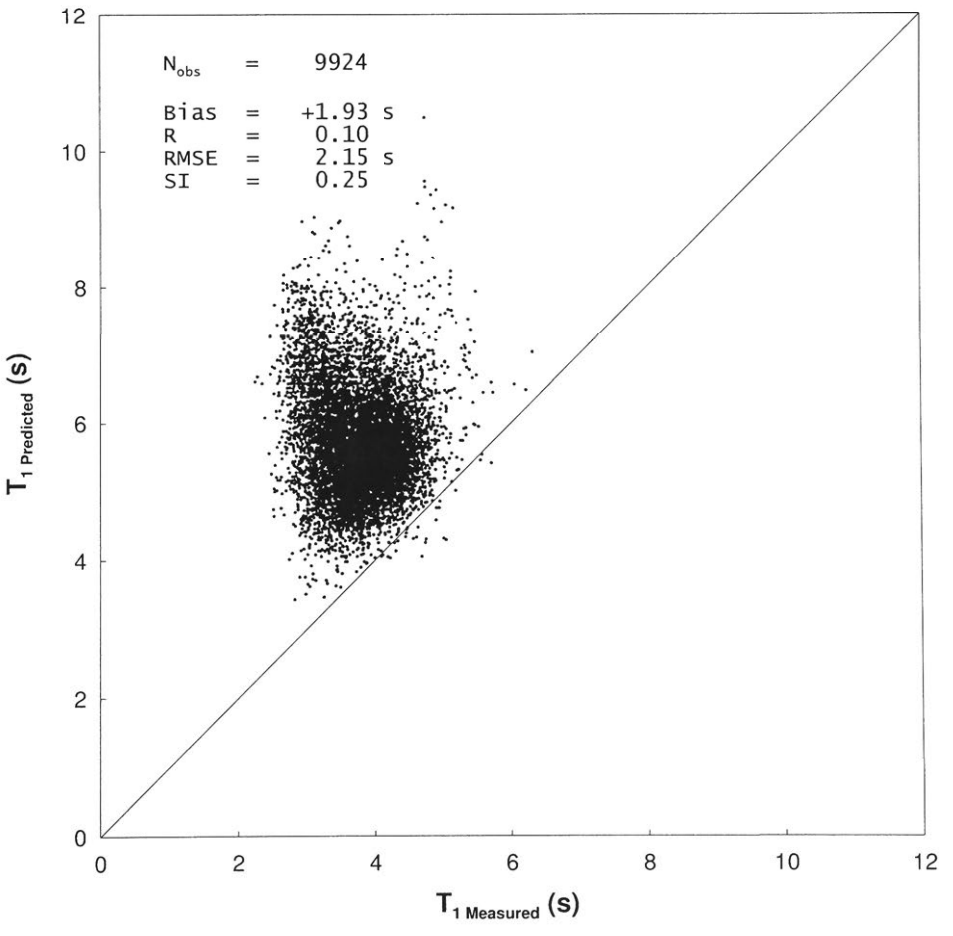

WRL
Report No. 237

COMPARISON OF MEASURED & PREDICTED T_1 VALUES
TOWNSVILLE, QUEENSLAND

Figure
7.02

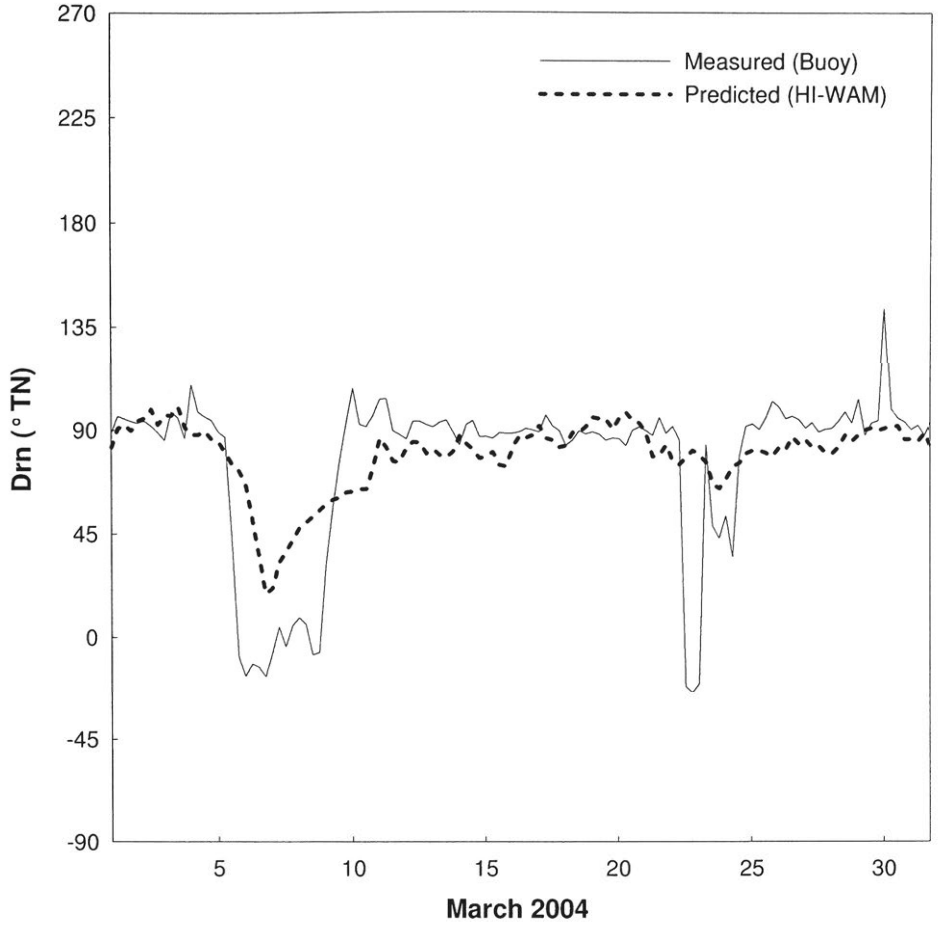

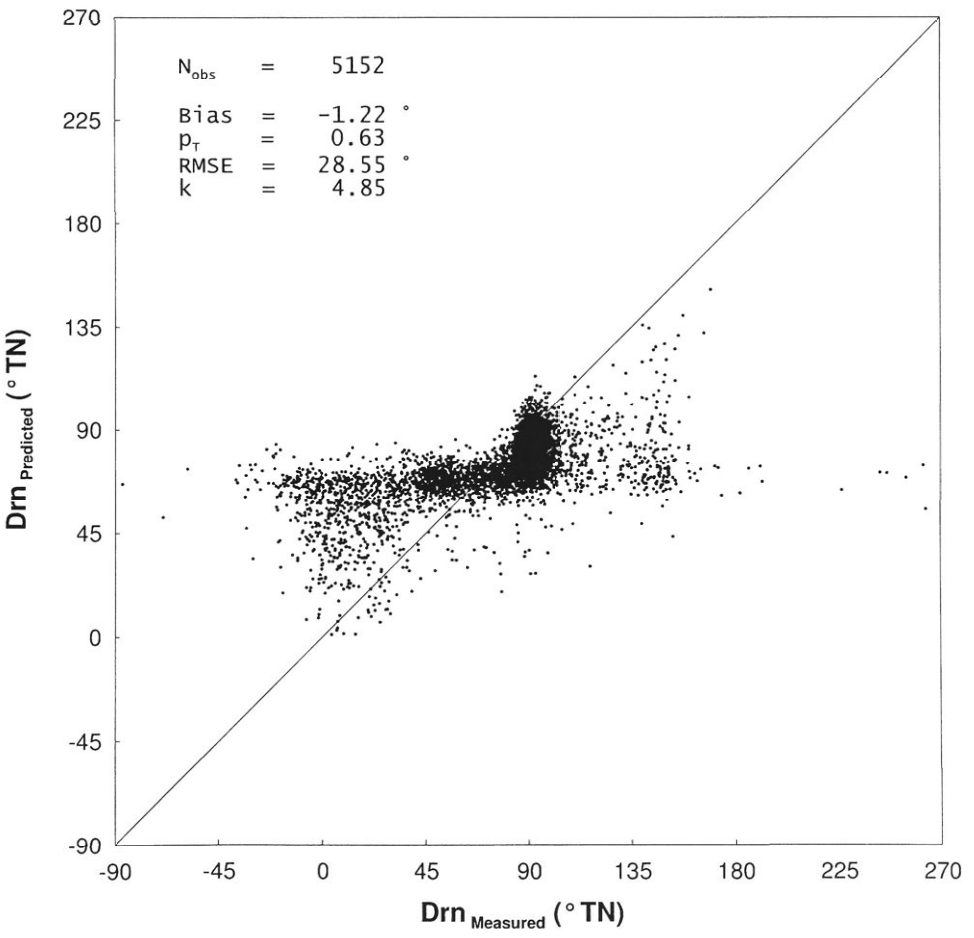

WRL Report No. 237	COMPARISON OF MEASURED & PREDICTED Drn VALUES TOWNSVILLE, QUEENSLAND	Figure 7.03

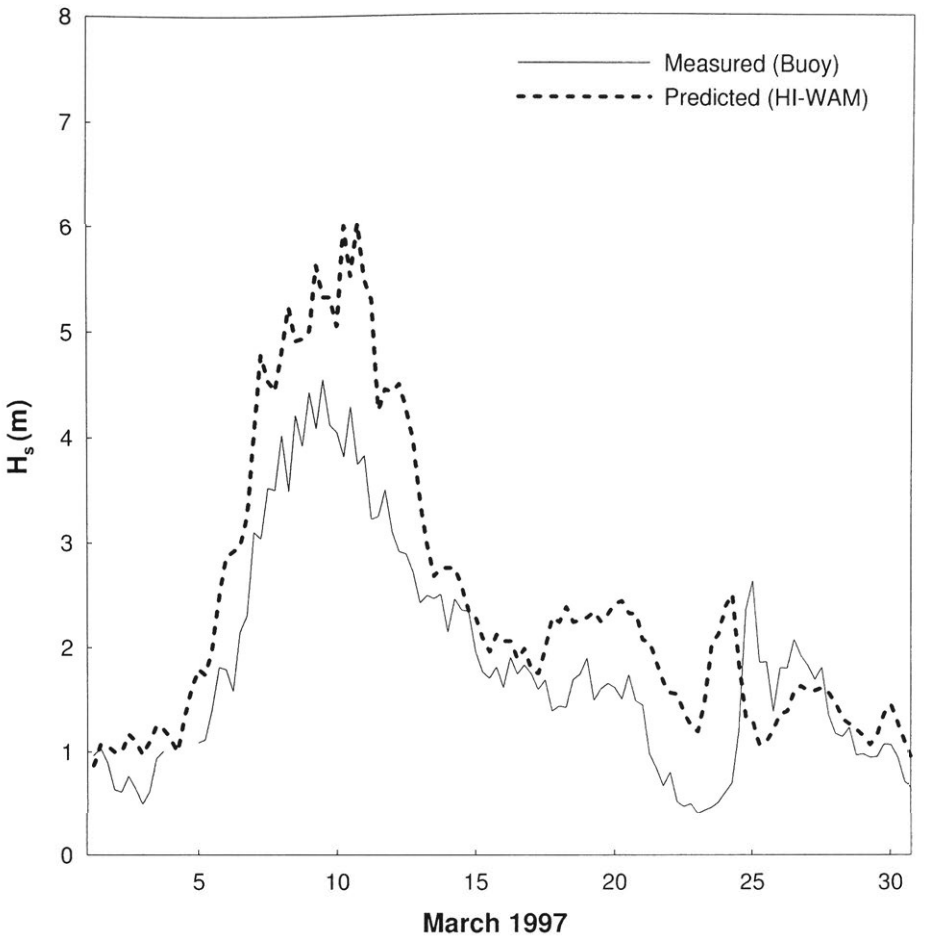

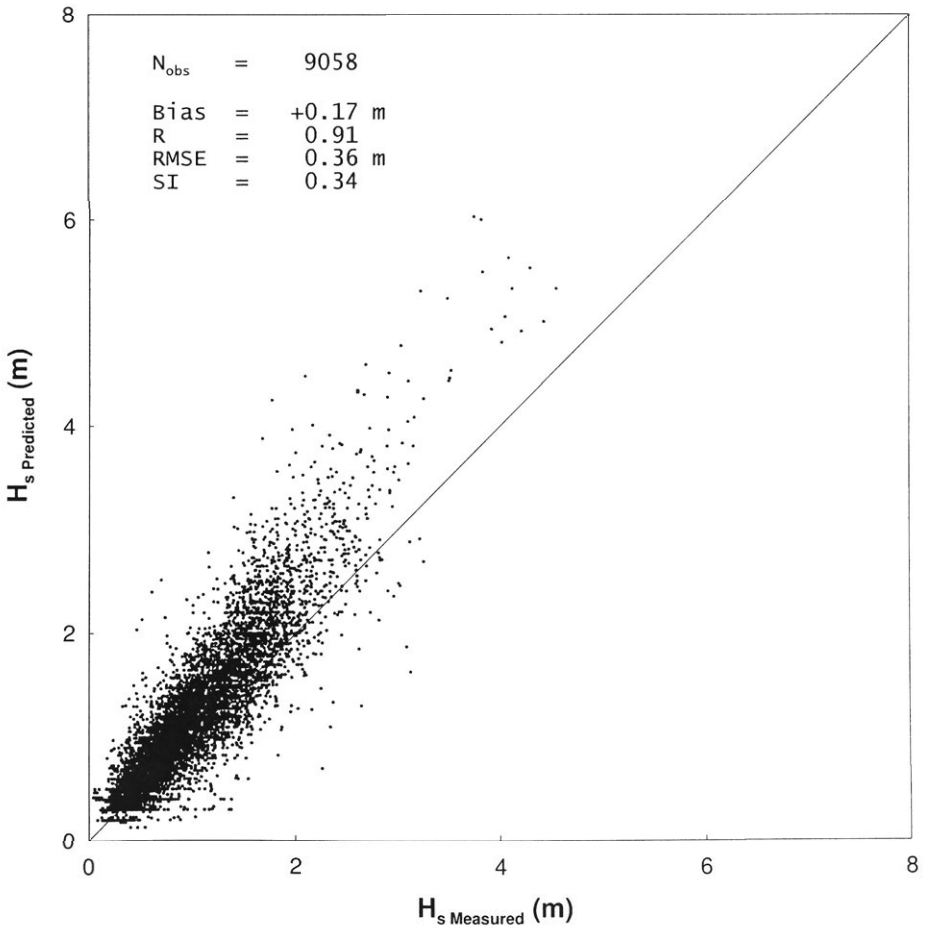

WRL Report No. 237	COMPARISON OF MEASURED & PREDICTED H_s VALUES MACKAY, QUEENSLAND	Figure 7.04

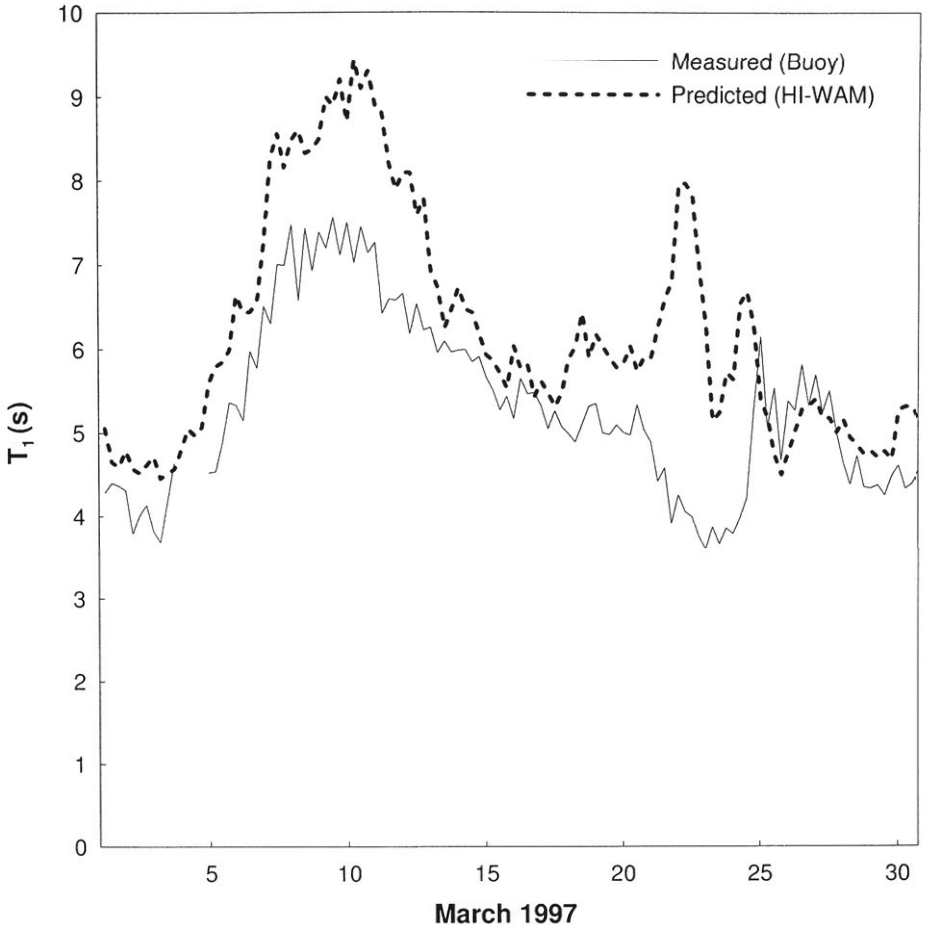

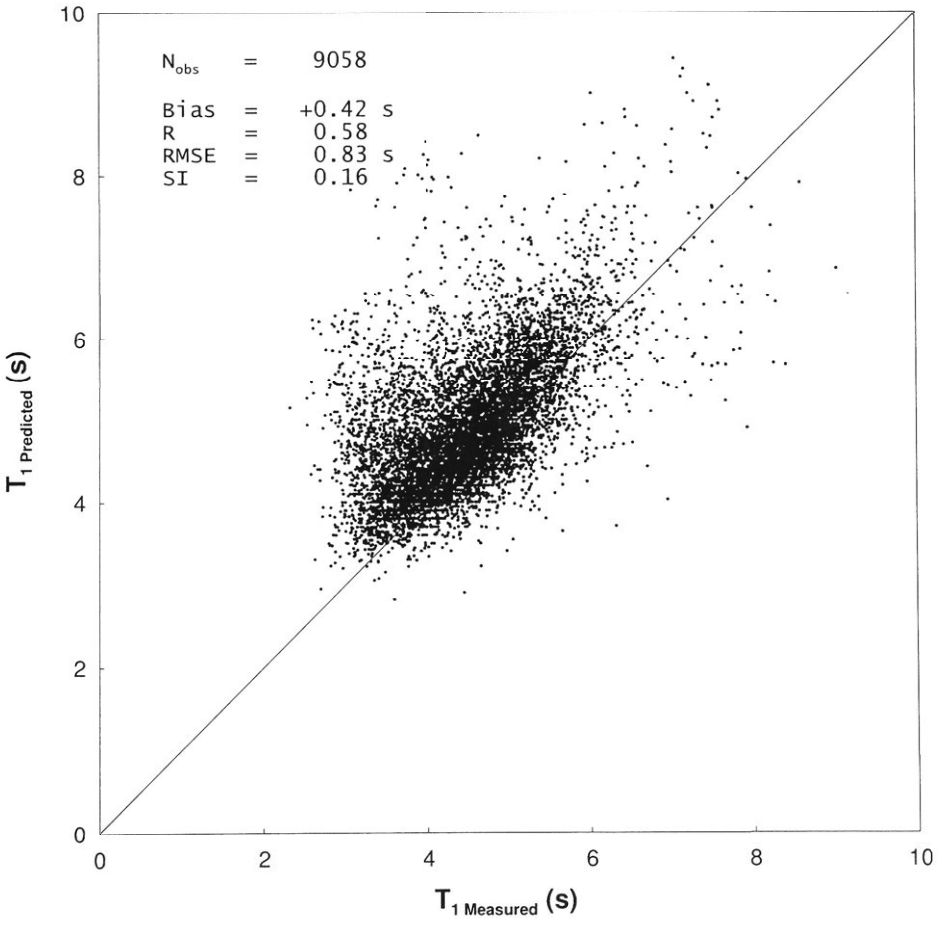

WRL
Report No. 237

COMPARISON OF MEASURED & PREDICTED T_1 VALUES
MACKAY, QUEENSLAND

Figure
7.05

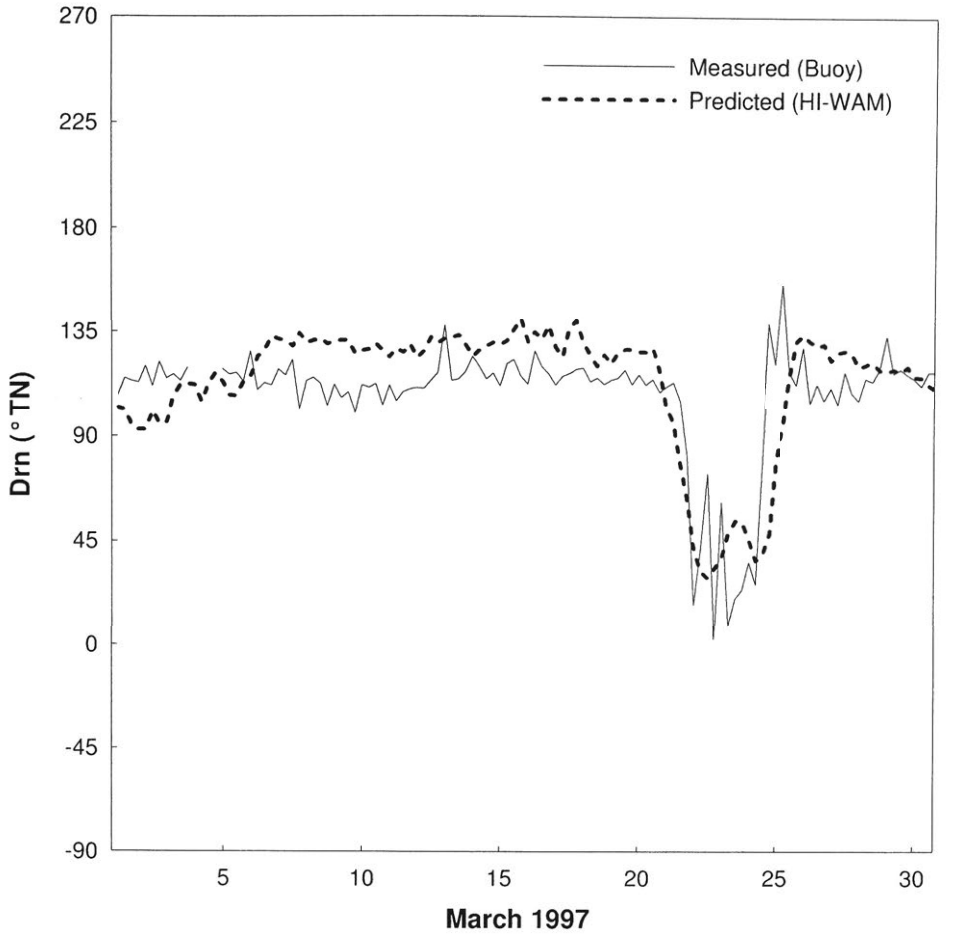

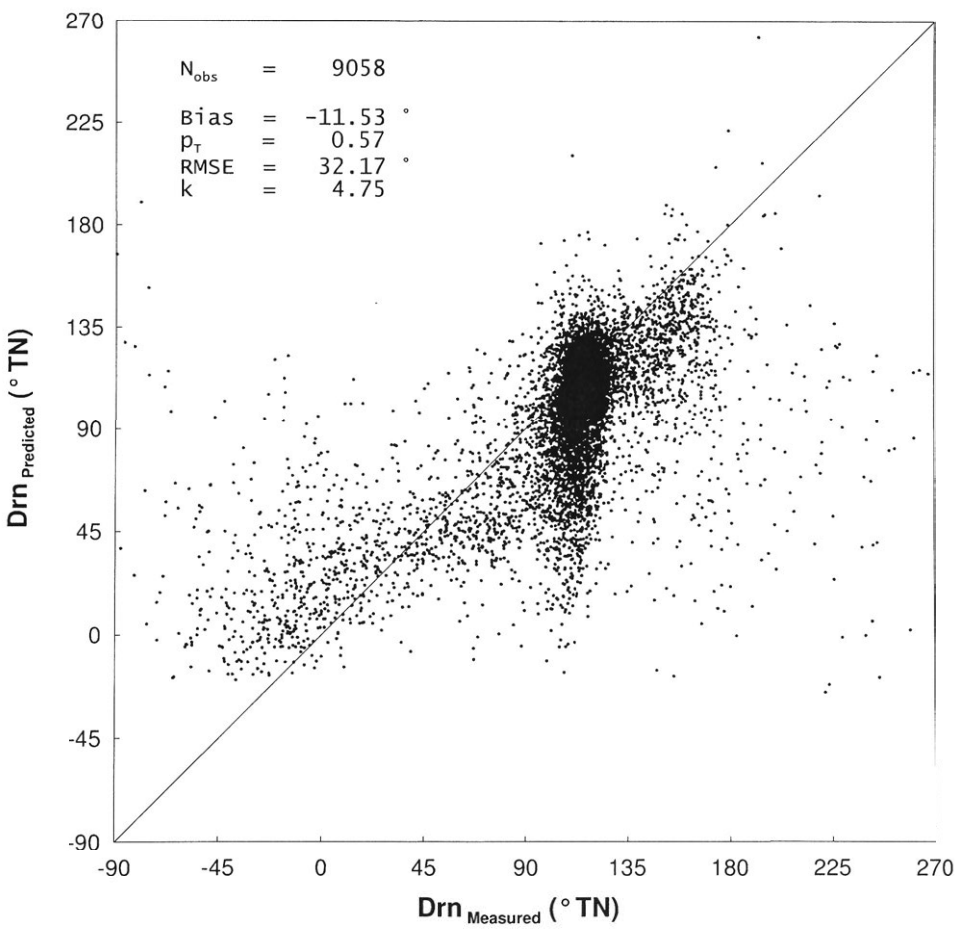

WRL Report No. 237	COMPARISON OF MEASURED & PREDICTED Drn VALUES MACKAY, QUEENSLAND	Figure 7.06

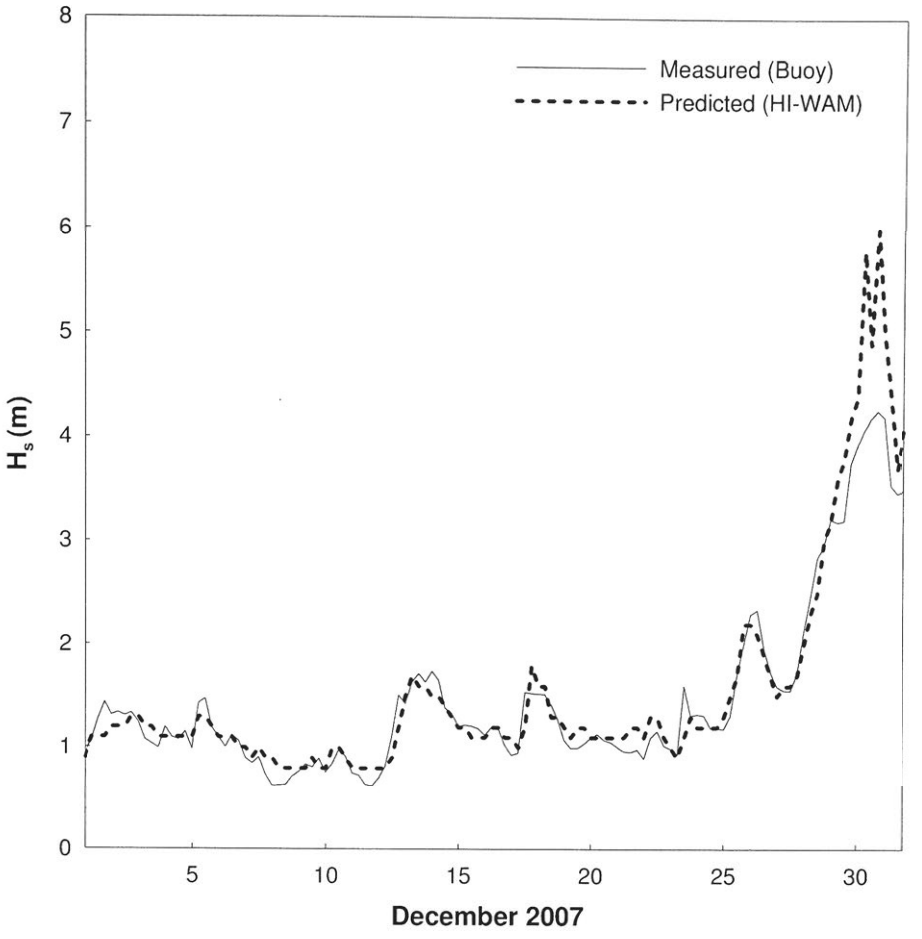

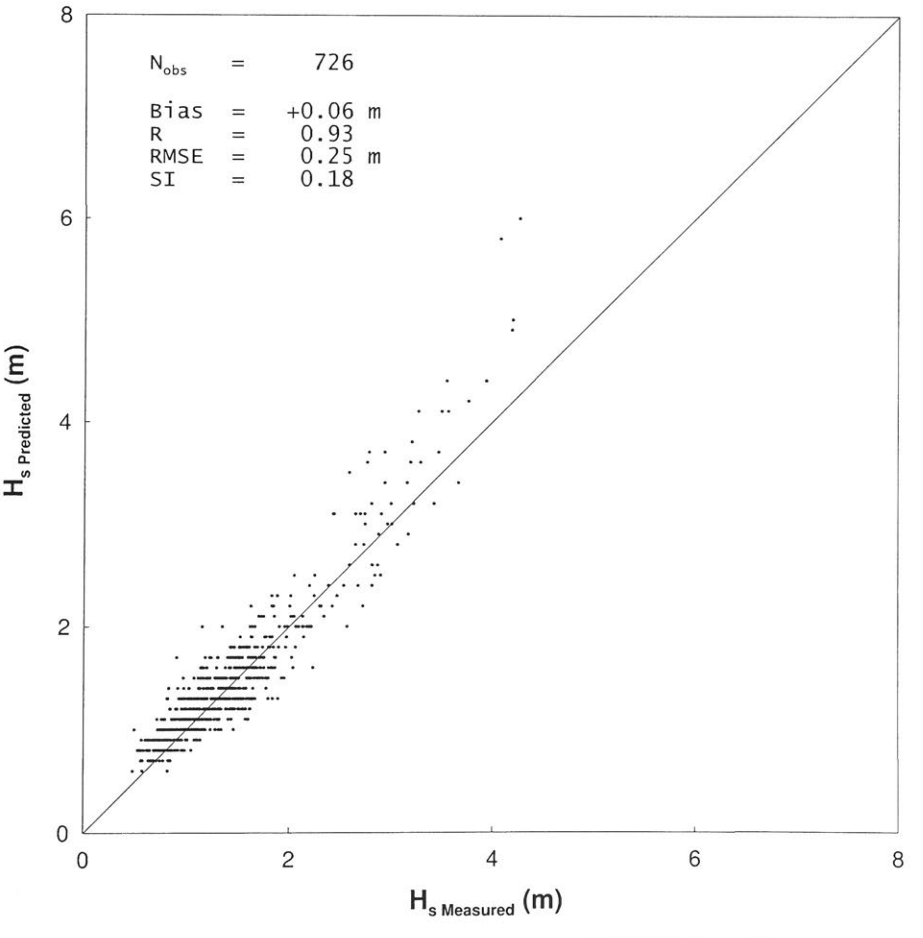

WRL Report No. 237	COMPARISON OF MEASURED & PREDICTED H_s VALUES MOOLOOLABA, QUEENSLAND	Figure 7.07

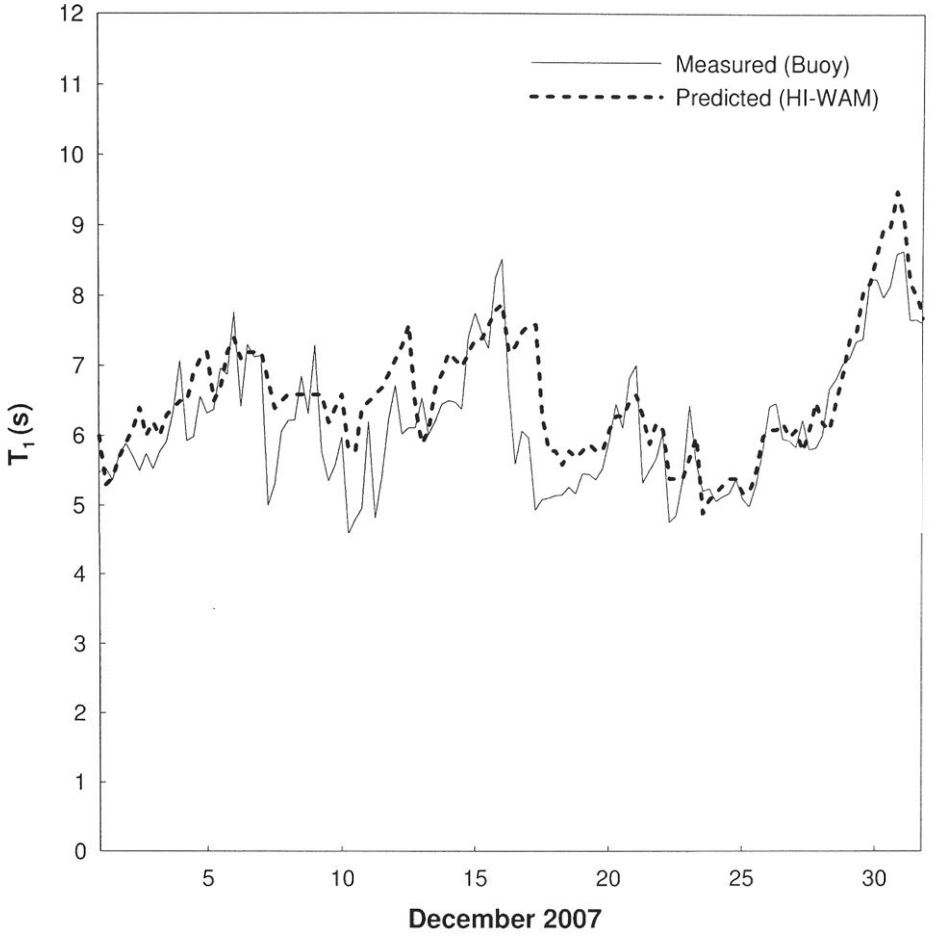

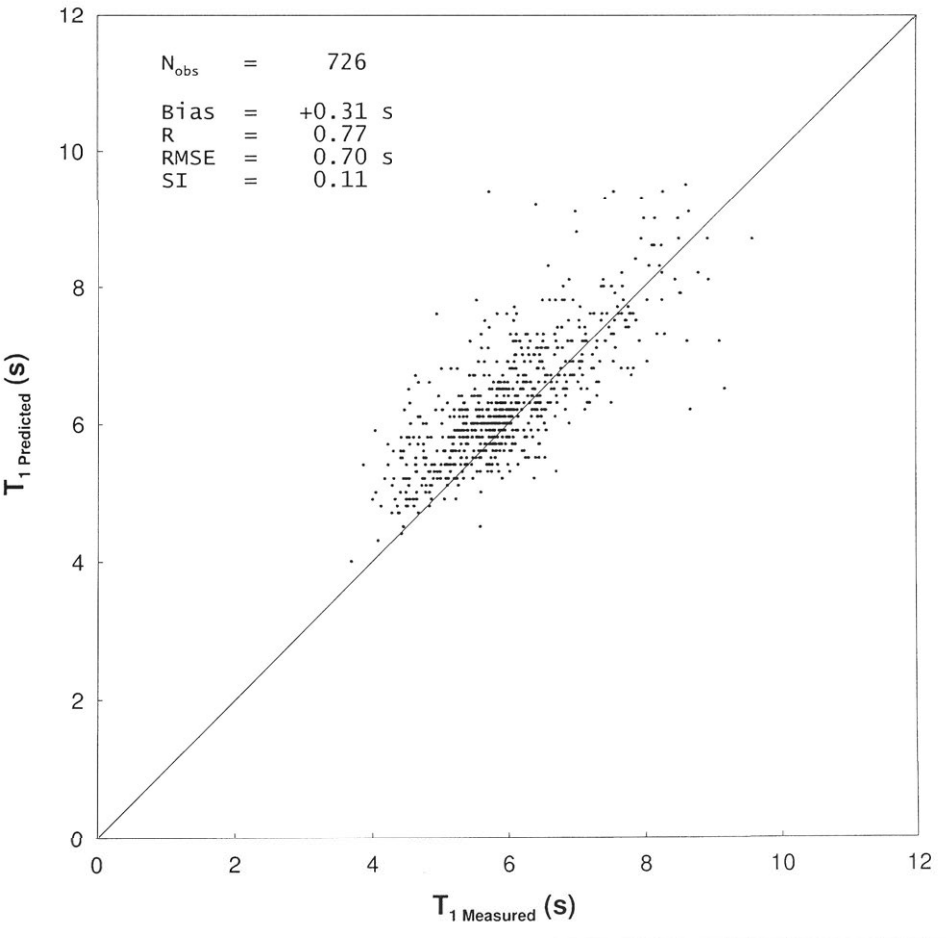

WRL Report No. 237	COMPARISON OF MEASURED & PREDICTED T_1 VALUES MOOLOOLABA, QUEENSLAND	Figure 7.08

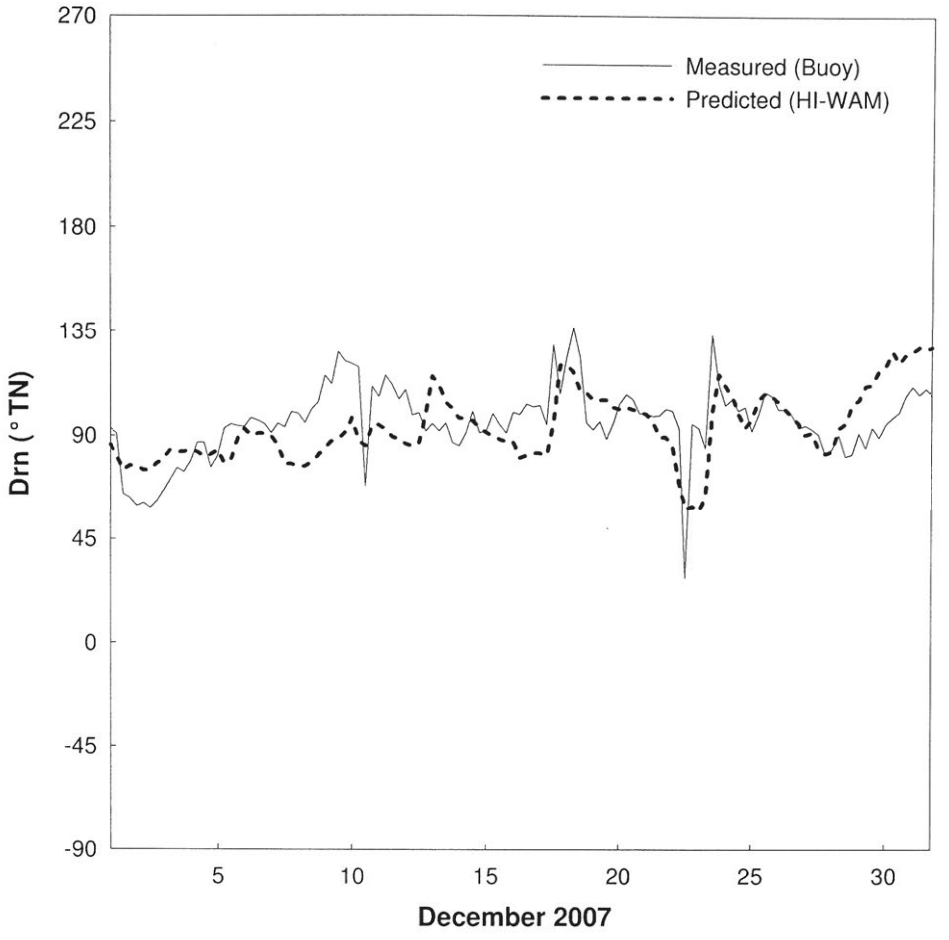

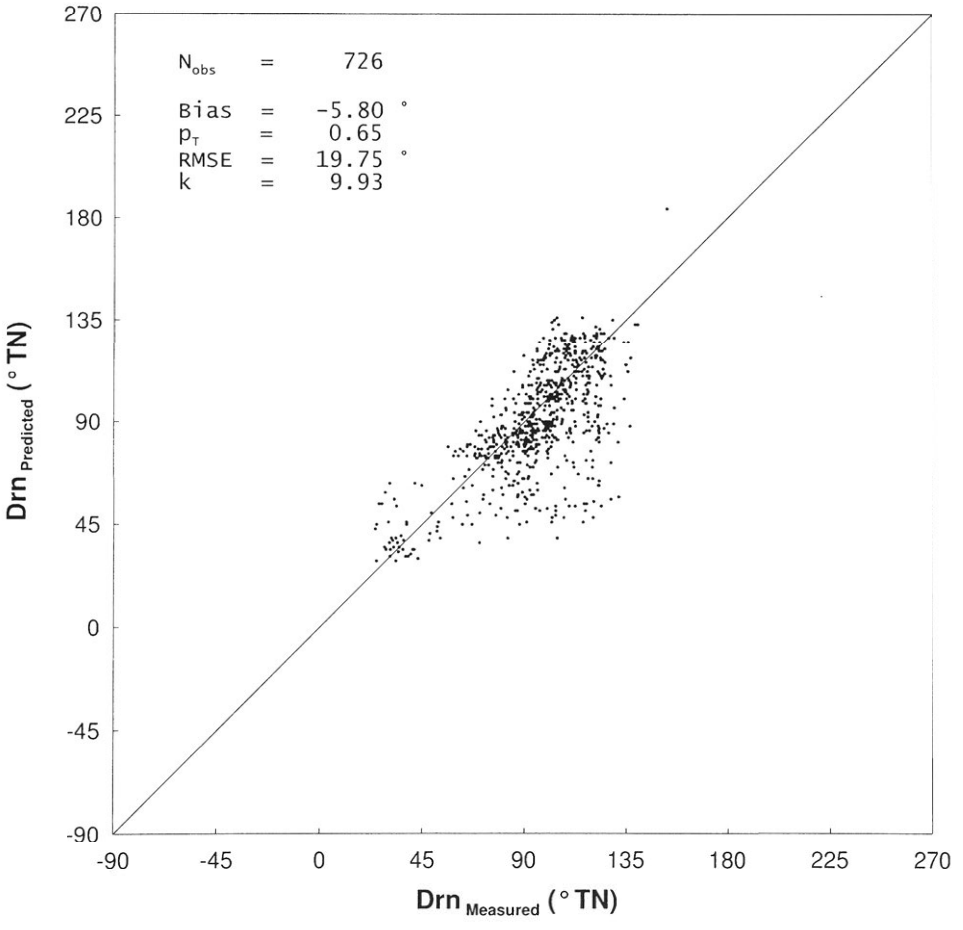

WRL Report No. 237	COMPARISON OF MEASURED & PREDICTED Drn VALUES MOOLOOLABA, QUEENSLAND	Figure 7.09

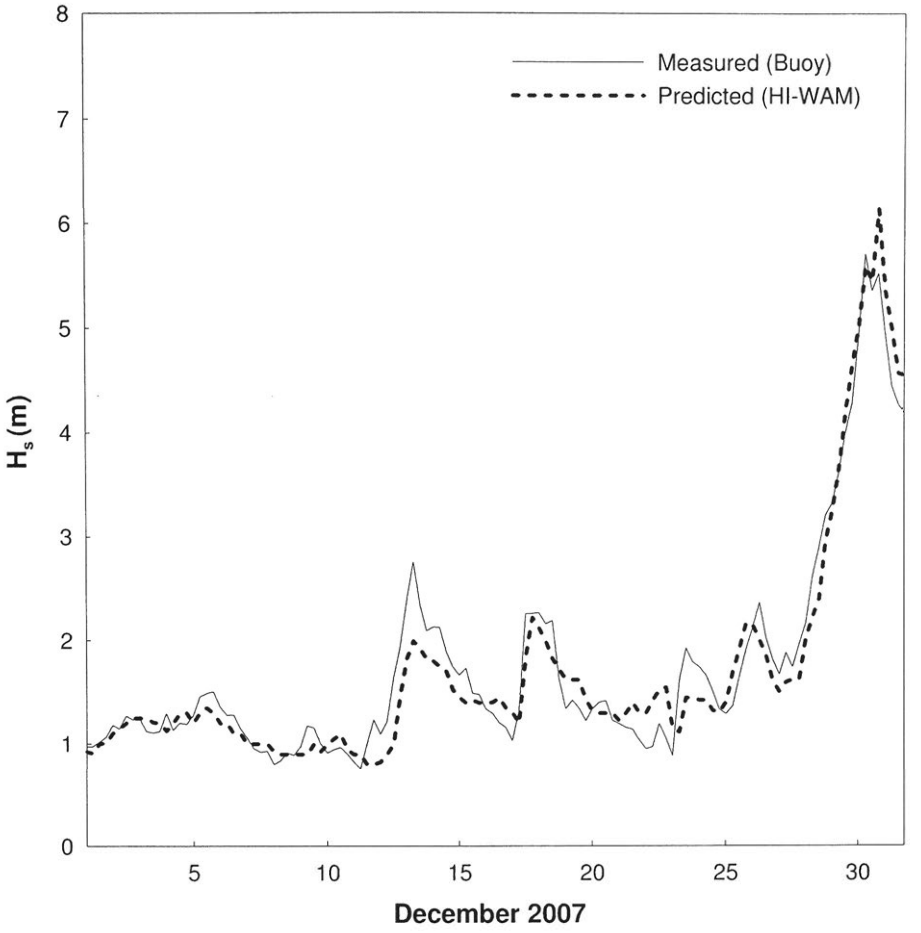

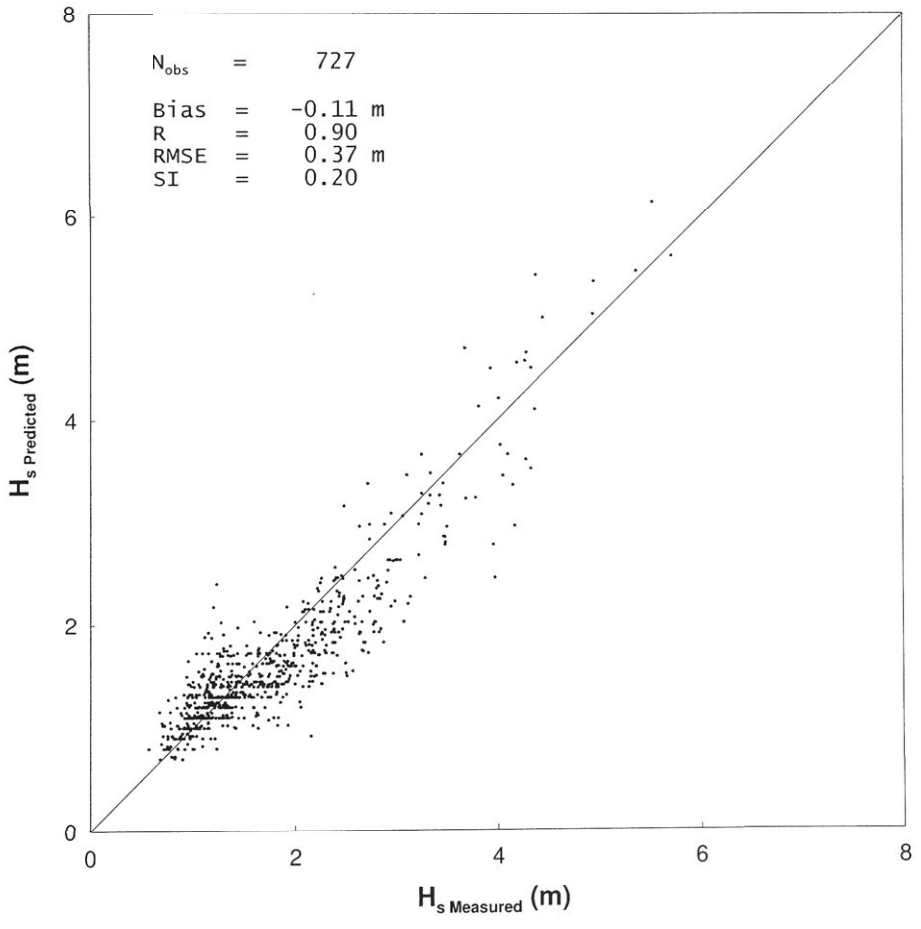

WRL
Report No. 237

COMPARISON OF MEASURED & PREDICTED H_s VALUES
BRISBANE, QUEENSLAND

Figure
7.10

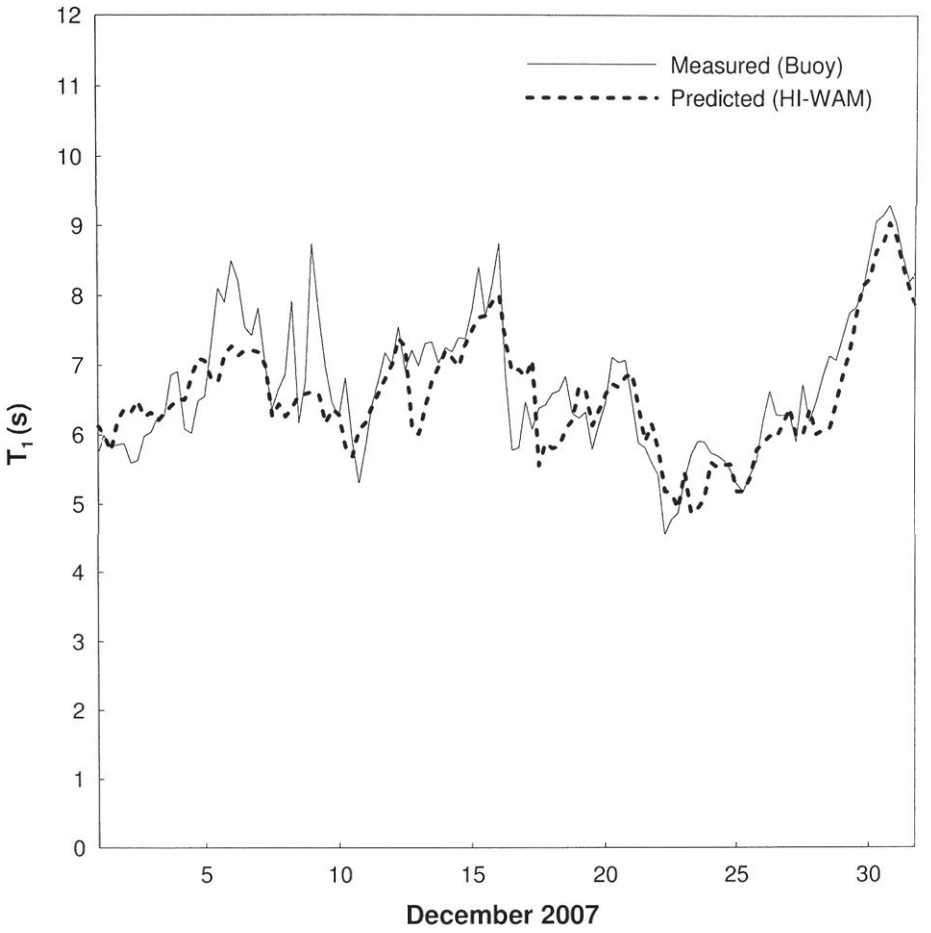

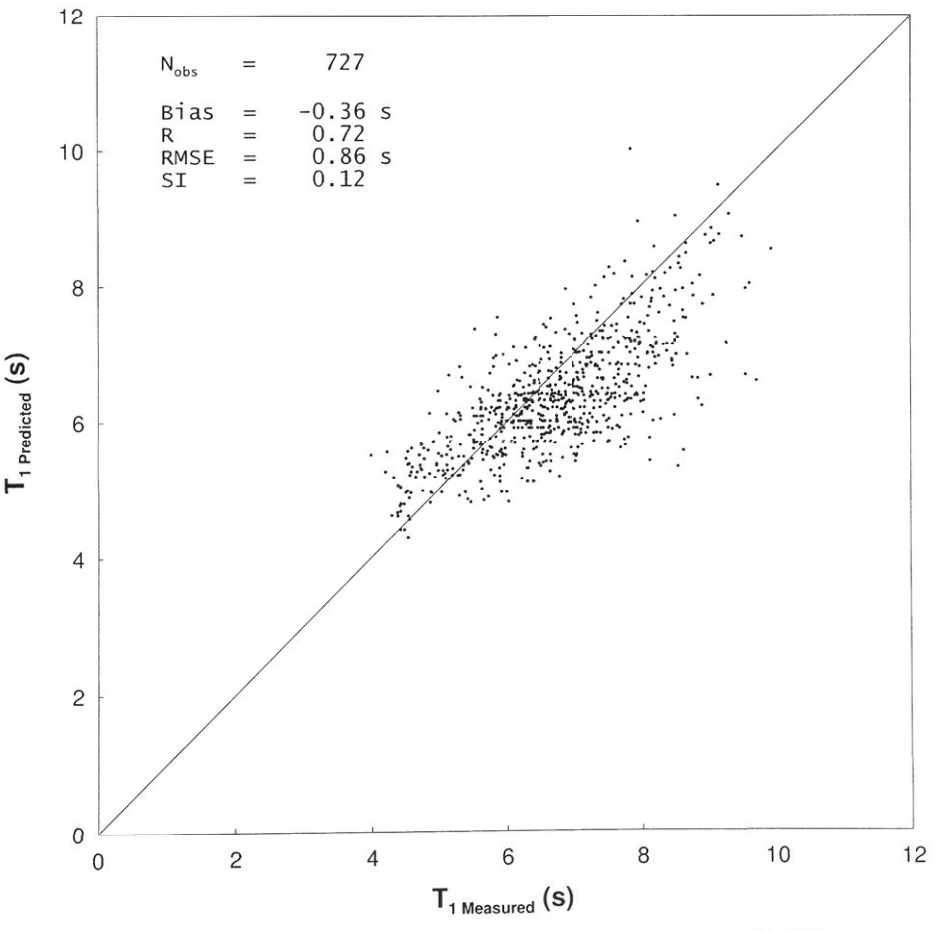

WRL Report No. 237	COMPARISON OF MEASURED & PREDICTED T_1 VALUES BRISBANE, QUEENSLAND	Figure 7.11

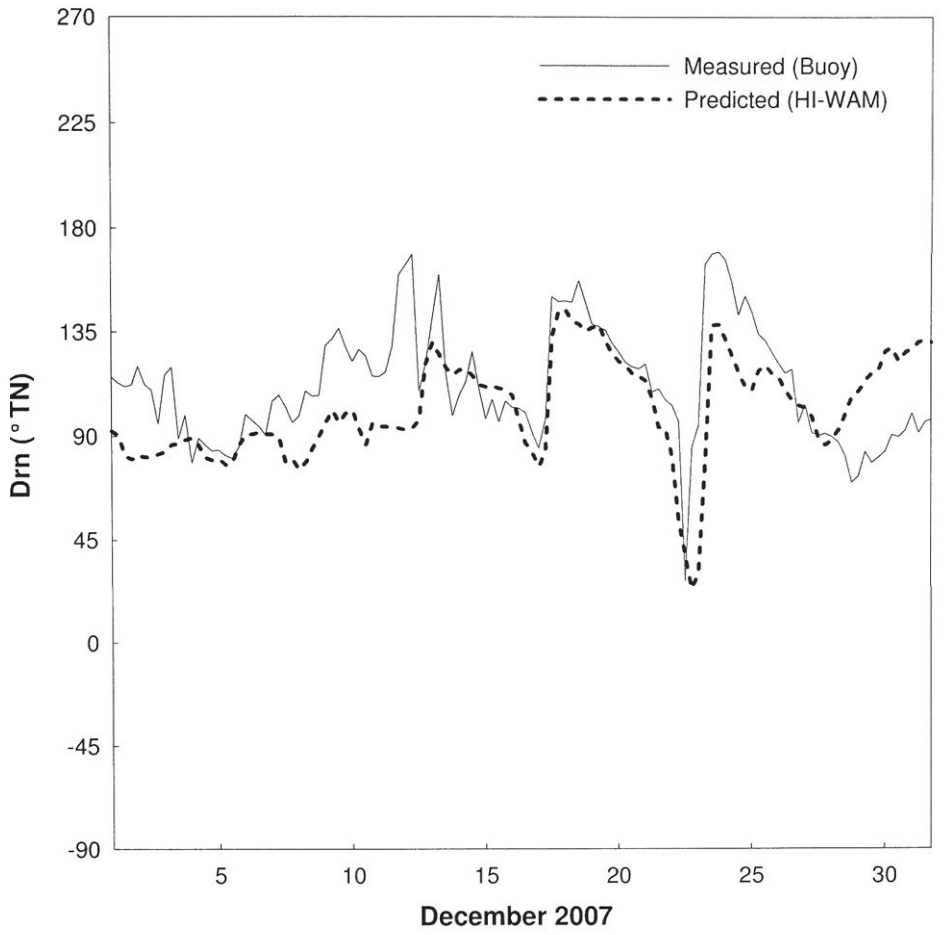

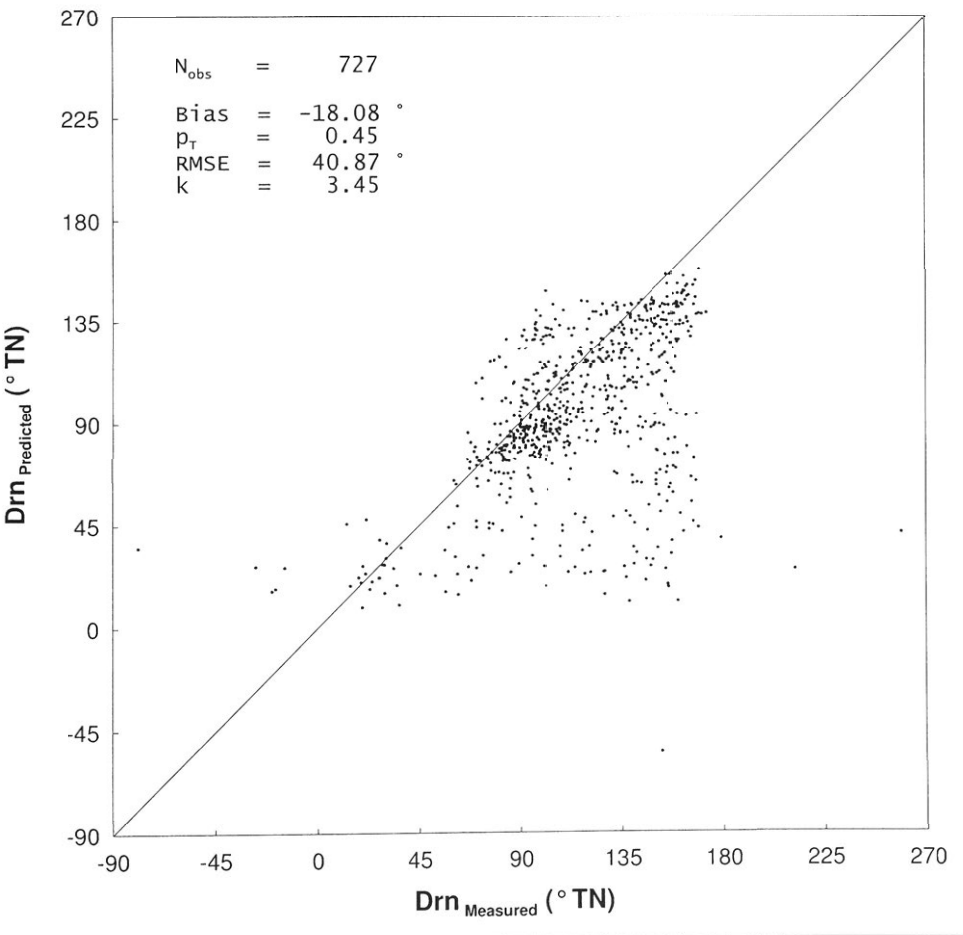

WRL Report No. 237	COMPARISON OF MEASURED & PREDICTED Drn VALUES BRISBANE, QUEENSLAND	Figure 7.12

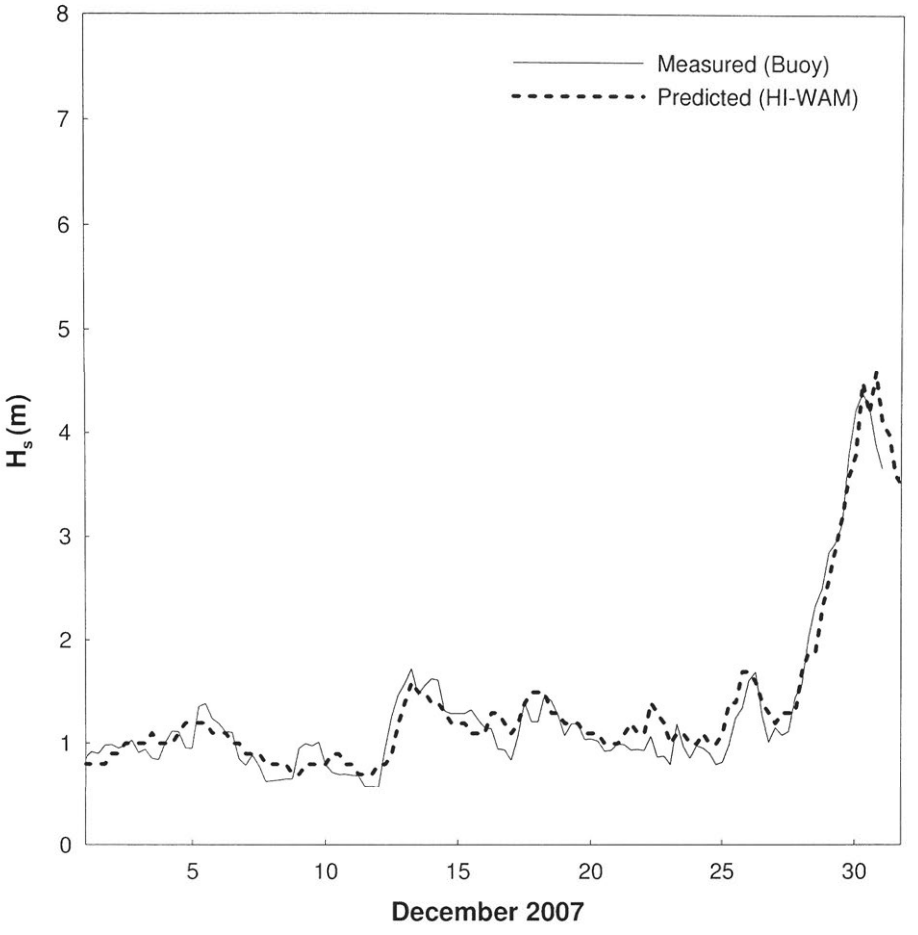

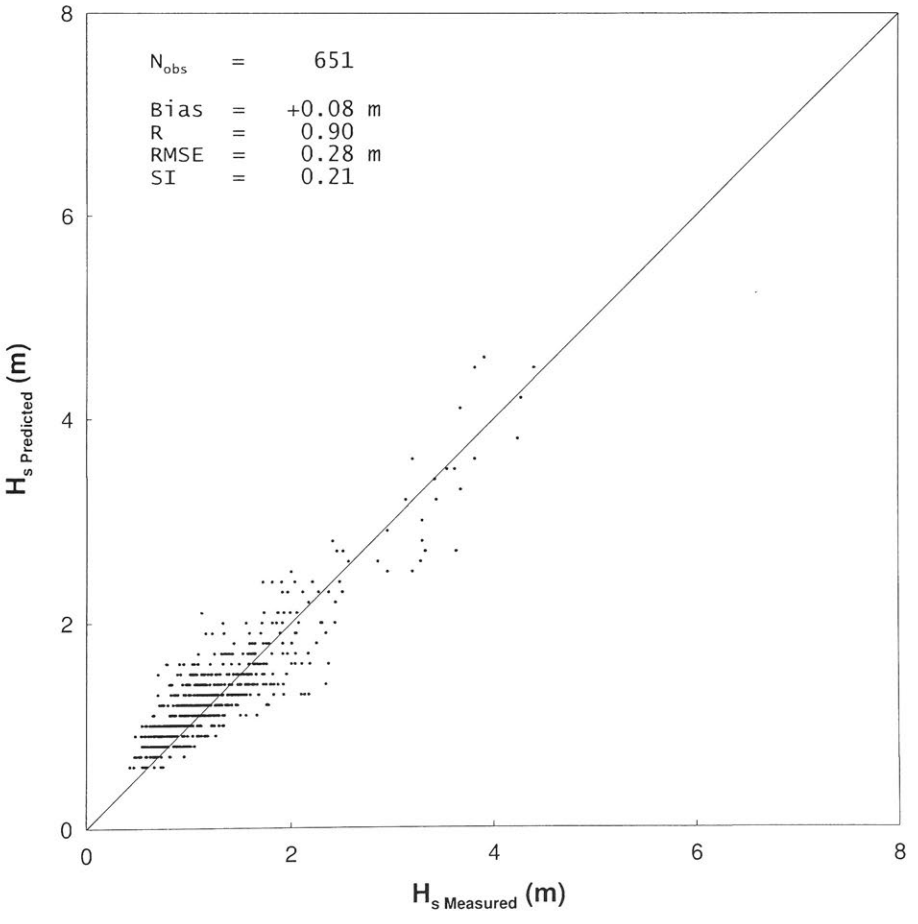

WRL
Report No. 237

COMPARISON OF MEASURED & PREDICTED H_s VALUES
GOLD COAST, QUEENSLAND

Figure
7.13

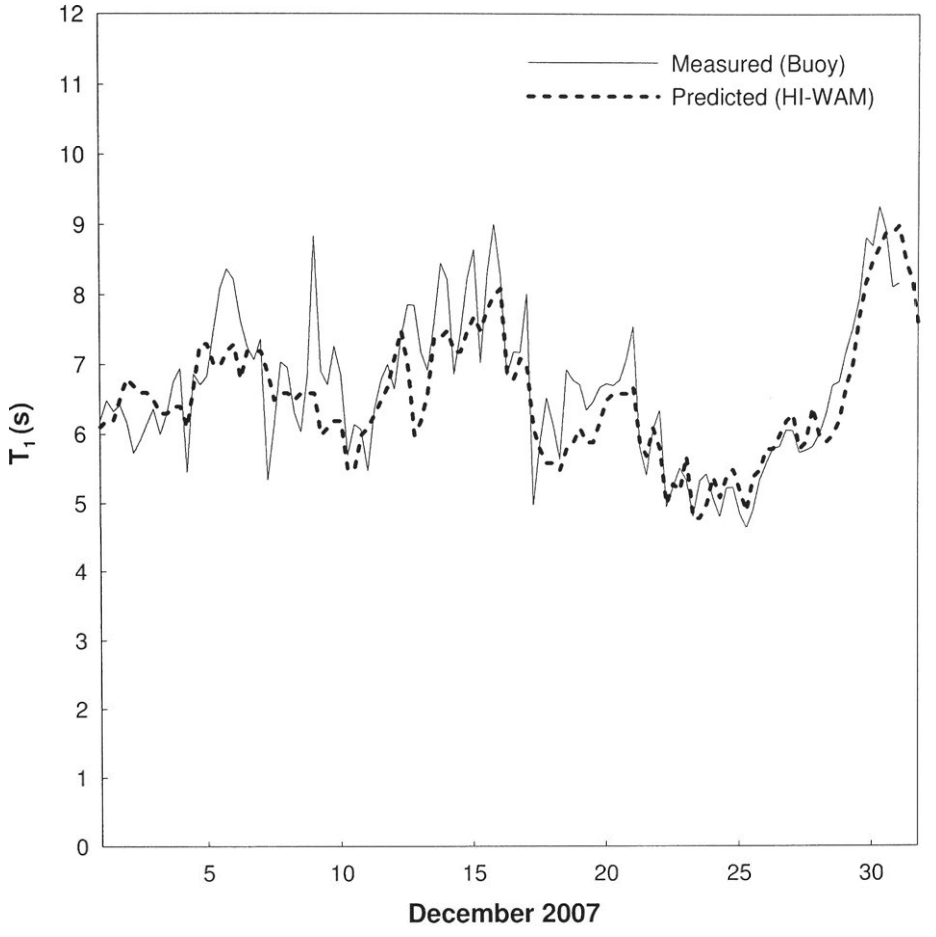

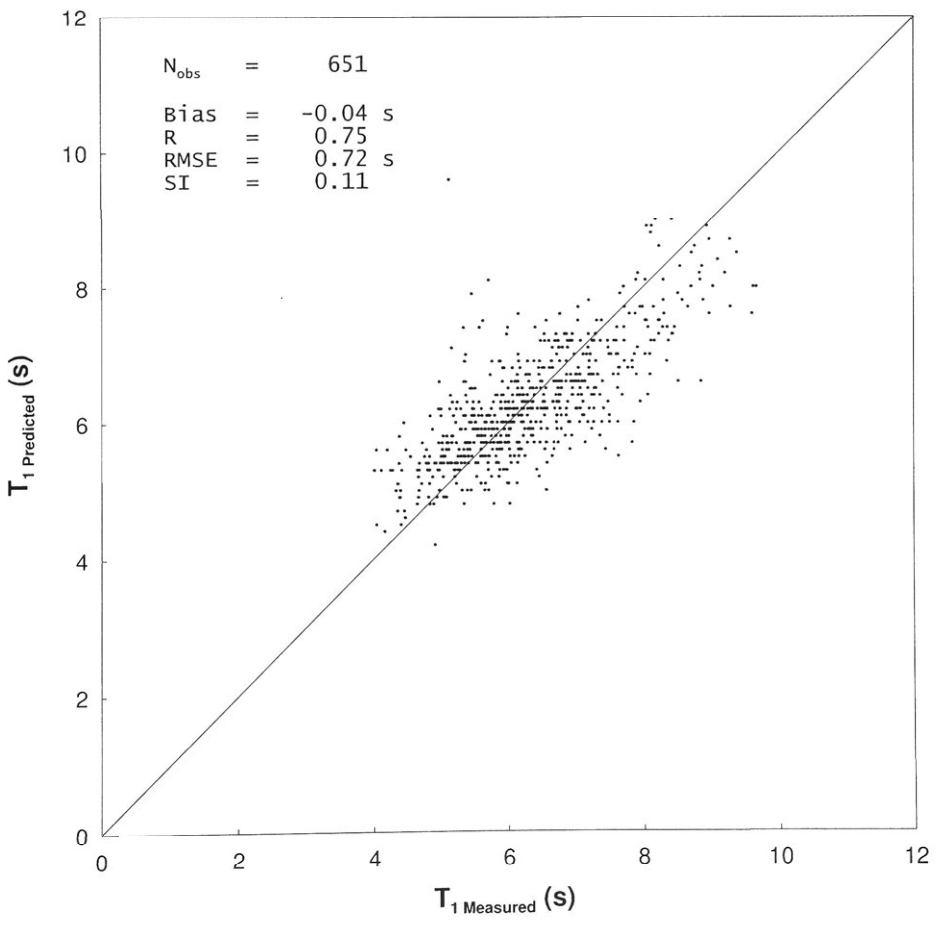

WRL
Report No. 237

COMPARISON OF MEASURED & PREDICTED T_1 VALUES
GOLD COAST, QUEENSLAND

Figure
7.14

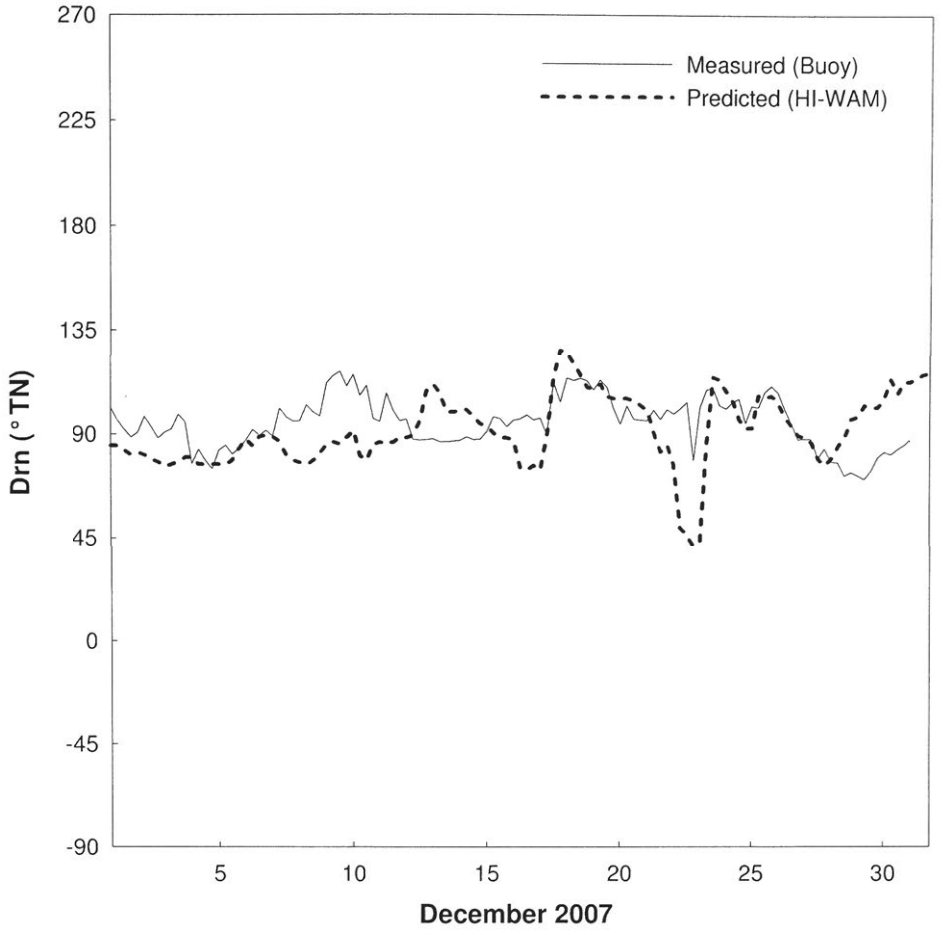

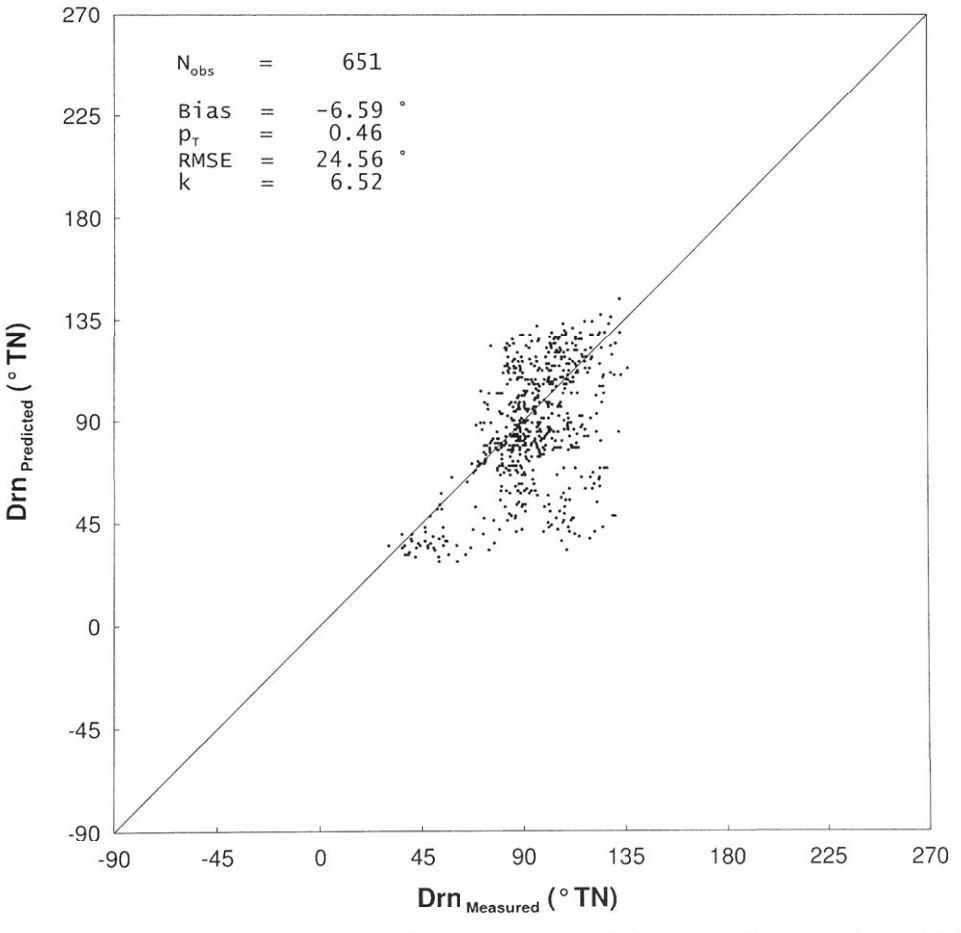

WRL Report No. 237	COMPARISON OF MEASURED & PREDICTED Drn VALUES GOLD COAST, QUEENSLAND	Figure 7.15

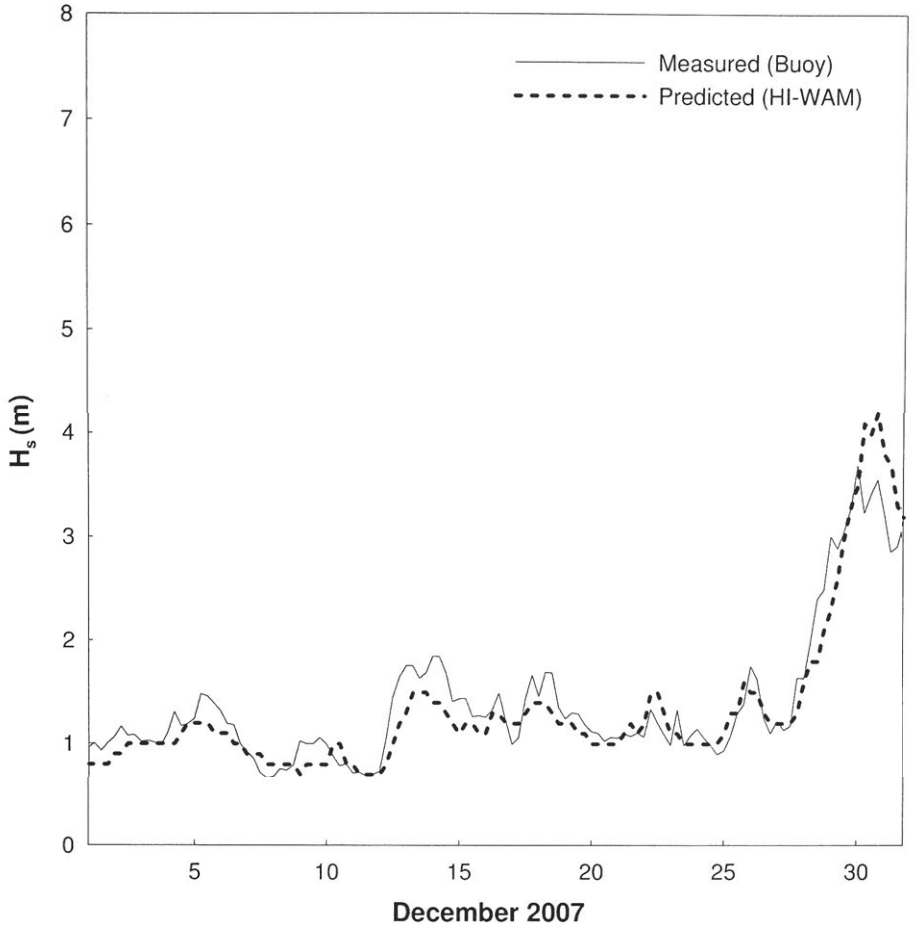

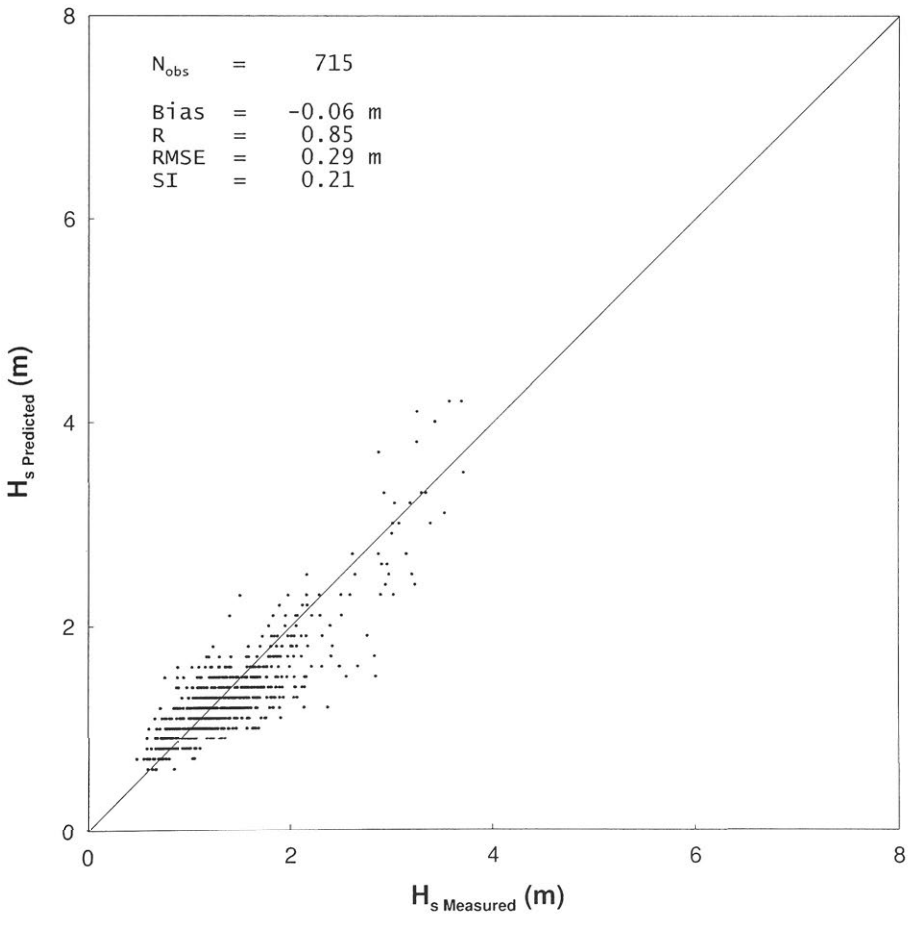

WRL
Report No. 237

COMPARISON OF MEASURED & PREDICTED H_s VALUES
TWEED RIVER, QUEENSLAND

Figure
7.16

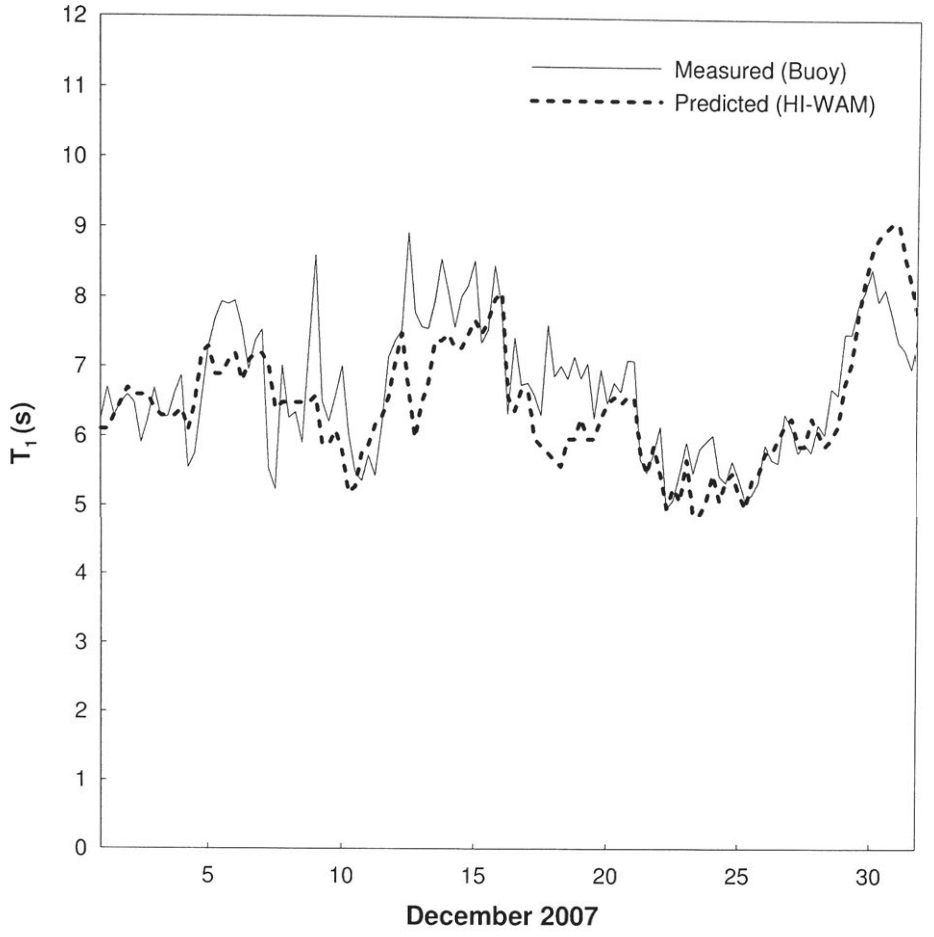

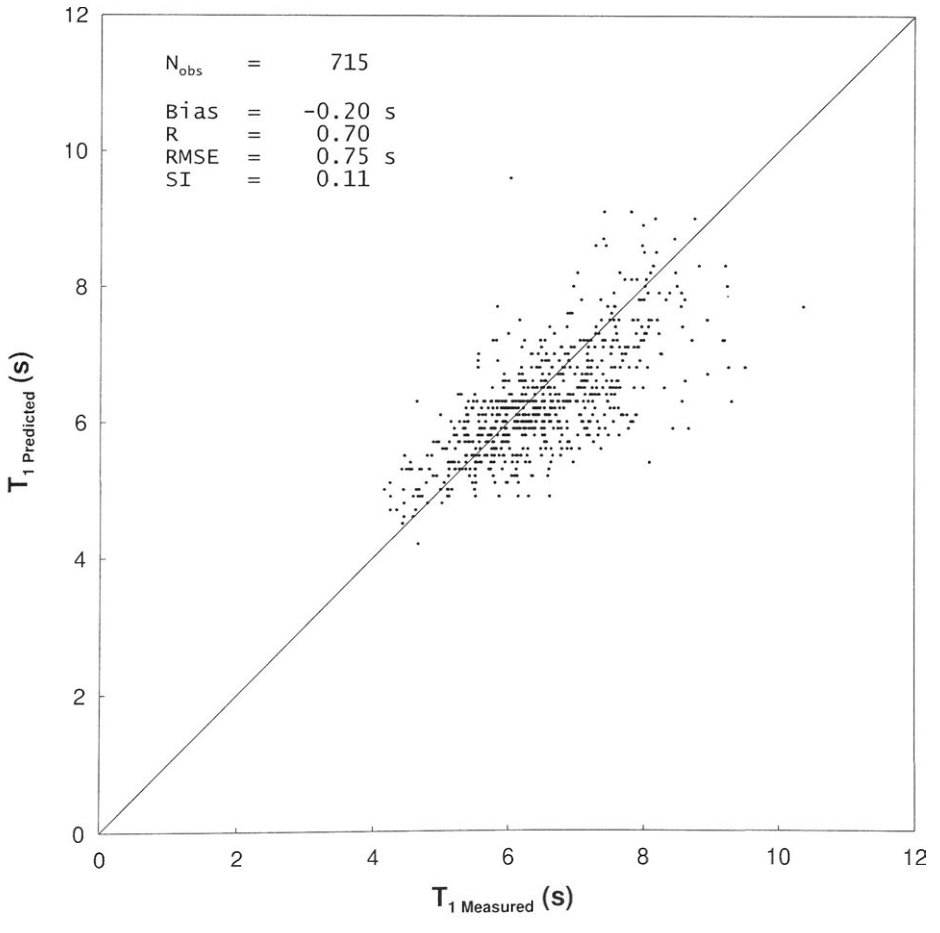

WRL
Report No. 237

COMPARISON OF MEASURED & PREDICTED T_1 VALUES
TWEED RIVER, QUEENSLAND

Figure
7.17

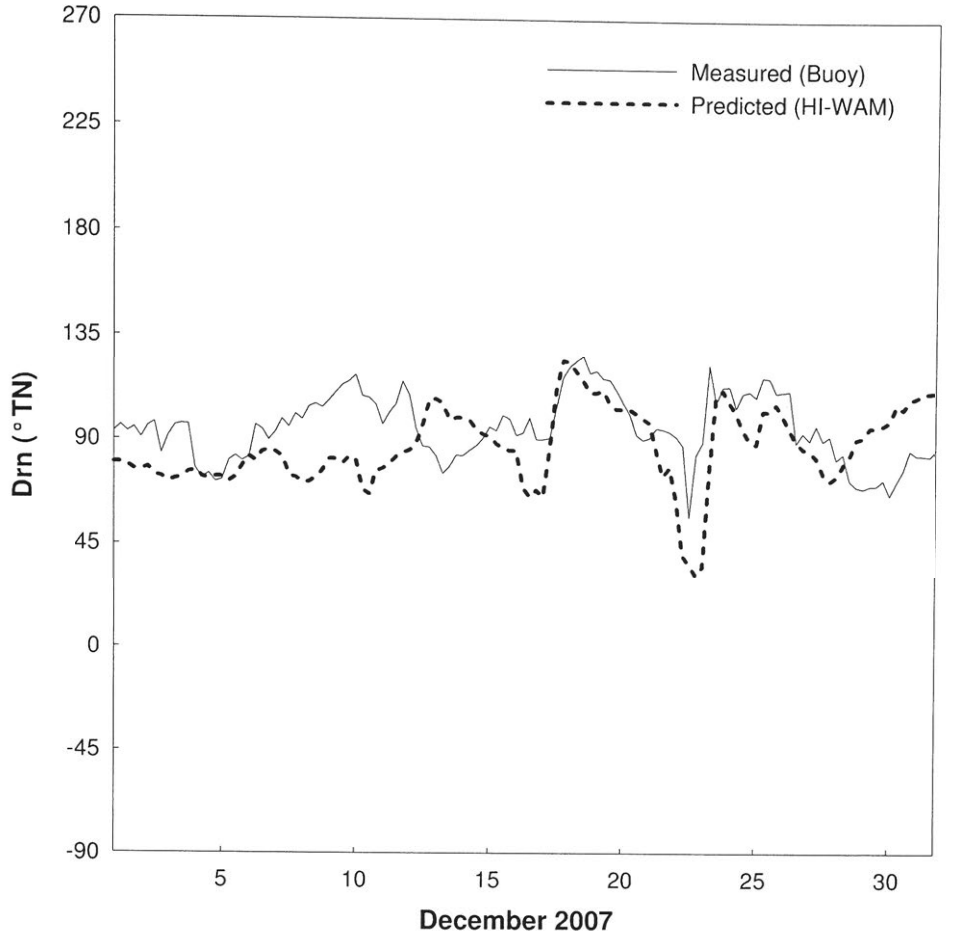

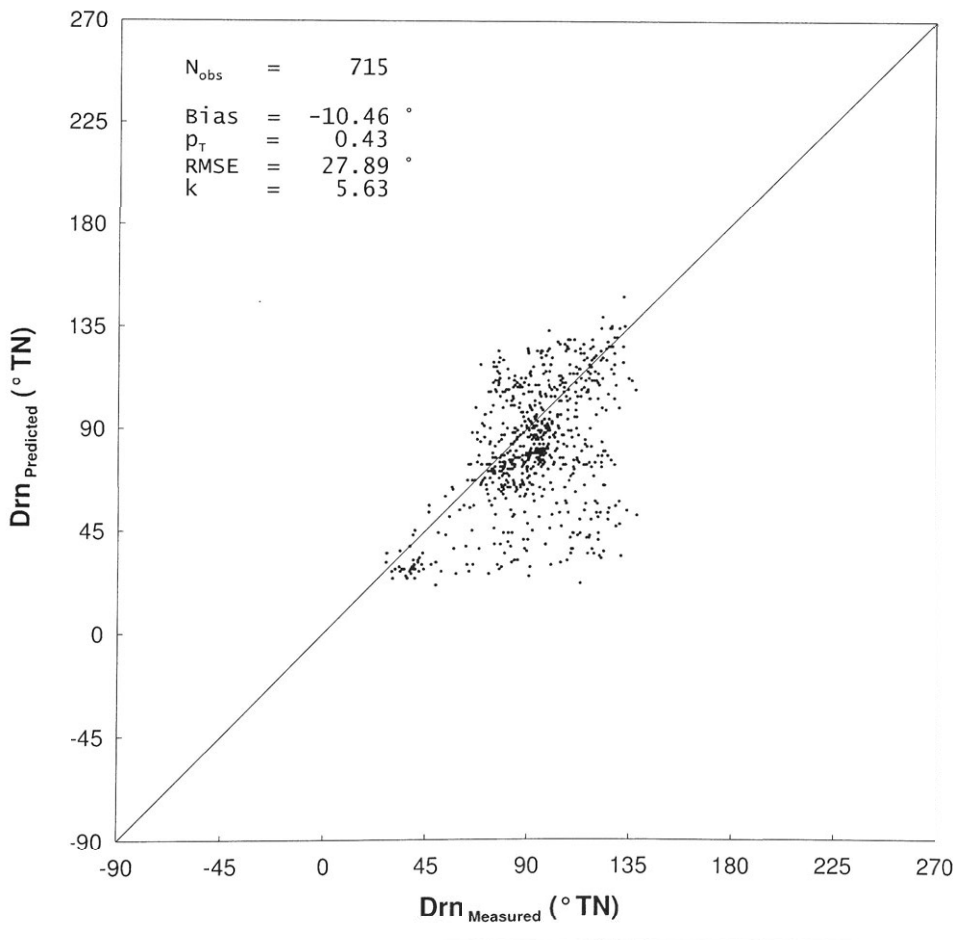

WRL Report No. 237	COMPARISON OF MEASURED & PREDICTED Drn VALUES TWEED RIVER, QUEENSLAND	Figure 7.18

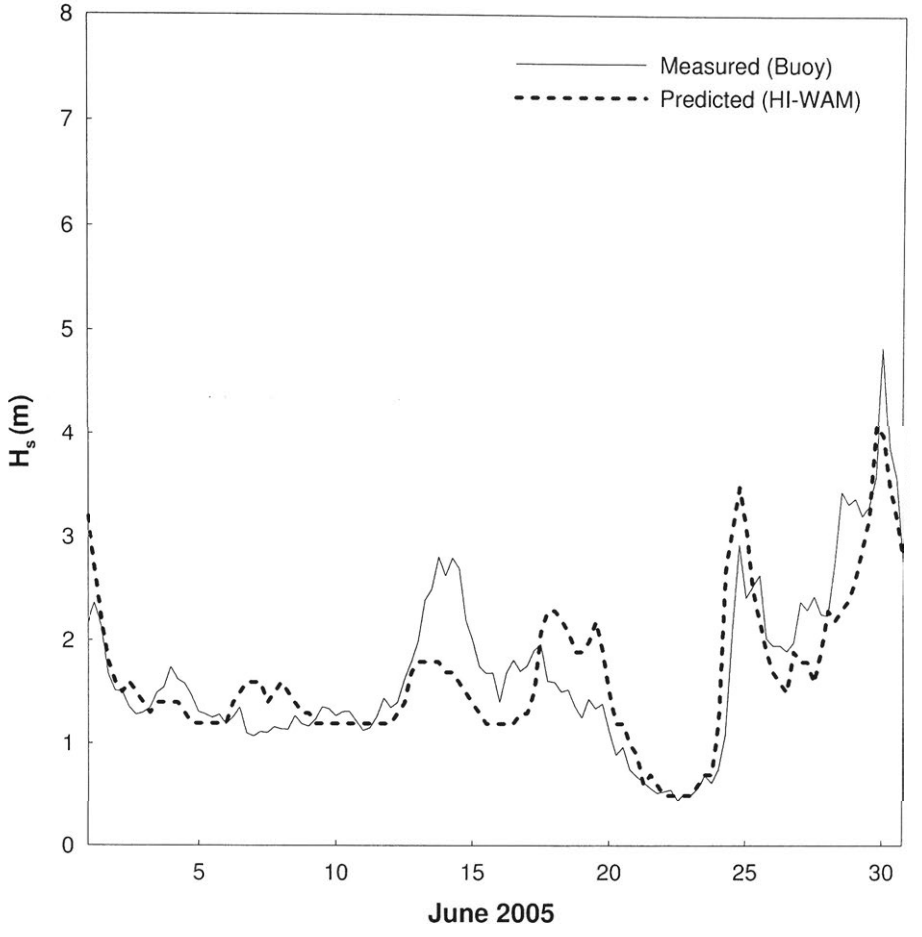

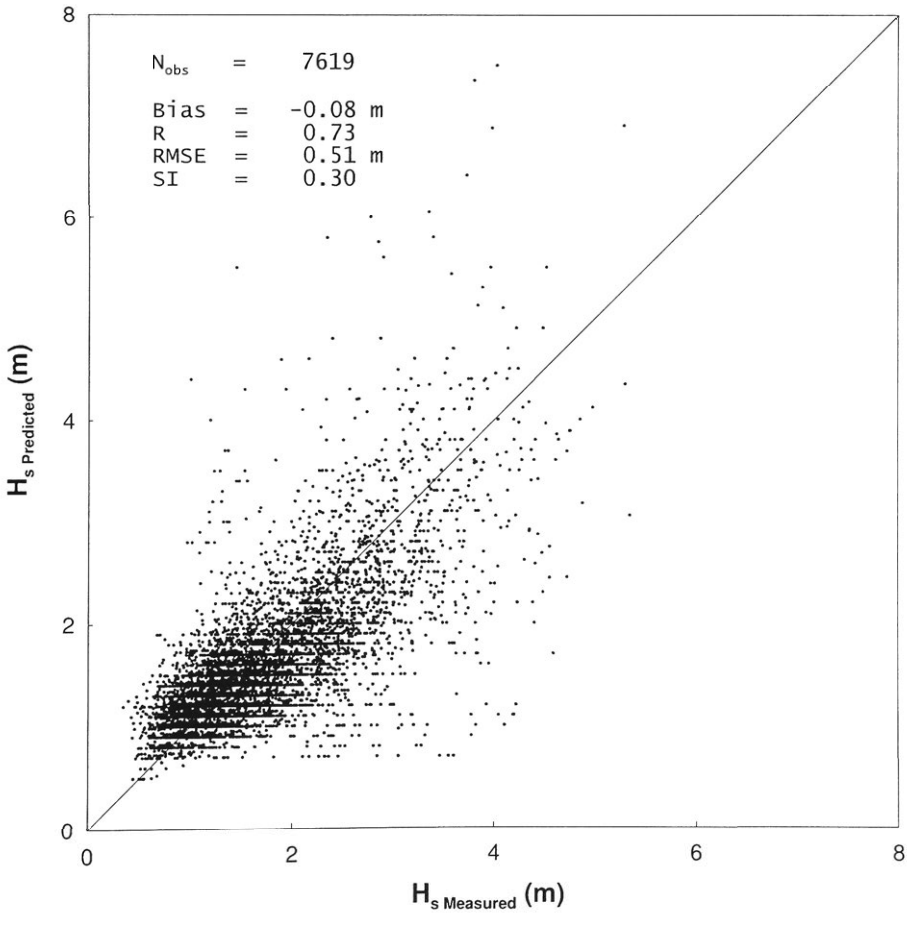

WRL Report No. 237	COMPARISON OF MEASURED & PREDICTED H_s VALUES BYRON BAY, NEW SOUTH WALES	Figure 7.19

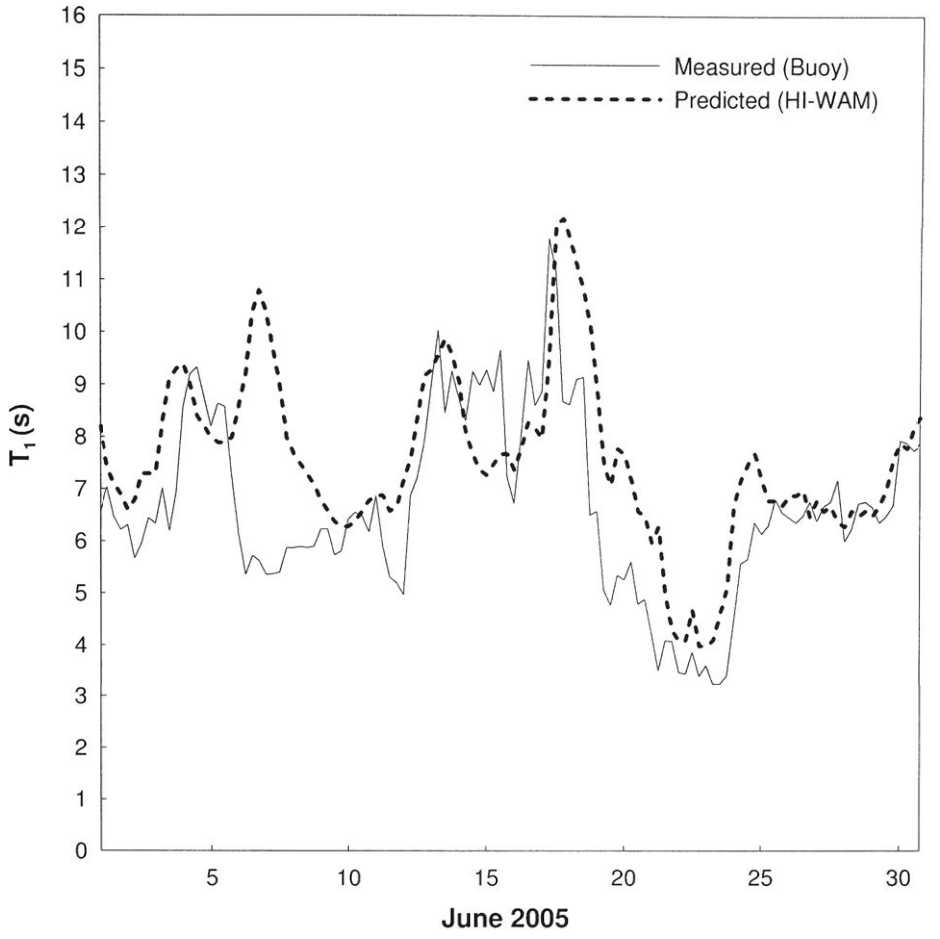

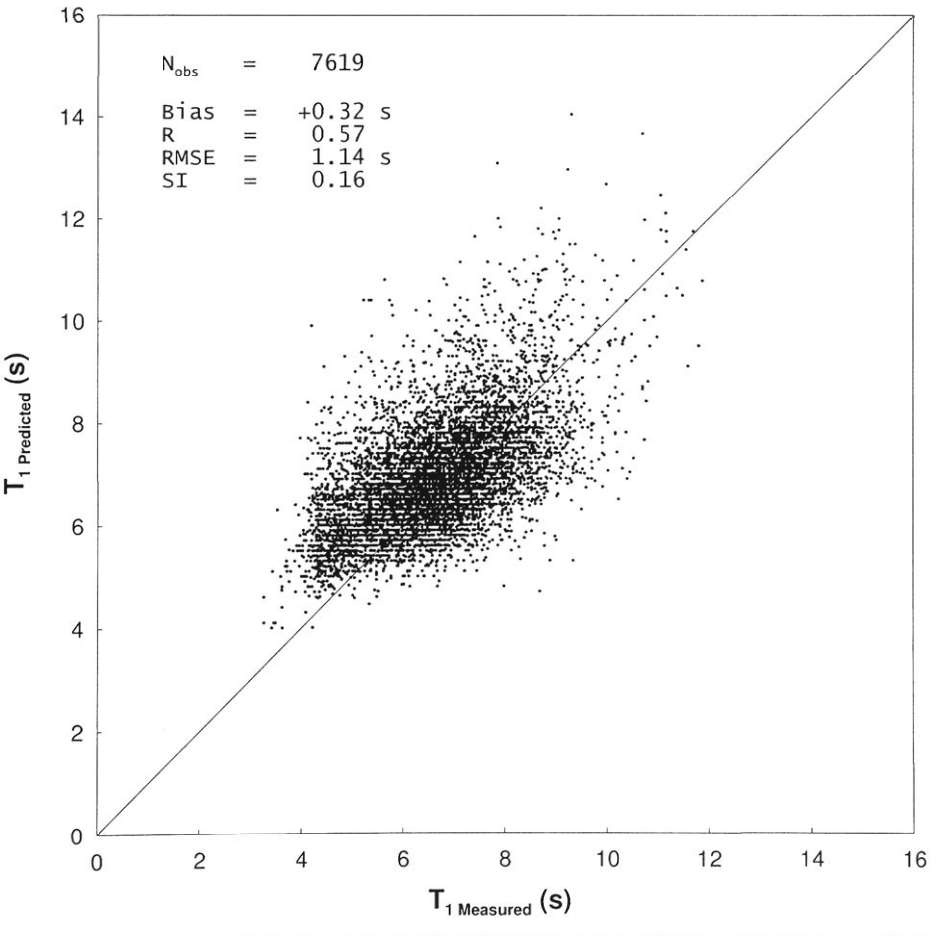

WRL Report No. 237	COMPARISON OF MEASURED & PREDICTED T_1 VALUES BYRON BAY, NEW SOUTH WALES	Figure 7.20

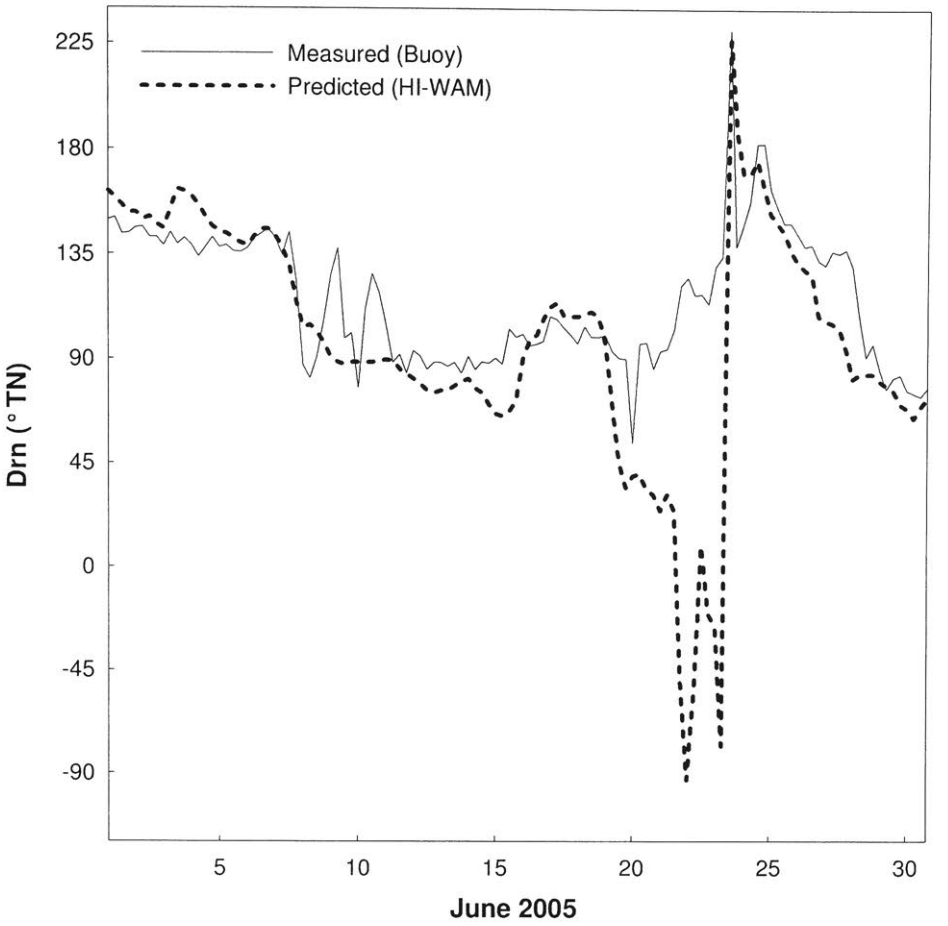

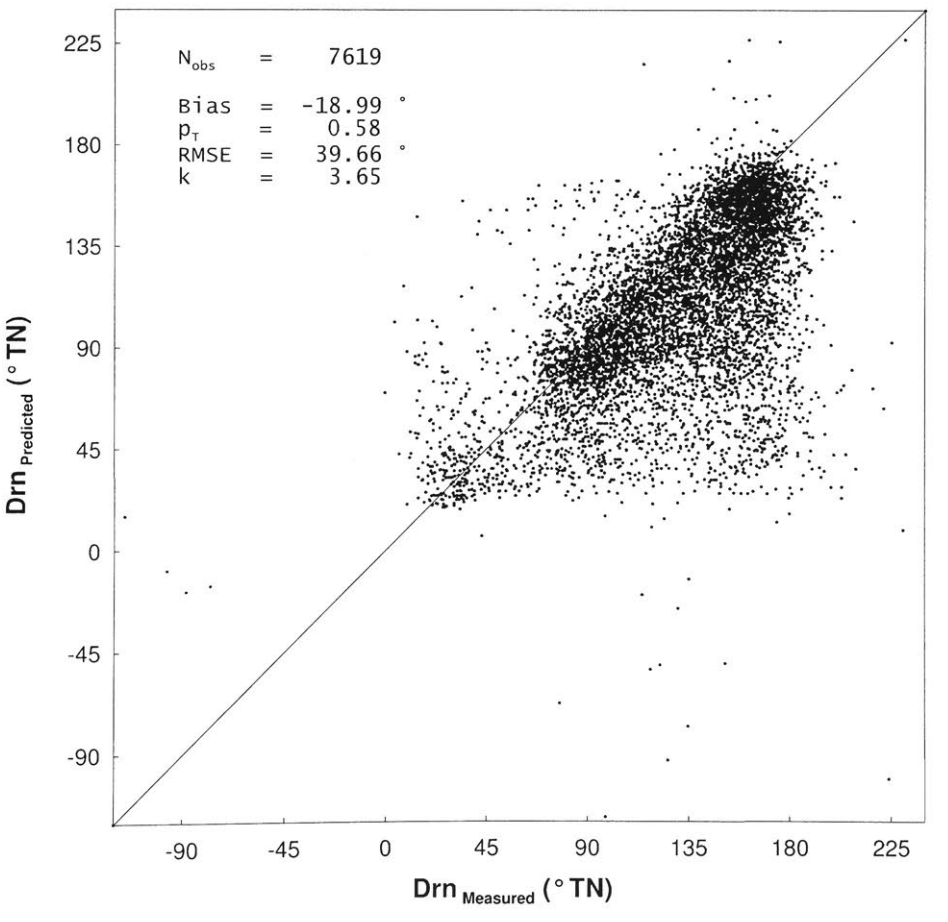

WRL Report No. 237	COMPARISON OF MEASURED & PREDICTED Drn VALUES BYRON BAY, NEW SOUTH WALES	Figure 7.21

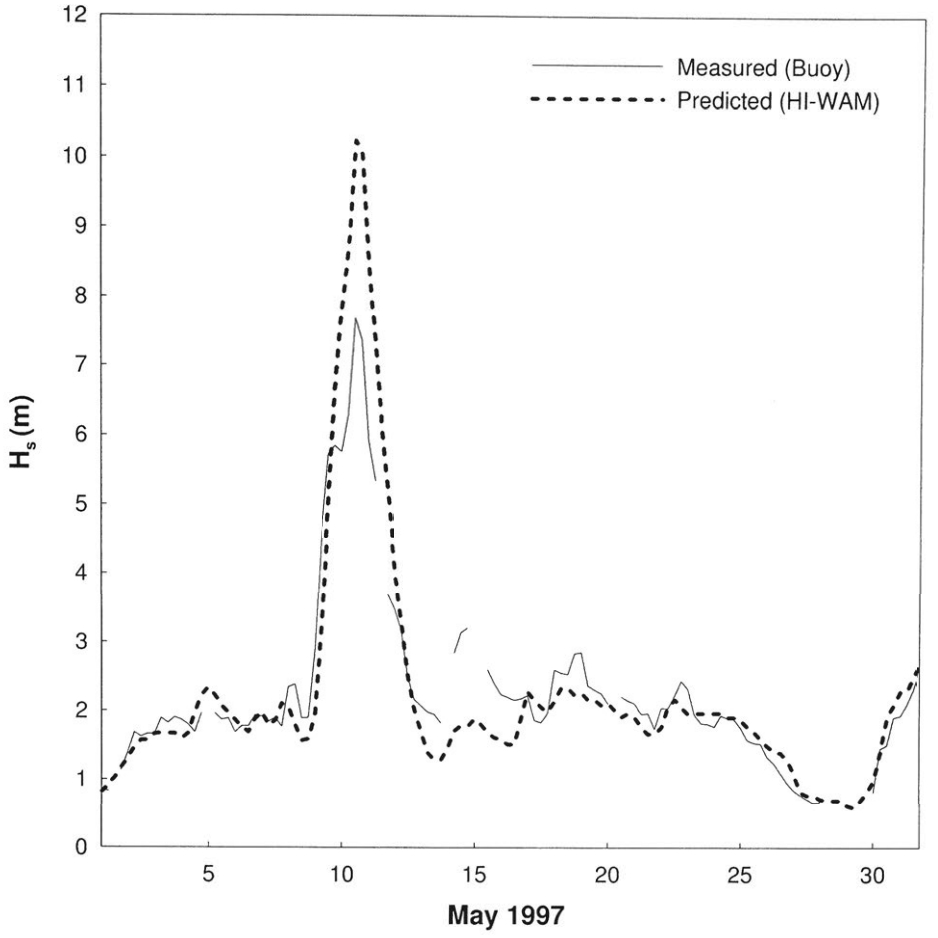

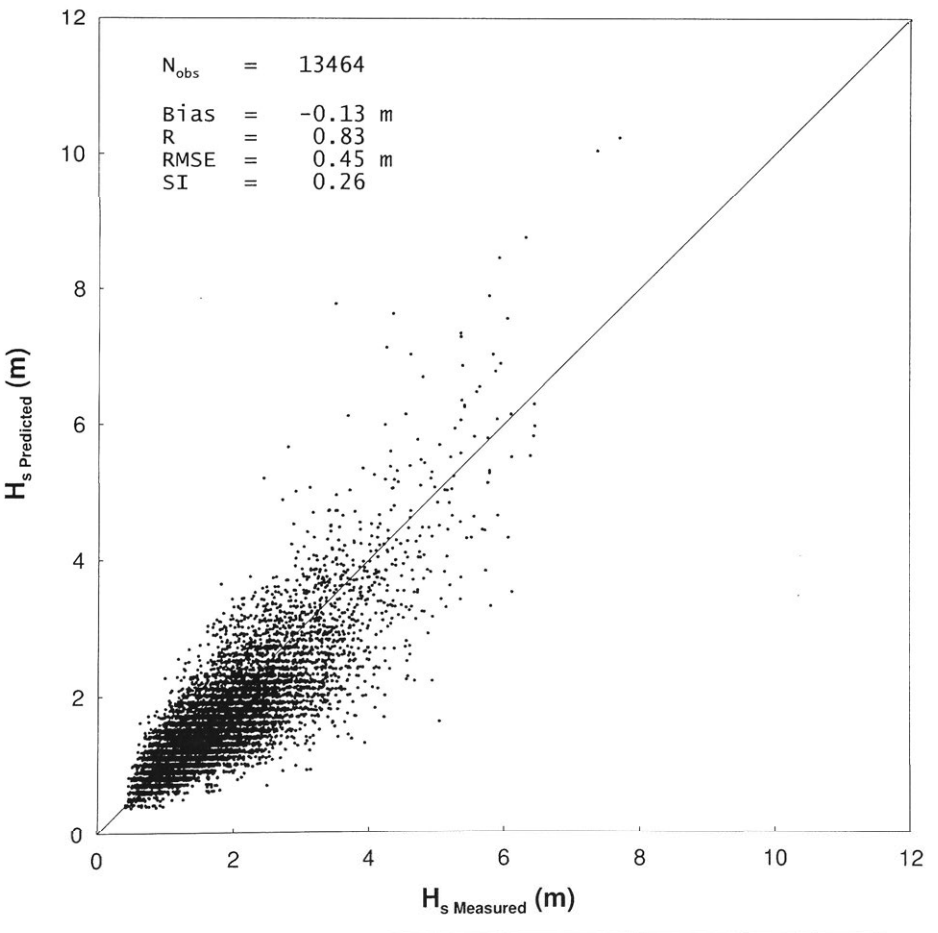

WRL
Report No. 237

COMPARISON OF MEASURED & PREDICTED H_s VALUES
SYDNEY, NEW SOUTH WALES

Figure
7.22

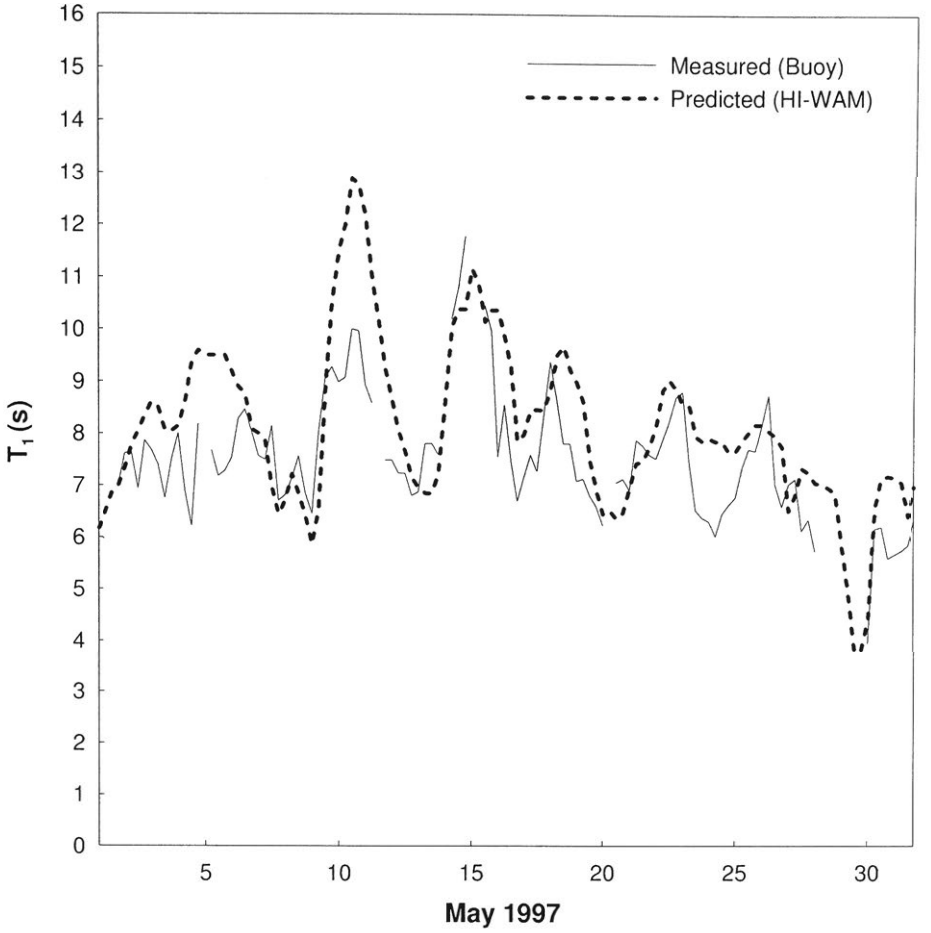

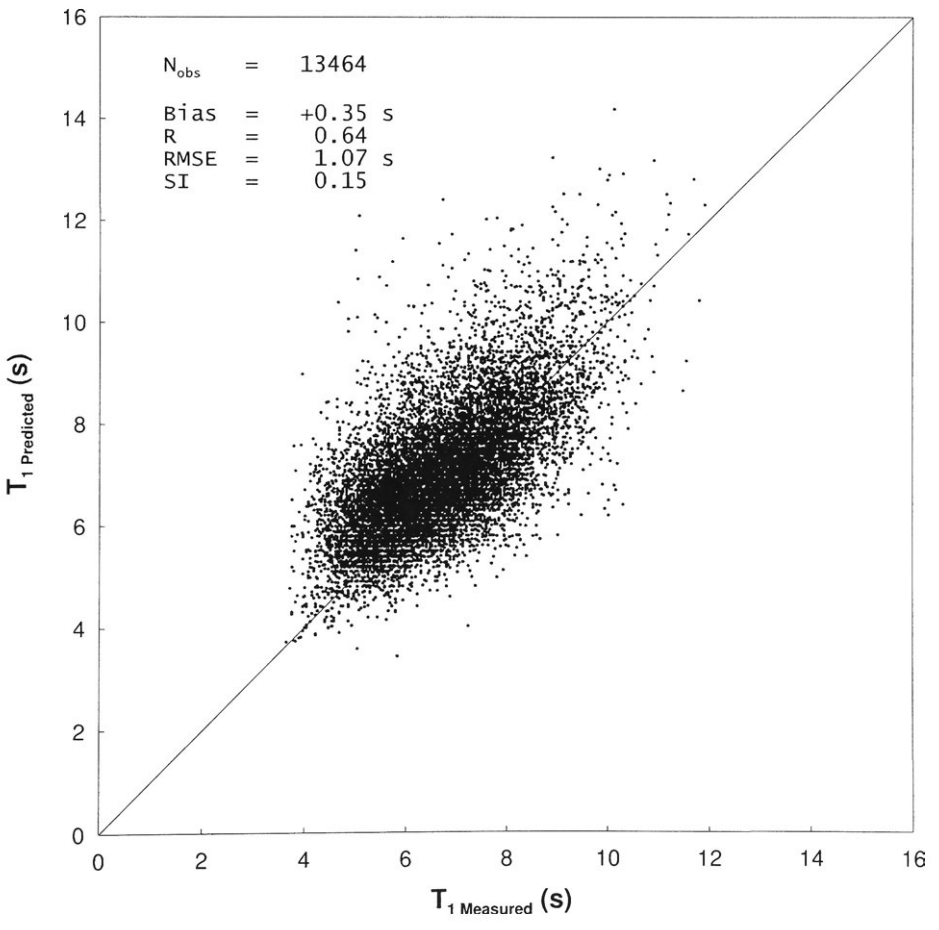

WRL Report No. 237	COMPARISON OF MEASURED & PREDICTED T_1 VALUES SYDNEY, NEW SOUTH WALES	Figure 7.23

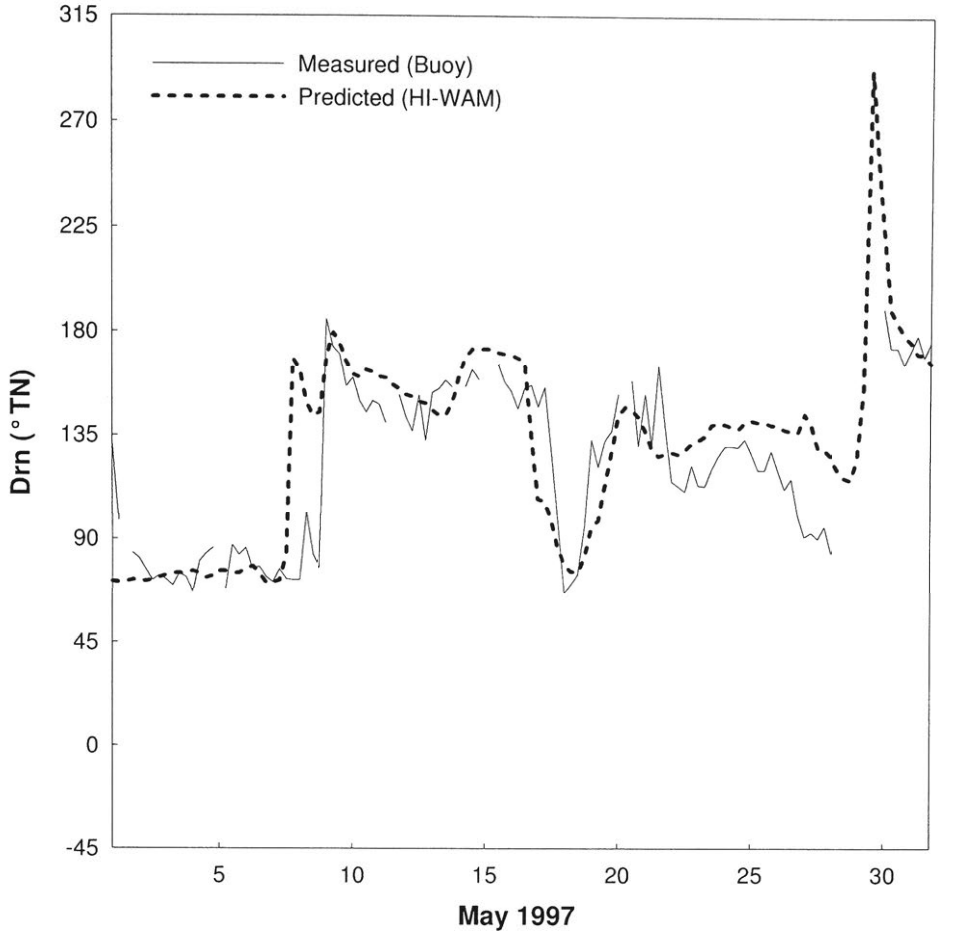

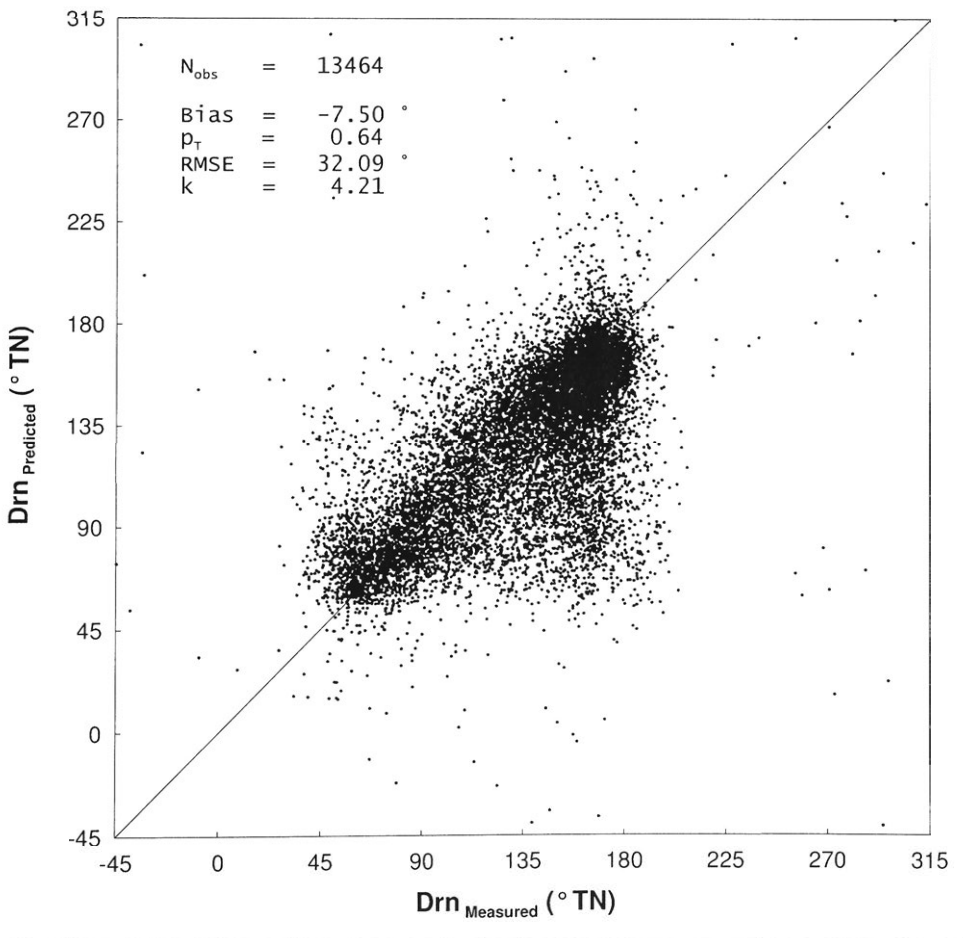

WRL Report No. 237	COMPARISON OF MEASURED & PREDICTED Drn VALUES SYDNEY, NEW SOUTH WALES	Figure 7.24

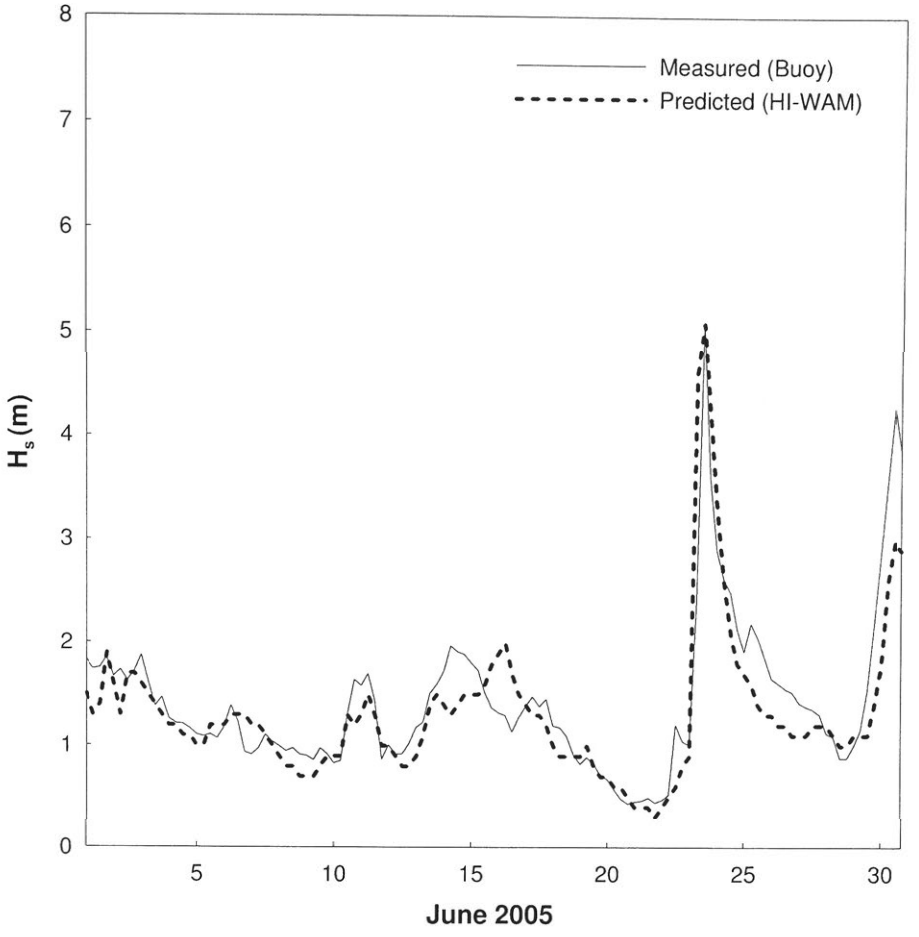

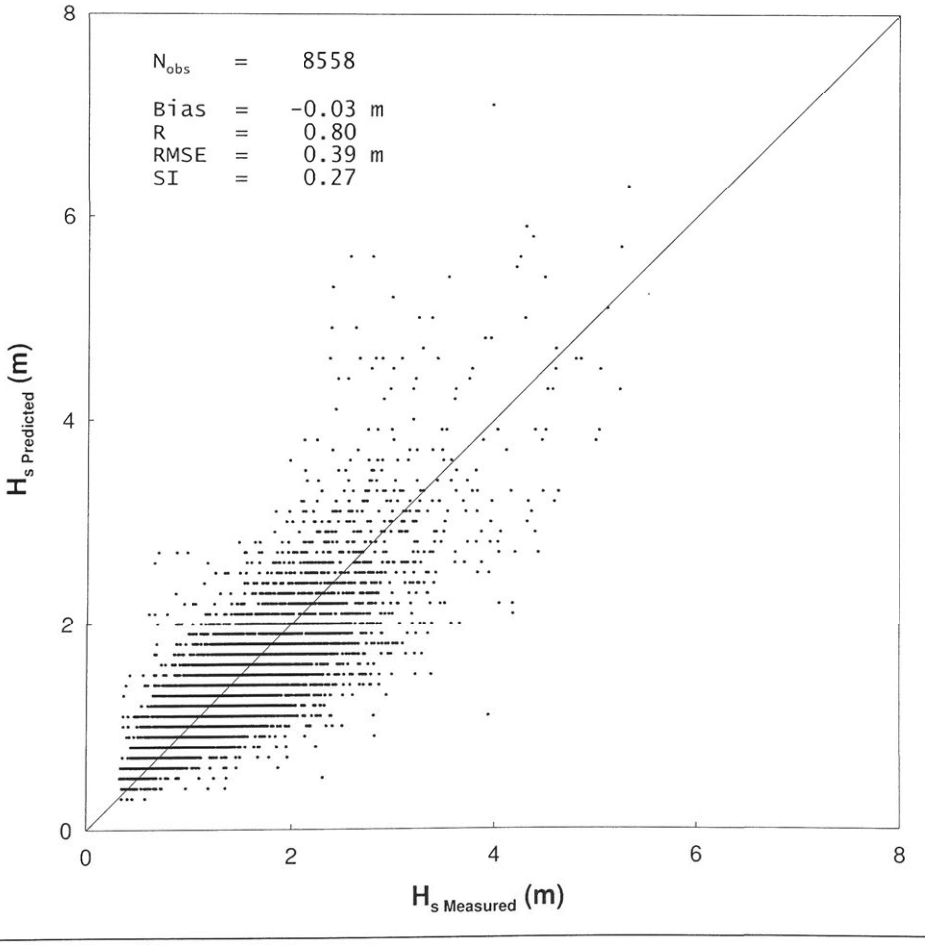

WRL
Report No. 237

COMPARISON OF MEASURED & PREDICTED H_s VALUES
BATEMANS BAY, NEW SOUTH WALES

Figure
7.25

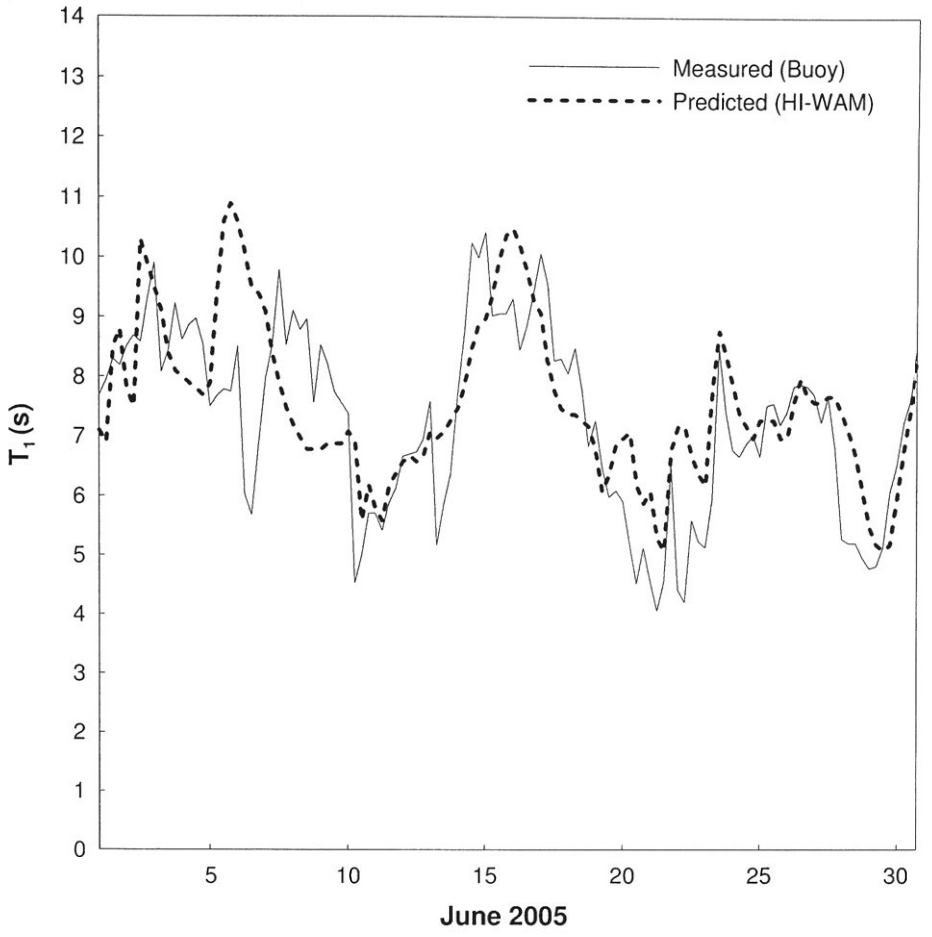

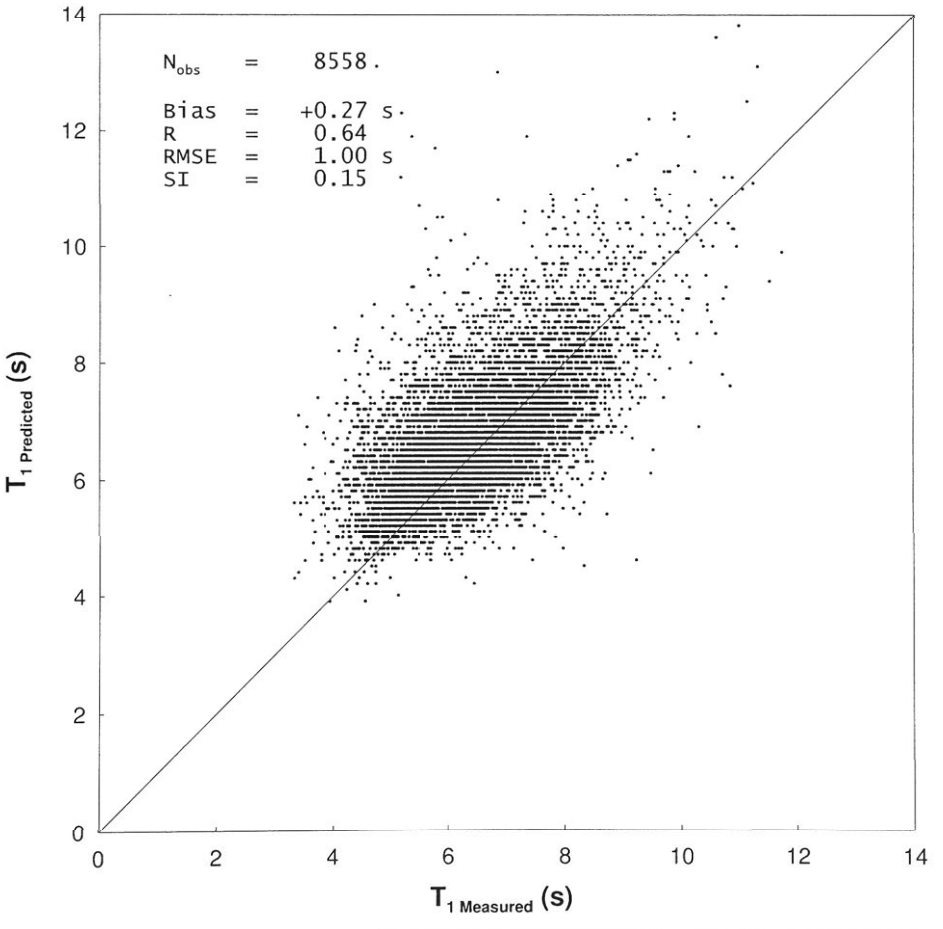

WRL Report No. 237	COMPARISON OF MEASURED & PREDICTED T_1 VALUES BATEMANS BAY, NEW SOUTH WALES	Figure 7.26

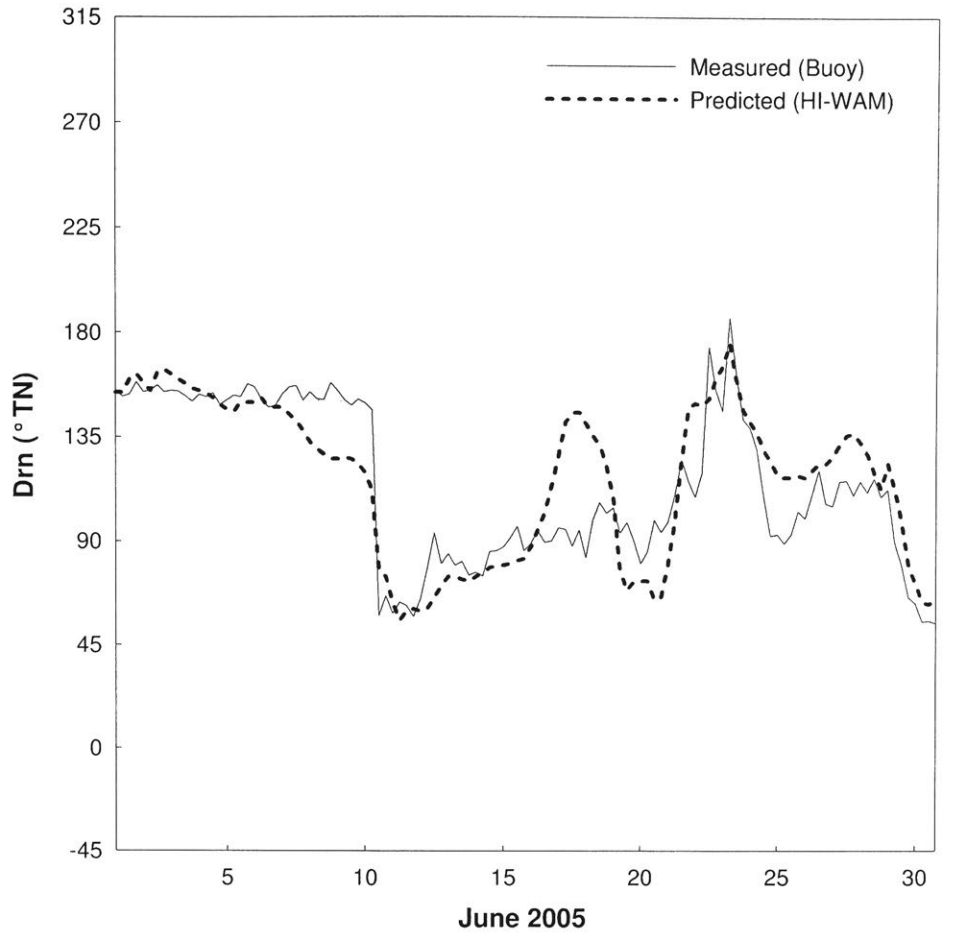

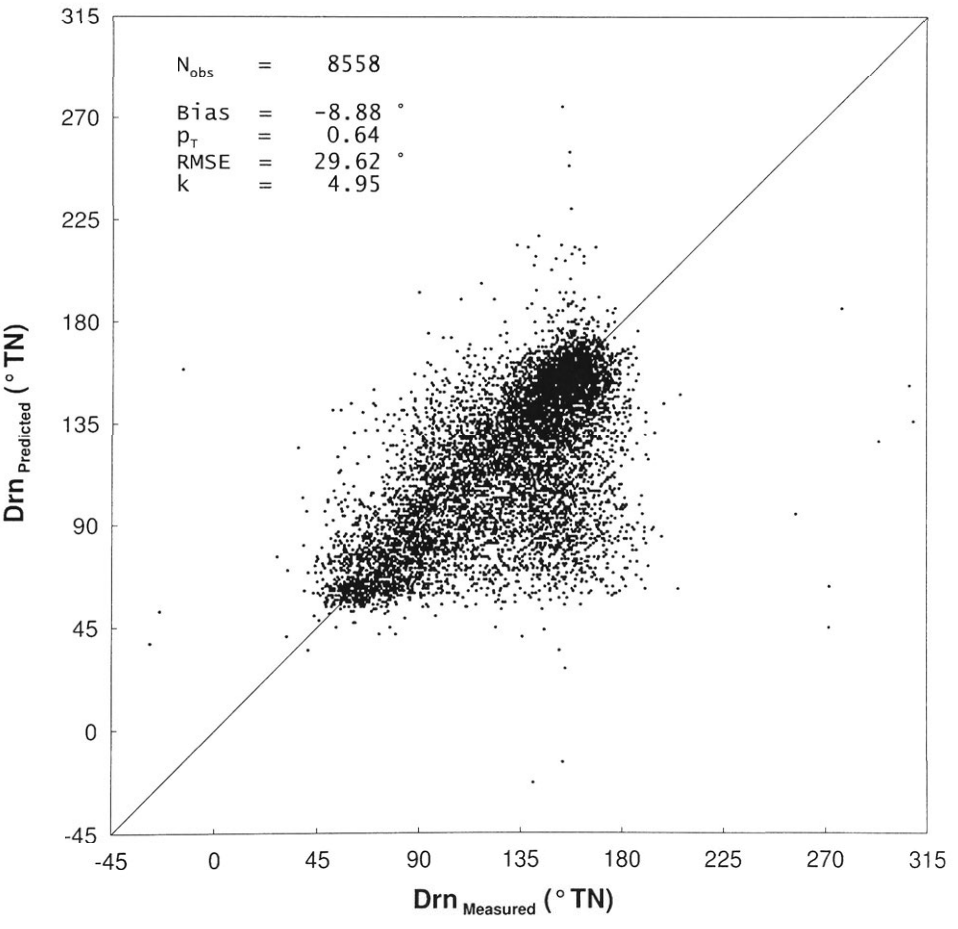

WRL Report No. 237	COMPARISON OF MEASURED & PREDICTED Drn VALUES BATEMANS BAY, NEW SOUTH WALES	Figure 7.27

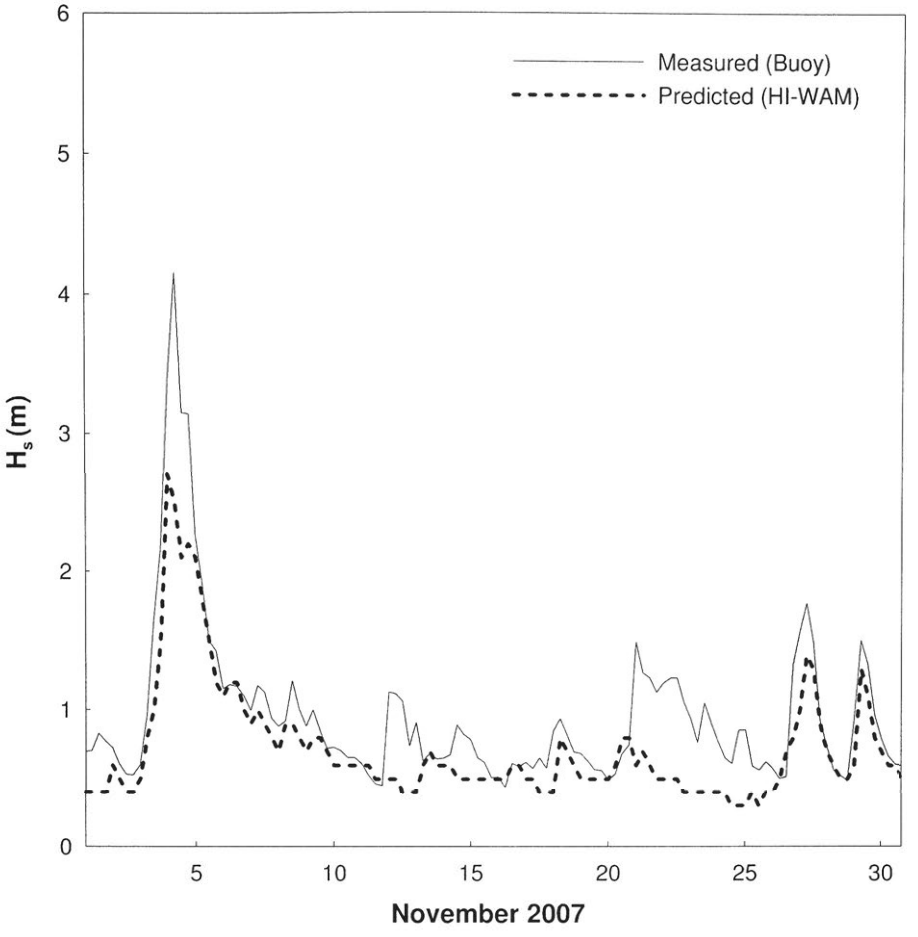

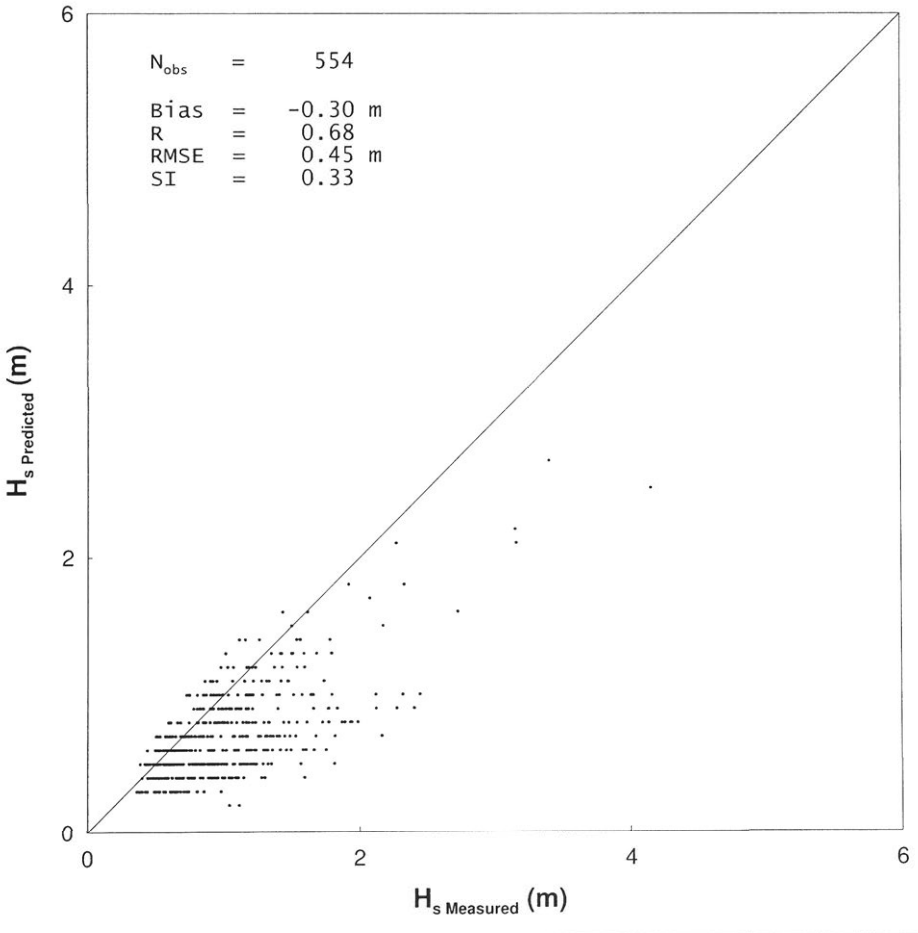

WRL
Report No. 237

COMPARISON OF MEASURED & PREDICTED H_s VALUES
LAKES ENTRANCE, VICTORIA

Figure
7.28

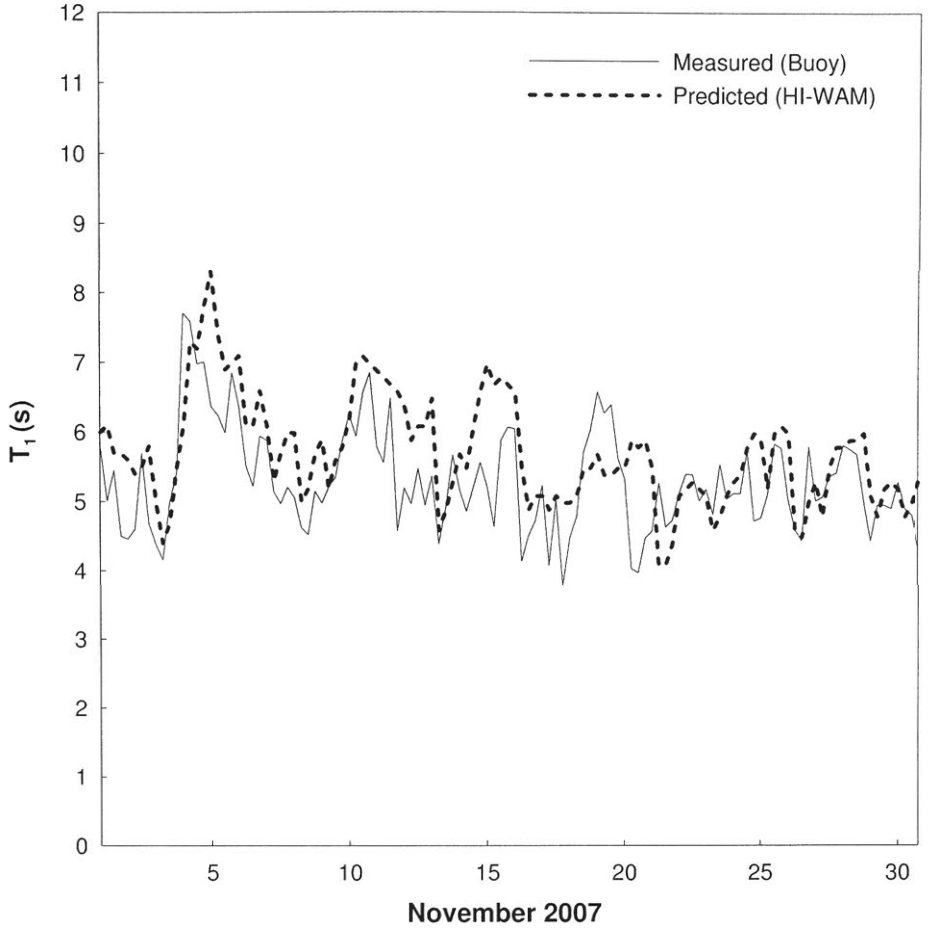

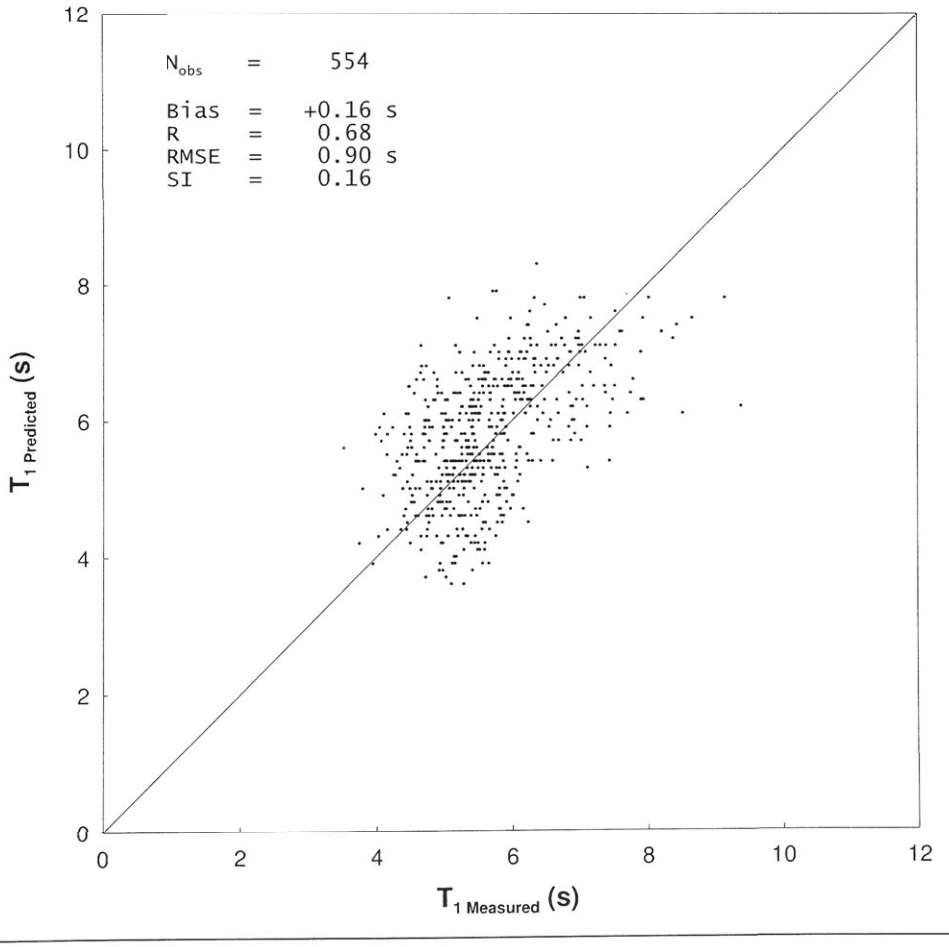

WRL
Report No. 237

COMPARISON OF MEASURED & PREDICTED T_1 VALUES
LAKES ENTRANCE, VICTORIA

Figure
7.29

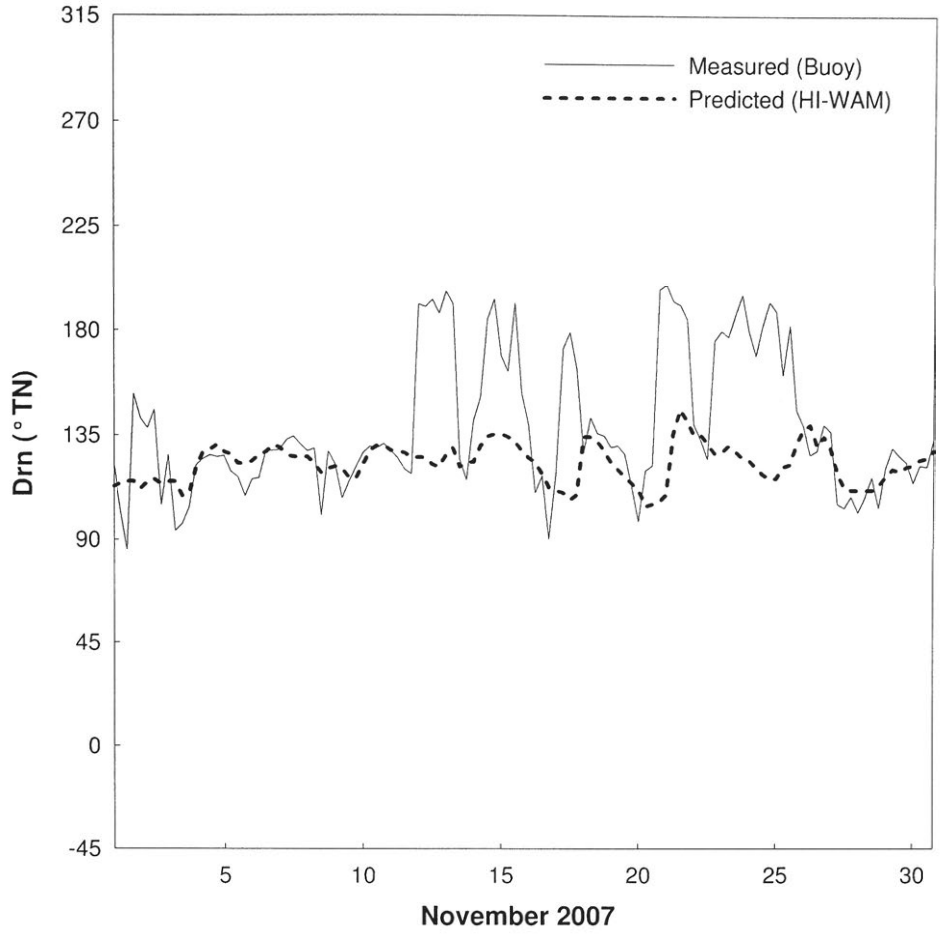

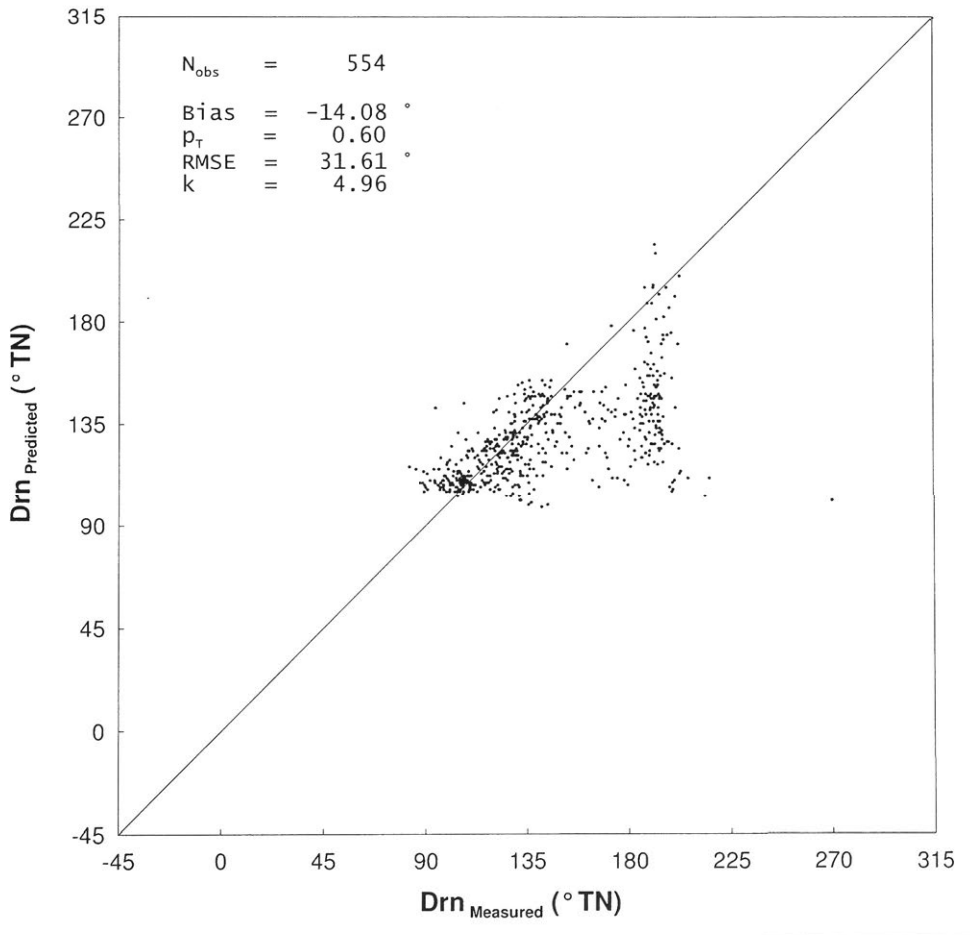

WRL Report No. 237	COMPARISON OF MEASURED & PREDICTED Drn VALUES LAKES ENTRANCE, VICTORIA	Figure 7.30

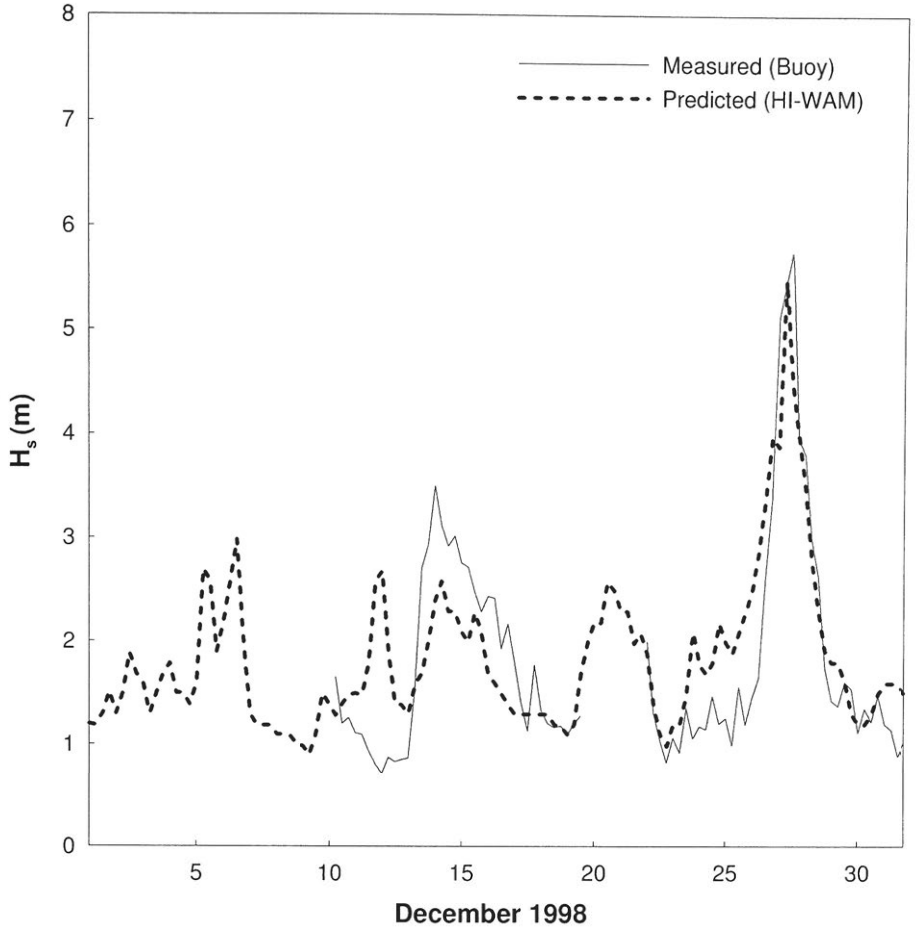

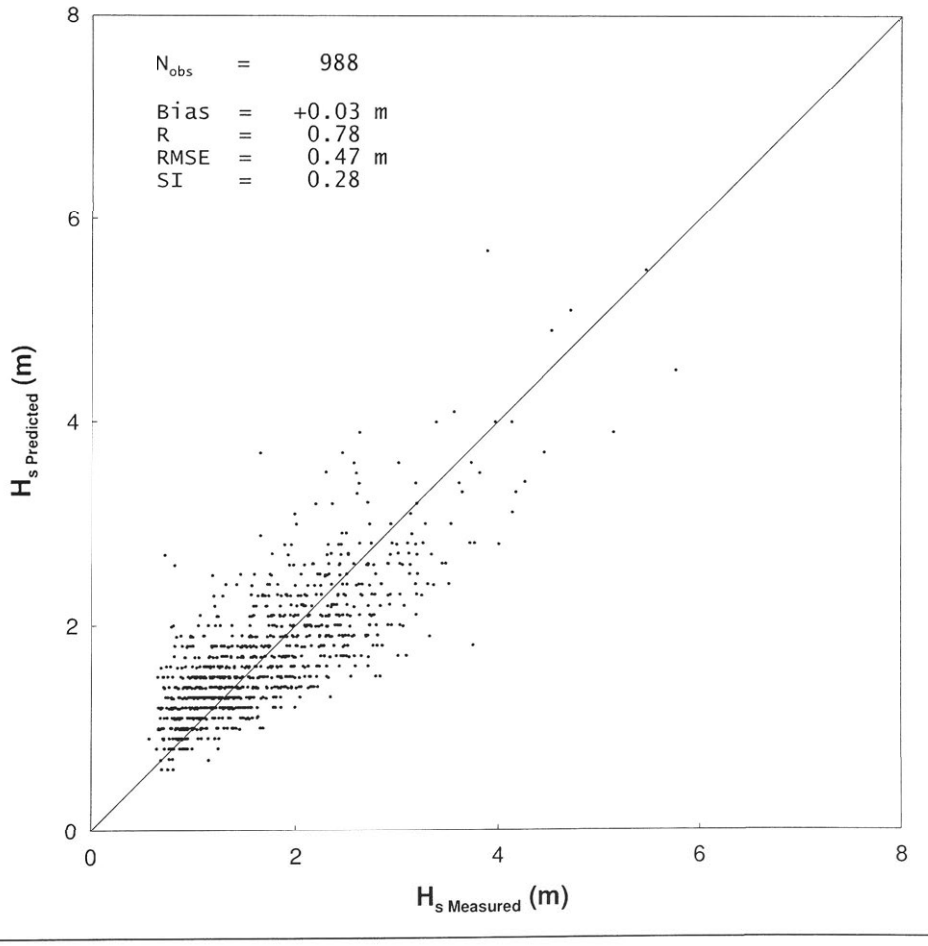

WRL Report No. 237	COMPARISON OF MEASURED & PREDICTED H_s VALUES KINGFISH B, VICTORIA	Figure 7.31

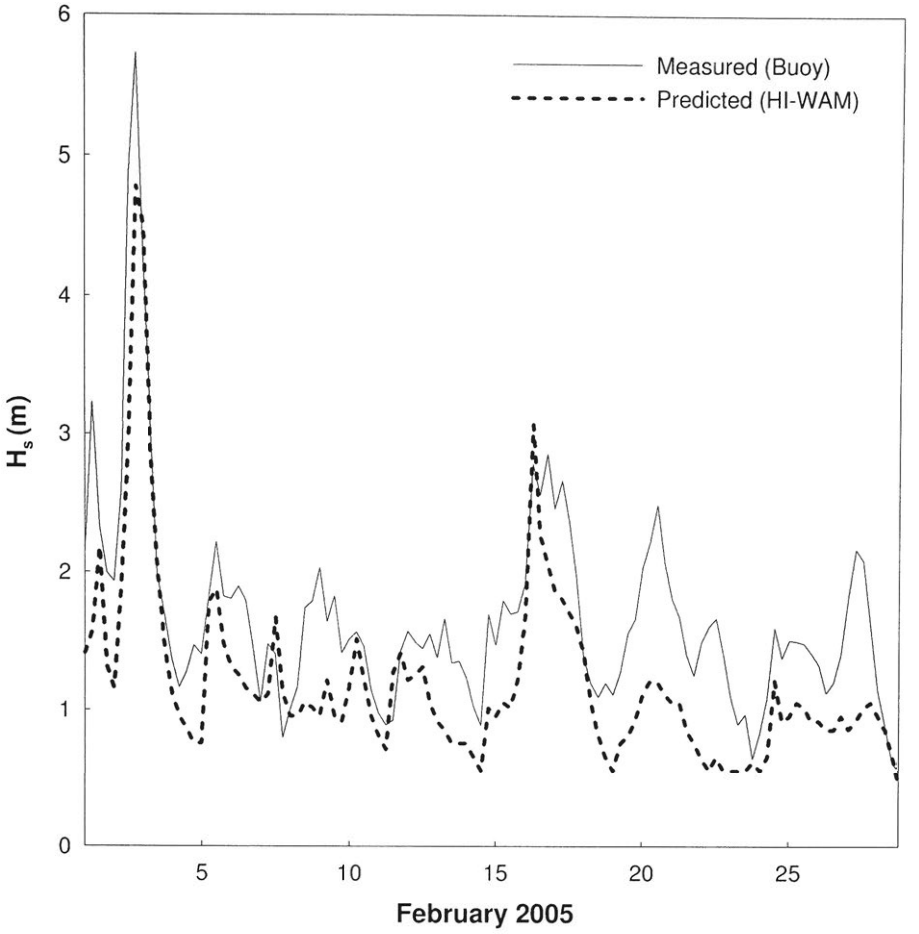

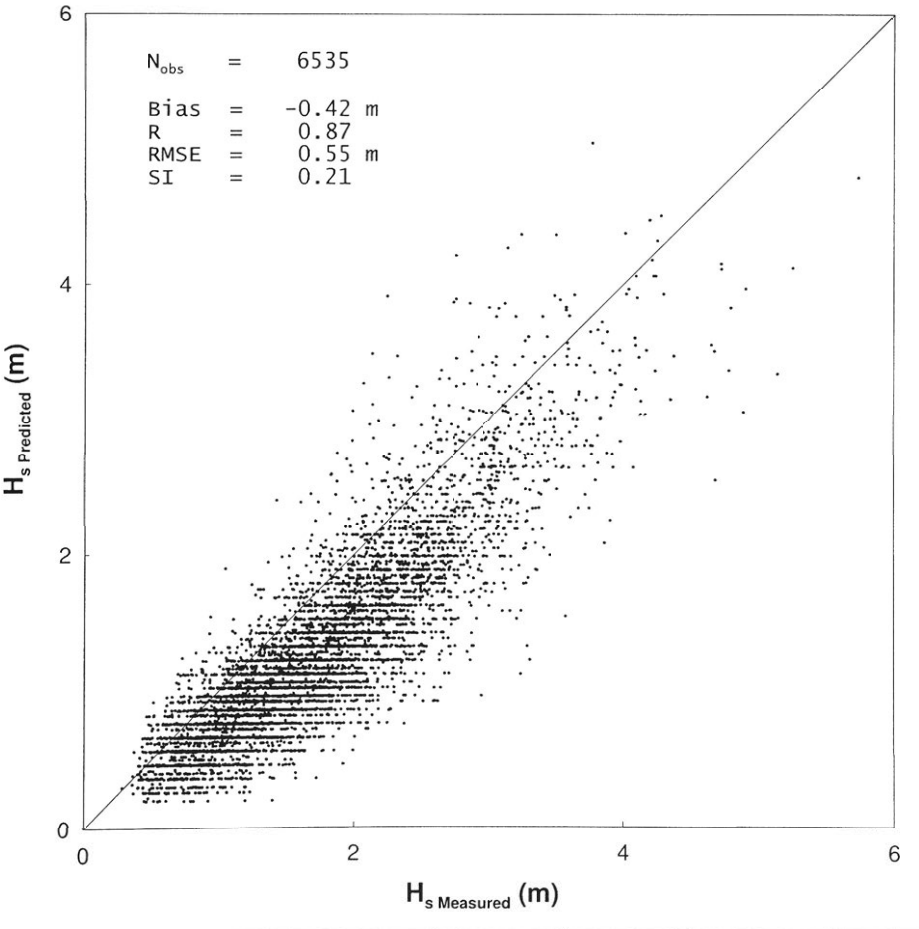

WRL Report No. 237	COMPARISON OF MEASURED & PREDICTED H_s VALUES POINT NEPEAN, VICTORIA	Figure 7.32

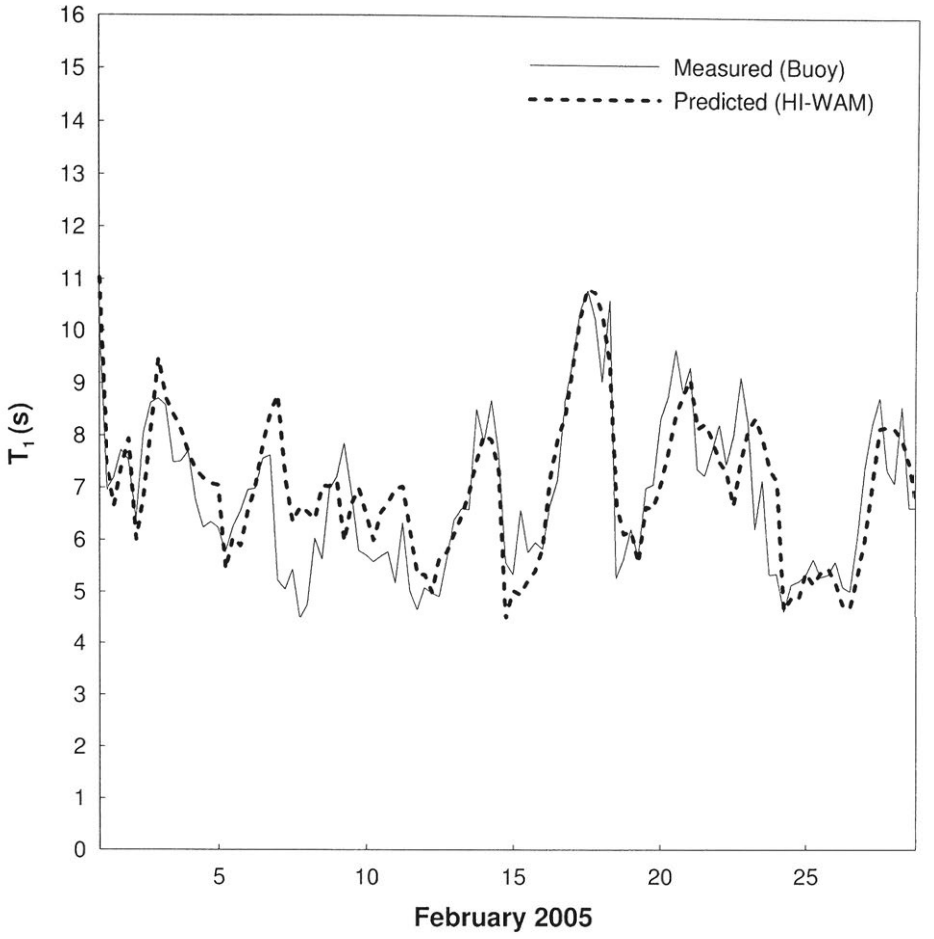

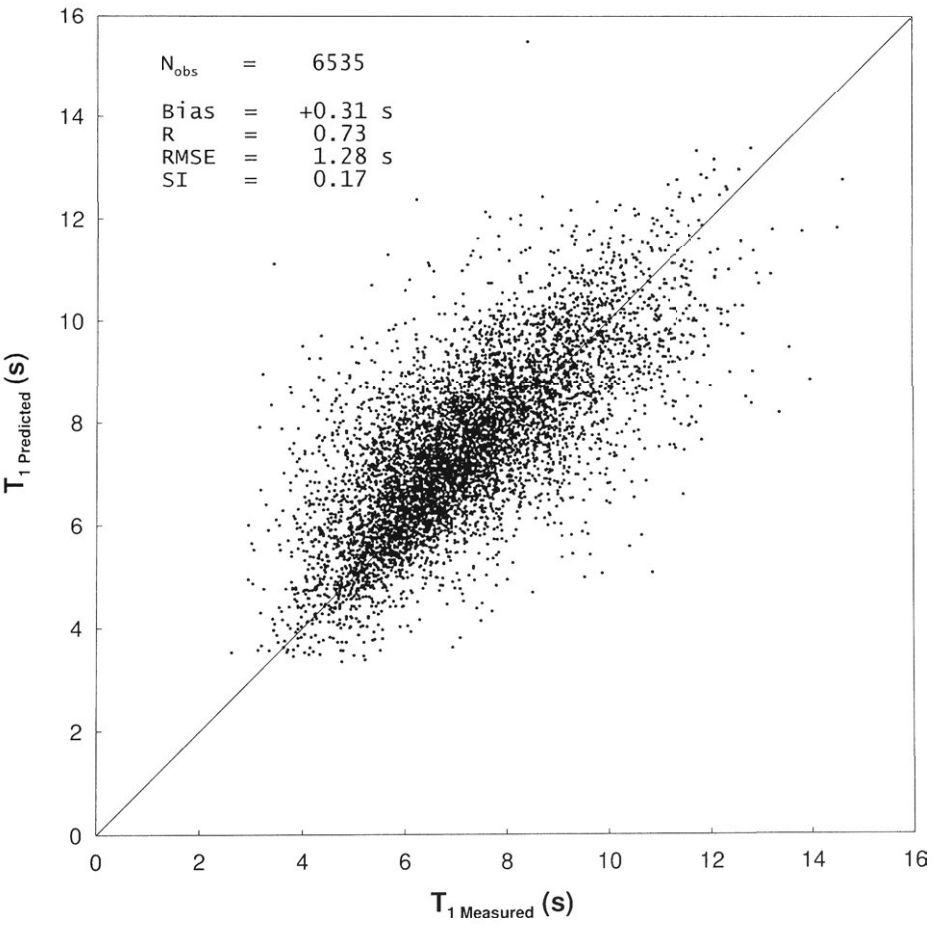

WRL Report No. 237	COMPARISON OF MEASURED & PREDICTED T_1 VALUES POINT NEPEAN, VICTORIA	Figure 7.33

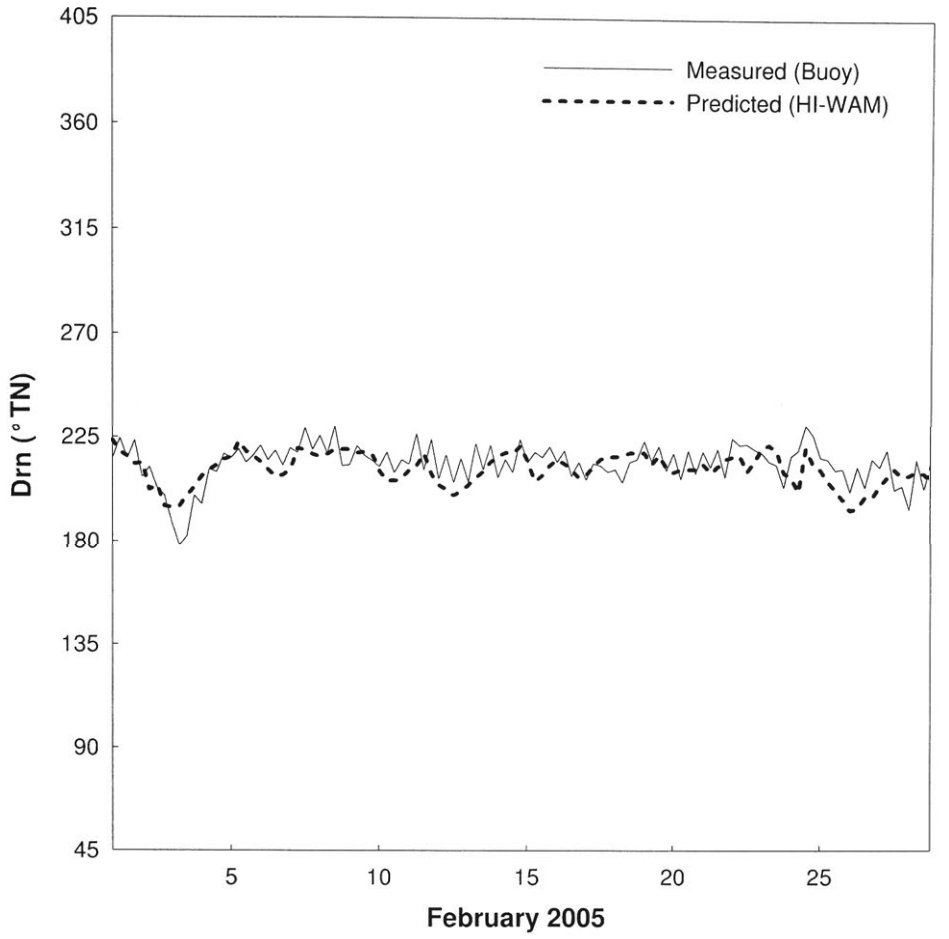

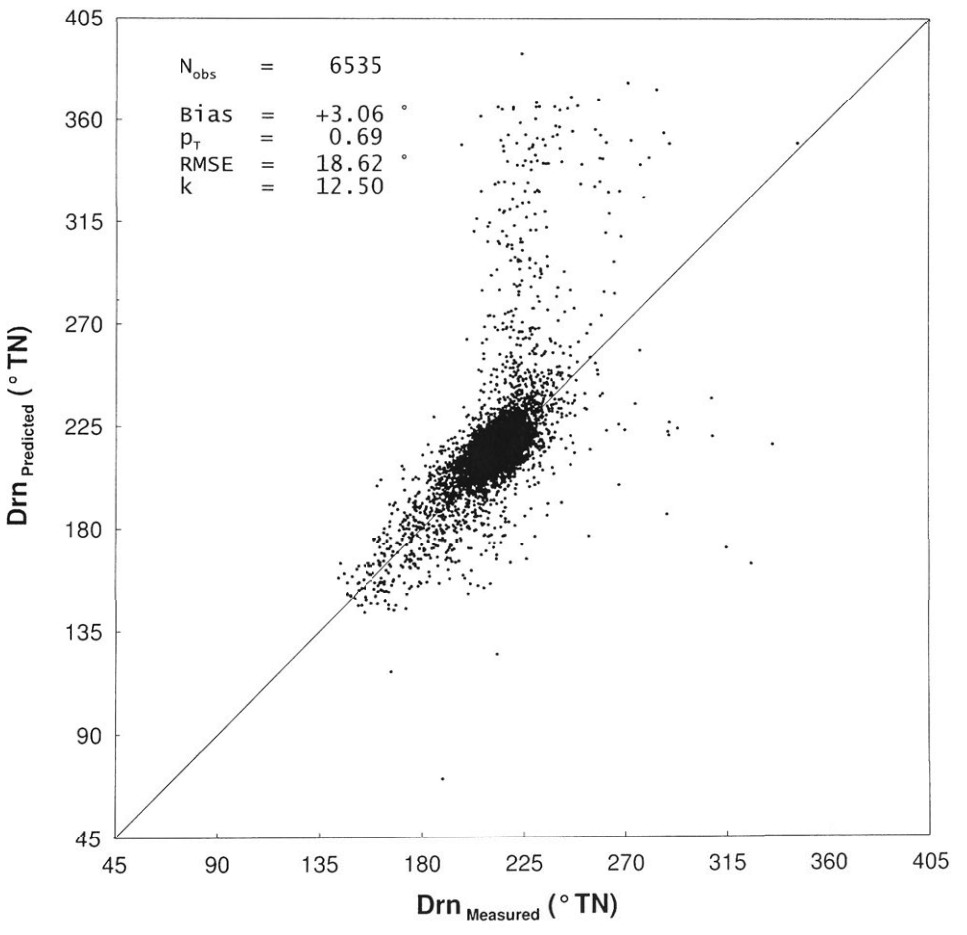

WRL Report No. 237	COMPARISON OF MEASURED & PREDICTED Drn VALUES POINT NEPEAN, VICTORIA	Figure 7.34

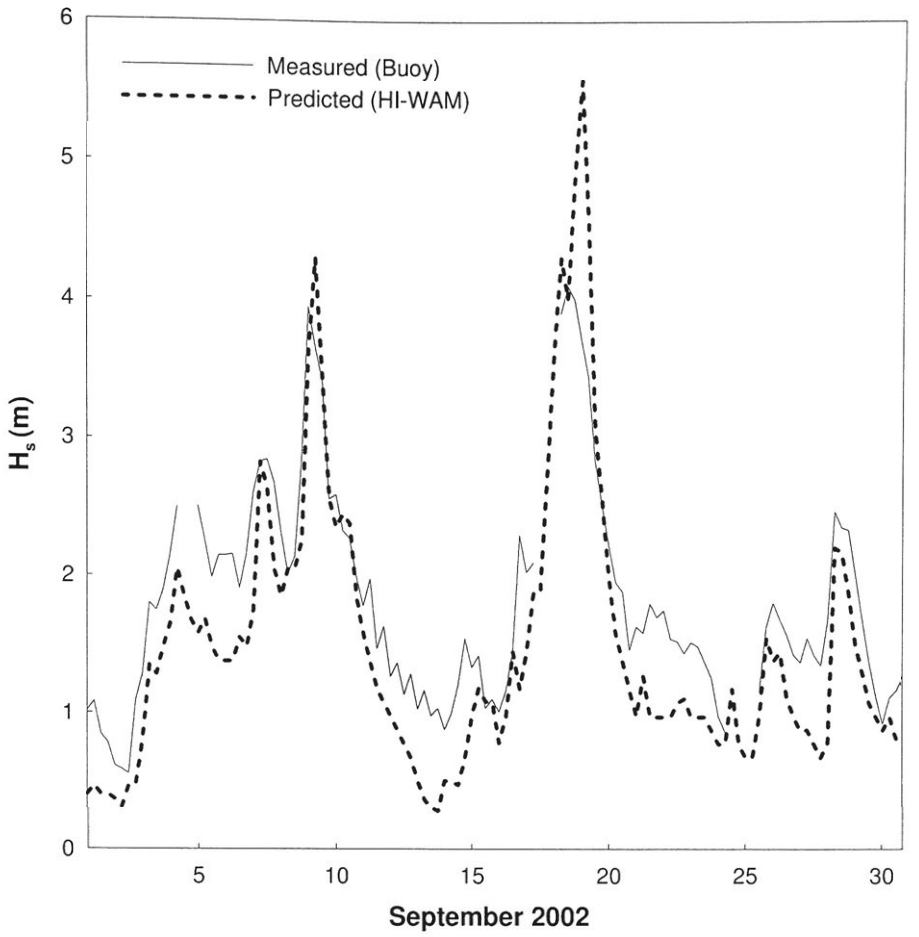

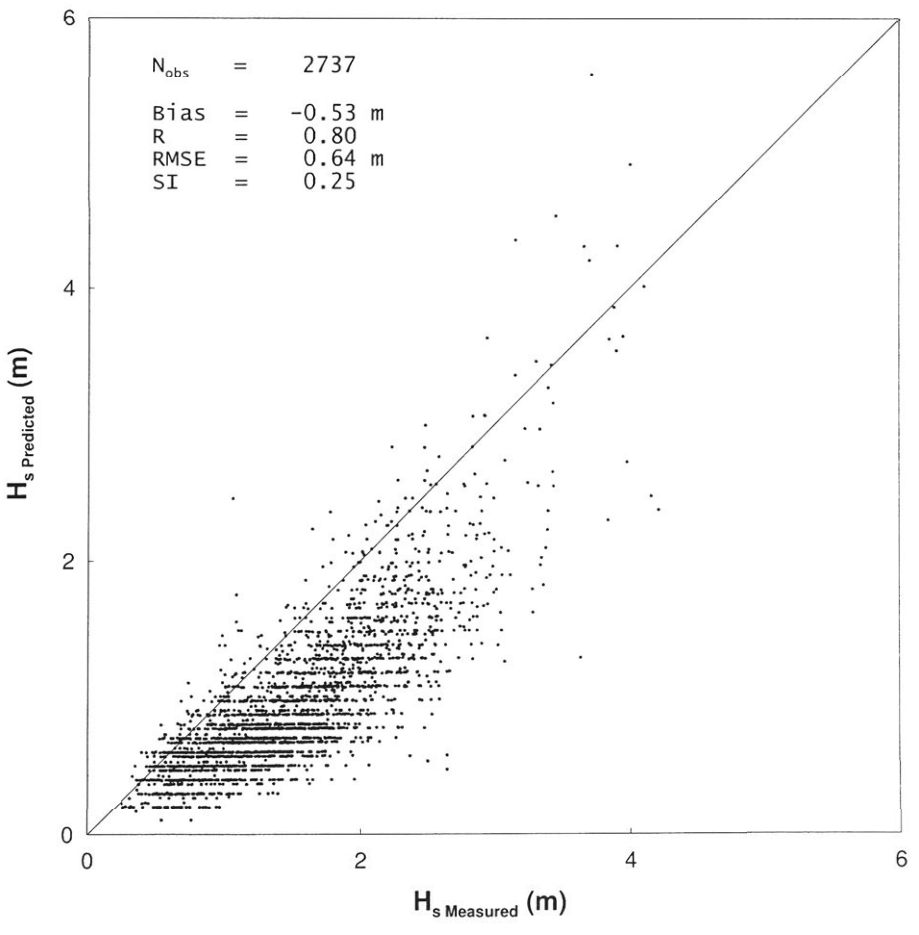

WRL Report No. 237	COMPARISON OF MEASURED & PREDICTED H_s VALUES POINT LONSDALE, VICTORIA	Figure 7.35

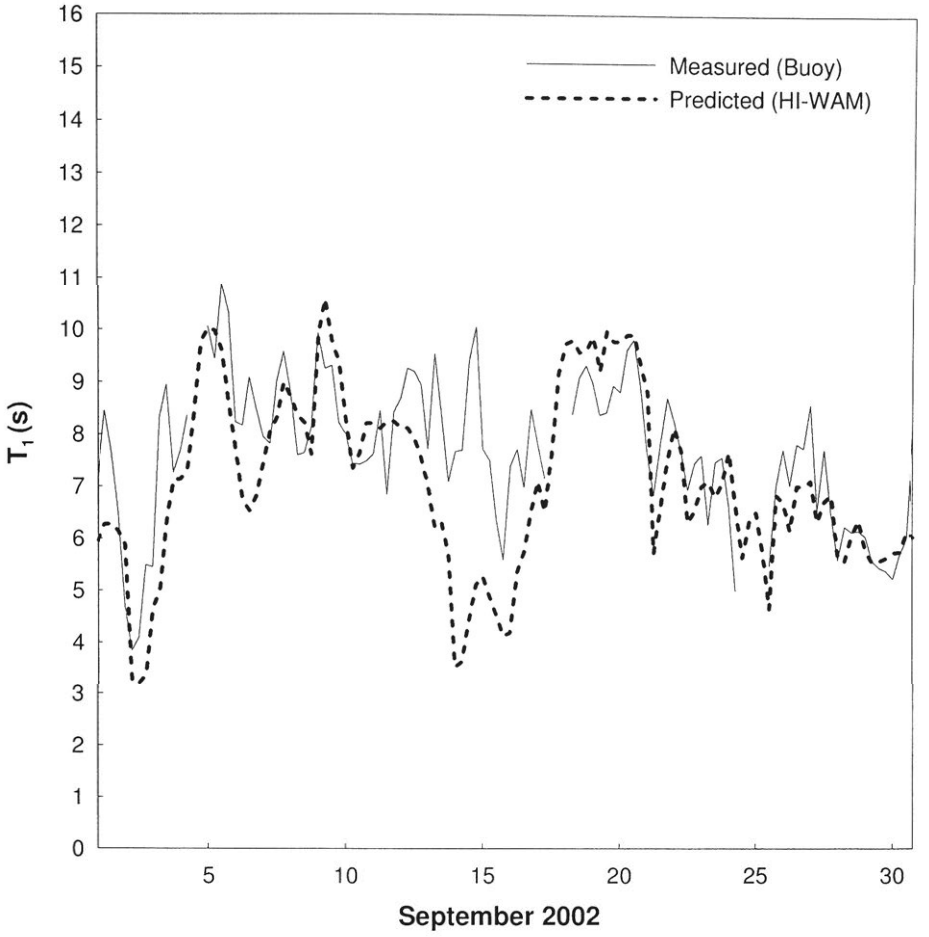

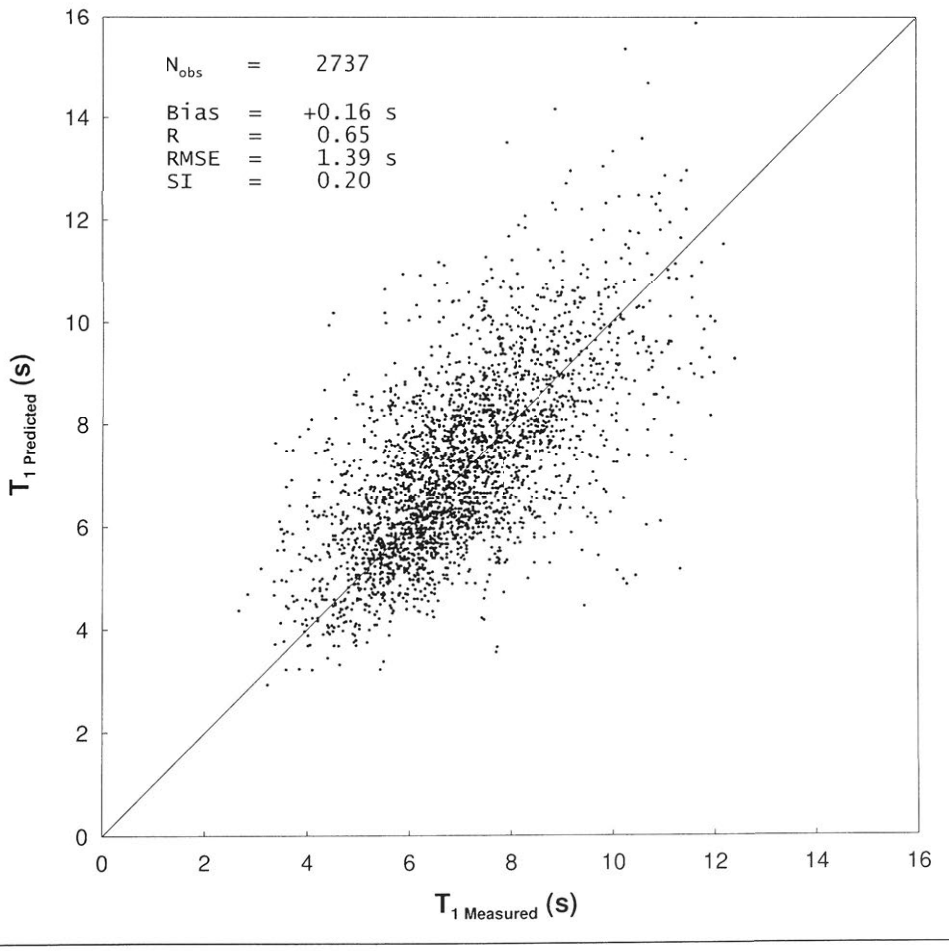

WRL Report No. 237	COMPARISON OF MEASURED & PREDICTED T_1 VALUES POINT LONSDALE, VICTORIA	Figure 7.36

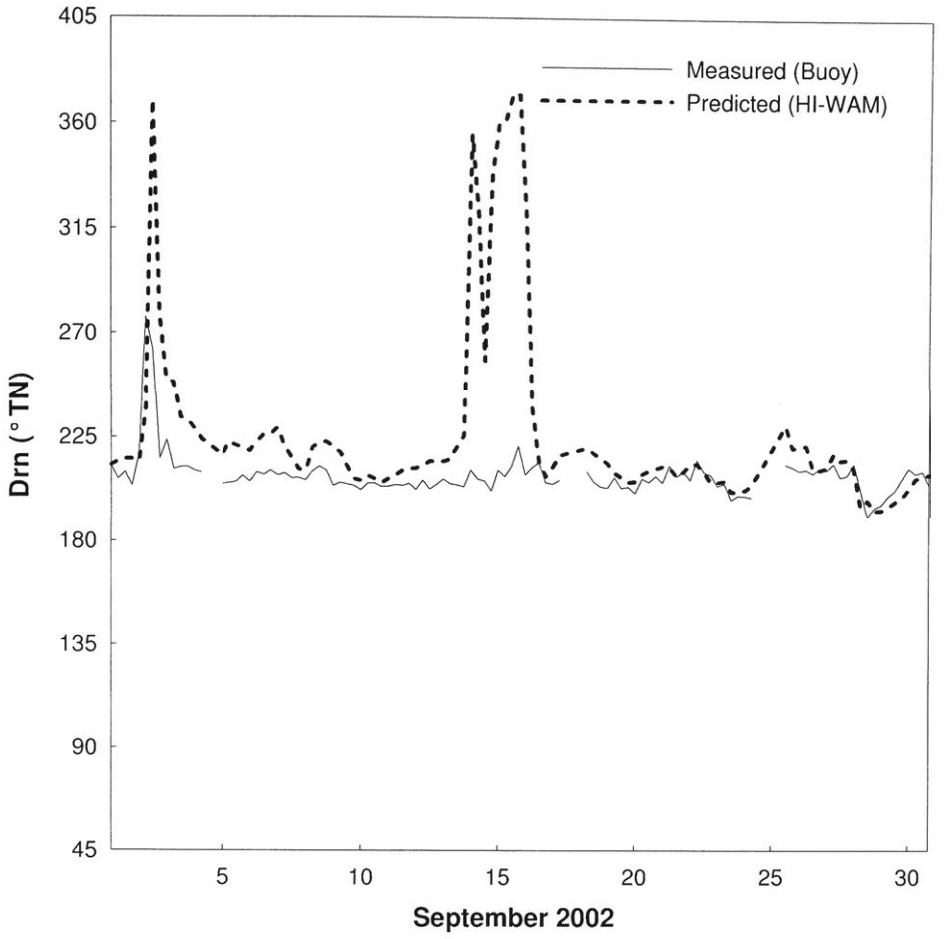

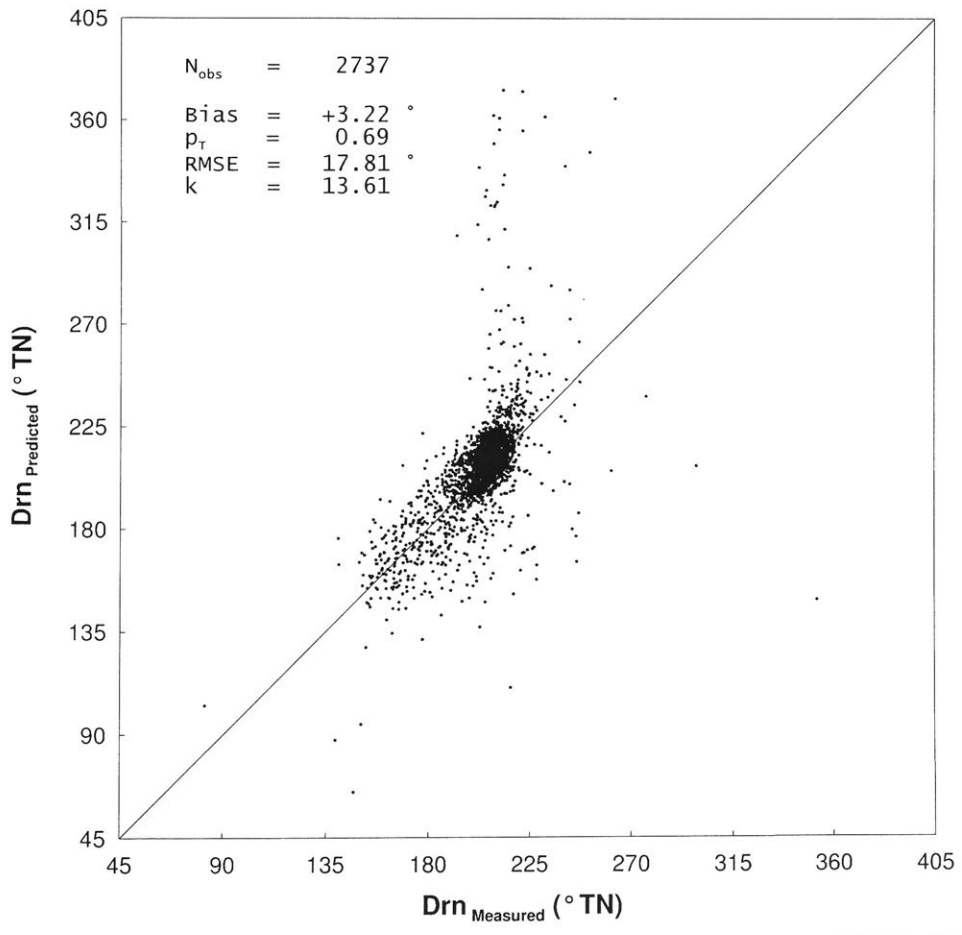

WRL Report No. 237	COMPARISON OF MEASURED & PREDICTED Drn VALUES POINT LONSDALE, VICTORIA	Figure 7.37

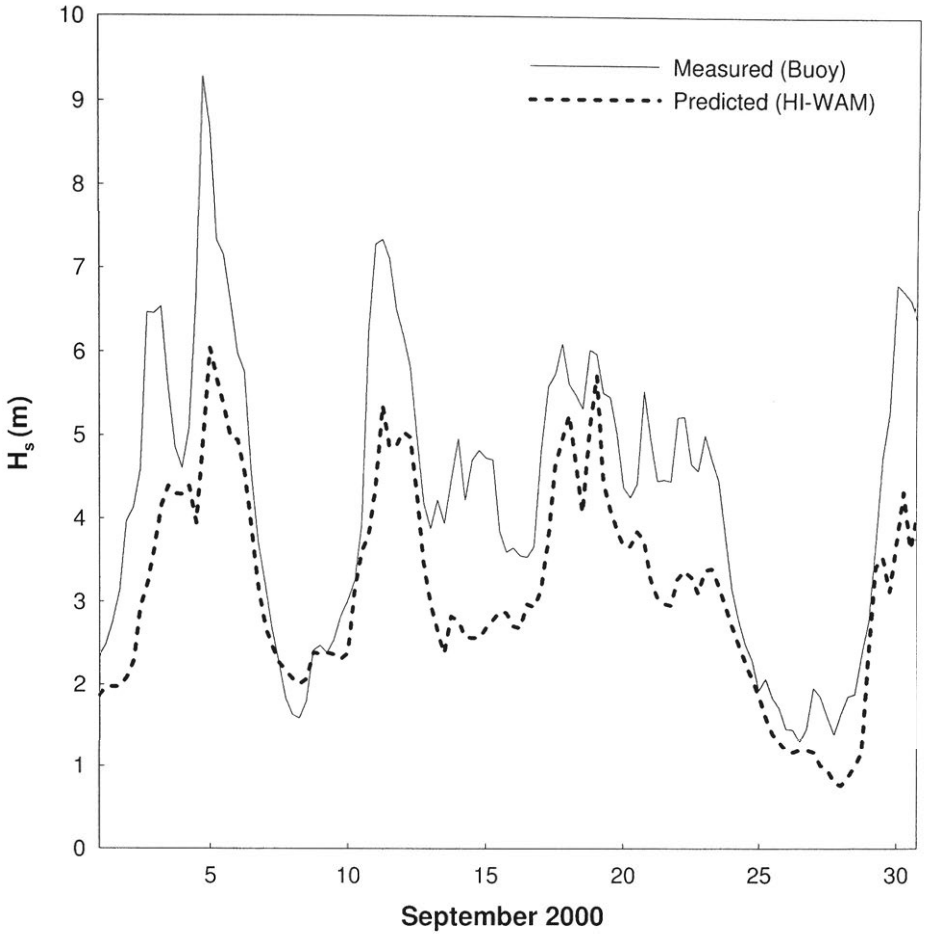

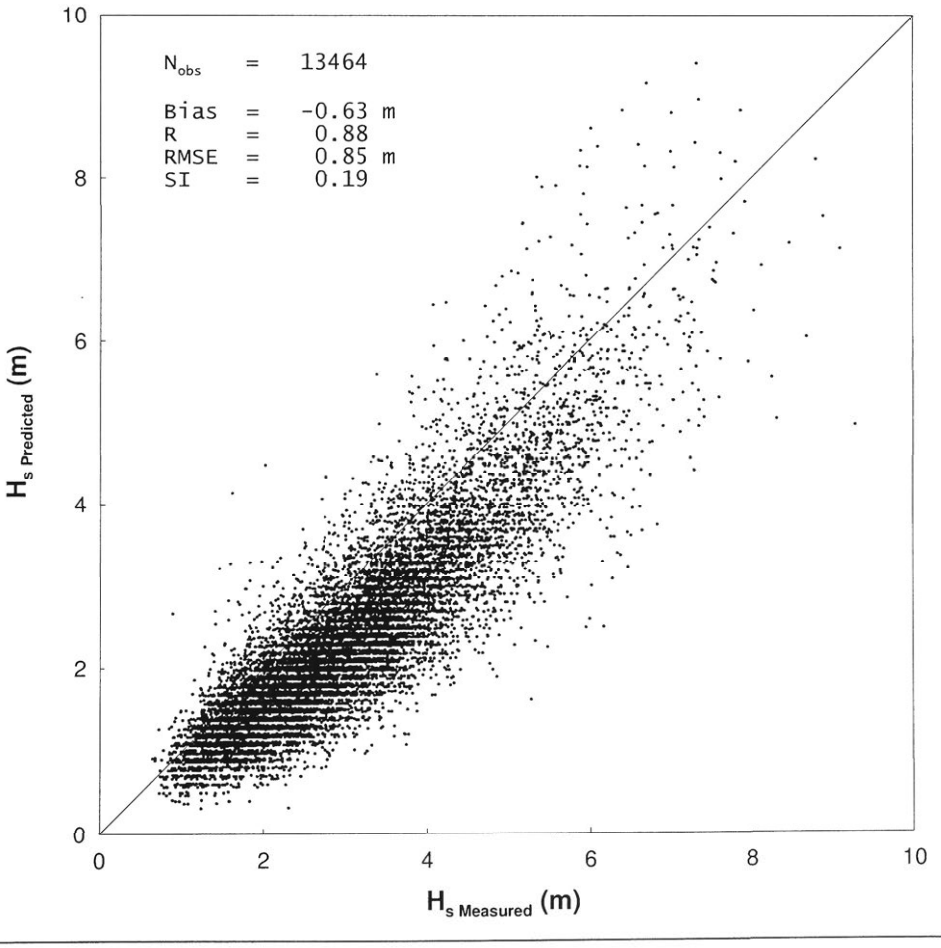

WRL
Report No. 237

COMPARISON OF MEASURED & PREDICTED H_s VALUES
CAPE SORRELL, TASMANIA

Figure
7.38

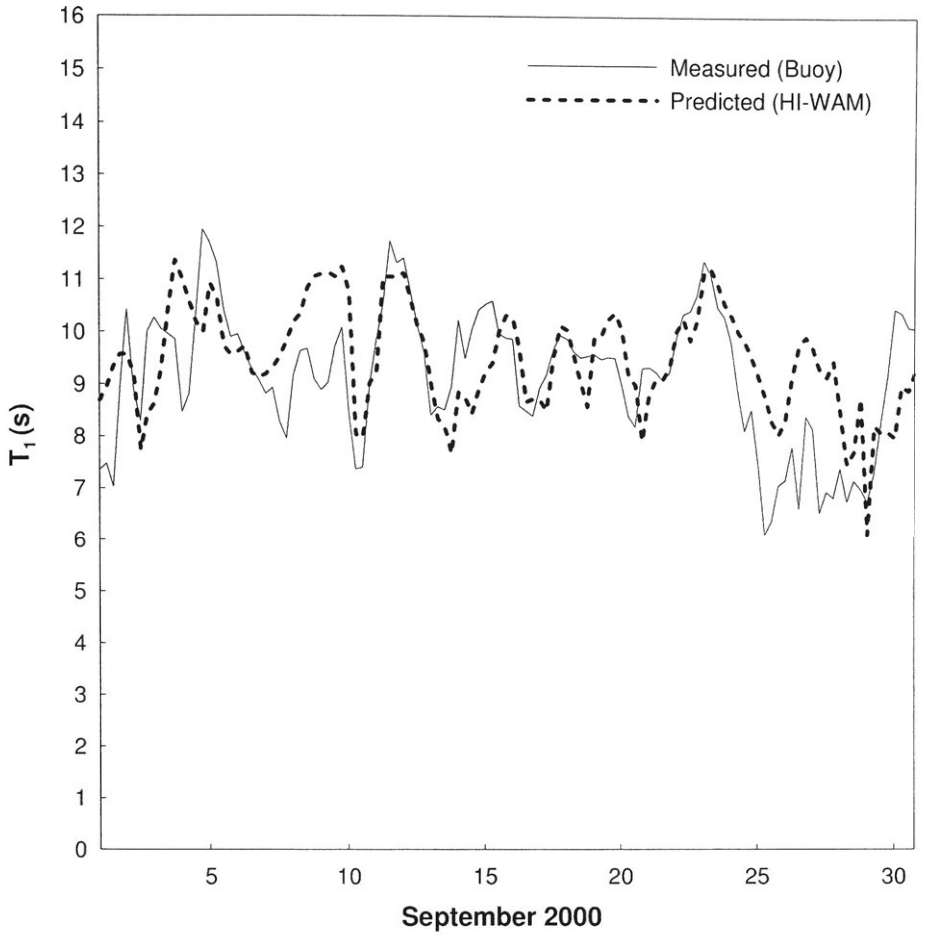

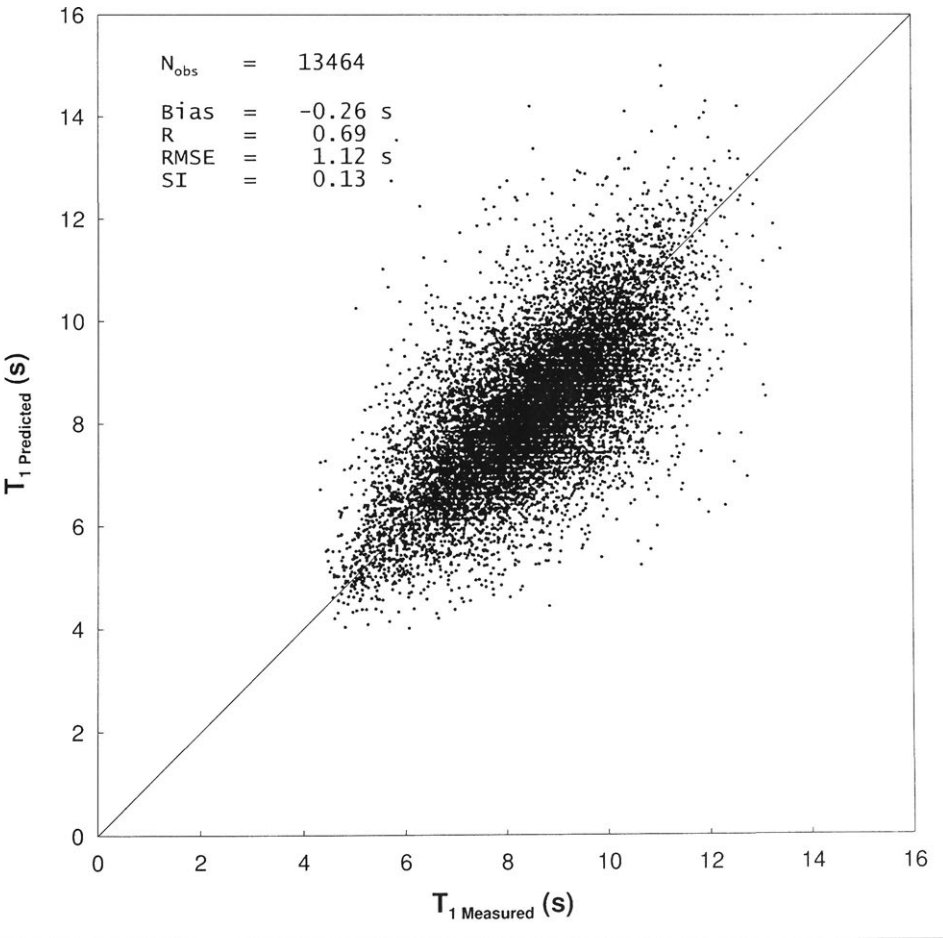

WRL Report No. 237	COMPARISON OF MEASURED & PREDICTED T_1 VALUES CAPE SORRELL, TASMANIA	Figure 7.39

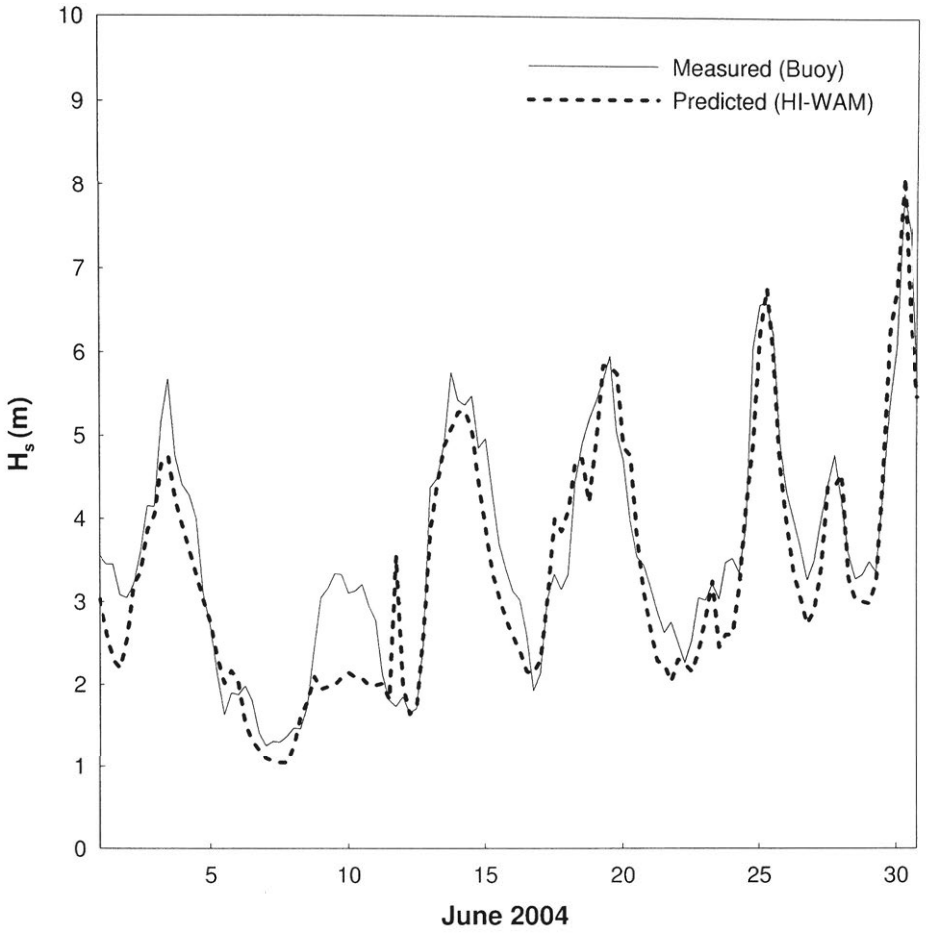

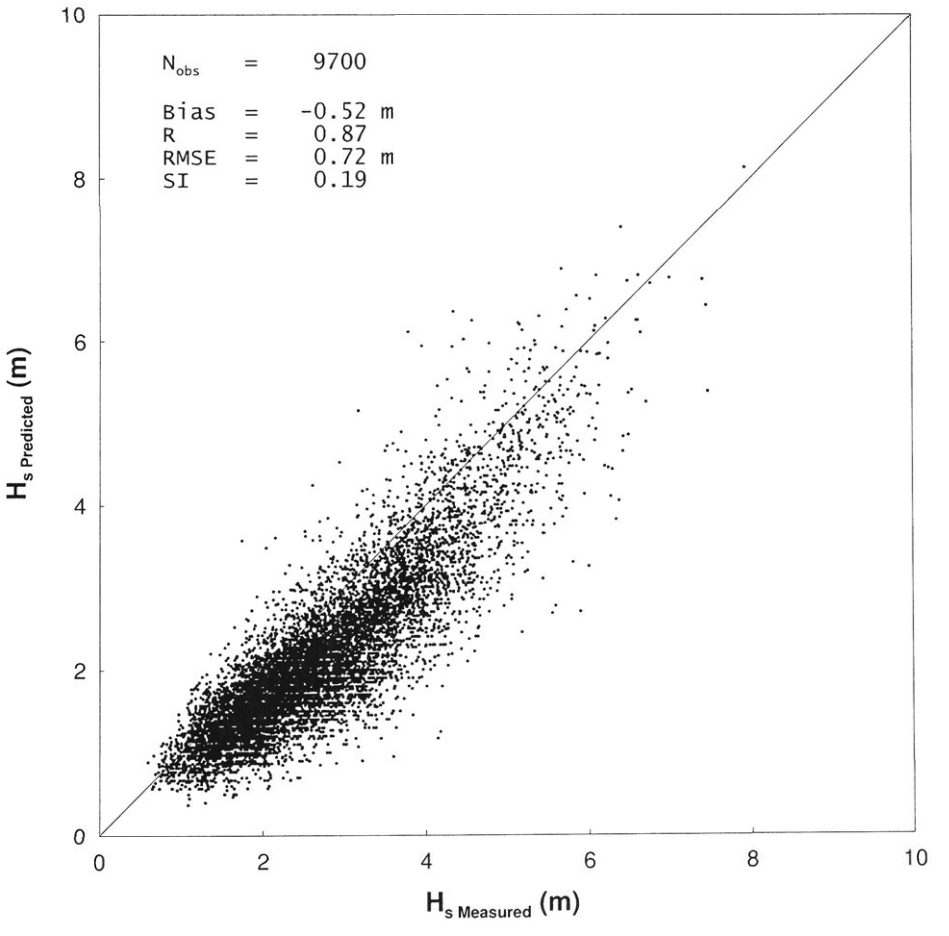

WRL Report No. 237	COMPARISON OF MEASURED & PREDICTED H_s VALUES CAPE DU COUEDIC, SOUTH AUSTRALIA	Figure 7.40

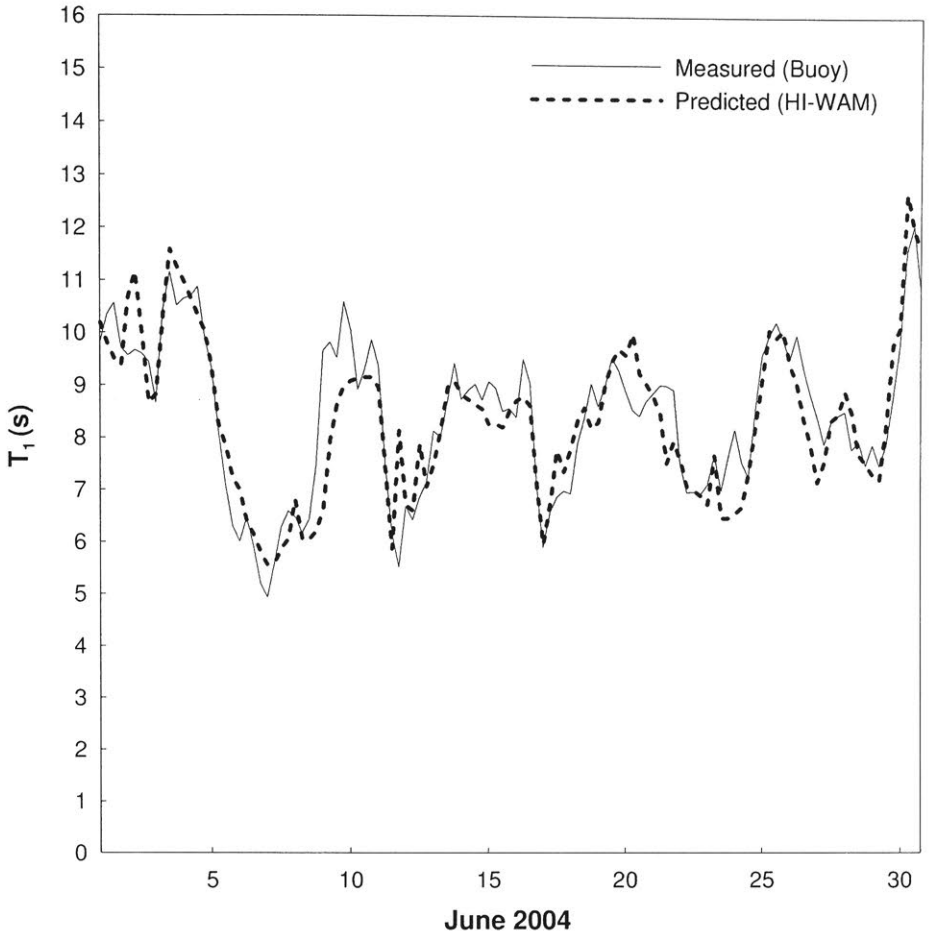

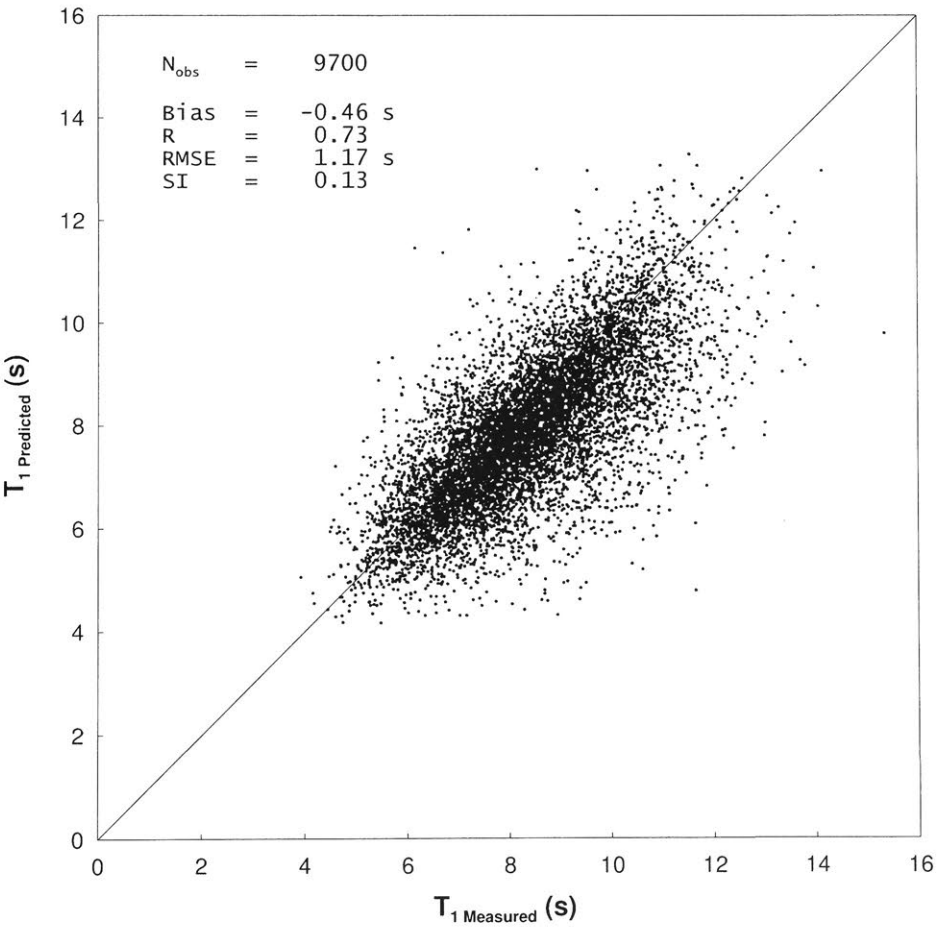

WRL
Report No. 237

COMPARISON OF MEASURED & PREDICTED T_1 VALUES
CAPE DU COUEDIC, SOUTH AUSTRALIA

Figure
7.41

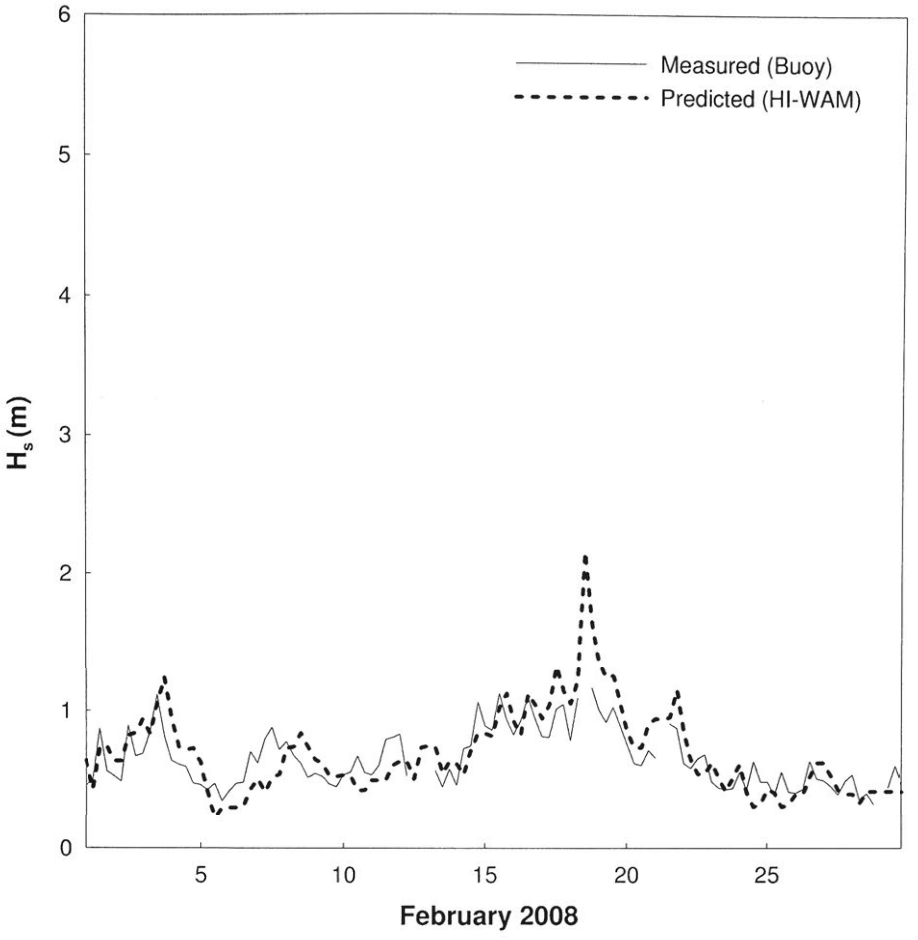

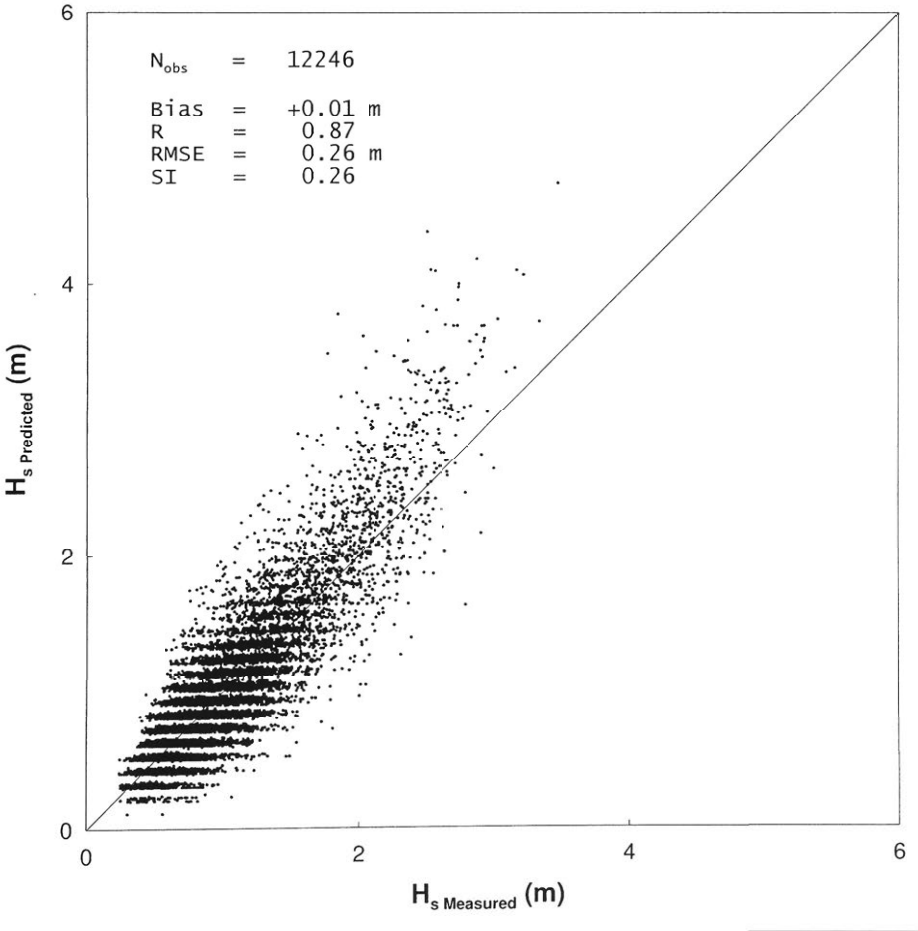

WRL Report No. 237	COMPARISON OF MEASURED & PREDICTED H_s VALUES COTTESLOE, WESTERN AUSTRALIA	Figure 7.42

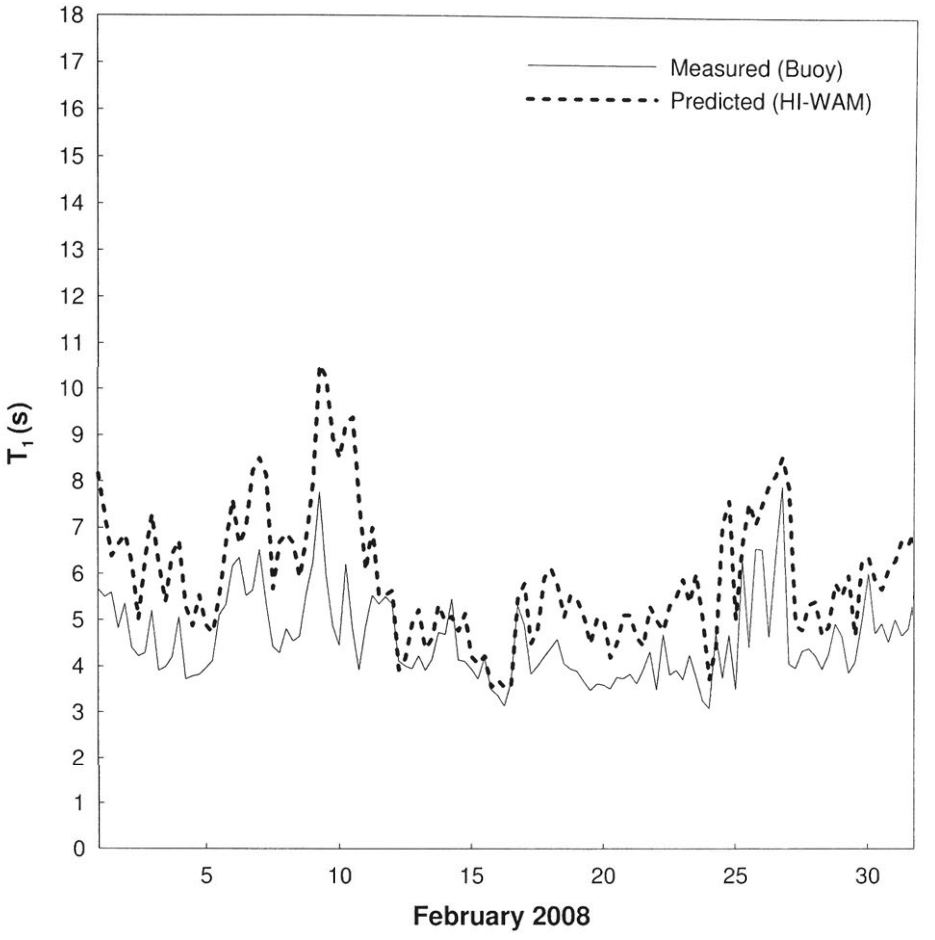

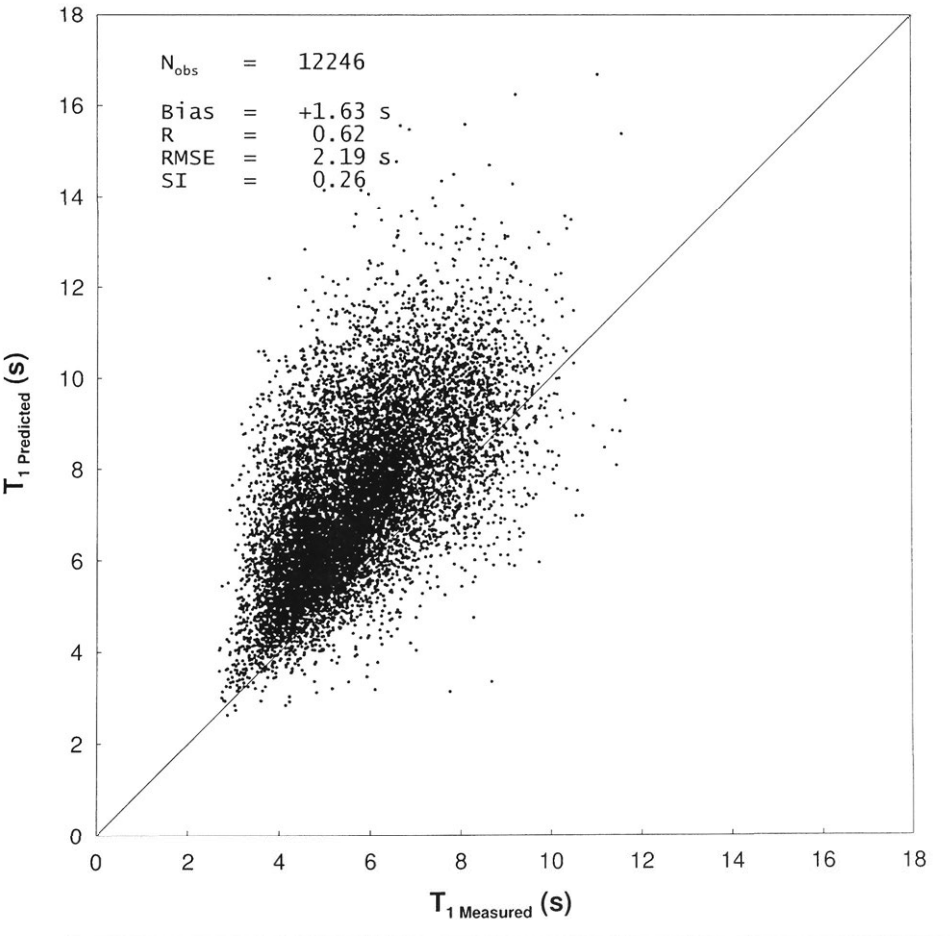

WRL
Report No. 237

COMPARISON OF MEASURED & PREDICTED T_1 VALUES
COTTESLOE, WESTERN AUSTRALIA

Figure
7.43

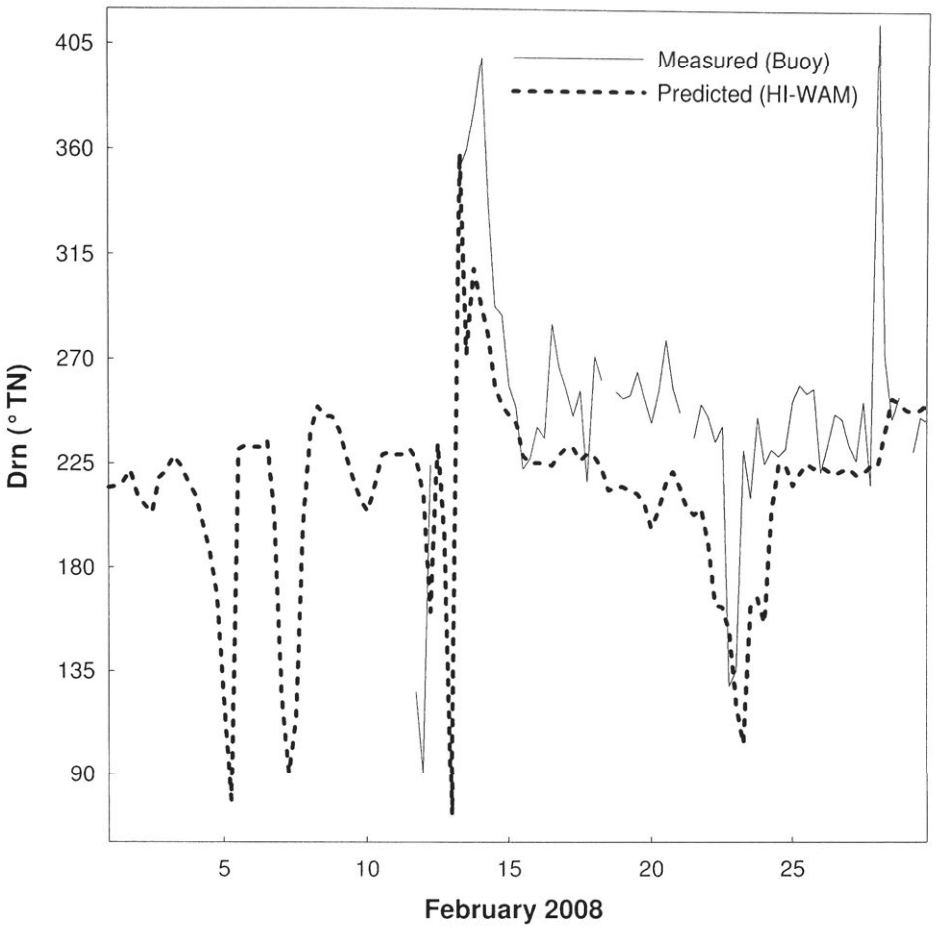

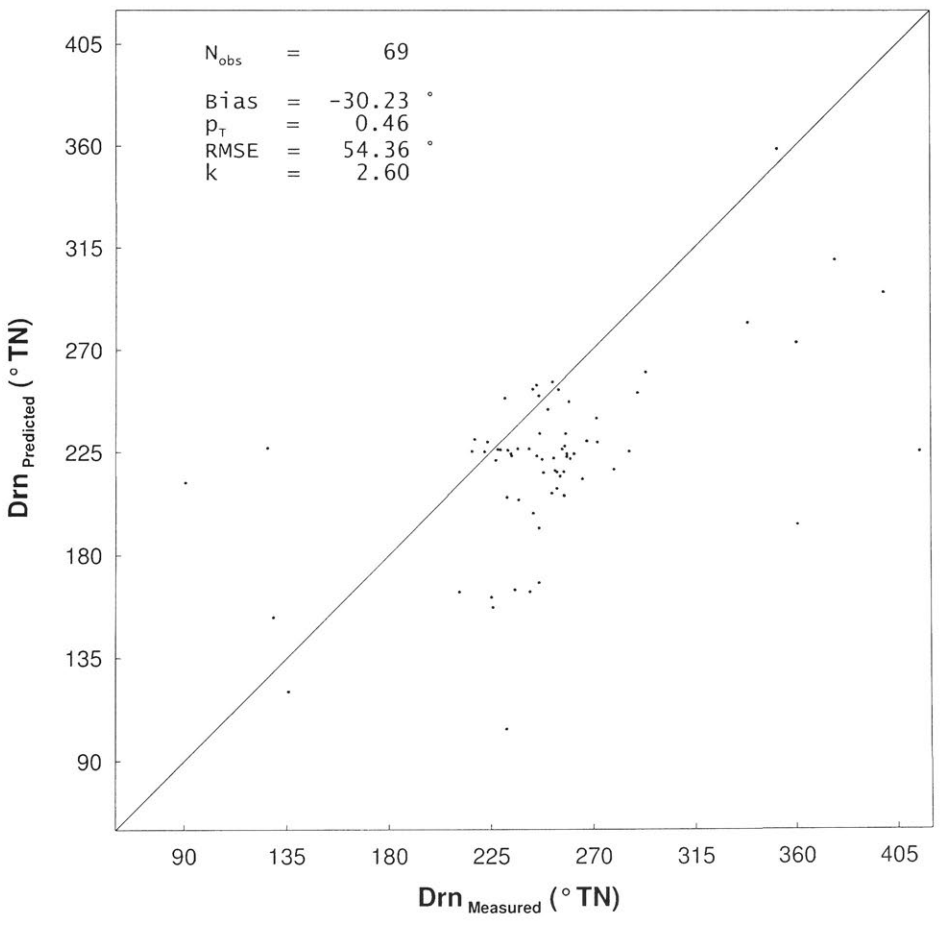

WRL Report No. 237	COMPARISON OF MEASURED & PREDICTED Drn VALUES COTTESLOE, WESTERN AUSTRALIA	Figure 7.44

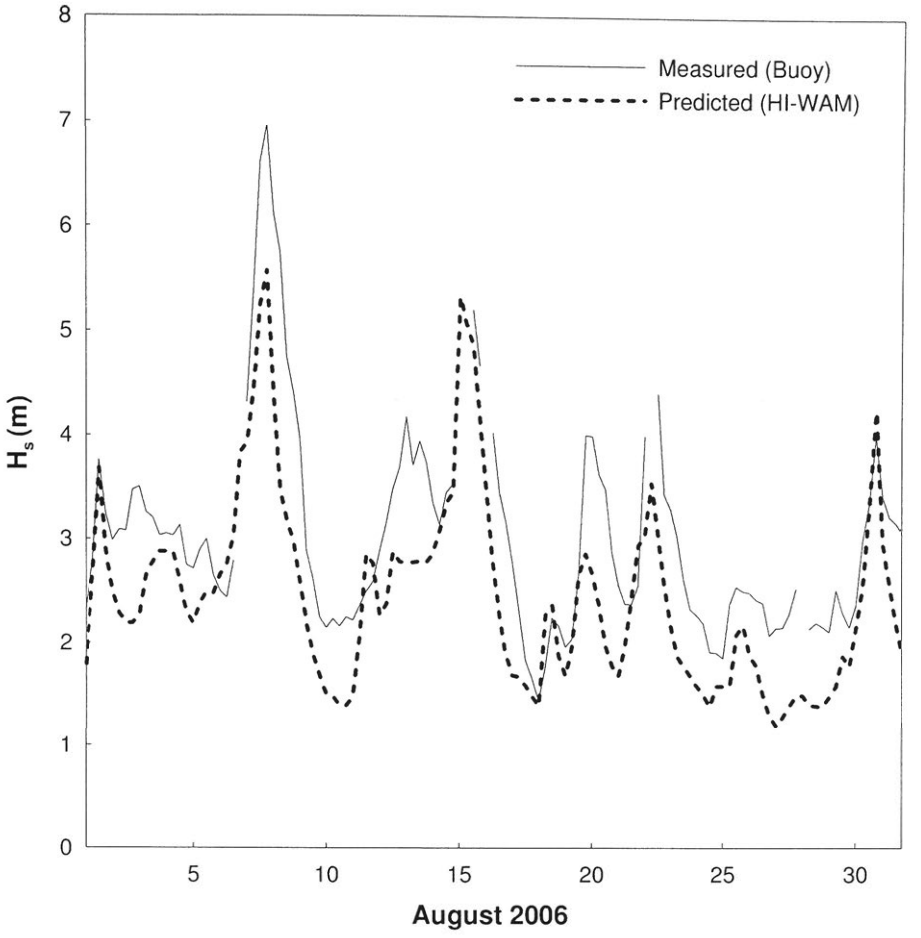

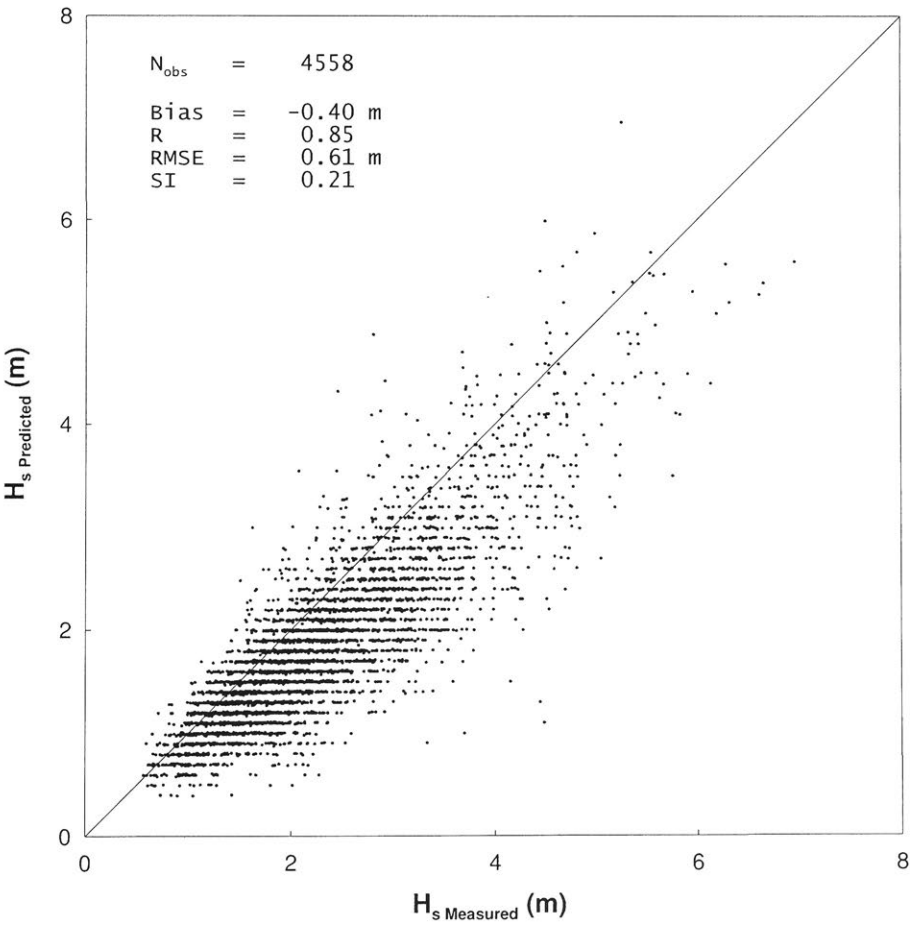

WRL
Report No. 237

COMPARISON OF MEASURED & PREDICTED H_s VALUES
ROTTNEST ISLAND, WESTERN AUSTRALIA

Figure
7.45

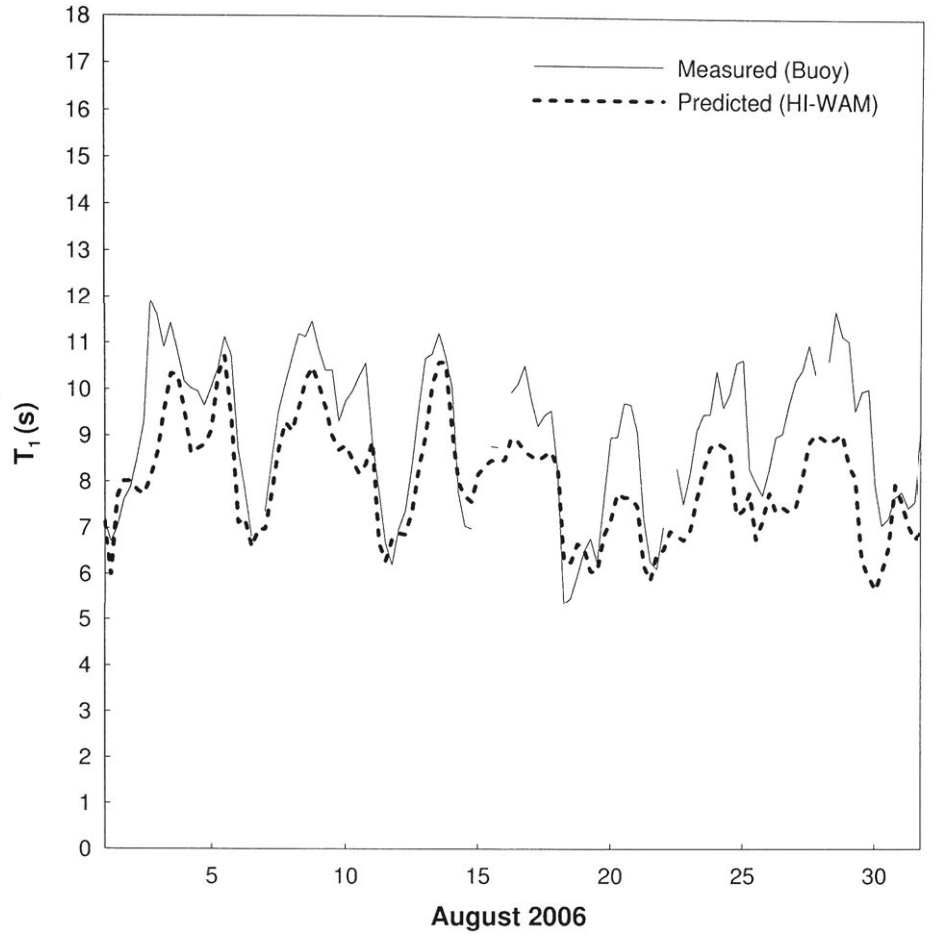

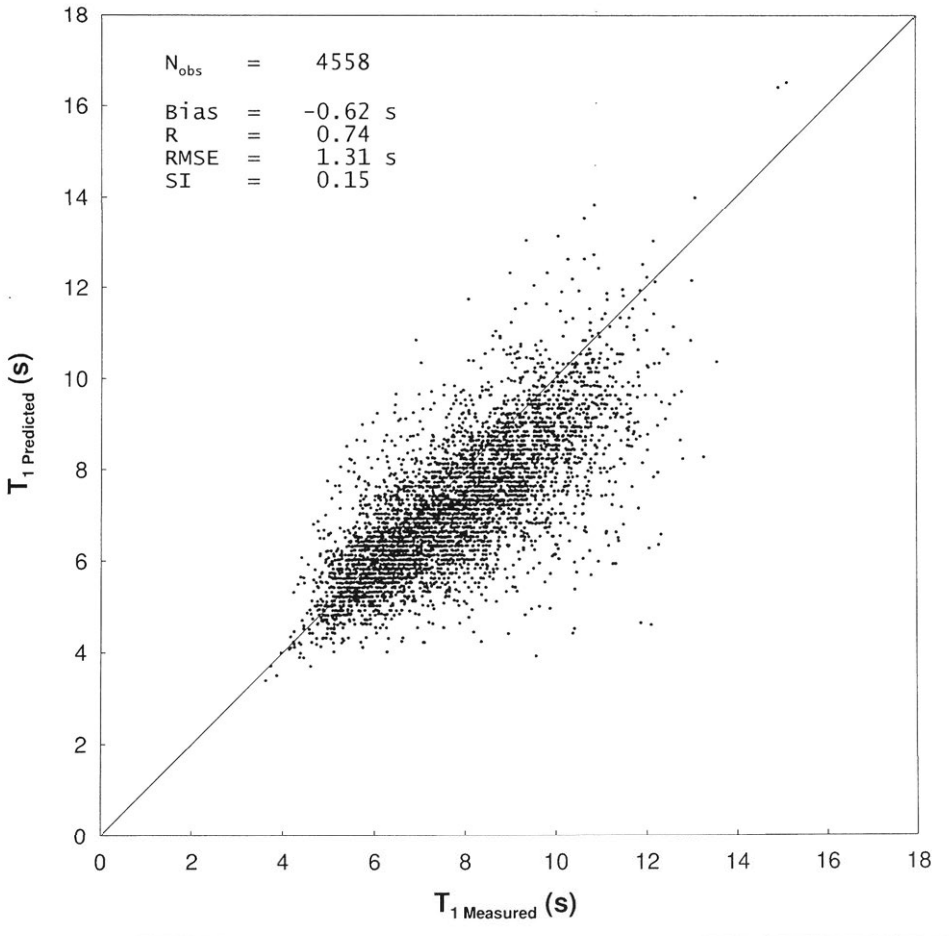

WRL
Report No. 237

COMPARISON OF MEASURED & PREDICTED T_1 VALUES
ROTTNEST ISLAND, WESTERN AUSTRALIA

Figure
7.46

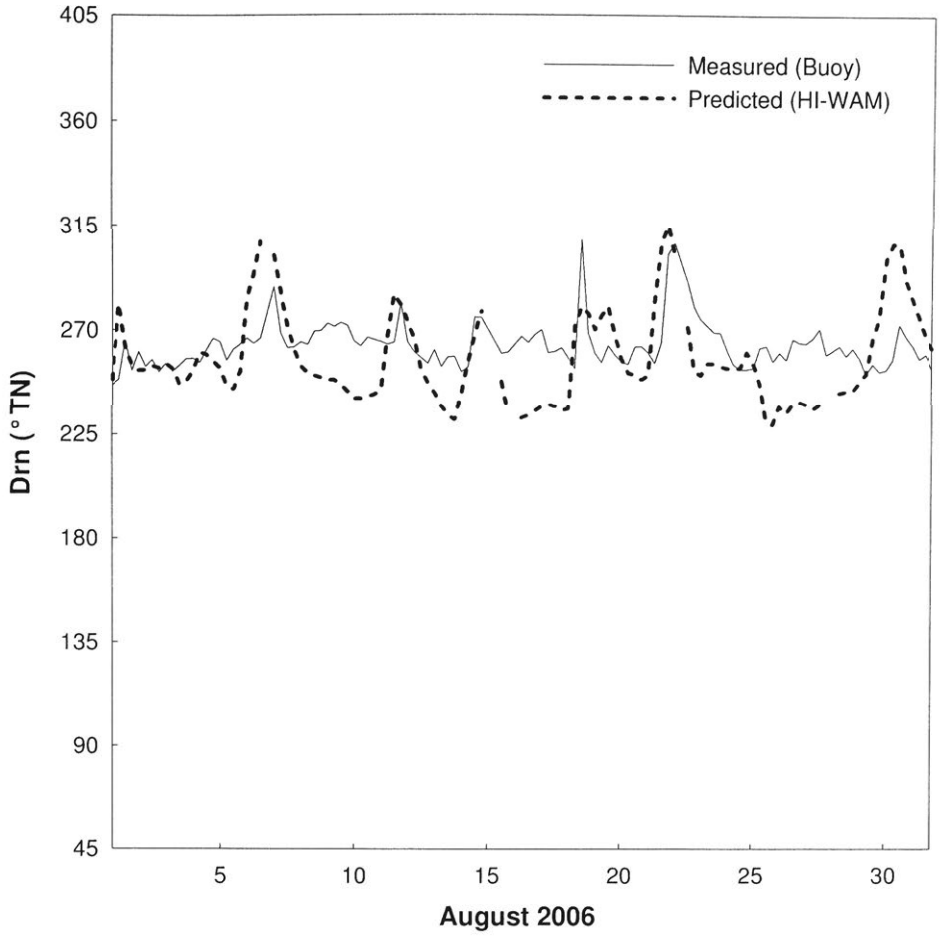

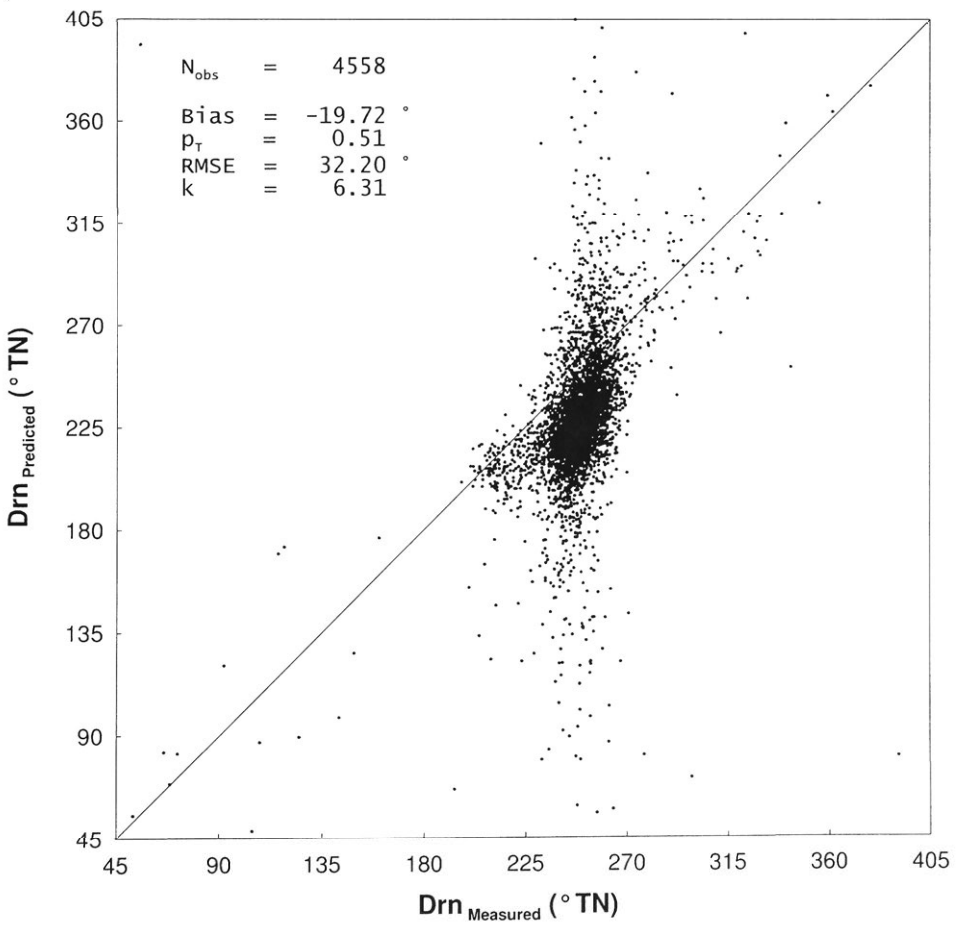

WRL Report No. 237	COMPARISON OF MEASURED & PREDICTED Drn VALUES ROTTNEST ISLAND, WESTERN AUSTRALIA	Figure 7.47

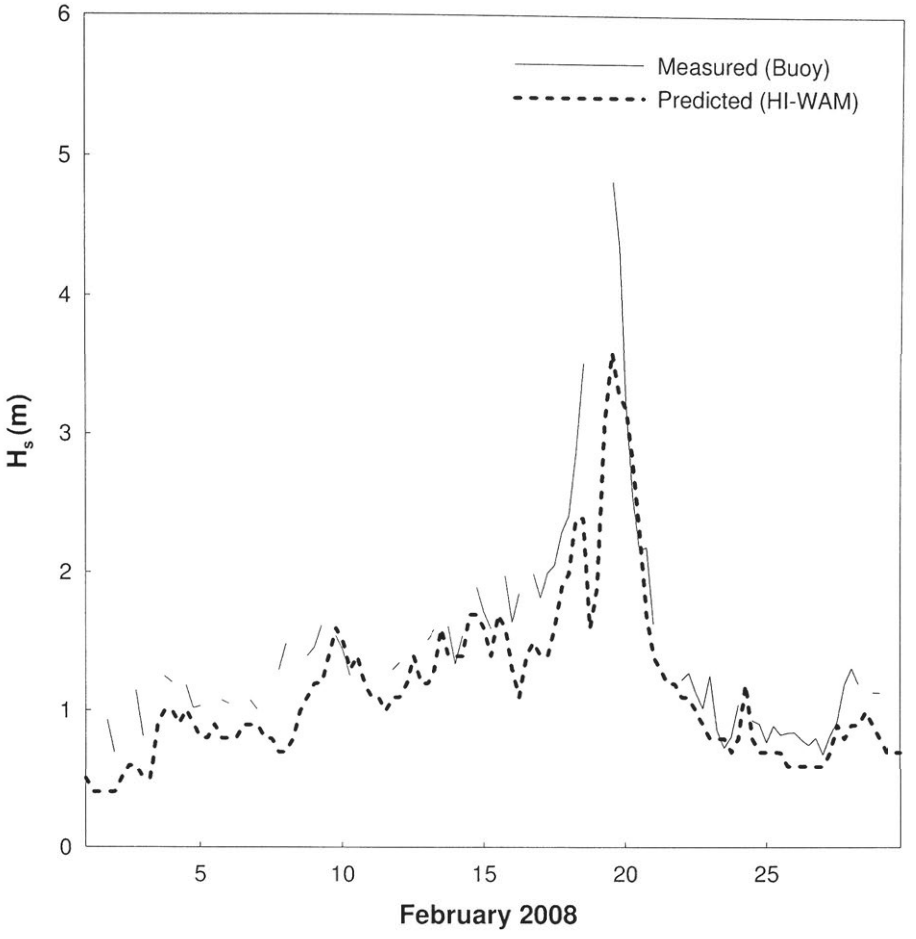

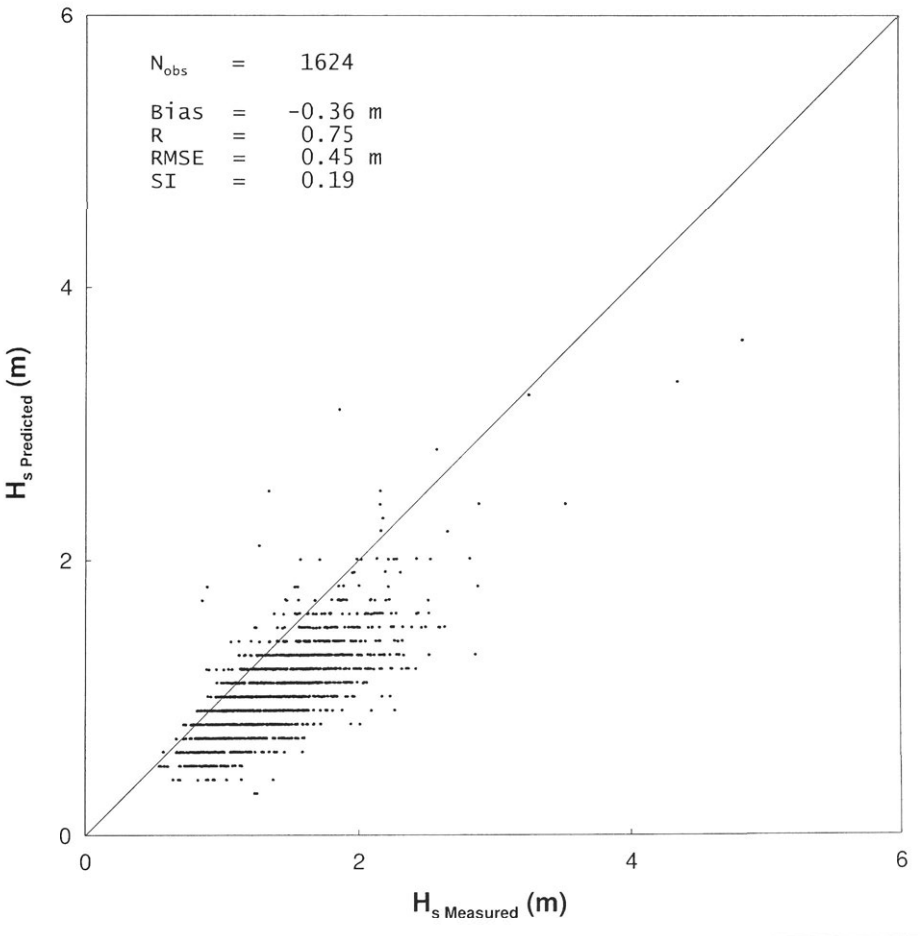

WRL Report No. 237	COMPARISON OF MEASURED & PREDICTED H_s VALUES EXMOUTH, WESTERN AUSTRALIA	Figure 7.48

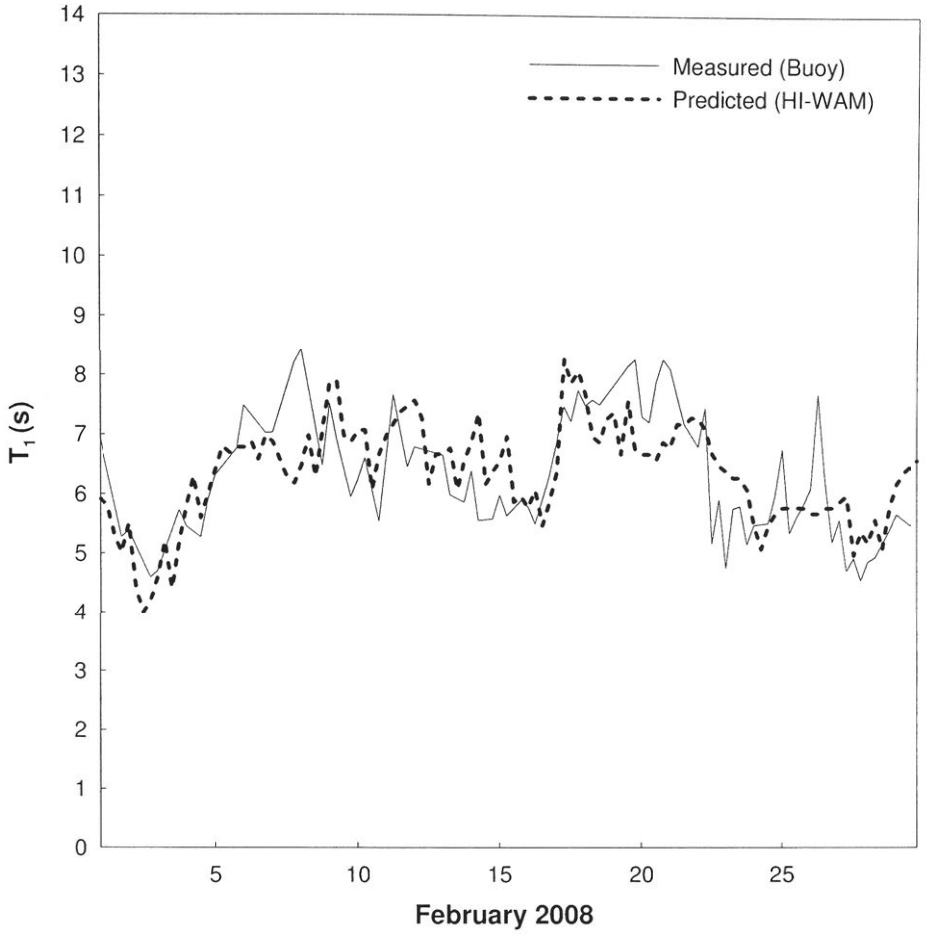

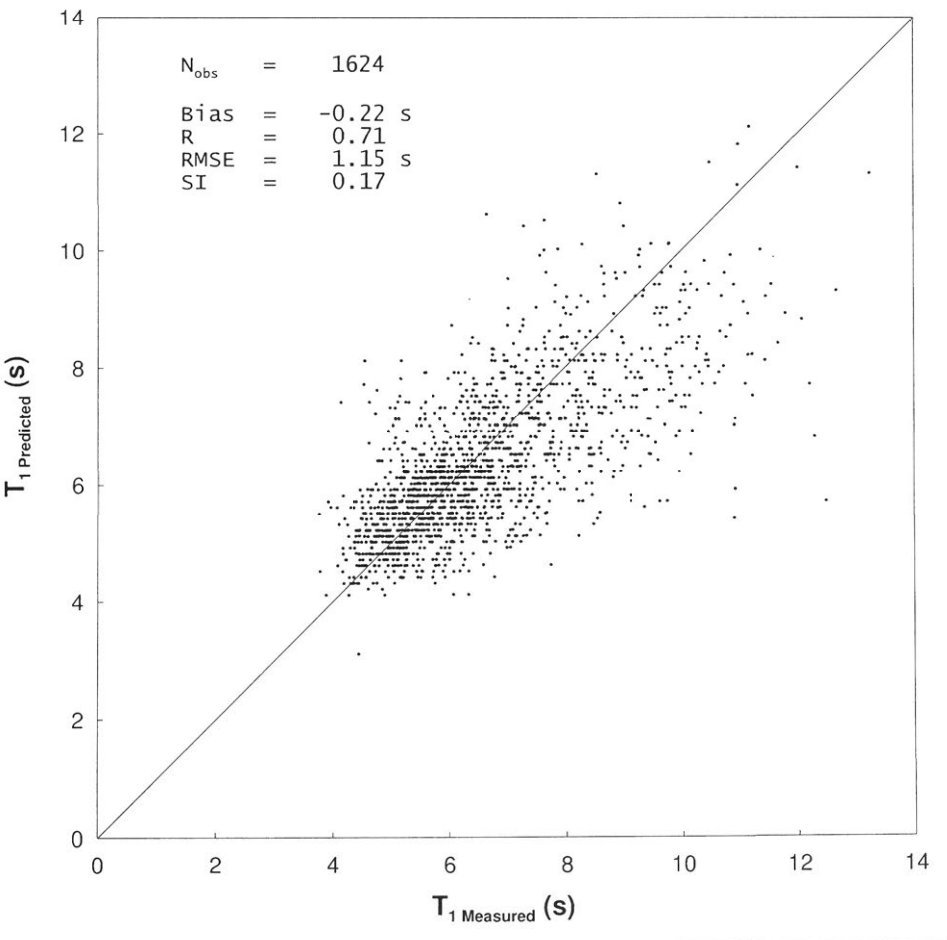

WRL
Report No. 237

COMPARISON OF MEASURED & PREDICTED T_1 VALUES
EXMOUTH, WESTERN AUSTRALIA

Figure
7.49

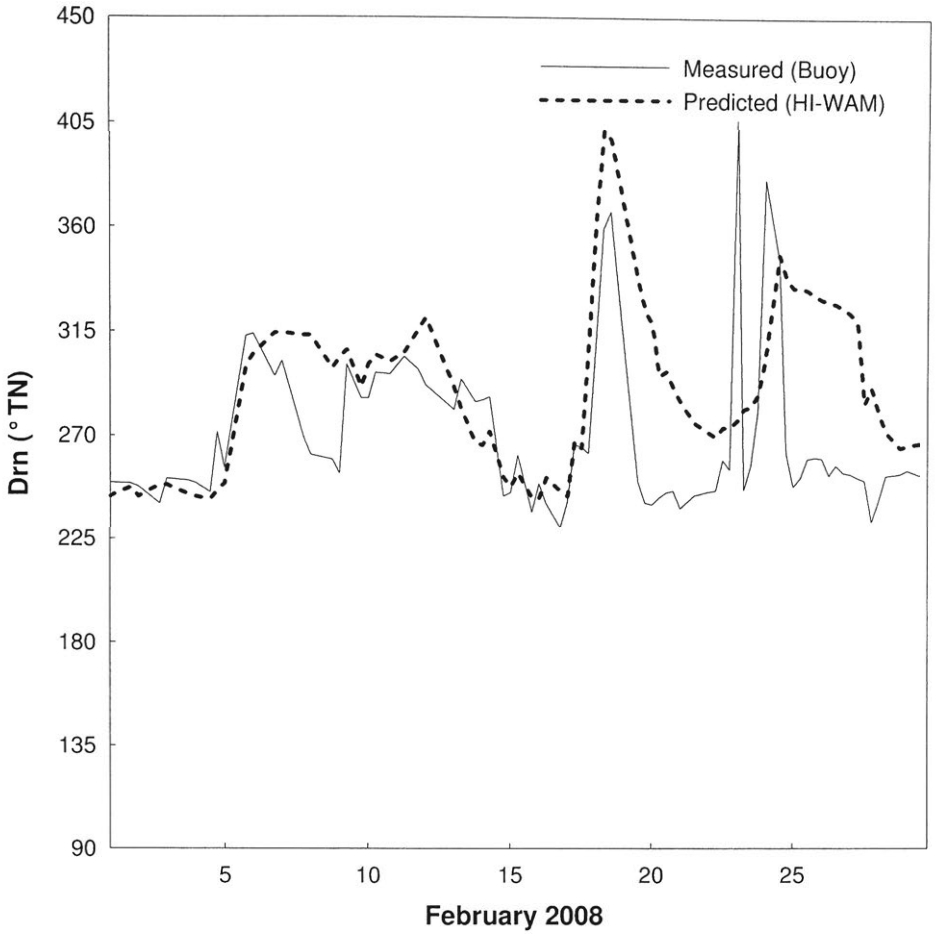

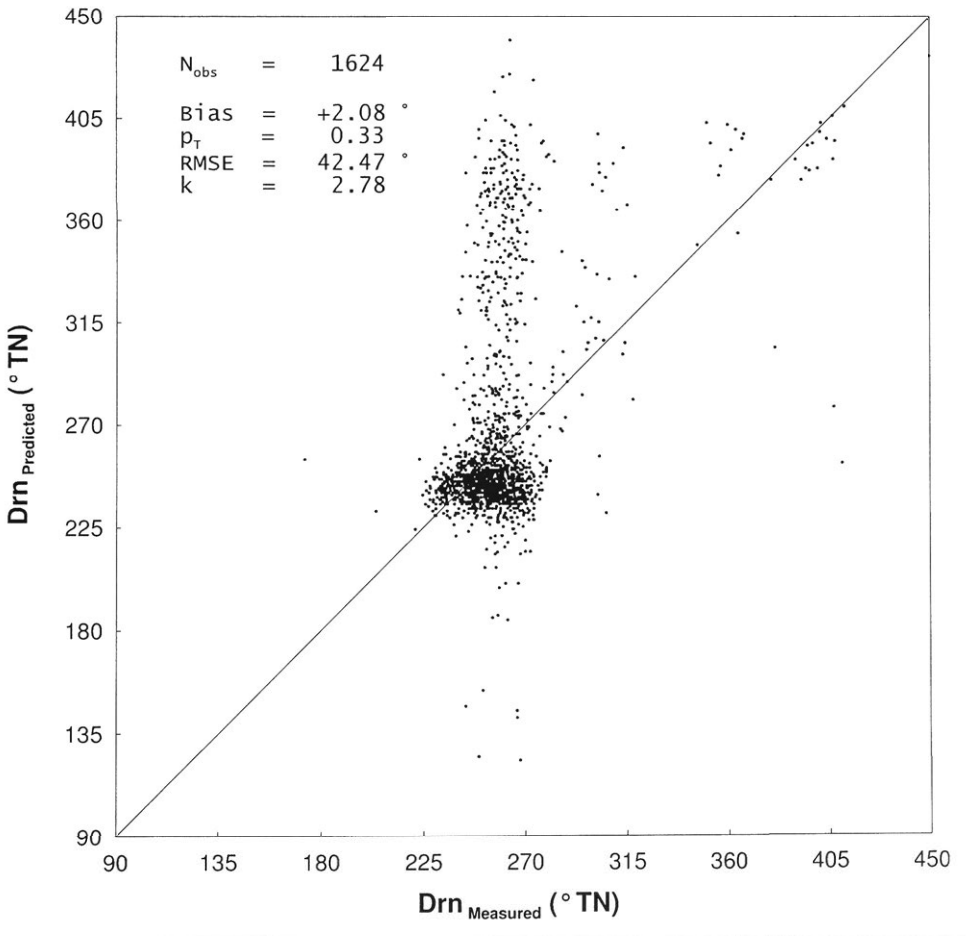

WRL Report No. 237	COMPARISON OF MEASURED & PREDICTED Drn VALUES EXMOUTH, WESTERN AUSTRALIA	Figure 7.50

SUMMARY TIME SERIES PLOTS of Hs FOR SELECTED MONTHS WITH HIGH WAVE ENERGY AROUND AUSTRALIAN COAST

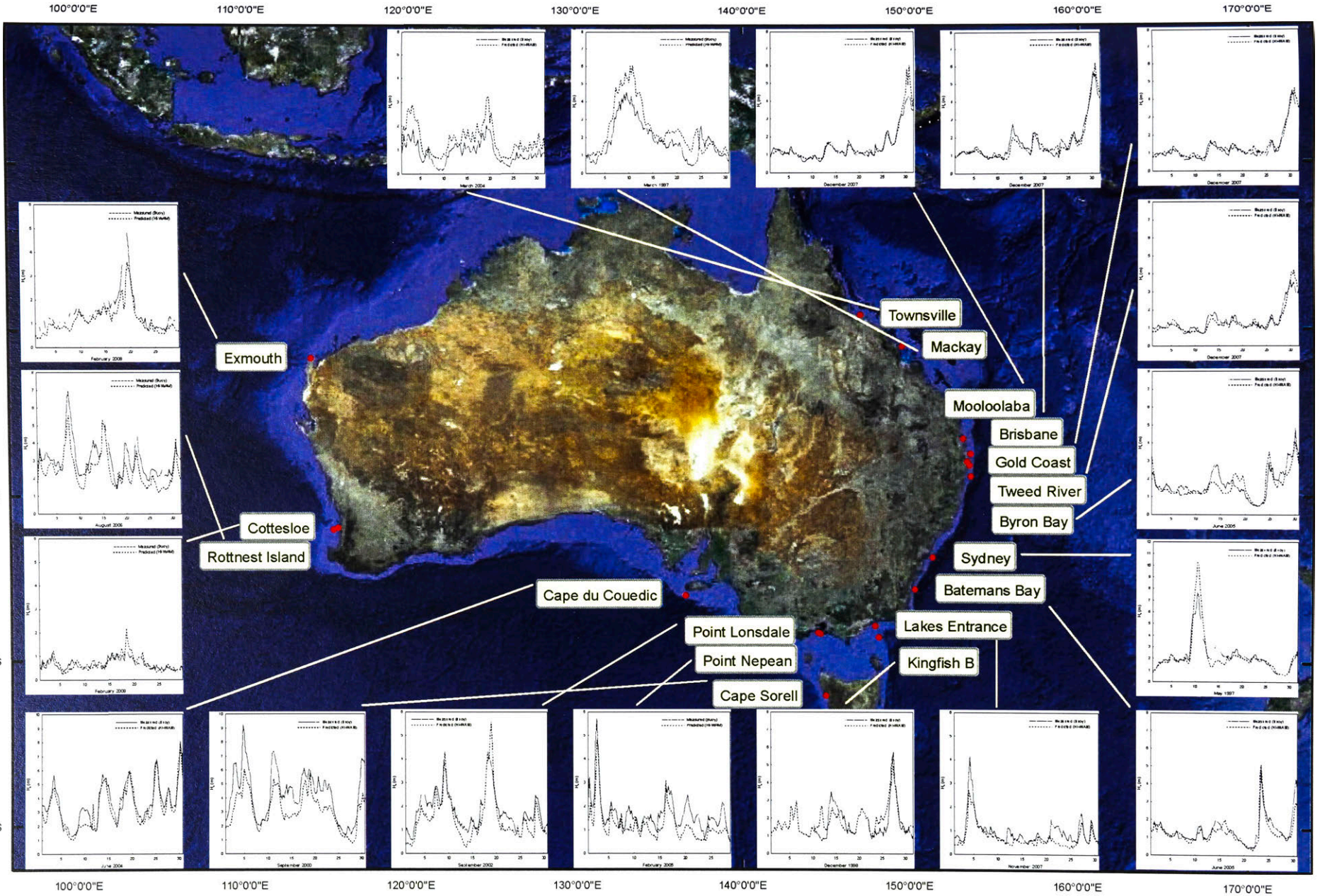

Figure 7.51

SUMMARY BOX PLOTS of Hs FOR ALL AVAILABLE DATA AROUND AUSTRALIAN COAST

Figure 7.52

SUMMARY TIME SERIES PLOTS of T1 FOR SELECTED MONTHS
WITH HIGH WAVE ENERGY AROUND AUSTRALIAN COAST

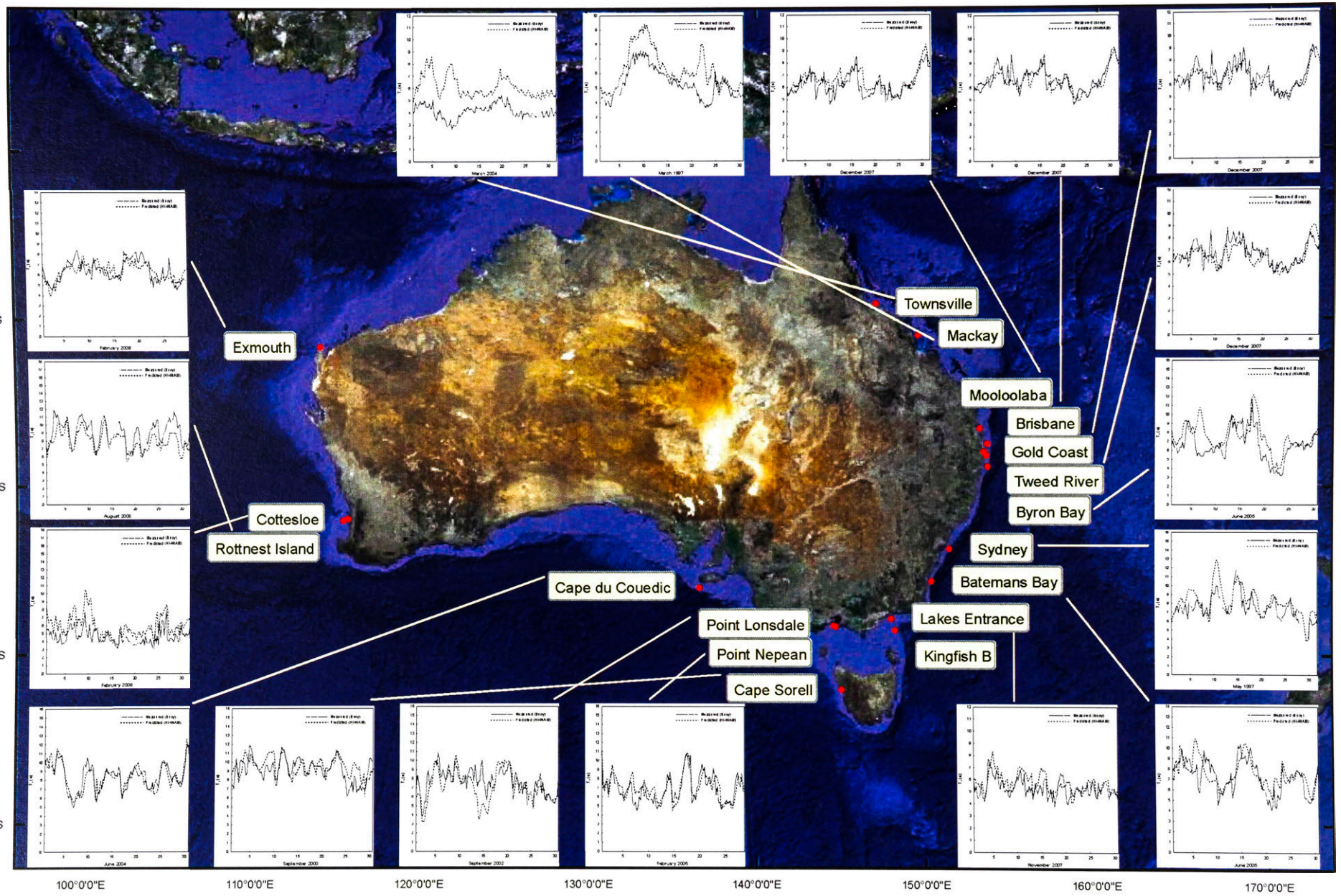

Figure 7.53

SUMMARY BOX PLOTS of T1 FOR ALL AVAILABLE DATA AROUND AUSTRALIAN COAST

Figure 7.54

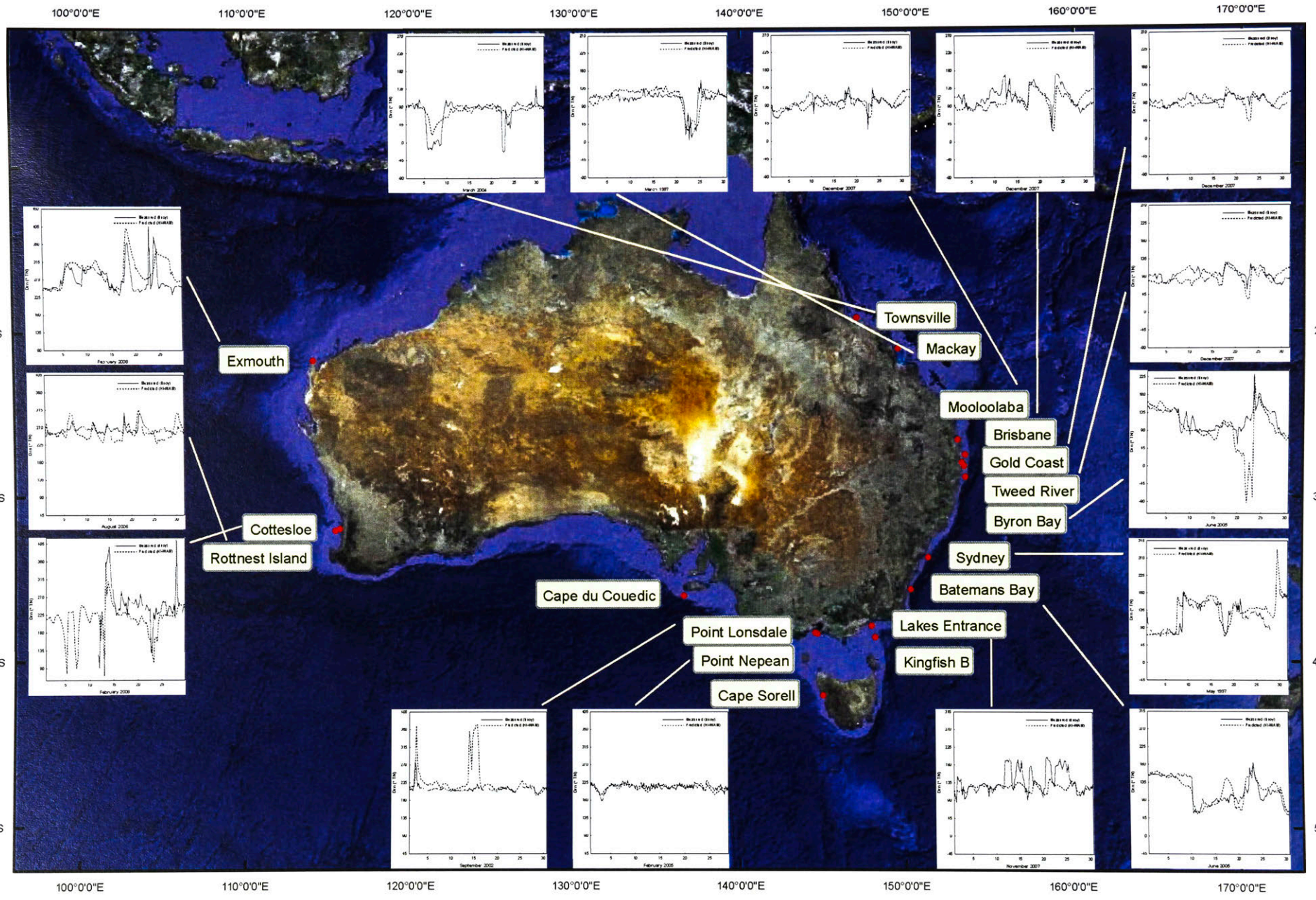

SUMMARY TIME SERIES PLOTS of Dm FOR SELECTED MONTHS
WITH HIGH WAVE ENERGY AROUND AUSTRALIAN COAST

Figure 7.55

SUMMARY BOX PLOTS of Drn FOR ALL AVAILABLE DATA AROUND AUSTRALIAN COAST

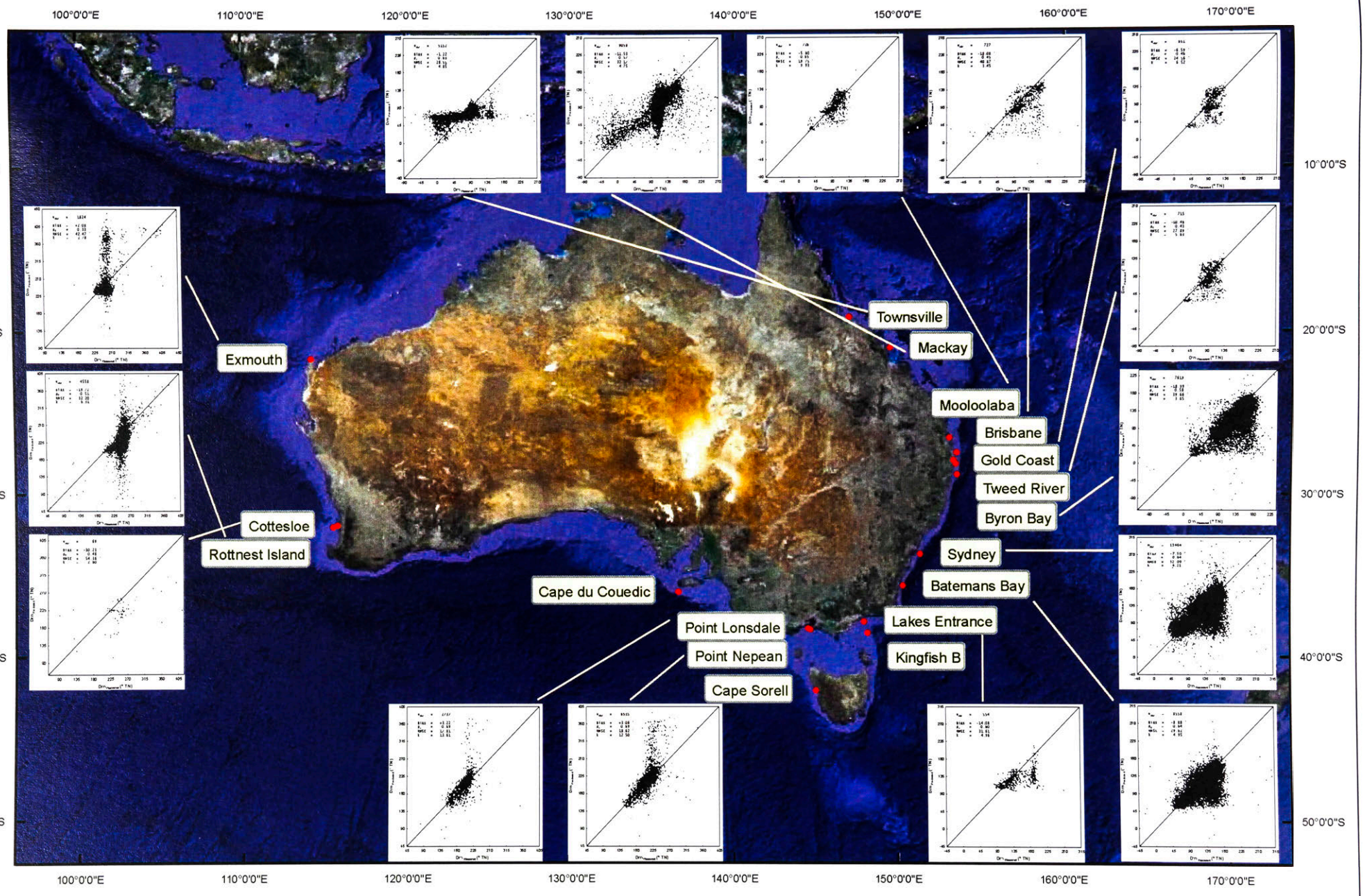

Figure 7.56

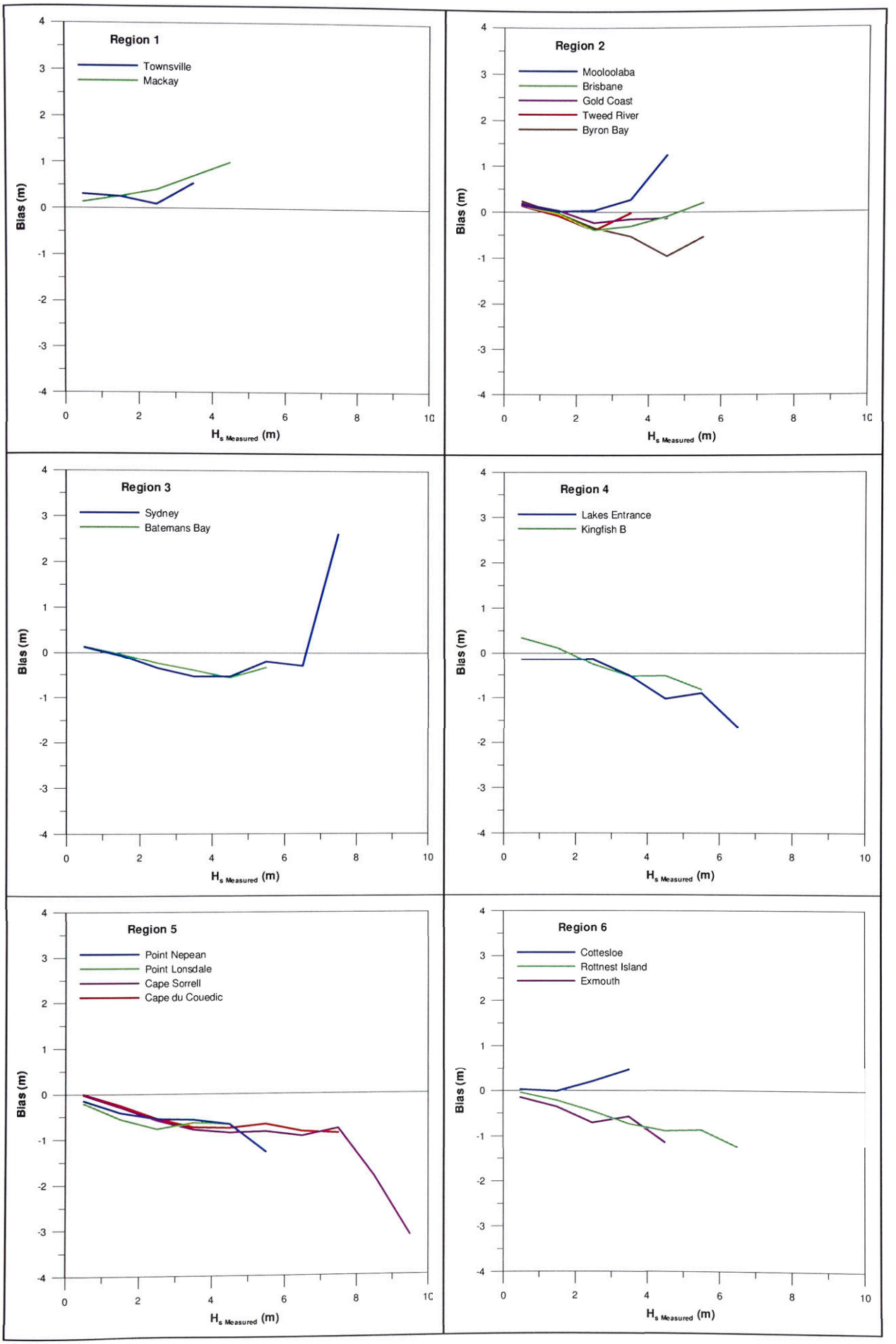

WRL
Report No. 237

MODEL SKILL PARAMETER (BIAS) FOR H_s WITH VARIATION IN MEASURED H_s FOR SIX REGIONS OF AUSTRALIA

Figure 7.57

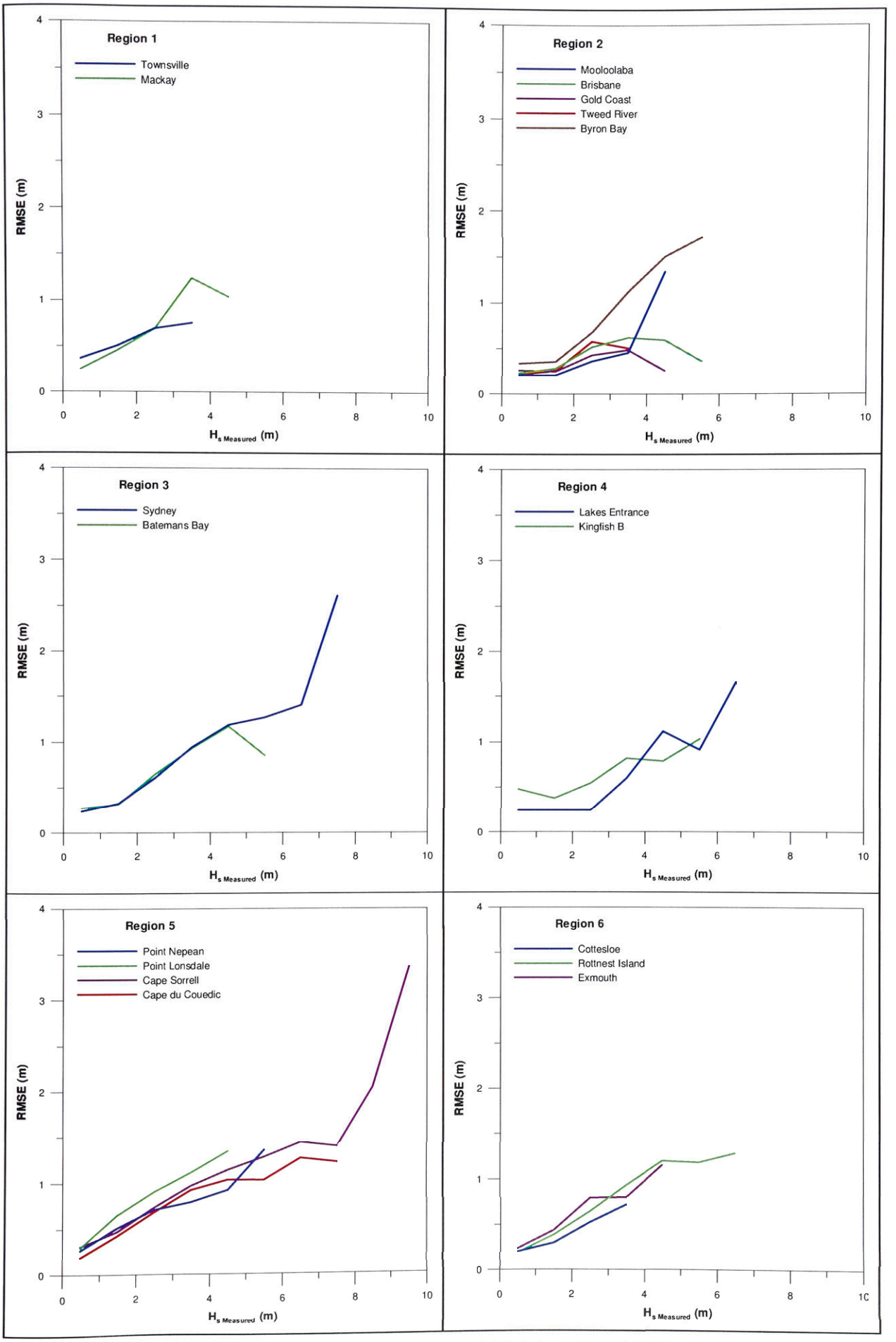

WRL
Report No. 237

MODEL SKILL PARAMETER (RMSE) FOR H_s WITH VARIATION IN MEASURED H_s FOR SIX REGIONS OF AUSTRALIA

Figure 7.58

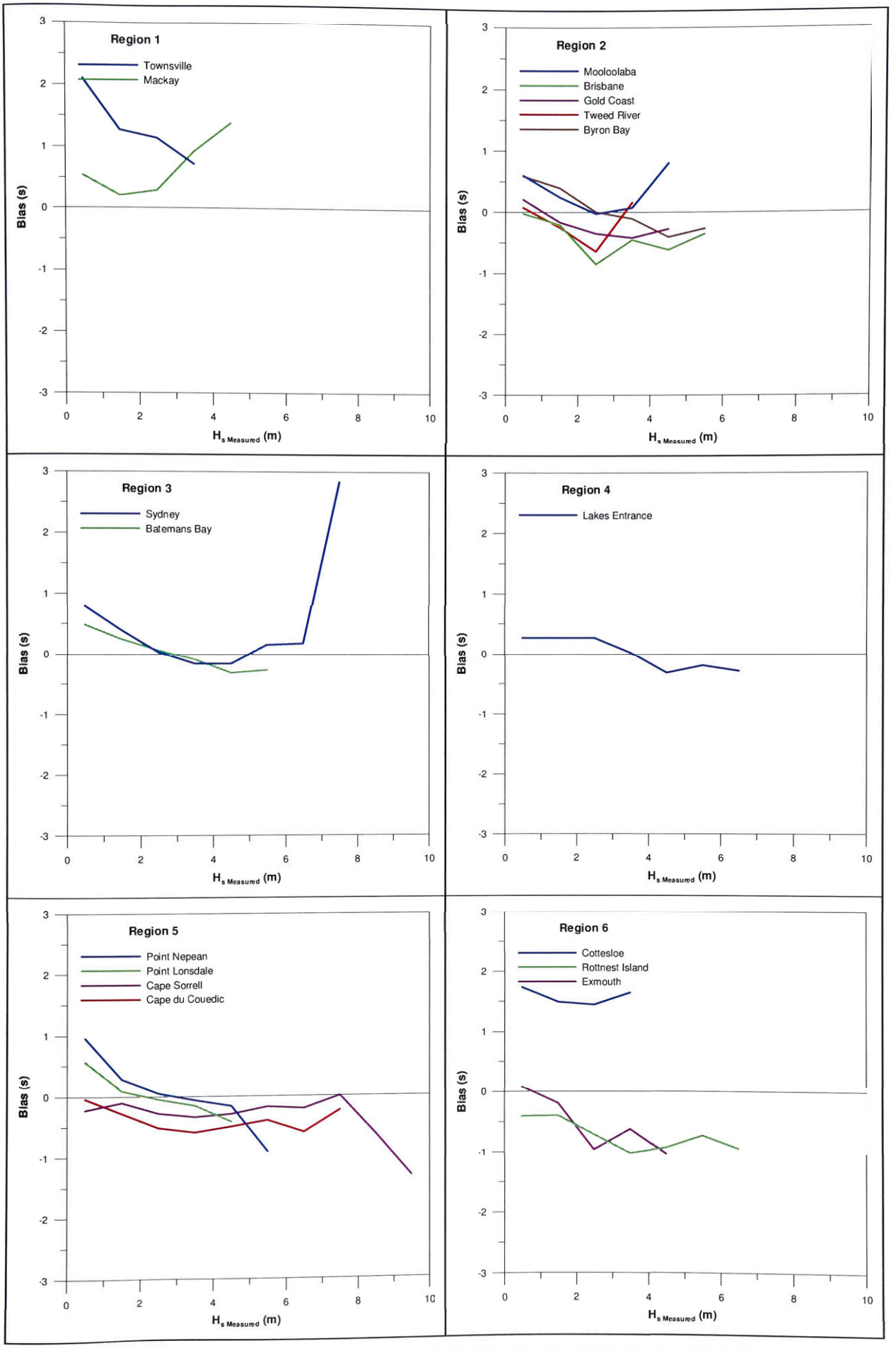

WRL
Report No. 237

MODEL SKILL PARAMETER (BIAS) FOR T_1 WITH VARIATION IN MEASURED H_s FOR SIX REGIONS OF AUSTRALIA

Figure 7.59

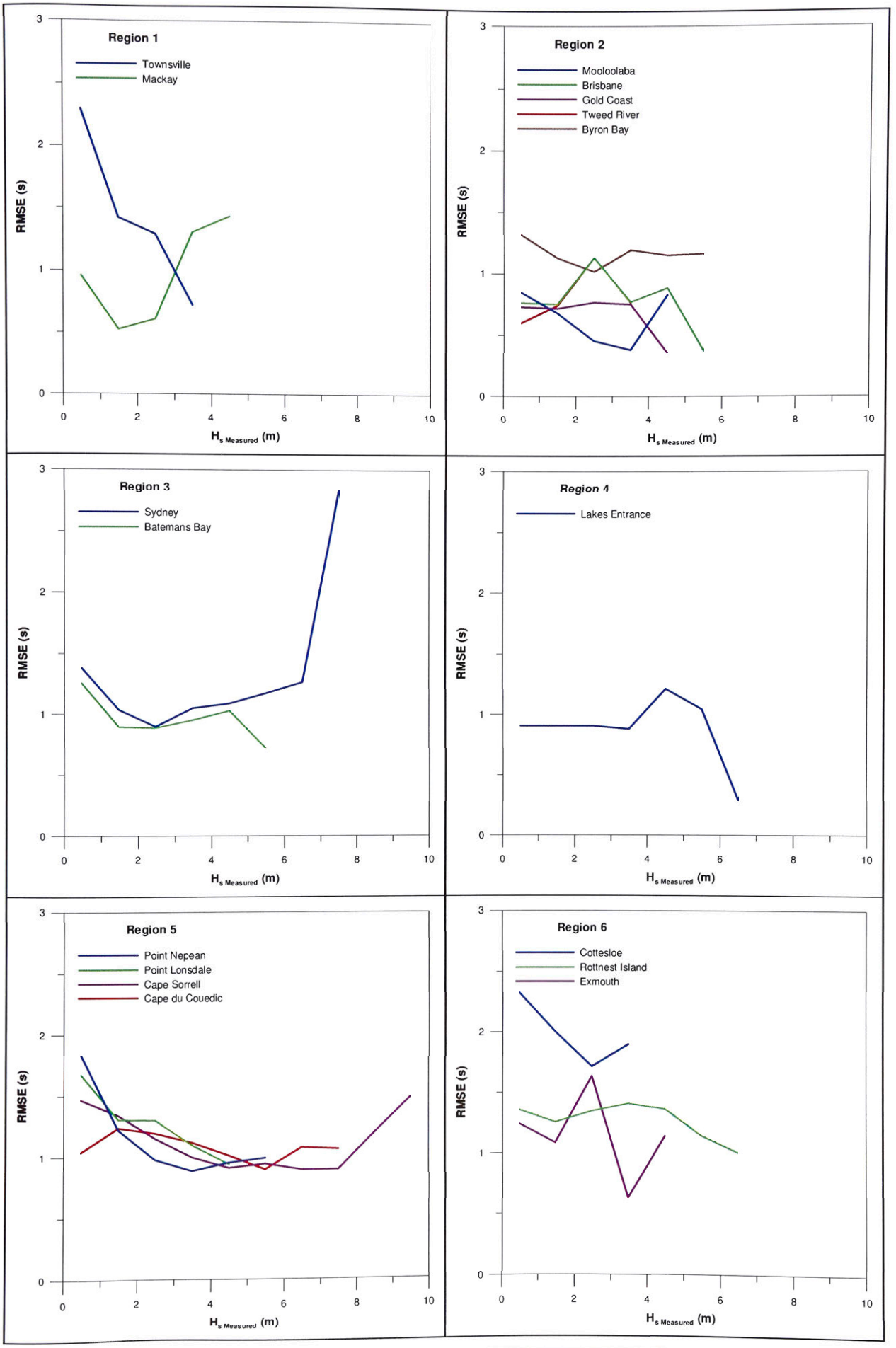

WRL
Report No. 237

MODEL SKILL PARAMETER (RMSE) FOR T_1 WITH VARIATION IN MEASURED H_s FOR SIX REGIONS OF AUSTRALIA

Figure 7.60

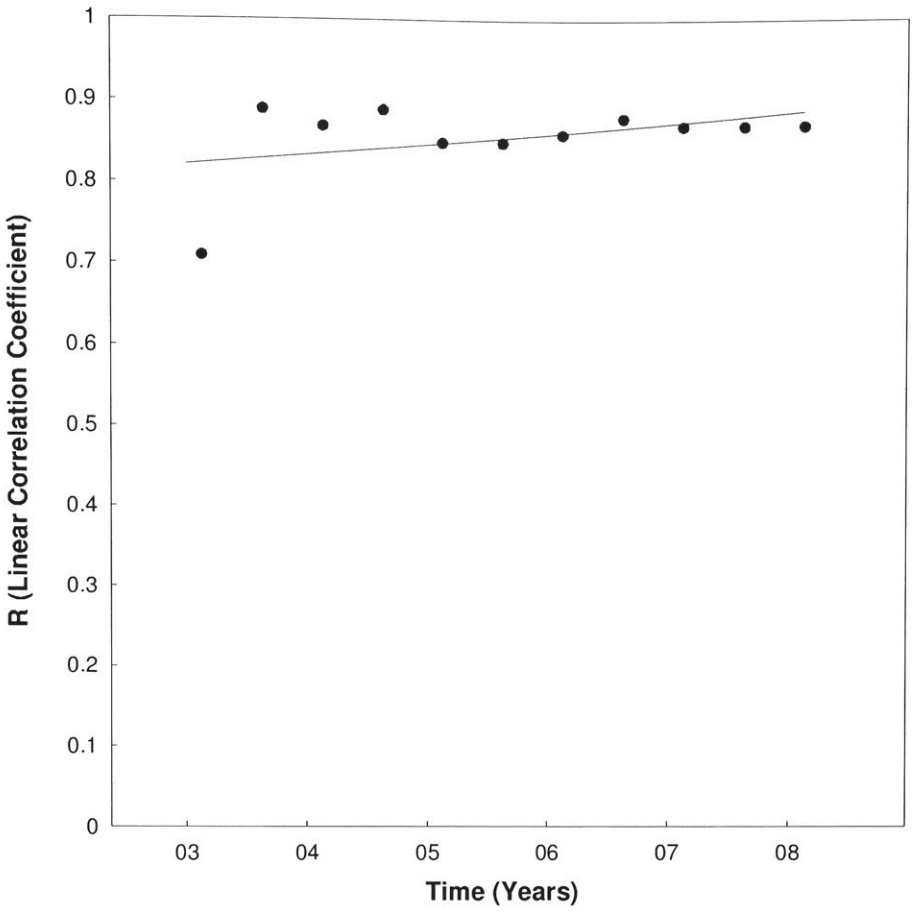

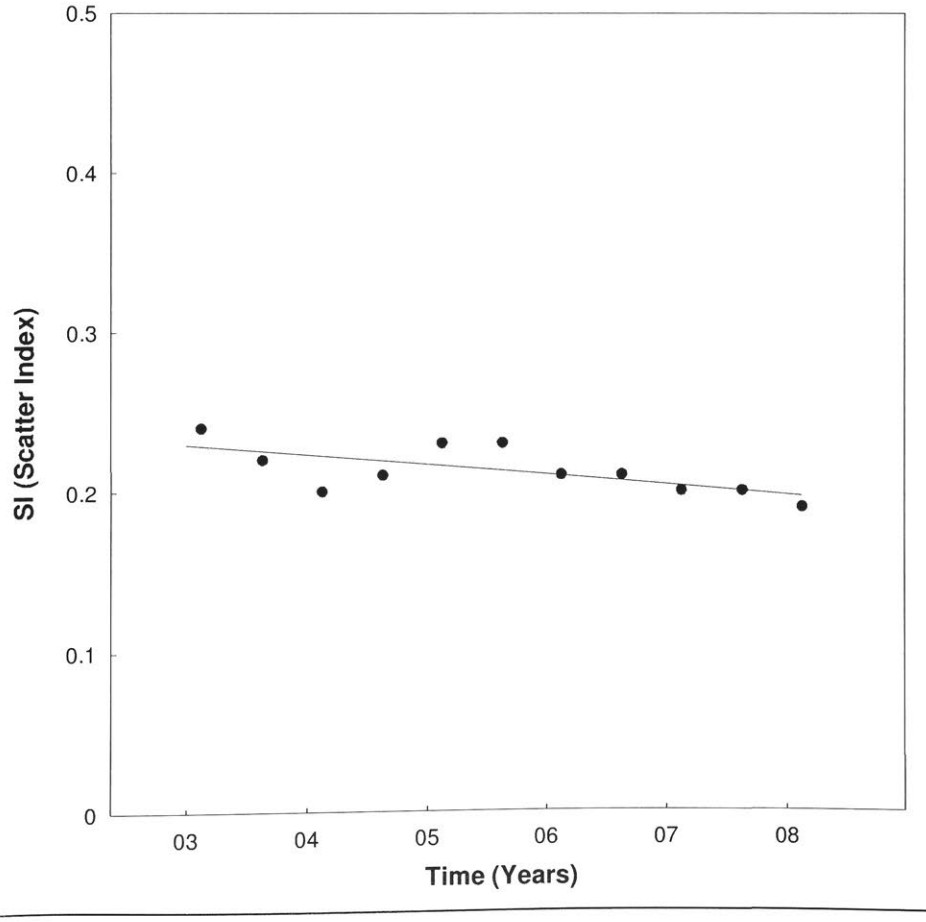

WRL Report No. 237	MODEL SKILL PARAMETERS (R and SI) FOR H_s HISTORICAL VARIATION WITH TIME FOR POINT NEPEAN	Figure 7.61

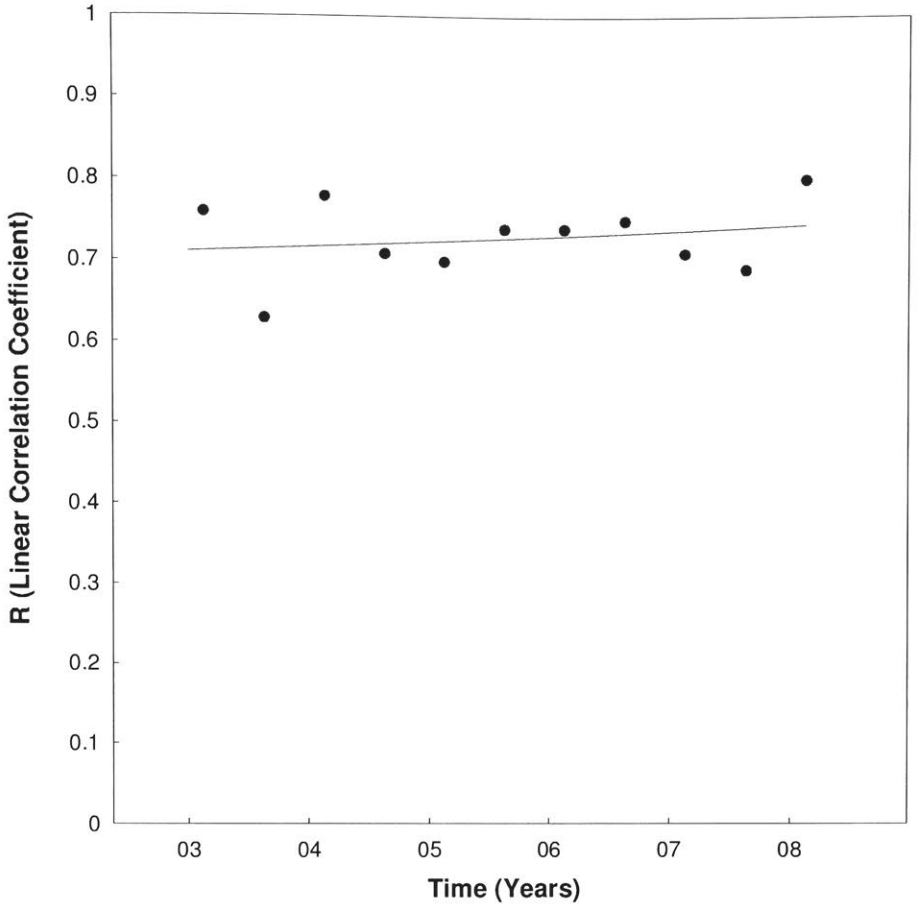

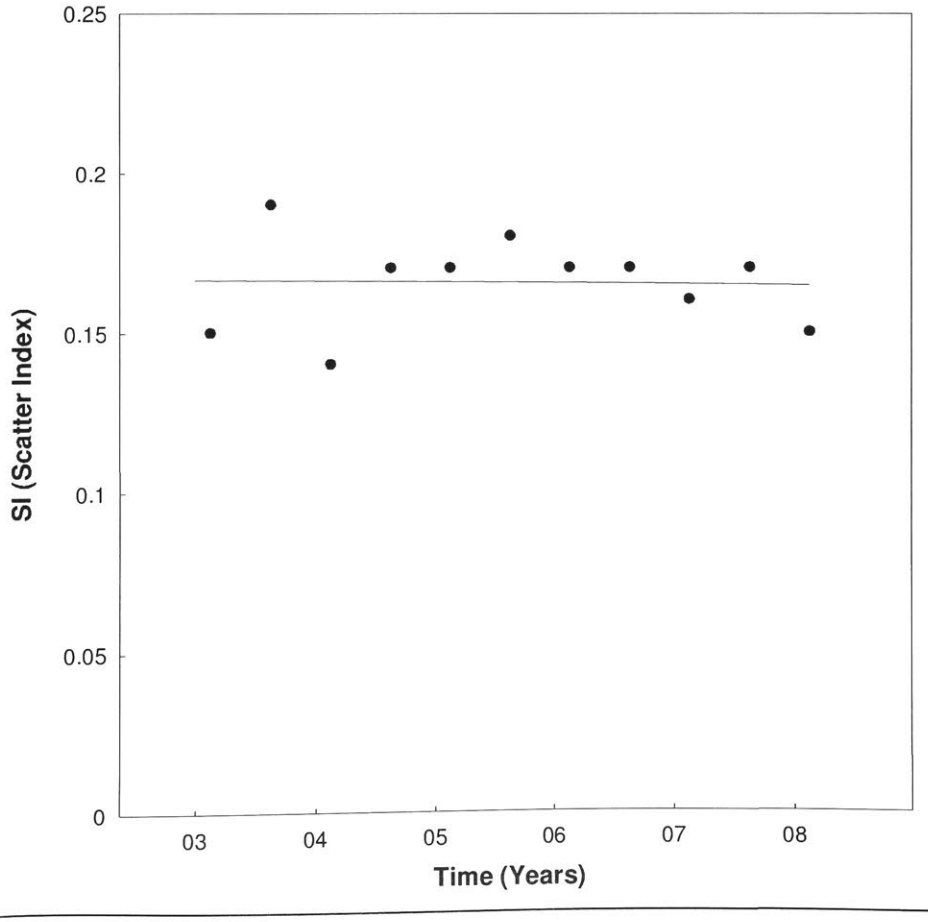

WRL Report No. 237	MODEL SKILL PARAMETERS (R and SI) FOR T_1 HISTORICAL VARIATION WITH TIME FOR POINT NEPEAN	Figure 7.62

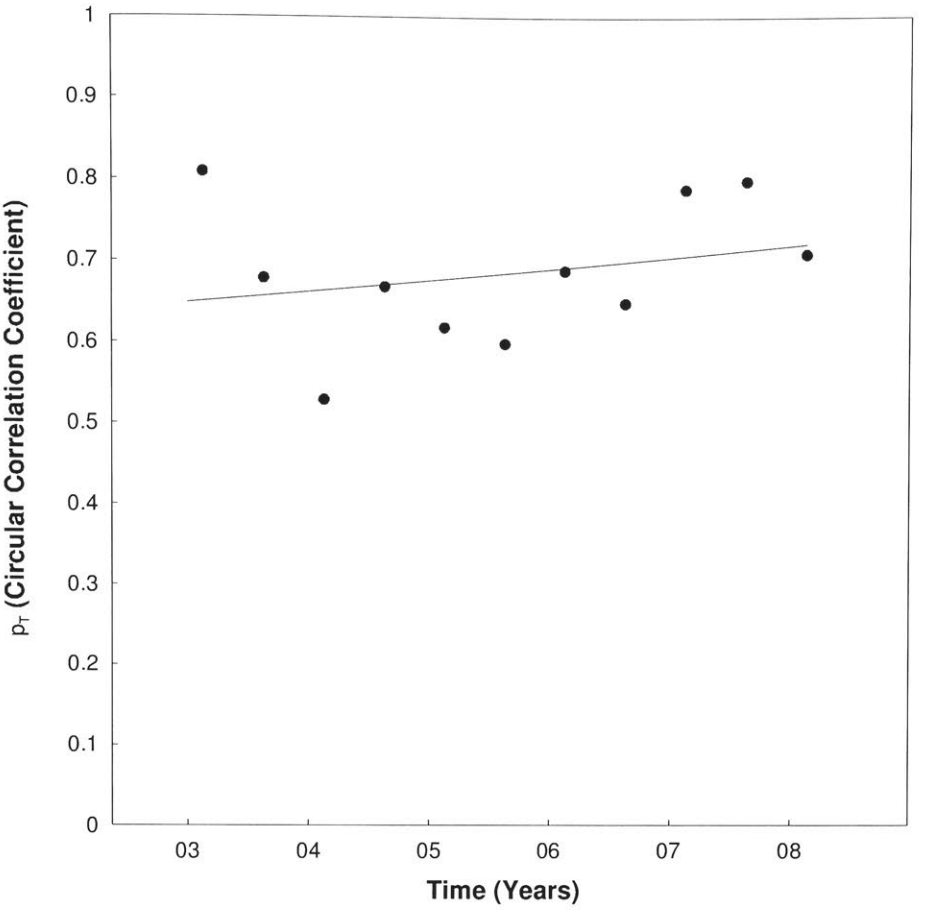

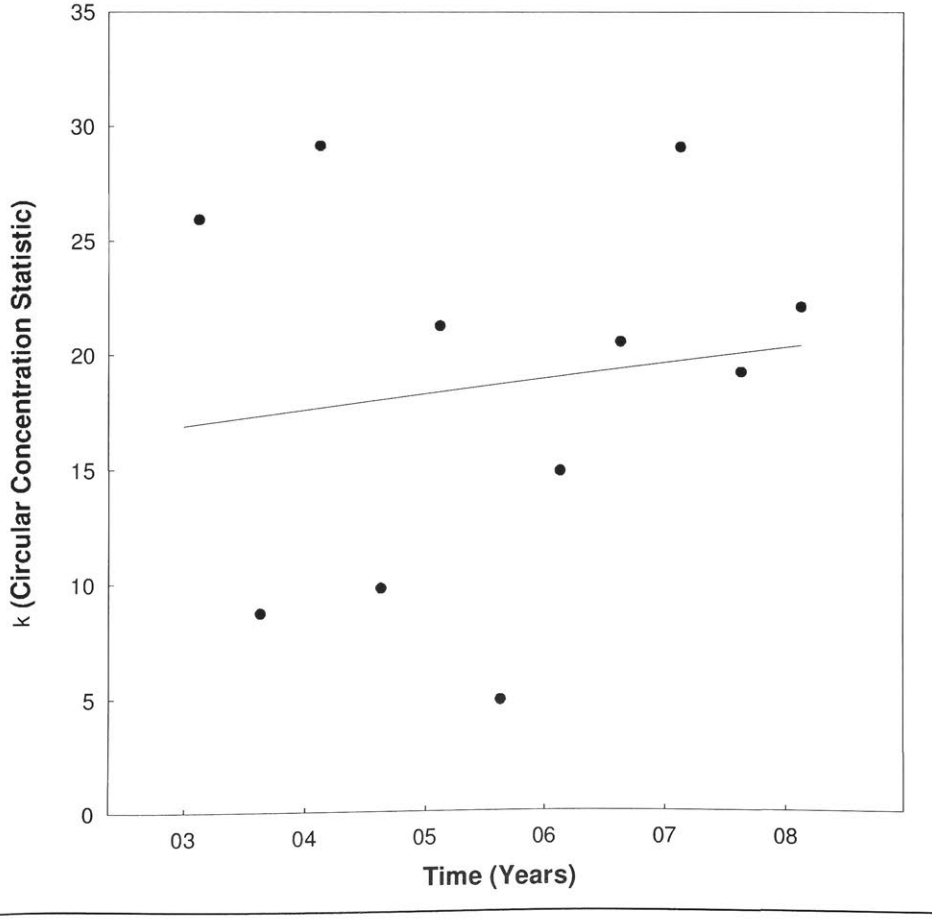

WRL Report No. 237	MODEL SKILL PARAMETERS (p_T and k) FOR Drn HISTORICAL VARIATION WITH TIME FOR POINT NEPEAN	Figure 7.63

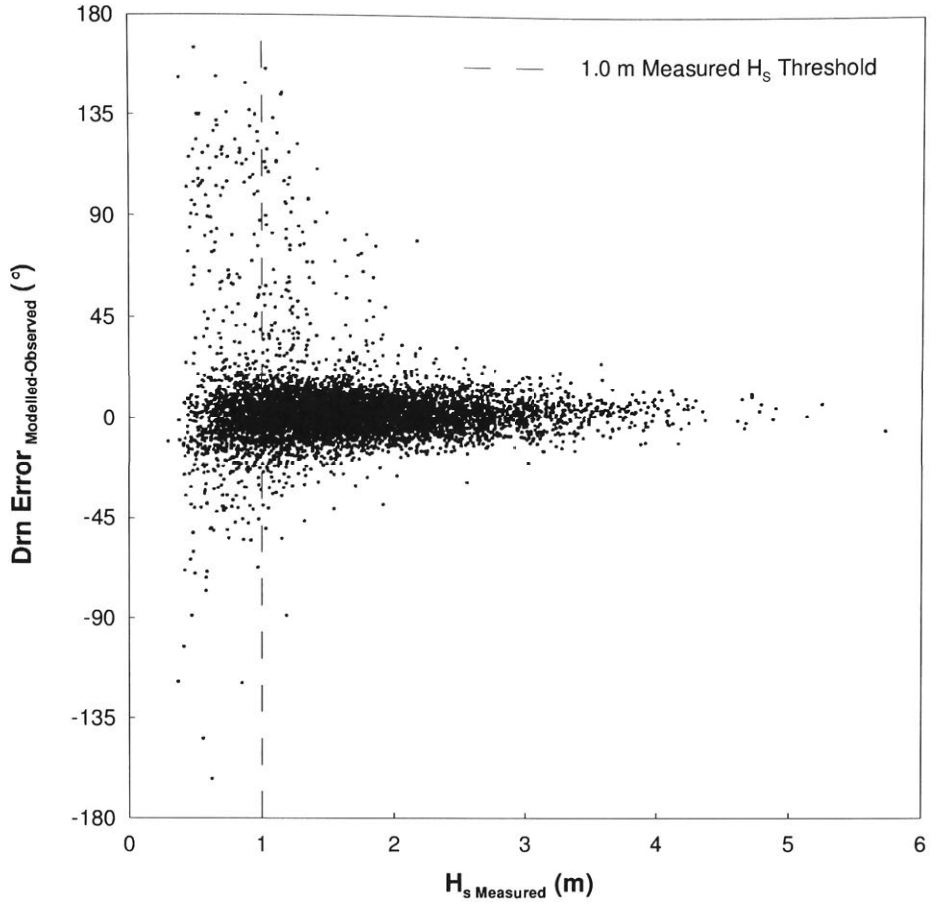

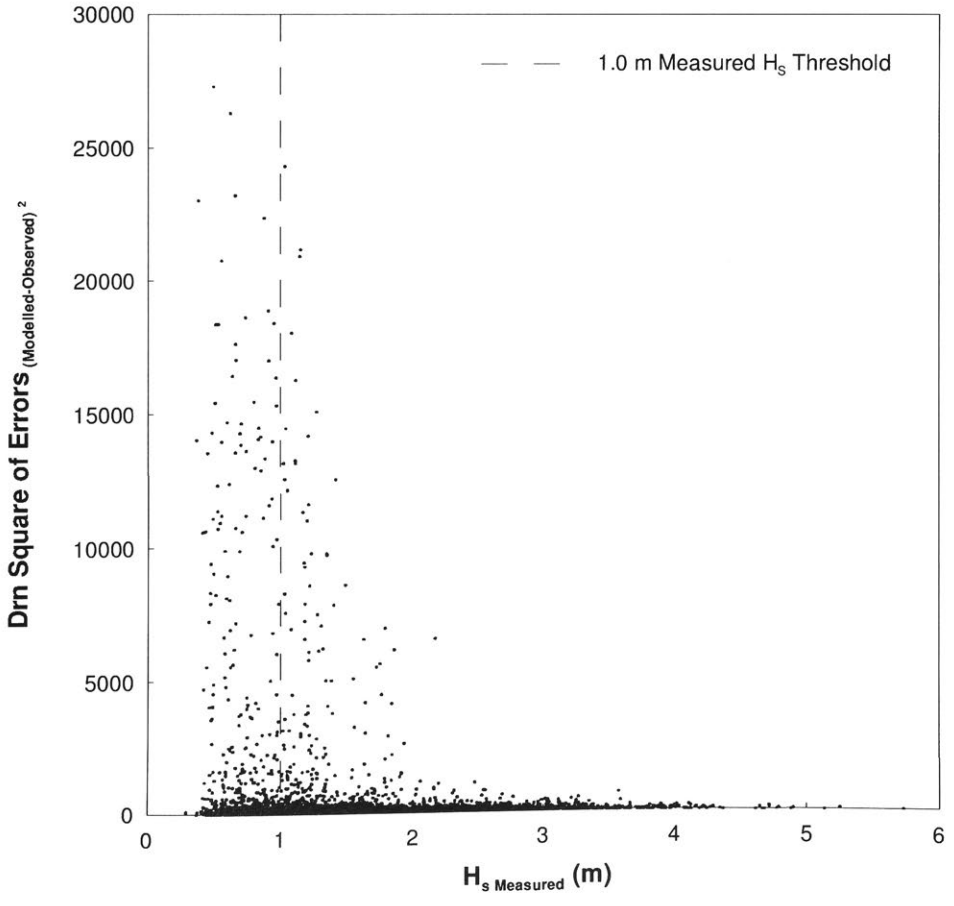

WRL Report No. 237	MEASURES OF ERROR FOR WAVE DIRECTION PREDICTION VARIATION WITH MEASURED H_S FOR POINT NEPEAN	Figure 7.64

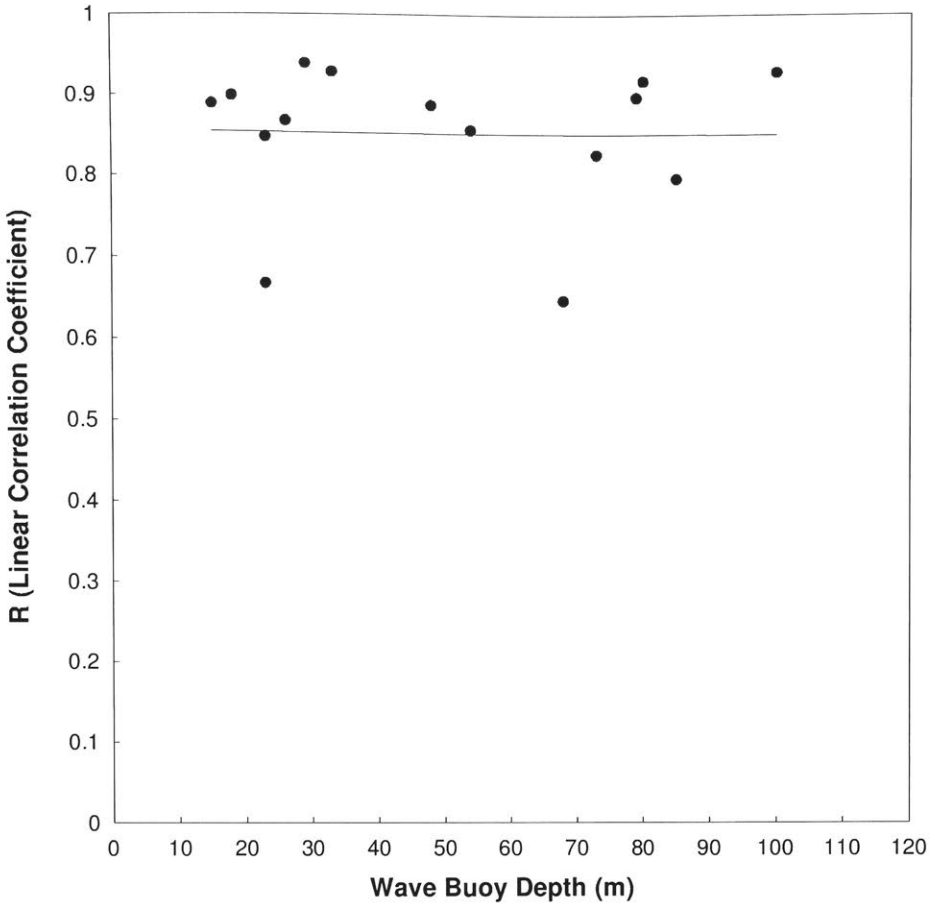

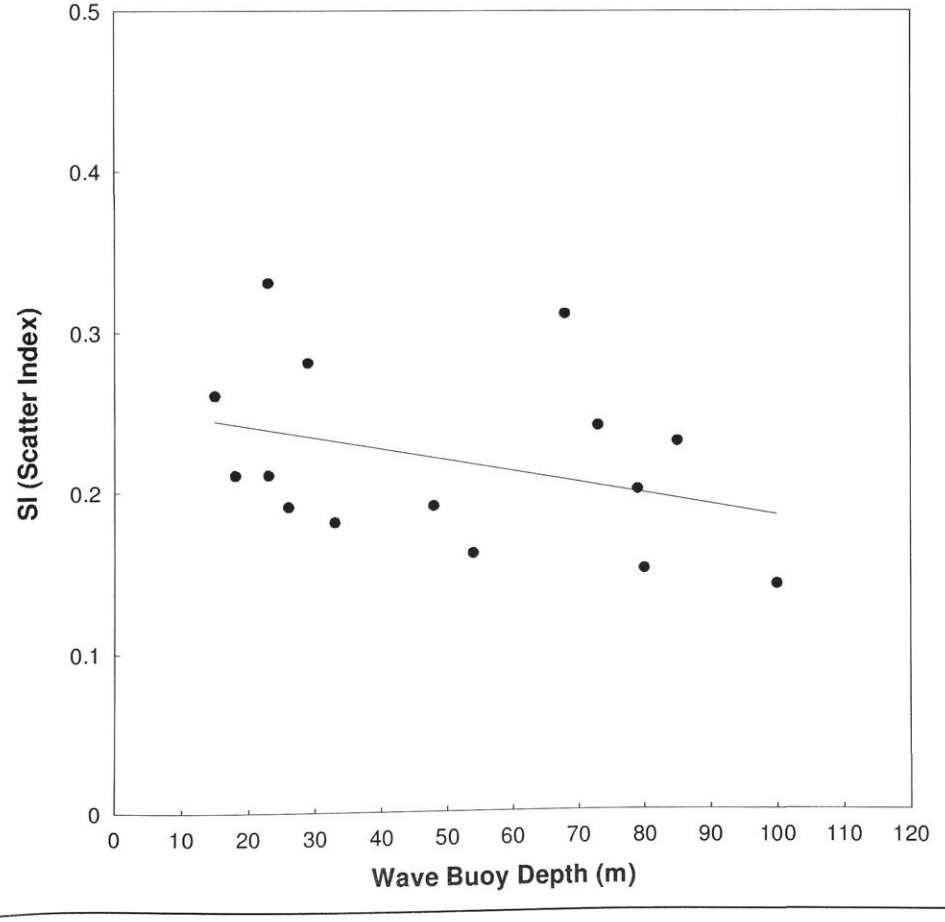

WRL
Report No. 237

MODEL SKILL PARAMETERS (R and SI) FOR H_s WITH VARIATION IN WAVE BUOY DEPTH

Figure 7.65

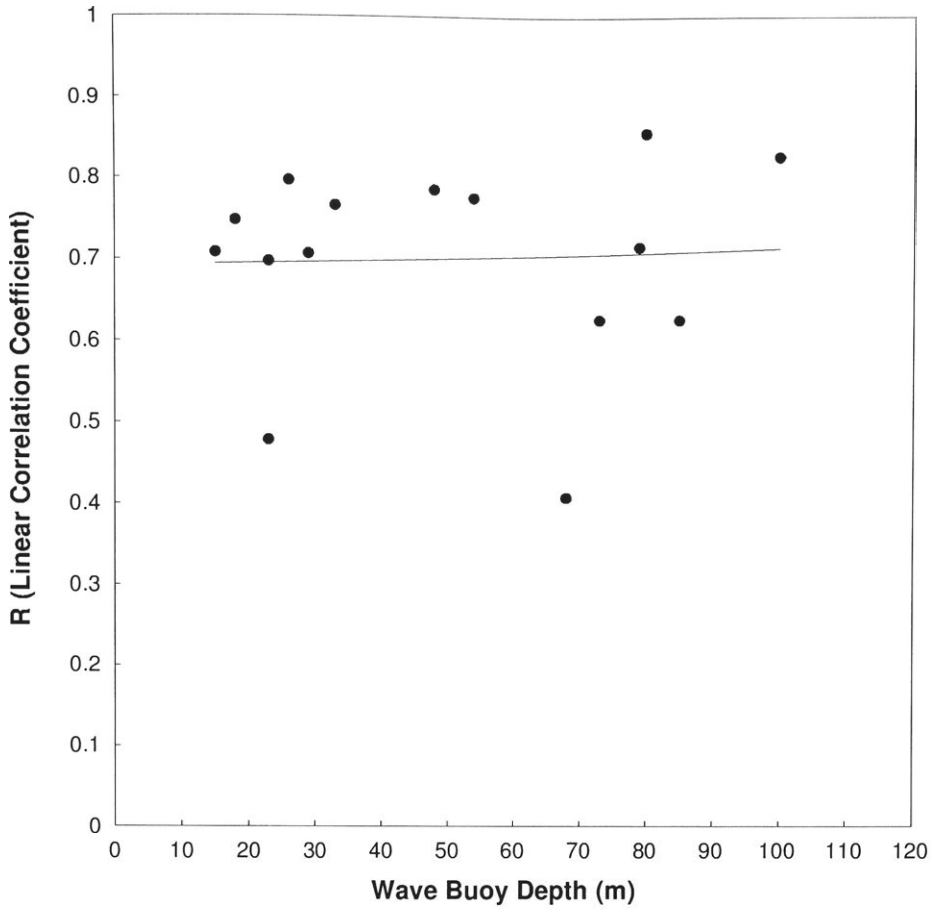

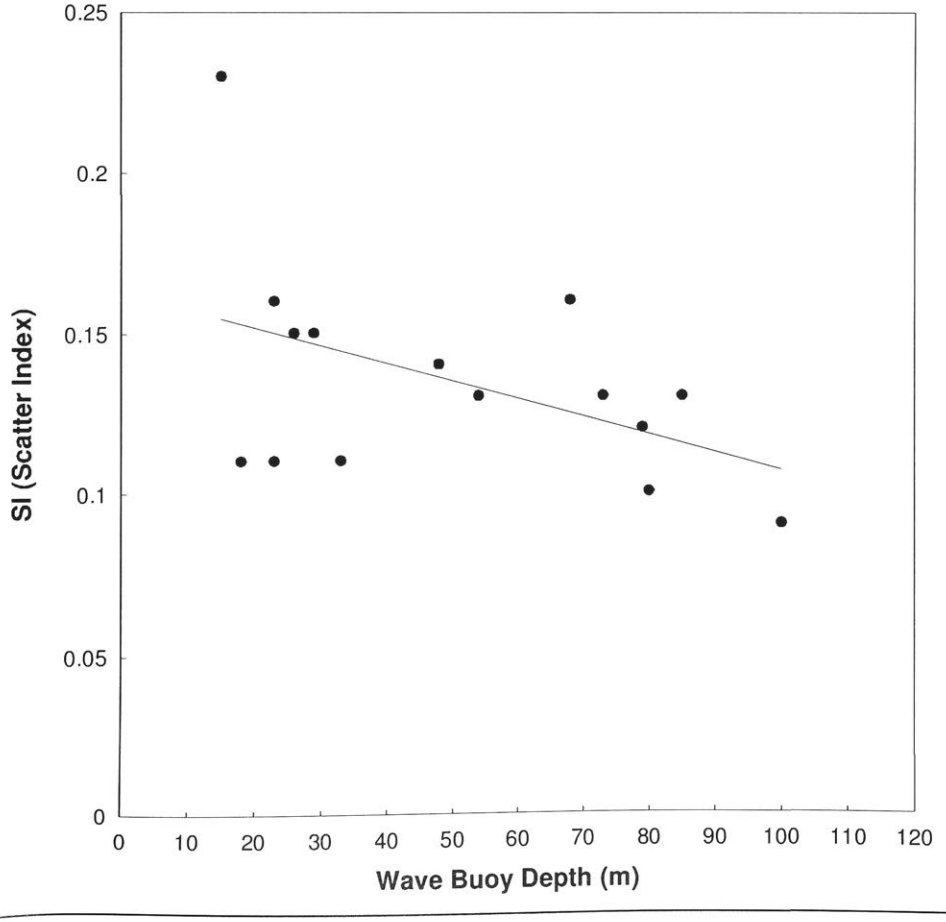

WRL
Report No. 237

MODEL SKILL PARAMETERS (R and SI) FOR T_1 WITH VARIATION IN WAVE BUOY DEPTH

Figure 7.66

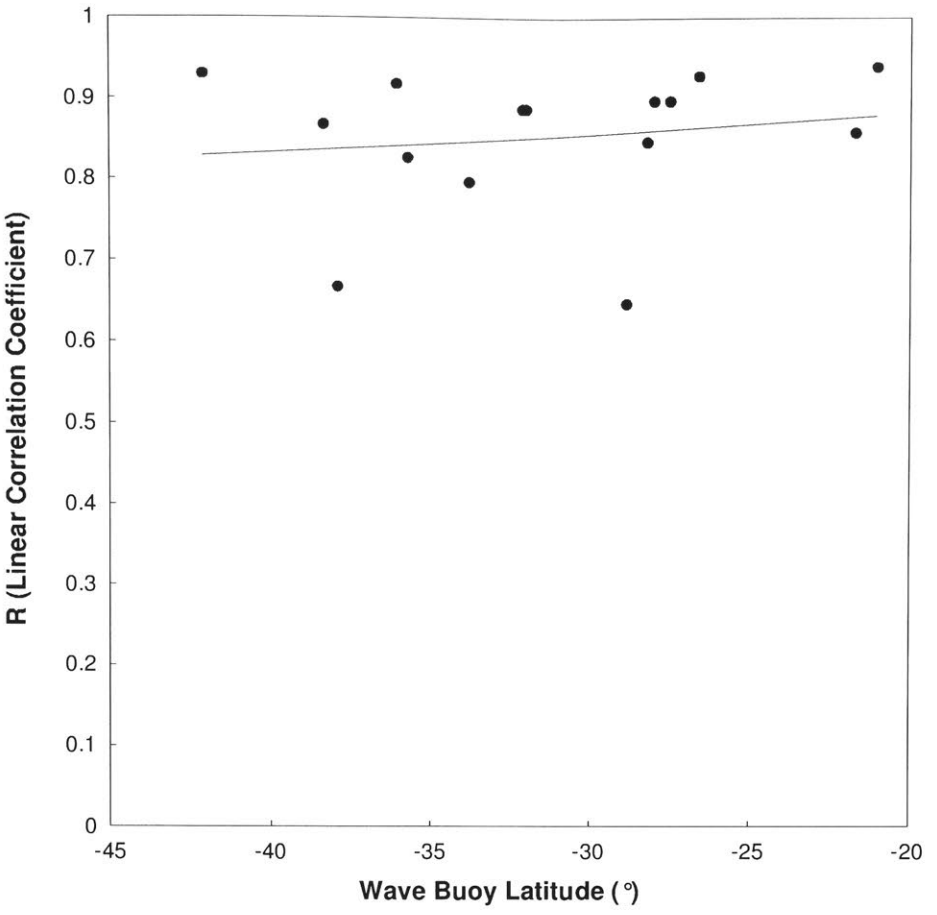

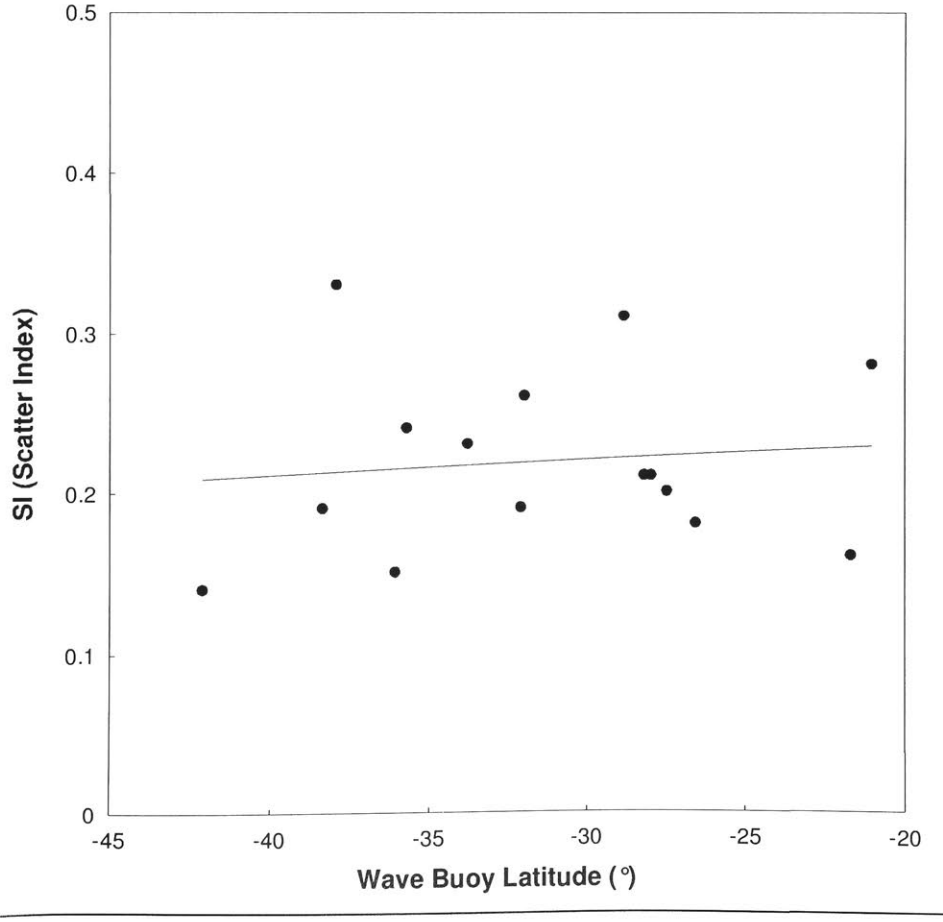

WRL Report No. 237	MODEL SKILL PARAMETERS (R and SI) FOR H_S WITH VARIATION IN WAVE BUOY LATITUDE	Figure 7.67

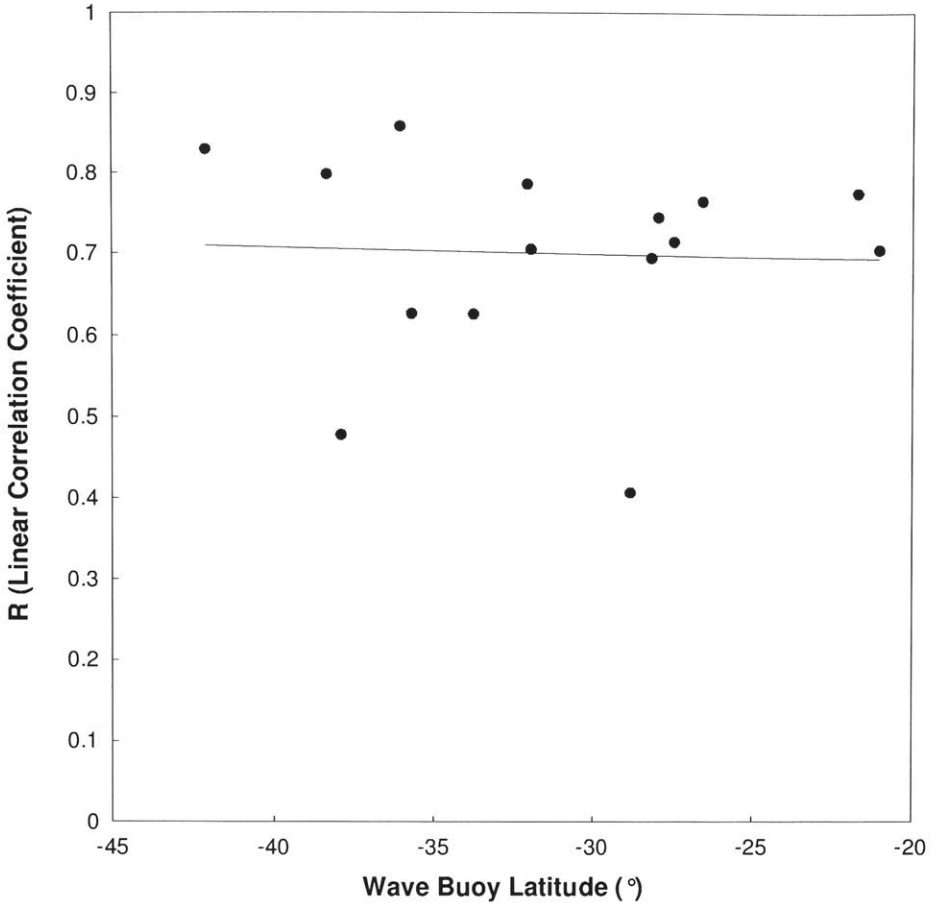

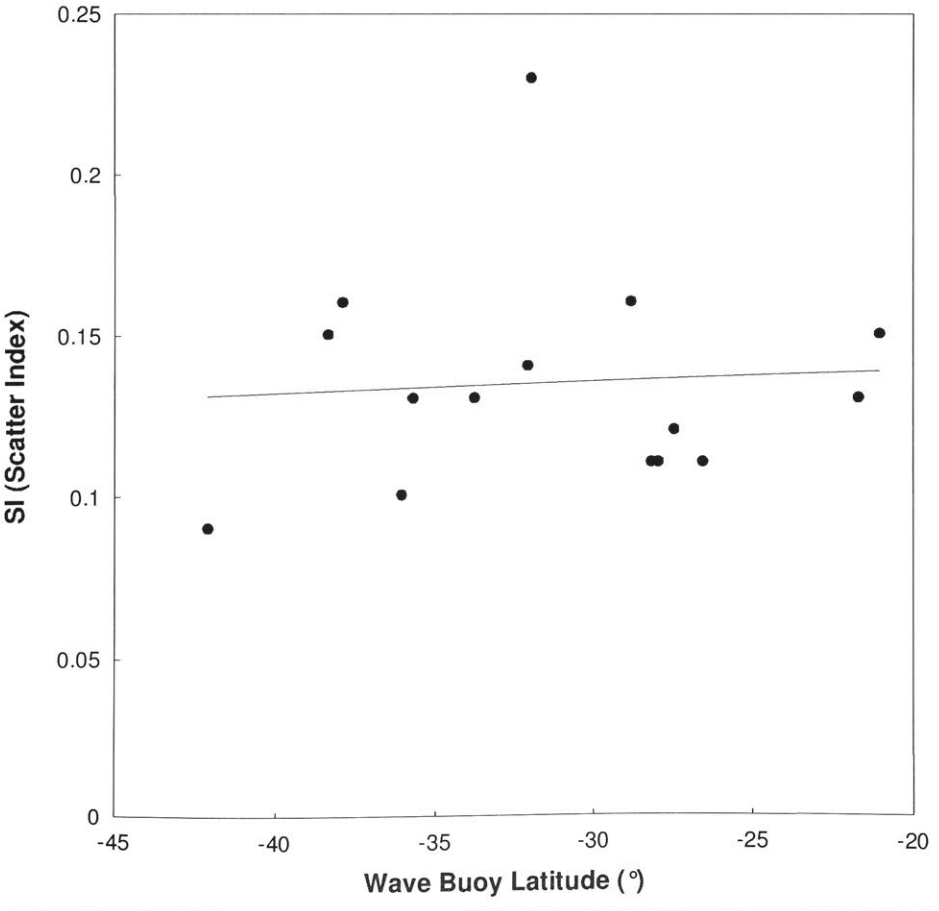

WRL Report No. 237	MODEL SKILL PARAMETERS (R and SI) FOR T_1 WITH VARIATION IN WAVE BUOY LATITUDE	Figure 7.68

The following information has been removed from the digital copy of this thesis. Please see the print copy of the thesis for a complete manuscript.

Title: Appendix A : Wave Buoy Data Consent Conditions

Title: Appendix B :Calculating Mean and Peak Wave Directions